Homologous and heterologous expression of magnetosome operons from *Magnetospirillum gryphiswaldense*

Dissertation der Fakultät für Biologie der
Ludwig-Maximilians-Universität München

vorgelegt von
Isabel Kolinko
aus München
2014

Die vorliegende Doktorarbeit wurde im Zeitraum von Februar 2010 bis Juni 2014 an der Ludwig-Maximilians-Universität München in Martinsried durchgeführt.

1. Gutachter: Prof. Dr. Dirk Schüler (Universität Bayreuth)
2. Gutachter: Prof. Dr. Kirsten Jung (Ludwig-Maximilians-Universität München)

Tag der Abgabe: 16.06.14

Tag der mündlichen Prüfung: 06.10.14

Publications and manuscripts originating from this thesis

Manuscript 1

Kolinko I., Jogler C., Katzmann E., and Schüler D. Frequent mutations within the genomic magnetosome island of *Magnetospirillum gryphiswaldense* are mediated by RecA. Journal of Bacteriology (2011), 19: 5328-34.

Manuscript 2

Lohße A.*, Kolinko I.*, Borg S., Uebe R., Raschdorf O., Plitzko J. M., Brachmann A., and Schüler D. Chromosomal multiplication of the *mam* and *mms* operons enables enhanced magnetosome biosynthesis in *Magnetospirillum gryphiswaldense.* In preparation.

* These authors contributed equally to this study.

Manuscript 3

Kolinko I., Lohße A., Borg S., Raschdorf O., Jogler C., Qiang T., Pósfai M., Tompa É., Plitzko J. M., Brachmann A., Wanner G., Müller R., Zhang Y., and Schüler D. Biosynthesis of magnetic nanostructures in a foreign organism by transfer of bacterial magnetosome gene clusters. Nature Nanotechnology (2014), 3: 193-7.

- Highlighted in: Staniland S. Nanoparticle biosynthesis: An accommodating host. Nature Nanotechnology (2014), 9: 163-4.

Manuscript 4

Lohße A., Borg S., Raschdorf A., Kolinko I., Tompa É., Pósfai M., Faivre D., Baumgartner J., and Schüler D. Genetic dissection of the *mamAB* and *mms6* operons reveals a gene set essential for magnetosome biogenesis in *Magnetospirillum gryphiswaldense.* Journal of Bacteriology (2014), doi: 10.1128/JB.01716-14, ahead of print.

Contributions to publications and manuscripts

Manuscript 1:

I.K., C.J. and D.S. designed the study. I.K. constructed the mutant and performed phenotypic characterization experiments. E.K. took transmission electron micrographs and I.K. analyzed the data. I.K. and D.S. wrote the manuscript.

Manuscript 2:

A.L., I.K. and D.S. designed the study. A.L. and I.K. established protocols and planned experiments. I.K. and A.L. constructed overexpression mutants and performed phenotypic characterization experiments. S.B. analyzed the mutants by transmission electron microscopy. R.U. performed fermentor cultivation experiments. J.P. and O.R. performed cryo-electron tomography experiments. A.B. performed Illumina genome sequencing. A.L. and I.K. analyzed the data. A.L., I.K. and D.S. wrote the manuscript.

Manuscript 3:

I.K., D.S., Y.Z., Q.T., C.J. and R.M. planned and performed cloning experiments. I.K. and A.L. performed genetic transfers and cultivation experiments. G.W. prepared cryo- and chemically fixed cells. S.B., O.R. and G.W. performed transmission electron micrographs and I.K. analyzed the data. J.P. and O.R. performed cryo-electron tomography experiments. E.T. and M.P. took high-resolution TEM micrographs and analyzed the data. I.K. and A.L. took fluorescence micrographs and performed phenotypization experiments. I.K. performed western blot experiments and analyzed proteomic data. A.B. performed Illumina genome sequencing and I.K. analyzed the data. I.K. and D.S. designed the study and wrote the paper.

Manuscript 4:

I.K. constructed the plasmids pBam_*mamI* and pBam_*mamA* and performed transcomplementation of *M. gryphiswaldense* Δ*mamI* and Δ*mamA*.

I hereby confirm the statements:

Isabel Kolinko Prof. Dirk Schüler

Index

Abbreviations

ABC	ATP-binding cassette
Bp	Base pairs
CDF	Cation diffusion facilitator
CDS	Coding sequence
CET	Cryo-electron tomography
CM	Cytoplasmic membrane
Fur	Ferric uptake regulator
EGFP	Enhanced green fluorescent protein
IR	Inverted repeat sequence
Kb	Kilobase pairs
MAI	Magnetosome island
Mad	magnetosome associated deltaproteobacteria
Mam	magnetosome membrane
MFS	Major facilitator superfamily
Mms	magnetic particle membrane-specific
MM	Magnetosome membrane
MRI	Magnetic resonance imaging
MTB	Magnetotactic bacteria
ORF	Open reading frame
PCR	Polymerase chain reaction
RBM	Reciprocal best matches
SDS-PAGE	Sodium dodecyl sulphate – polyacrylamide gel electrophoresis
TEM	Transmission electron microscopy
TPR	Tetra tricopeptid
WT	Wild type

Summary

The magnetotactic model organism *Magnetospirillum gryphiswaldense* synthesizes membrane-bounded, nano-sized magnetite (Fe_3O_4) crystals, referred to as magnetosomes. Most genes governing the biosynthesis pathway of these unique organelles are clustered in a contiguous genomic magnetosome island (MAI). It has been shown that four major operons (*mamAB*, *mamGDFC*, *mms6*, *mamXY*) within the MAI encode factors for the stepwise magnetosome assembly, involving the invagination of vesicles from the cytoplasmic membrane, magnetosomal uptake of iron, redox-controlled biomineralization of magnetite crystals, as well as their assembly into highly ordered nanochains along a dedicated cytoskeletal structure.

Rearrangements occurring within the MAI frequently cause the accumulation of unmagnetic mutants during subcultivation in the laboratory, which hampers the genetic analysis of magnetosome formation in *M. gryphiswaldense*. In previous studies it was speculated that this instability is due to RecA-dependent homologous recombination between numerous sequence repeats present within the MAI. To verify this hypothesis, a *recA* mutant strain of *M. gryphiswaldense* was constructed. Besides a slightly higher sensitivity to UV-light, homologous recombination was severely reduced in strain IK-1. Remarkably, in contrast to the wild type (WT), no spontaneous non-magnetic mutants accumulated after serial passaging under physiological stress conditions. This demonstrates that the observed rearrangements in the MAI are in fact RecA-driven and that the *recA* mutant is genetically more stable than the WT.

In the second part of this thesis, we aimed to clone all known *mam* and *mms* genes from *M. gryphiswaldense* for their subsequent transfer into various homologous and heterologous hosts. Modular expression cassettes comprising single as well as all major magnetosome operons were constructed by recombinogenic engineering based on phage-derived recombination. Transposable elements (MycoMar or Tn5 transposase) were utilized to enable transfer and random chromosomal integration in single copy into a broad host range of bacteria.

In the third part of this thesis, we investigated whether it is possible overproduce magnetosomes by chromosomal amplification of the *mam* and *mms* operons. While an insertion of additional copies of single operons enhanced the magnetosome size in the genetically stable *recA* mutant, duplication of the four major magnetosome operons caused a more than twofold increase in magnetosome numbers per cell. These findings demonstrate that a higher gene dosage provides an efficient strategy to specifically enhance magnetosome numbers and size in *M. gryphiswaldense*.

Finally, the expression cassettes were transferred into the photosynthetic model organism *Rhodospirillum rubrum* and other alphaproteobacteria via transposition. While we failed to detect phenotypic effects in most tested heterologous hosts, membrane-bounded magnetite crystals were formed in *R. rubrum* after transfer of all four major operons. This proves that the 29 transferred magnetosome genes constitute an autonomous expression unit that is sufficient to transplant the controlled synthesis of magnetite nanocrystals and their self-assembly within a foreign organism. However, a MTB-specific ferrous iron transport system encoded outside the *mam* and *mms* operons was necessary for biomineralization of donor-like magnetosomes. Altogether, this finding provides the first evidence that the magnetotactic trait can be disseminated to different species by only few events of transfer. Furthermore, it represents a step towards the endogenous magnetization of various organisms by synthetic biology.

Zusammenfassung

Der magnetotaktische Modellorganismus *Magnetospirillum gryphiswaldense* synthetisiert nanometergroße, membranumhüllte Magnetitkristalle (Fe_3O_4), so genannte Magnetosomen. Der Großteil der Gene, welche die Synthese dieser einzigartigen Organelle steuern, ist in einer zusammenhängenden genomischen Magnetosomeninsel (MAI) lokalisiert. Es wurde gezeigt, dass vier Operons (*mamAB*, *mamGDFC*, *mms6*, *mamXY*) innerhalb der MAI Faktoren für die schrittweise Synthese der Magnetosomen kodieren. Die intrazelluläre Bildung dieser Organelle beinhaltet die Invagination der Vesikel aus der cytoplasmatischen Membran, die magnetosomale Eisenaufnahme, die redoxkontrollierte Biomineralisation der Magnetitkristalle sowie ihre Assemblierung zu Nanoketten entlang eines zytoskelettalen Filaments.

Aufgrund von spontanen Umstrukturierungen und Deletionen innerhalb der MAI kommt es während der Kultivierung unter Laborbedingungen häufig zur Akkumulierung von unmagnetischen Mutanten. Dies erschwert die genetische Analyse der Magnetosomenbildung in *M. gryphiswaldense*. Es wurde vermutet, dass die beobachtete genetische Instabilität durch RecA-vermittelte homologe Rekombination zwischen repetitiven Sequenzen in der MAI hervorgerufen wird. Um diese Hypothese zu überprüfen, wurde eine *recA*-Mutante von *M. gryphiswaldense* konstruiert. Der Stamm IK-1 zeichnete sich neben einer höheren Sensitivität gegenüber UV-Licht durch eine erheblich verringerte Rekombinationsrate aus. Bemerkenswerterweise häuften sich im Gegensatz zum Wildtyp (WT) keine spontanen Mutanten nach mehreren Passagen unter physiologischen Stressbedingungen an. Dies beweist, dass die beobachteten Umstrukturierungen in der MAI tatsächlich durch RecA hervorgerufen werden und dass die *recA* Mutante eine höhere genetische Stabilität im Vergleich zum WT aufweist.

Der zweite Teil der Dissertation hatte die Klonierung aller bekannten *mam*- und *mms*-Gene zum Ziel, um einen Transfer der Magnetosomenoperons in unterschiedliche homologe und heterologe Wirte zu ermöglichen. Zu diesem Zweck wurden mittels einer auf Phagen-basierten Klonierungsstrategie modulare Expressionkassetten konstruiert, welche entweder einzelne oder alle

Magnetosomenoperons beinhalteten. Um ihre chromosomale Insertion in eine große Bandbreite unterschiedlicher Bakterien zu ermöglichen, wurden transposable Elemente (MycoMar oder Transposase 5) verwendet.

In dem dritten Teil dieser Dissertation wurde überprüft, ob es möglich ist mittels chromosomaler Amplifikation der *mam*- und *mms*-Operons eine Magnetosomenüberproduktion zu erzielen. Während eine Erhöhung der Kopienzahl einzelner Operons zur Bildung von größeren Magnetosomen in der genetisch stabilen *recA*-Mutante führte, verursachte die Duplikation aller *mam*- und *mms*- Gene einen mehr als zweifachen Anstieg der Magnetosomenzahl pro Zelle. Die Ergebnisse zeigen, dass eine Erhöhung der Gendosis eine effiziente Strategie darstellt, um spezifisch die Magnetosomenzahl oder –größe zu erhöhen.

Schließlich wurden die Transposonplasmide in den photosynthetischen Modellorganismus *Rhodospirillum rubrum* und andere Alphaproteobakterien transferiert. Während wir in den meisten getesteten heterologen Wirten keine phänotypischen Veränderungen feststellen konnten, bildete *R. rubrum* membranumhüllte Magnetitkristalle nach dem Transfer der vier Magnetosomenoperons. Das Ergebnis zeigt, dass die 29 Gene eine eigenständige Expressionseinheit darstellen, welche ausreichend ist, um die Fähigkeit zur kontrollierten Synthese von Magnetitkristallen in einen fremden Wirt zu übertragen. Allerdings wurde ein MTB-spezifisches Eisen(II)-Transportsystem, welches außerhalb der *mam*- und *mms*-Operons kodiert ist, für die Bildung von Donor-ähnlichen Magnetosomen in *R. rubrum* benötigt. Insgesamt betrachtet beweist diese Ergebnis zum ersten Mal, dass der magnetotaktische Phänotyp durch wenige Transferereignisse in einen anderen Organismus übertragen werden kann. Zudem ist es einen wichtiger Schritt auf dem Weg zur endogenen Magnetisierung verschiedener Organismen mit Hilfe von synthetischer Biologie.

Chapter I

1. Introduction

The genetic diversity of prokaryotes is illustrated by their metabolic versatility, ability to sense and quickly adapt to environmental changes, and to synthesize macromolecular structures and organelles. Shaping of each of these complex phenotypes requires the balanced expression of numerous genes, which are often found to be organized as gene clusters in the genome [1, 2]. Intriguing examples of such a group of functionally related genes are the magnetosome gene clusters found in magnetotactic bacteria (MTB). Coordinated action of >30 genes drives the formation of membrane-enveloped, magnetic nanocrystals (magnetosomes) that are assembled into highly ordered chains within the cell. The molecular and genetic mechanisms underlying the stepwise assembly of these organelles have attracted interdisciplinary interest. Furthermore, magnetosomes also offer various biomedical and biotechnological applications due to their high chemical purity, unprecedented magnetic properties and inherent biocompatibility. However, magnetotactic bacteria are recalcitrant organisms and genetic engineering of the few culturable representatives is cumbersome. Furthermore, the magnetic phenotype is unstable in several cultivable MTB, leading to rapid accumulation of spontaneous mutants during subcultivation [3-5]. For a long time, these drawbacks have prompted ideas to transplant the magnetosome biosynthesis pathway into more amenable hosts [6, 7]. So far, this has remained unachieved due to the structural and genetic complexity of this organelle and insufficient knowledge of the biosynthetic functions involved [1].

This thesis addressed the above-mentioned issues. The magnetotactic bacterium *Magnetospirillum gryphiswaldense* was engineered for more stable and enhanced production of magnetosomes. Most importantly, we demonstrate the genetic transfer of the magnetosome biosynthesis pathway into a foreign host.

1.1 The alphaproteobacterium *Magnetospirillum gryphiswaldense*

The ability to synthesize magnetosomes, which are membrane-enveloped crystals of the iron mineral magnetite (Fe_3O_4) or greigite (Fe_3S_4) [8-10], has been found in a heterogeneous group of prokaryotes, called magnetotactic bacteria [11-13]. Despite their differences in morphology, physiology and phylogeny, MTB share a lifestyle as gradient organisms inhabiting in or below the oxic-anoxic transition zone in aquatic sediments. Therefore, it has been speculated that their ability to sense and orient along the Earth's magnetic field, termed magnetotaxis, helps guiding the cells towards their favored growth zone [11, 13]. However, due to their fastidiousness and unknown growth requirements, only very few representatives have been isolated in axenic culture so far [11]. The majority of MTB is affiliated with the *Alphaproteobacteria*, including the best characterized organisms *Magnetospirillum gryphiswaldense* (the model organism used in this thesis) and the closely related *Magnetospirillum magneticum* (16S rRNA identity = 96%) [14]. Cells of *M. gryphiswaldense* produce cuboctahedral magnetite crystals (30-40 magnetosomes per cell) [15-17], which are assembled along a cytoskeletal structure into one or two linear chains within the cell (see Fig. 1) [18-20].

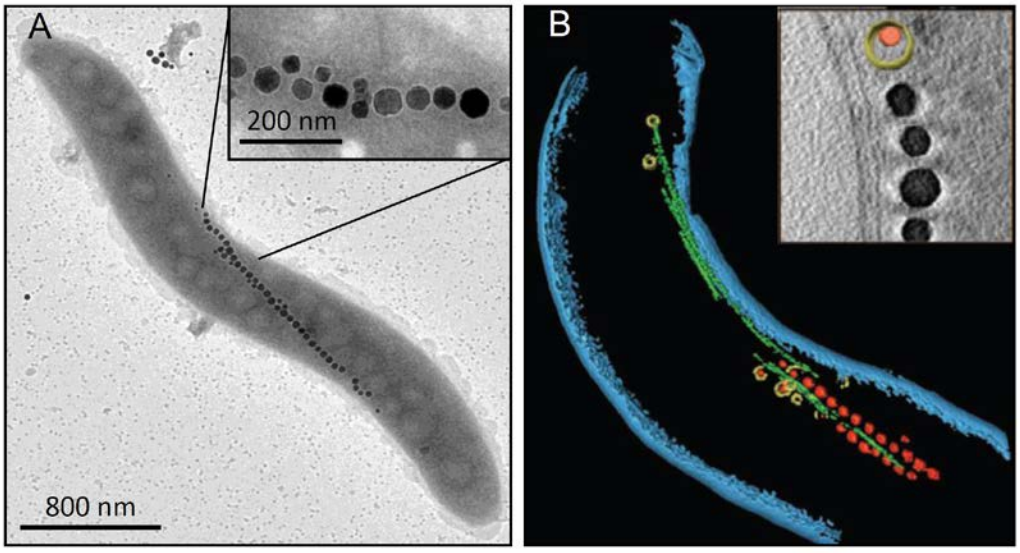

Figure 1: Transmission electron micrograph (A) and cryo-electron tomograph (B) of a *Magnetospirillum gryphiswaldense* cell, which produces membrane enveloped (yellow) magnetic particles (red) aligned into a chain-like structure along a dedicated cytoskeletal filament (green). (B) adapted from [19].

This microaerophilic bacterium was originally isolated from the sediment of a river near the city of Greifswald and can grow chemoorganoheterotrophically with oxygen or nitrate as terminal electron acceptors [15, 21]. Compared to other MTB, *M. gryphiswaldense* is easier to cultivate since it is more tolerant towards oxygen [22]. Additionally, the genome sequence [23, 24], as well as a recently established genetic system [25-27], are available for *M. gryphiswaldense*. These different prerequisites make this bacterium a model organism to study the genetic and biochemical processes underlying magnetosome formation and to engineer magnetosomes for various functionalization approaches [28].

1.2 Characteristics and applications of magnetosomes

Mature magnetite crystals of *M. gryphiswaldense* have a size of 35-50 nm [16, 17], and dependent on the species, monocrystalline particles ranging from 30-120 nm have been described in MTB [29-32]. Crystals within this narrow size range are in a permanent single-domain state [32, 33]. In such a particle, all elementary magnetic dipoles are aligned in parallel and thus form a uniform magnetization, which is maximal for a given volume [33]. In contrast, smaller crystals (<30 nm) also consist of a single magnetic domain, but possess superparamagnetic characteristics and do not retain a temporally stable magnetization at room temperature because of thermal fluctuations [29]. Larger multidomain particles (>120 nm), on the other hand, consist of several magnetic domains with magnetic moments oriented in different directions and therefore have a reduced magnetization compared to single-domain particles [29, 33]. Consequently, magnetosomes bear optimal magnetic properties for magnetotaxis [32]. Not only the size, but also the crystal morphology in MTB underlies species-specific control [32]: While *M. gryphiswaldense* produces cuboctahedral magnetosomes, prismatic, or bullet shaped crystals (see also Fig. 2A) were reported in other MTB [32, 34, 35]. Although variations in the size and morphology exist, particles produced by MTB are chemically pure [33] and have a high degree of crystallographic perfection [36-38]. Altogether, these above-mentioned characteristics are difficult or even impossible to reconstruct by chemical synthesis.

A prerequisite for the formation of crystals with such remarkable properties is a tight physiochemical control over the crystallization process within the cell. This is achieved by compartmentalization in subcellular membrane vesicles, which serve as “nanoreactors” for crystal nucleation and growth (see also 1.3) [33, 39]. The so called magnetosome membrane (MM) consists of phospholipids and specific proteins (see also 1.4) and is as a “natural coating” stably surrounding the crystals even after cell lysis [40, 41] (Fig. 2B). Similar to other organic shell structures (e.g. polymers, polysaccharides) used for coating of artificial core/shell nanoparticles [42], the MM ensures the dispersibility of the magnetosomes [40]. Furthermore, it also offers a large biocompatible surface for the display of different functional moieties. Using either chemical or genetic engineering, magnetosomes have been coupled with drugs, antibodies, oligonuncleotides, fluorophores and enzymes, and therefore offer numerous applications, including magnetic drug targeting, immunoassays and magnetic resonance imaging [40, 43-47].

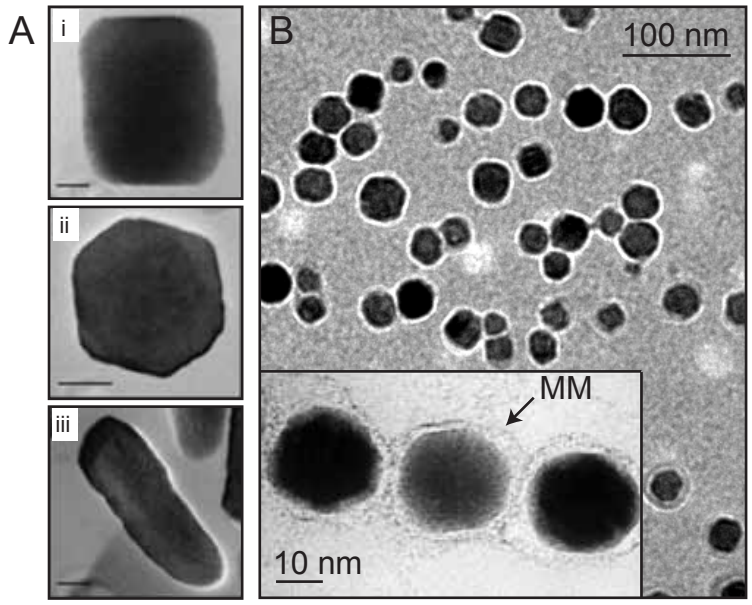

Figure 2: A.TEM micrographs of i) prismatic, ii) cuboctahedral and iii) bullet shaped magnetosomes. Scale bar: 20 nm. Adapted from [40]. B. Isolated magnetosomes of *M. gryphiswaldense* (micrograph taken by E. Katzmann), which are surrounded by a magnetosome membrane (MM), negatively stained with uranyl acetate (inset adapted from [39]).

1.3 The process of magnetosome biosynthesis

For the biomineralization of magnetite crystals and their subsequent organization into well-ordered chains, several steps need to be coordinated in the cell, including: i) vesicle formation, ii) cellular and magnetosomal iron uptake, iii) crystal nucleation and growth, and iv) chain-like assembly.

Using cryo-electron tomography (CET), it has been shown in both *M. gryphiswaldense* and *M. magneticum* that the vesicles for magnetosome biosynthesis are formed prior to magnetite crystallization via invaginations of the cytoplasmic membrane (see Fig. 3) [19, 48]. This observation is consistent with the results of a biochemical analysis of the MM from *M. gryphiswaldense*, which revealed a lipid composition nearly identical to that of the cytoplasmic membrane (CM) [41]. In contrast, the protein composition of the MM is distinct compared to that of the CM, which suggests that a sorting of MM-specific proteins takes place during the membrane vesicle formation process [49]. However, it is still under debate whether the vesicles detach from the cytosplasmic membrane or stay connected with the periplasm during subsequent steps of magnetosome biosynthesis and assembly [11, 39].

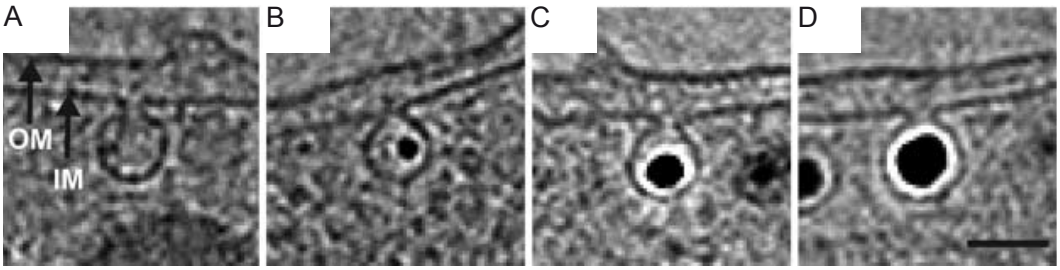

Figure 3: CET images illustrating the process of vesicle formation and crystal growth in *M. magneticum*. A. Vesicle synthesis proceeds via invagination of the inner/cytoplasmic membrane (IM). Afterwards, crystal nucleation and growth (B-D) occur within the vesicles. OM: outer membrane. Scale bar: 50 nm. Adapted from [48].

Prior to crystal precipitation, large amounts of iron are transported into the cell (account up to 4% of the dry weight) [33]. Cells of *M. gryphiswaldense* import extracellular ferrous iron by a slow, diffusion-like process [50]. In contrast, ferric iron is incorporated by a low-affinity, but high-velocity transport system that follows Michaelis-Menten kinetics (V_{max} = 0.86 nmol Fe min^{-1} (mg dry weight)$^{-1}$; K_m = 3 µM) [50]. Bioinformatic analysis of the genome of

M. gryphiswaldense revealed the presence of ferrous iron uptake systems (FeoAB transporters), as well as a putative ATP binding cassette (ABC) ferric iron transporter, and a putative ABC-type ferric siderophore transporter [51-53]. However, only deletion of genes encoding constituents of two ferrous iron uptake systems (FeoB1 and FeoB2) had an influence on magnetosome formation (see also 1.4.2) [52, 53]. Recently, two enzymes (FeR5, FeR6) were characterized, which indirectly influence magnetosome formation by reducing extracellular ferric iron for its subsequent uptake into the cell [54].

Next, the iron is transported into the magnetosome vesicles. Several MM-specific proteins have been suggested to act as magnetosomal ferric (MamH, MamZ) or ferrous (MamB, MamM) iron uptake systems (see also 1.4.2) [55, 56]. However, it is still unknown whether the iron is taken up from the cytoplasm and/or via the periplasm into the magnetosome vesicles [57]. The latter transport pathway would only be possible as long as the magnetosome vesicles did no detach from the cytoplasmic membrane [51].

Upon accumulation of supersaturating iron concentrations, magnetite nucleation and crystal growth occur within the vesicles. In general, the biomineralization of the mixed-valence iron oxide magnetite depends on a strict control of the physicochemical parameters, since protons are released during the formation of this mineral (equation 1).

$$\text{(eq. 1)}\ 2\ Fe^{3+} + Fe^{2+} + 4\ H_2O \rightarrow Fe_3O_4 + 8\ H^+ \text{ [57, 58]}$$

Based on the conditions required for precipitation of abiotically formed magnetite crystals, it has been proposed that biomineralization within the magnetosome vesicles occurs under slightly reducing conditions (E_h from -0.2 to -0.4 V) and at basic pH [33, 58, 59]. The chemical process of crystallization is still under debate, although it has recently been speculated that magnetite coprecipitates with ferrous iron from a phosphate-rich ferritine (ferric hydroxide) via a transient ferrihydrite phase [60].

Lastly, the magnetosomes are assembled into well-ordered chains along a cytoskeletal structure, thereby maximizing the magnetic dipole moment of the cell, resulting in cellular alignment along the weak geomagnetic field lines [18, 48, 61]. Despite the strict biochemical control exerted on magnetosome biosynthesis, formation of these complex nanostructures is also influenced by

several environmental factors. Specifically, besides the need of micromolar amounts of iron in the medium [50], magnetite biomineralization in *M. gryphiswaldense* occurs only under microaerophilic or anaerobic conditions [22, 62]. This might derive from abiogenic perturbation of the redox balance required for magnetite biomineralization [63]. However, several protein involved in denitrification and aerobic respiration have recently also been found to play a role in magnetosome formation in *M. gryphiswaldense*, indicating that the repression of biomineralization under aerobic conditions is also biologically controlled (see also 1.4.3) [63]. Furthermore, it has also been found that temperatures of >30 °C have inhibitory effects on magnetosome biomineralization and chain assembly. This might be caused by cellular heat stress or altered membrane fluidity [64].

1.4 Genetics of magnetosome formation

1.4.1 The magnetosome island

A set of >20 proteins was found to be specifically associated with the MM in *M. gryphiswaldense* [16, 41]. The corresponding genes were designated magnetosome membrane (*mam*) or magnetic particle membrane-specific (*mms*) and are clustered in a 115 kb large genomic region, termed the “Magnetosome Island” (MAI) [3, 16, 65, 66]. Generally, genomic islands are defined as mobile regions that enable horizontal transfer of a “flexible gene pool” to unrelated species [2, 67]. Their coding capacity is diverse, including the synthesis of virulence factors and bioactive compounds as well as different degradation pathways [68, 69]. Acquisition and expression of these genetic elements has been speculated to provide a selective advantage for the host by conferring a novel function, thereby significantly contributing to adaptive genome evolution in bacteria [67, 70].

The MAI of *M. gryphiswaldense* harbors several operons, which are interspersed by numerous hypothetical genes and mobile elements, such as transposase genes and insertion sequences (Fig. 4A, 4B) [3, 16, 23]. Furthermore, it was observed that rearrangements and deletions within the MAI can quickly arise during subcultivation, causing the accumulation of unmagnetic

or only weakly magnetic mutants [3, 71]. With the increasing availability of genomic information from additional MTB, MAIs were also described in other alphaproteobacteria, like *M. magneticum* and *Magnetovibrio blakemorei*, as well as in the deltaproteobacterium *Desulfovibrio magneticus* [5, 72, 73]. Thus, given the phylogenetic diversity of MTB and the high degree of homology between some magnetosome genes of remotely related groups, a horizontal distribution of the magnetotactic trait has been speculated by Jogler and coworkers [72, 74]. However, no indications for characteristic features of genomic islands (e.g. mobile element sequences) were found in the MAI of other analyzed MTB [75, 76]. Furthermore, a comparison of 16S rRNA genes and the amino acid sequence of magnetosome genes from different MTB indicated a congruent evolution among these genes [77]. This led to the recent hypothesis that magnetotaxis may have evolved vertically [11]. However, none of the above-mentioned hypotheses has been unambiguously proven so far.

1.4.2 Molecular organization and functions of magnetosome genes within the MAI

The MAI of *M. gryphiswaldense* comprises the 4 major magnetosome operons *mms6*, *mamGFDC*, *mamAB*, *mamXY* (30 genes, ~27 kb in total), which are each transcribed as single, polycistronic messenger RNA under control of the P_{mms6}, P_{mamDC}, P_{mamH}, and P_{mamXY} promoters, respectively (Fig. 4A) [16, 55, 78]. By construction of single gene and operon deletion mutants, their essential or accessory roles during magnetosome biosynthesis and assembly have been elucidated. However, up to date the functions of several *mam* and *mms* genes are still unknown.

Deletion of the 3.7 kb *mms6* operon resulted in significantly smaller crystals, which were aligned in short chains or loosely scattered within the cell (see also Fig. 4C) [16]. Consistent with this finding, the MTB-specific MmsF and Mms6 proteins are predicted to be major regulators of crystal size and shape in *M. magneticum* [7, 79]. In *M. gryphiswaldense*, two additional genes in the *mms6* operon, namely *mms36* and *mms48*, have been found to play a role in crystal size regulation. Elimination of either *mms36* or *mms48* caused the synthesis of fewer, but larger magnetite crystals compared to that of the WT

[80]. Therefore, a cumulative effect on biomineralization by various proteins encoded by the *mms6* operon has been suggested [80].

The 2.4 kb *mamGFDC* operon encodes the small hydrophobic proteins MamG, MamF, MamD and MamC (Fig. 4A), which belong to a set of specific signature proteins with no homology to proteins in non-magnetic organisms [23]. They are most abundant and together account for approximately 35% of all magnetosome associated polypeptides in the MM of *M. gryphiswaldense* [41]. A Δ*mamGFDC* mutant (see Fig. 4B) displays smaller crystals with aberrant shapes, therefore indicating an accessory role for magnetite biosynthesis [17]. In a recent sequencing effort, a *mamF-like* (*mamF2*, 74% sequence identity to *mamF*) and *mamD-like* (*mamD2*, 76% sequence identity to *mamD*) gene were identified in the MAI of *M. gryphiswaldense* [24] (A. Lohße, R. Uebe, unpublished). Transcomplementation studies in different *M. gryphiswaldense* mutants suggest that MamD2 and MamD, as well as MamF and MamF2, are functionally redundant and not essential for magnetosome formation (R. Uebe, unpublished).

Deletion of the 5.1 kb *mamXY* operon resulted in cells that formed two distinct types of magnetosomes: short chains of nearly regularly shaped, cuboctahedral crystals were flanked by small particles with poorly defined morphologies (see also Fig. 4C) [16]. The proteins MamX, MamZ (formerly known as MamH-like) and FtsZm were hypothesized to maintain the redox balance of Fe^{2+}/Fe^{3+} during magnetite biomineralization [55, 81]. A MTB-specific double c-type cytochrome signature motif CXXCH referred to as “magnetochrome” motif has been identified in MamX (consistent with MamP, MamE and MamT). MamZ contains a major facilitator superfamily (MFS) transporter domain and was speculated to be a ferric iron transporter [55]. Although MamY was implicated in constricting the magnetosome membrane during vesicle biogenesis [82], recent studies rather suggest a role in magnetosome chain assembly (F. Müller, unpublished) [83].

Recently, a MTB-specific *feoAB*-like operon encoding a ferrous iron transport system has been identified in the MAI of all so far analyzed MTB [76]. Deletion of *feoB1* and the entire operon in *M. gryphiswaldense* caused formation of fewer and smaller magnetosomes, indicating an accessory role in magnetosomal iron uptake [52] (R. Uebe, unpublished).

The *mamAB* operon of *M. gryphiswaldense* is 16.4 kb large, and a *mamAB*-like operon has been found in all analyzed MTB so far [76]. In particular, 10 genes (*mamABEIKLMOPQ*) are conserved in the *mamAB* operon of all magnetite-producing MTB [11, 76]. Furthermore, it is the only operon, which is necessary and sufficient for magnetite biomineralization in *M. gryphiswaldense.* It contains genes for vesicle biogenesis, protein sorting, iron transport, magnetite crystallization, crystal size control, and chain-like assembly (see Fig. 4B) [16]. Below the putative functions of the corresponding proteins are shortly described.

MamL, MamQ and MamB have been speculated to be involved in vesicle biogenesis, since deletion of the corresponding genes results in non-magnetic cells that also lack the ability to form vesicles [56, 80]. While MamL has no predicted function [23, 84], MamB belongs to the cation diffusion facilitator (CDF) superfamily, which have been shown to contribute to divalent metal ion homeostasis [56]. Although a potential role of MamB in protein-protein interactions has been suggested, its function during membrane vesicle formation has remained elusive so far [56]. MamQ shares homology with LemA proteins [41], which are conserved in several bacteria but whose function is uncertain [80]. In its predicted secondary structure, MamQ has a high content of α-helices that are somewhat reminiscent to several eukaryotic proteins such as the EFC/BAR domain of Formin Binding Protein 17 [49]. BAR domains have the ability to sense and stabilize membrane curvatures [85]. Therefore, the weak similarity of MamQ to BAR domain proteins might hint towards a related function in MM vesicle genesis [80]. MamE and MamA, which belong to the family of HtrA family of serine proteases and the tetratrico-peptide repeat (TPR) proteins, respectively, were hypothesized to coordinate the sorting of magnetosome proteins during or before vesicle biogenesis [49, 86-88]. However, the existence of a ‘magnetochrome’ domain also suggests a putative function of MamE during magnetite crystallization by participating in redox control [89]. The interacting CDF proteins MamM and MamB, as well as the MFS protein MamH and MamZ, have been speculated to play a role in magnetosomal iron transport [55, 56]. Alternatively, a different role of MamH as phosphate exporter during biomineralization has recently also been suggested by Nudelman *et al.*, who built homology models to investigate the function of

magnetosome proteins [90]. However, the latter predicted function is based on a model from Baumgartner *et al.* [60] suggesting that biomineralization proceeds from a phosphate-rich ferritine, which needs to be further investigated. So far, there is no direct experimental evidence for the transport of iron or phosphate by MamH. Recently, the crystal structure of MamP was solved, and *in vitro* studies indicated a role as iron oxidase contributing to the formation of iron(III) ferrihydrite via its magnetochrome domain [91]. MamI, MamT and MamO were also implicated in magnetite crystallization and crystal maturation. Notably, while *mamI* has been found to be essential for vesicle biogenesis in *M. magneticum* [49], magnetosome vesicles as well as small, poorly crystalline iron oxide particles were still formed in *M. gryphiswaldense* Δ*mamI* [80]. These findings indicate a distinct role of MamI within both magnetospirilla strains. Also MamN was described to be essential for magnetosome biosynthesis, as indicated by the absence of electron dense crystals in *M. magneticum*. In contrast, few, small magnetite particles were still formed in Δ*mamN* of *M. gryphiswaldense*. MamN shares weak similarity to H^+-translocation proteins and might therefore be involved in crystal growth by regulating the intramagnetosomal pH via mediation of an H^+ efflux from the magnetosome compartment [39, 80].

The actin-like protein MamK forms a filamentous structure for magnetosome assembly [19, 48], and interacts with the acidic protein MamJ that is involved in connecting magnetosomes to the filament [18, 92, 93]. Both proteins, however, have no effect on vesicle biogenesis and no or only minor effects on biomineralization [18, 19].

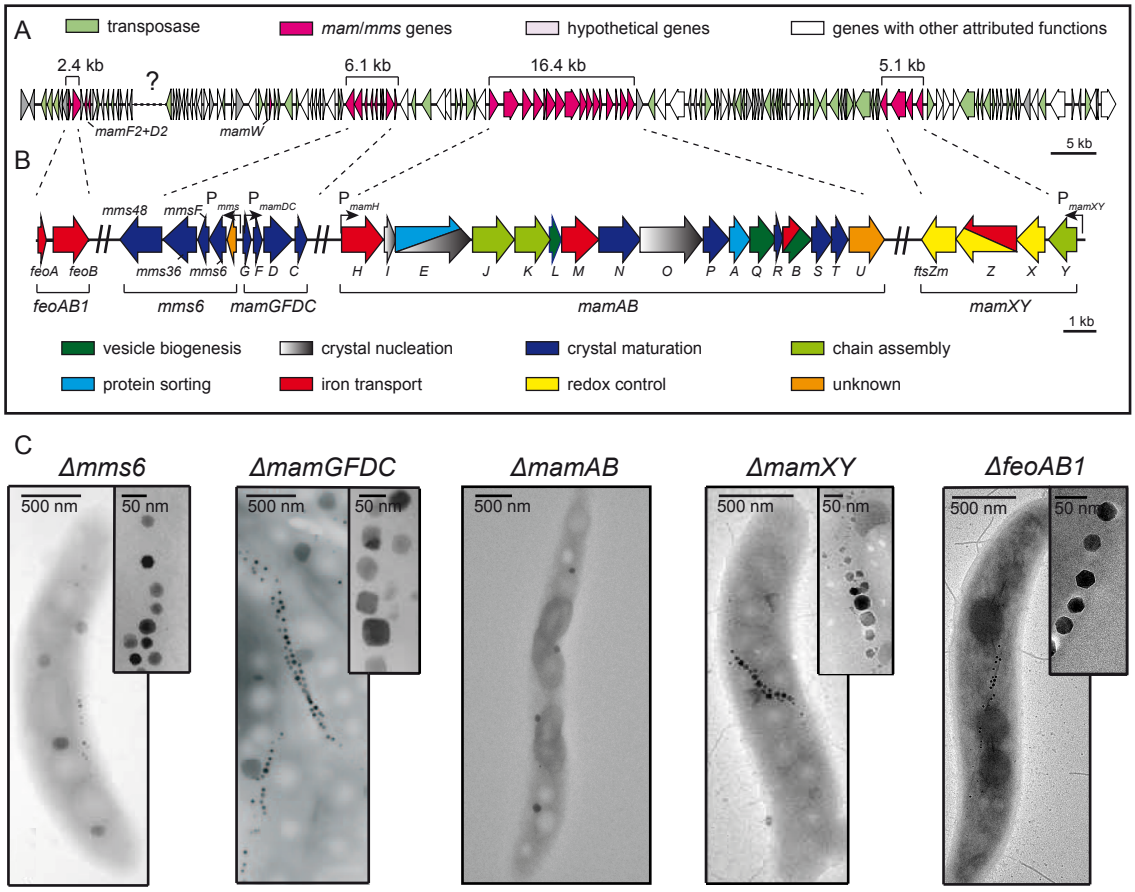

Figure 4: A. Molecular organization and characteristics of the MAI in *M. gryphiswaldense*. Hypothetical genes, transposase genes, *mam* and *mms* genes and genes encoding other assigned functions are shown in different colors. The asterisk indicates a region, in which the gene organization is still unknown due to the high number of repetitive sequences. B. Schematic representation of the molecular operon organization in the MAI of *M. gryphiswaldense*. Colors of different arrows indicate putative functions of encoded proteins. Crossed lines represent interspersed regions devoid of genes required for magnetosome formation. C. Transmission electron micrographs illustrating the phenotypes of different operon deletion mutants in *M. gryphiswaldense*. Upon deletion of the *mms6*, *mamGFDC*, *mamXY* or *feoAB1* operon, the mutant strains are still able to form magnetite particles, although the numbers, sizes and/or shape of the crystals differ from that of the WT. In contrast, deletion of the *mamAB* operon completely abolishes magnetosome formation. Images of Δ*mms6* and Δ*mamXY* mutants were adapted from [16], and of Δ*mamGFDC* from [17]. Images of Δ*feoAB1* were kindly provided by R. Uebe (unpublished).

Altogether, the comprehensive genetic analysis of the *mam* and *mms* operons in *M. gryphiswaldense* showed that numerous factors participate in magnetosome formation. Surprisingly, only few of them are essential: Whereas in *M. magneticum* eight proteins (MamI, E, L, M, N, O, B, Q) were found to be required for magnetosome formation [49], in *M. gryphiswaldense* only six

proteins (MamE, L, M, O, B, Q) are essential for at least some rudimentary iron biomineralization and, if including MamI, seven proteins for the biosynthesis of magnetite-containing magnetosomes [80]. However, so far this has been only investigated by construction of single gene deletion mutants in *M. gryphiswaldense* or *M. magneticum*. Therefore, it remains to be shown whether these essential magnetosome proteins are also sufficient for vesicle formation and crystallization in the absence of the other factors encoded by the *mamAB,* or other magnetsome operons.

1.4.3 Accessory genetic determinants outside the MAI influencing magnetosome formation

In addition to various proteins encoded within the MAI, genes localized elsewhere in the genome are also involved in magnetite biomineralization in *M. gryphiswaldense*. For instance, the ferric uptake regulator protein Fur plays a role in global iron homeostasis in *M. gryphiswaldense*, and a *fur* deletion mutant synthesized fewer and slightly smaller magnetite crystals than the WT [94]. However, the rather weak effects on magnetosome formation upon deletion of *fur* suggest an indirect role of this regulator for magnetosomal iron uptake, probably by balancing the competing demands for biochemical iron supply and magnetite biomineralization [51, 94]. Furthermore, deletion of genes encoding several enzymes participating in denitrification (nitrate reductase Nap, nitrite reductase NirS [95, 96]), and aerobic respiration (cytochrome c oxidase cbb_3 [97]) also resulted in smaller and aberrantly shaped crystals compared to that of the WT. It has been speculated that besides their participation in energy metabolism, these proteins are also involved in maintaining the redox balance of Fe^{2+}/Fe^{3+} for magnetite biomineralization [63]. Furthermore, also the oxygen sensor Fnr (Fumarate and Nitrate reductase regulatory protein) is indirectly involved in magnetite biomineralization by regulating denitrification genes such as *nap* and *nirS* [63]. However, by contrast to several *mam* and *mms* genes, none of these genetic determinants are essential for magnetosome biomineralization in *M. gryphiswaldense*.

1.5 Genetic manipulation of *M. gryphiswaldense*

Despite considerable progress within the last years, genetic manipulation of culturable MTB, such as *M. gryphiswaldense*, is still cumbersome. This is mostly attributed to their slow growth and the limited number of available genetic tools [98]. For plasmid-based gene expression in *M. gryphiswaldense* mostly vectors of the pBBR1 group were used [25]. Additionally, a limited number of plasmids from the IncP and IncQ incompatibility group were also found to be capable of replication in *M. gryphiswaldense* and *M. magneticum* [25, 99]. For chromosomal integration of a sequence site-specific *recA*-dependent insertion [16, 26] or random transposon mediated genomic insertion was applied [25, 86, 100]. Very recently, the toolbox for genetic manipulation of *M. gryphiswaldense* was extended by a GalK counterselection system for markerless gene deletion and chromosomal tagging [101].

In general, replicative and insertional plasmids are transferred from *Escherichia coli* to *M. gryphiswaldense* via conjugation [25, 100]. Despite considerable effort, no reliable electroporation protocol has been established in MTB so far [25]. Several hypotheses related to the low electroporation efficiency, such as adverse effects of the magnetosome chains in the strong electric field [99] or a restriction barrier [25], have been disapproved [25] (C. Jogler, unpublished). Therefore, the reasons for the low number of transformants after electroporation are still unknown.

Additional obstacles in the engineering of MTB are the rearrangements and deletions, which frequently occur within the MAI during subcultivation. It has been shown that spontaneous mutants affected in magnetosome formation arise at a frequency of up to 10^{-2} in *M. gryphiswaldense*. It has been speculated that the genetic instability of the MAI might derive from RecA-driven homologous recombination [3, 71]. RecA is a ubiquitous and highly conserved protein and catalyzes strand exchanges between homologous DNA molecules via RecA–single-stranded DNA (ssDNA) complexes [102, 103]. Furthermore, it also plays a key role in signal transduction following DNA damage [104, 105].

1.6 Heterologous expression of single magnetosome genes

The problems associated with the cultivation and genetic manipulation of MTB stimulated ideas for the transplantation of the magnetosome biosynthesis pathway into more amenable host. Such an approach would open up several new possibilities: For instance, it could enable the comprehensive dissection of the biosynthesis pathway in a surrogate host, which is easier to manipulate than MTB. Even more important, it facilitates to elucidate the minimal gene set required for magnetosome formation, since the heterologous system will probably lack any unknown accessory factors that influence biomineralization in the native host. Ultimately, the synthesis of magnetosomes in organisms that can be grown and manipulated more easily, such as *E. coli*, might facilitate the high yield production of nanocrystals for various biotechnological and biomedical applications.

In previous studies, only single or few magnetosome genes from MTB have been heterologously expressed. Typically, the well-characterized *E. coli* served as host, which is also widely used for expression of other recombinant proteins from various organisms [106]. To this end, the coding sequences were cloned into medium copy number plasmids (pBBR1, pET) and placed under control of strong, inducible promoters (P_{lac}, P_{tet} or P_{t7}), since the native promoters of the *mam* and *mms* operons have been shown to be inactive in *E. coli* [45]. Using such a setup, MamP and MamA have been overexpressed in *E. coli* for protein purification and crystal structure analysis [88, 91]. Also the localization pattern of the actin- and tubulin-like proteins MamK and FtsZm has been studied in *E. coli* [19, 81, 107]. In contrast, expression of the magnetosome membrane proteins MamB and MamM, which have been speculated to form a heterodimer complex *in vivo* [56], has been found to be inefficient in *E. coli* DH5α (K. Junge, R. Uebe, unpublished). This problem could be partially overcome by coexpression of both proteins and the utilization of a Rosetta strain as host. This BL21 derivative contains an additional tRNA pool to enhance the expression of genes containing codons, which are rarely used in *E. coli* (Novagen). Consequently, the variations in the expression level of some magnetosome proteins might derive from a differing codon usage preference between *M. gryphiswaldense* and *E. coli*, which is partially compensated by the

additional tRNA pool in the Rosetta strain. Additionally, the limited product yields of some magnetosome membrane proteins might also indicate a high metabolic burden on the cells, as often observed for heterologous expression of membrane proteins in *E. coli* [108].

However, so far no multigene cassettes containing several magnetosome operons have been constructed that potentially facilitates the transplantation of magnetosome biosynthesis into a foreign host.

1.7 Challenges in cloning and transfer of multigene clusters

The introduction of novel functions into foreign hosts by gene cluster transfer faces several challenges. First, the DNA fragments have to be mobilized into a vector backbone that allows stable maintenance in the recipient strain [109]. Second, numerous genes have to be expressed in a balanced manner [1]. This depends on different factors such as promoters, ribosome binding sites and the codon usage in the sequence [109-111]. Functional expression of the gene cluster also relies on a suitable heterologous host, which has to be chosen carefully based on its physiological and genetic compatibility [109]. However, these attempts will not be successful if the gene cluster is not sufficient for a particular function and depends on auxiliary determinants localized elsewhere in the hosts genome [1].

Despite the challenges in transfer and expression of gene clusters, several studies already reported successful transplantation of metabolic pathways. Chromosomal integration of the nitrogen fixation gene cluster from *Klebsiella pneumoniae* (~20 kb) resulted in a N_2-fixing *E. coli* [112]. Using chromosomal insertion via transposable elements or bacteriophage derived PhiC31 integrases, large expression cassettes encoding secondary metabolites, for example the epothilone gene cluster (58 kb) from *Sorangium cellulosum* [113] or the 128 kb daptomycin gene cluster from *Streptomyces roseosporus*, have been heterologously expressed [114]. Likewise, the ability to form complex intracellular structures has been transferred genetically: The carboxysomes, Pdu and Eut microcompartments, which serve as proteinaceous nanoreactors to isolate distinct metabolic pathways from the cytoplasm, were transplanted into *E. coli* [115-118]. In contrast to the genetic transfer of natural product

biosynthesis pathways, these gene clusters (up to ~20 kb) were stably maintained via replicative systems in the heterologous host. Also the gas vesicle compartment from *Serratia* sp. was reconstituted in *E. coli* by transfer of a cosmid harboring the ~16 kb large cluster [119].

However, by contrast to previous approaches with other synthesis pathways, magnetosome operons encode a large number of membrane proteins (25 of 30), which are generally difficult to express in non-native species due to potential toxic effects on the cells, low expression levels and mis- or unfolding of the proteins [120]. As mentioned in a previous section (see 1.4.2), the functions of many *mam* and *mms* genes are still unknown. Furthermore, other factors encoded outside the canonical *mam* and *mms* operons directly or indirectly regulate magnetosome formation in *M. gryphiswaldense* (see also 1.4.3). Therefore, it was not known if the *mam* and *mms* operons are also sufficient for magnetosome biosynthesis in a heterologous system.

1.8 Scope of this work

This thesis had 4 key objectives: In the first part, we investigated whether RecA in fact mediates the observed genetic instability of the MAI, as speculated before [3]. To this end, a *recA* mutant of *M. gryphiswaldense* was constructed. Besides its phenotypic characterization, we also investigated its potential for further genetic engineering approaches.

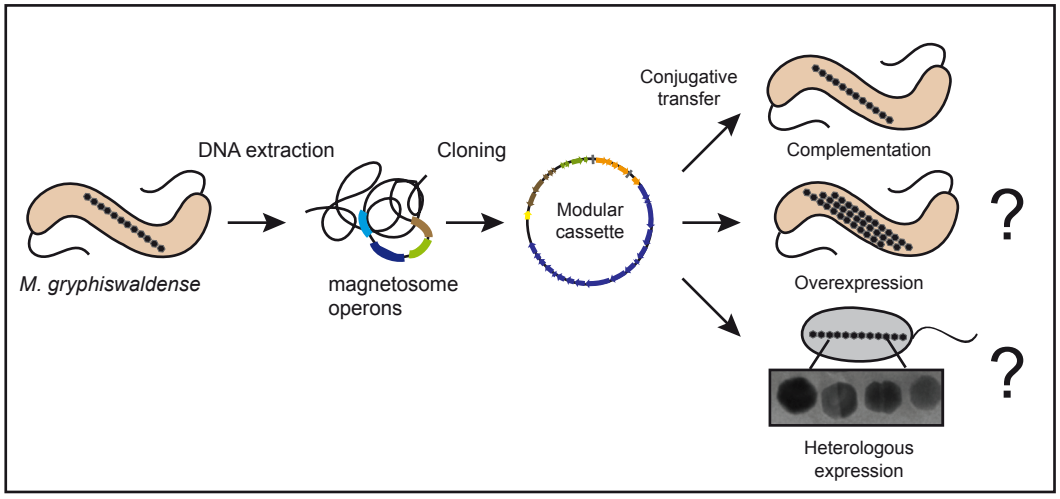

Figure 5: Schematic outline and aims of this thesis (key objectives 2-4). Native magnetosome operons of *M. gryphiswaldense* were used for construction of modular plasmids. These expression cassettes can be transferred into homologous and heterologous hosts.

The second aim was the construction of cassettes encoding parts or the entire magnetosome biosynthesis pathway of *M. gryphiswaldense* (see Fig. 5). Since so far no large plasmids comprising several magnetosome operons were constructed, suitable cloning techniques, as well as vector backbones for efficient transfer and stable maintenance, had to be developed.

The plasmids were tested for their functionality by transcomplementation studies in the native host. Based on the developed system, we investigated in the third part of this thesis, if magnetosome production can be enhanced in *M. gryphiswaldense* by a gene dosage increase of the *mam* and *mms* operons.

Ultimately, the expression cassettes were investigated for their sufficiency to transplant the magnetosome biosynthesis pathway into different, hitherto non-magnetic organisms.

2. Discussion

2.1 Deletion of *recA* in *M. gryphiswaldense* results in increased genetic stability of the magnetosome island

Cultivation and genetic manipulation of *M. gryphiswaldense* has been hampered so far by the accumulation of spontaneous unmagnetic mutants after prolonged cold storage or exposure to oxidative stress [3, 71]. While the genotypes were polymorphic with respect to the sites and extent of deletions, all mutations were found to be associated with the loss of various copies of insertion elements and magnetosome genes within the MAI [3]. It has been speculated that the observed genetic instability might derive from RecA-mediated homologous recombination. Genomic instability caused by RecA has also been observed in other organisms like *Leptospira biflexa* [121] and *Mycobacterium bovis* [122]. In MTB the effects of *recA* loss have not been investigated so far. Therefore, we constructed a *recA* deletion mutant of *M. gryphiswaldense*. Strain IK-1 displayed similar characteristics to other already described *recA*$^-$ strains like increased UV-sensitivity and very low rates of homologous recombination events [123, 124], while the ability to synthesize WT-like magnetosomes was not affected. However, in contrast to the WT, we failed to detect spontaneous unmagnetic mutants after prolonged incubation under physiological stress conditions. This finding indicates that the observed polymorphic mutations in the MAI rely on RecA and that the mutant displays a higher genetic stability compared to the WT. In a similar study, Bo *et al.* recently reported that deletion of *uvrA*, which leads to high mutation frequencies within the MAI of *M. magneticum*, was compensated by additional deletion of *recA* [125]. Based on these observations, it seems very likely that the spontaneous loss of magnetosome formation in other MTB, such as the magnetic vibrio *Magnetovibrio blakemorei* [4], is also RecA-driven.

Additionally, the increased genetic stability in the absence of RecA also makes strain IK-1 promising for the expression of recombinant proteins and further genetic engineering. As shown below, we also investigated IK-1 as potential chassis for the construction of various overexpression strains (see 2.3).

2.2 Construction of large expression cassettes comprising the magnetosome operons

The aim of the second part of this thesis was the construction of large expression cassettes encoding parts or the entire magnetosome biosynthesis pathway of *M. gryphiswaldense*. To this end, the *mam* and *mms* operons (~ 27 kb in total) had to be cloned into a suitable vector backbone for transfer and stable maintenance of the genes in different hosts.

Despite the availability of a broad set of restriction enzymes and vector backbones, cloning of large DNA fragments (>20 kb) is challenging. The lack of unique restriction sites and the limitations of error-prone PCR steps hamper the use of conventional cloning or recently developed Gibson [126] or Golden Gate assembly strategies [127]. In previous studies with secondary metabolite gene clusters from different marine and soil-derived organisms [109], genomic libraries based on BACs, cosmids or fosmids were constructed for cloning of large sequences. These plasmids allow stable maintenance of very large sequences (up to several hundred kb) [128-130]. However, they are often not suitable for subsequent mobilization and maintenance in different hosts. To this end, constructs carrying the target sequence can be modified by phage-derived Red/ET homologous recombination in *E. coli*. This technique enables the modification of plasmids without the necessity of unique endonuclease cleavage sites [131-133]. For instance, it has facilitated successful cloning of the large secondary metabolite myxochromide S (30 kb) or myxothiazol (57 kb) gene clusters from *Stigmatella aurantiaca* from genomic libraries [134, 135].

The construction of modular expression cassettes harboring the four major magnetosome operons of *M. gryphiswaldense* (*mamAB*, *mms6*, *mamGFDC*, *mamXY*) was facilitated by the availability of a BAC clone containing the large 16.4 kb *mamAB* sequence [71]. Red/ET-recombination was performed to stitch together all genes from the native *mam* and *mms* operons (29 genes), but lacking the tubulin-like ftsZm. This gene was omitted from its native *mamXY* operon because of its known interference with cell division during cloning [81]. Regions 200-400 bp upstream of all operons were retained to ensure transcription from native promoters [55, 78]. In parallel to the insertion of additional operons into the *mamAB*-BAC, a recently described recombineering

method for direct cloning of genomic fragments was used [136]. This strategy was chosen to circumvent possible mutations in the target sequence caused by an observed genetic instability of the BAC (S. Schübbe, unpublished).

Overall, the cloning efficiency was considerably low, with only one correct clone among >100. This is at least 10-fold lower compared to the percentage of correct clones obtained after recombineering of various polyketide gene clusters [136, 137]. Furthermore, the growth of *E. coli* recombinants containing correct plasmids was significantly impaired. This might derive from a general burden (by e.g. additional demands for precursors for DNA synthesis) caused by the maintenance of several copies (10-15) of large plasmids (>23 kb) within the cell [138]. However, similar growth defects have not been observed in *E. coli* cells carrying even larger constructs based on the same transposon vector (Y. Zhang, personal communication). Therefore, the observed impairment of cell growth might be related to basal expression of several magnetosome membrane proteins in *E. coli*, possibly under control of the kanamycin promoter located upstream of the *mamAB* operon in the constructed large plasmids.

2.2.1 Chromosomal insertion is required for stable maintenance of the magnetosome operons in various hosts

As in previous studies with other multigene cassettes (see 1.7), two different approaches were tested for stable maintenance of the magnetosome operons: episomal maintenance of the genes by a host-compatible plasmid or integration of the target sequence into the genome [109].

Until recently, functional expression of single magnetosome genes from *M. gryphiswaldense* was predominantly performed via broad host range pBBR1 based plasmids [19, 25, 139]. This was mostly attributed to the limited number of vectors available for transfer and maintenance in *M. gryphiswaldense*. However, after transfer of a *mamAB*-pBBR1 plasmid (23 kb) into *M. gryphiswaldense*, as well as different heterologous hosts (e.g. *Agrobacterium tumefaciens*, *Rhodospirillum rubrum*), severe rearrangements and deletions were observed in the reisolated plasmids (see also Fig. S1) [140]. Several attempts were made to circumvent the occurrence of rearrangements in the plasmids, e.g. by usage of the Δ*recA* strain IK-1 or a constructed Δ*hsdR*

mutant (deficient in restriction subunit of a type I restriction-modification system) as acceptor organism. However, for all different tested hosts or cultivation conditions the *mamAB*-pBBR1 plasmid was still unstable. The observed rearrangements could derive from structural instability, in which some plasmids contain a mutated DNA sequence that causes incorrect expression. Additionally, allelic segregation could be responsible for the rearrangements within the large *mamAB*-pBBR1 plasmid. Here, functional plasmids are displaced by rearranged variants, leading to accumulation of non-productive clones that still contain the respective antibiotic resistance marker [141, 142].

In contrast to *in trans* expression, chromosomal engineering has the advantage of a constant copy number of the inserted genes. One possible strategy is the site-specific chromosomal integration of a target sequence via homologous recombination. This approach is commonly applied for the construction of *M. gryphiswaldense* mutant strains by replacement of a gene of interest against an antibiotic resistance marker [26, 27]. However, in other studies with *Myxococcus xanthus* it has been shown that the insertion efficiency via homologous recombination severely decreases with the size of the target sequence [113]. Therefore, an alternative strategy based on chromosomal integration of a specific sequence via transposition was chosen. In general, transposable elements, such as mariner or transposon 5 (Tn5), recognize two inverted repeat (IR) sequences and catalyze random insertion of a target sequence via a “cut and paste” mechanism into various prokaryotic organisms [143]. Compared to site-specific homologous recombination, the insertion efficiency via transposable elements is known to be 2-3 orders of magnitude higher [113]. This makes transposition particularly suitable for genomic integration of large DNA fragments. For instance, a MycoMar mariner transposon has been used for insertion and heterologous expression of a 56 kb polyketide gene cluster in *Myxococcus xanthus* and *Pseudomonas putida* [113]. As a negative side effect of the efficient random insertion, the target sequence can potentially integrate into functional genes. This can result in growth defects of the mutants or can even prevent functional expression of the inserted genes. Therefore, the insertion site of the transferred sequence has to be verified.

In this work, it was found that transposable elements are suitable for chromosomal integration and stable expression of the four major magnetosome

operons. We used a mariner and a Tn5 transposon system [144], since both can be applied for a broad range of gram-negative bacteria with similar efficiencies [86, 145-147]. Chromosomal reintegration of plasmids harboring the *mamAB* operon alone, or in combination with accessory operons, resulted in stable WT-like restoration of magnetosome biomineralization in various *M. gryphiswaldense* deletion mutants. This indicates that the transferred operons maintained functionality upon cloning and transfer. Insertions were stable for at least 40 generations without selection pressure. The magnetosome operons inserted into neutral genomic sites, as verified by whole genome sequencing of the insertants.

2.3 Multiplication of the *mam* and *mms* operons results in increased magnetosome biosynthesis in *M. gryphiswaldense*

Previous studies indicated that magnetosome production in *M. gryphiswaldense* can be potentially enhanced by selective overexpression of single or few *mam* or *mms* genes. For instance, Scheffel *et al.* showed that *in trans* expression of additional copies of the entire *mamGFDC* operon in the WT caused the formation of magnetite particles that were enlarged by a few nm compared to those produced by the WT control [17]. Recently, overexpression of *mms48* encoded by the *mms6* operon also resulted in a slight increase in the particle numbers per cell (40 per cell instead of 36 for the WT) [80]. However, the effects of a further gene dosage increase of single operons or even multiplication of all *mam* and *mms* genes on magnetosome formation have not been investigated so far. Here, we used transposon plasmids (see 2.2.1) to insert additional copies of single as well as all major magnetosome operons into the genetically stable *recA* mutant.

In different studies with other biosynthesis pathways, chromosomal integration of a target sequence has already been successfully used for overexpression of gene clusters. For instance, Tang *et al.* recently increased the production of the secondary metabolite spinosyn in the native host by partial gene cluster duplication [148]. Using a chemically inducible chromosomal evolution approach, 40 consecutive copies of a poly-3-hydroxybutyrate gene

cluster were inserted into the chromosome of *E. coli*, thereby causing a significant increase in the productivity of this biopolymer [142].

In our approach, we found that dupli- or triplication of the *mms6* operon (strains ΔRecA+*mms6* 2x and 3x) already caused magnetosome overproduction of up to 70% (see also Table S2). Remarkably, also the mean crystal size was significantly increased (up to 33%). Further copies of the *mms6* operon alone or in combination with the *mamGFDC* operon did not further augment the overexpression phenotype. Duplication of the large *mamAB* operon alone had pleiotropic phenotypic effects: While some cells contained increased numbers of regularly sized magnetosomes (by ~50% compared to that of IK-1), we also detected a morphotype harboring small, aberrantly shaped magnetic nanoparticles (see Fig. 6B). In contrast, overexpression of all magnetosome operons (ΔRecA+*ABG6X*) strongly enhanced magnetosome numbers per cell by 118%, and no heterogeneity among different cells was visible.

Altogether, these findings demonstrate that a gene dosage increase of the *mam* and *mms* operons provides an efficient strategy for magnetosome overexpression in *M. gryphiswaldense*. In the mutants that overexpressed single magnetosome operons, the biomineralization seemed to be limited by the lack of accessory factors encoded in the non-amplified magnetosome operons. In contrast, chromosomal duplication of all major operons resulted in the strongest increase in magnetosome production.

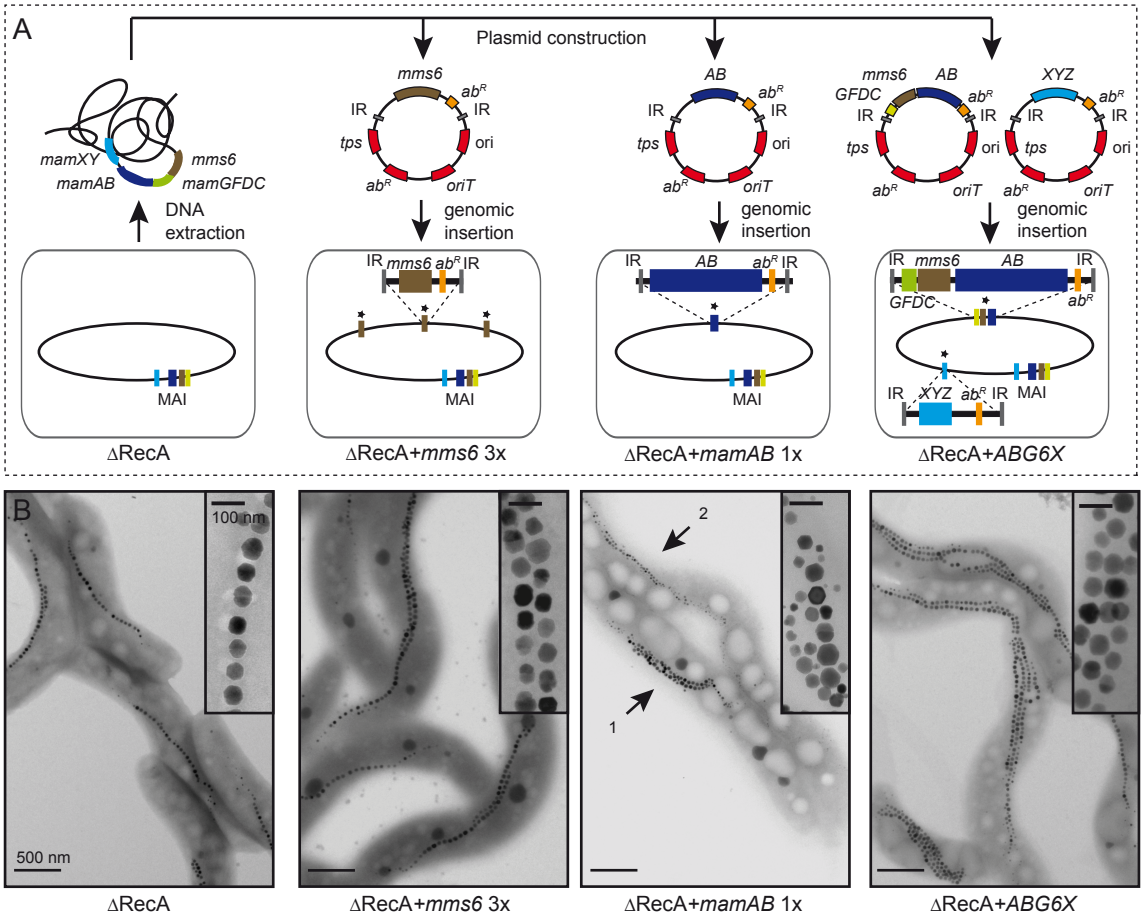

Figure 6: A. Strategy for construction of overexpression strains by amplification of different magnetosome operons. Insertional plasmids were constructed based on genomic DNA from *M. gryphiswaldense*. Plasmids contain the magnetosome operons *mamAB* (blue, *AB*), *mamGFDC* (green, GFDC), *mms6* (brown) and the *mamXY* operon lacking *ftsZm* (pale blue, *XYZ*). The vector backbone (genes are indicated in red) contains a transposase gene (*tps*), inverted repeats (IR), origin of transfer (*oriT*), an R6K or p15A origin of replication (*ori*) and antibiotic resistance cassette (ab^R). After conjugative transfer of the plasmids, the transposase recognizes IR sequences and catalyzes chromosomal insertion of the target sequence. Additional copies of respective magnetosome operons in the chromosome (oval shape) are marked with asterisks. B. TEM analysis of overexpression strains compared to the parental strain IK-1 (ΔRecA). 1 and 2 illustrate the different morphotypes found in ΔRecA+*mamAB* 1x.

However, several questions regarding the regulation of the magnetosome numbers as well as size in the different overexpression still remain elusive. For instance it is unknown, to what extent overexpression of the *mms6* operon alone causes formation of larger crystals. One important factor spatially constraining growth of the crystals is the size of the magnetosome vesicles. We sometimes found significantly enlarged vesicles in the *mms6* insertion strains by CET (119 nm instead of up to 54 nm in the parental strain). This finding indicates that overexpression of a set of genes might also directly influence the

vesicle diameter prior to crystallization, thereby defining the increase in crystal size. This could be caused by accumulation of proteins encoded by the *mms6* operon in the MM, thereby having a marked effect on the vesicle size. In strain ΔRecA+*mamAB* 1x, we observed that MamM and MamA were enriched in the MM compared to that of strain IK-1 (by 128% and 145%, respectively). As expected, no changes in the expression level of MamC were detectable in ΔRecA+*mamAB* 1x. This finding demonstrates that the protein composition of the MM changes by overexpression of only a set of genes. However, besides the formation of larger crystals in the *mms6* overexpression strains, also the numbers of magnetosomes were increased. This observation suggests that overexpression of a set of magnetosome genes influences the expression or the recruitment of accessory proteins controlling other processes during magnetosome formation, such as magnetosomal iron transport, vesicle biogenesis, or magnetosome chain assembly.

Altogether, our findings indicate that the expression level of magnetosome proteins seems to be one important factor, which determines the number and size of magnetite crystals. However, we did not compare the transcript or protein levels of all expressed magnetosome genes in the insertional mutants with that of the parental *recA*$^-$ strain. Therefore, it is unknown whether a gene dosage increase of the *mam* and *mms* operons results in uniform overexpression of all amplified magnetosome genes.

Our findings also raise the question, which accessory factors encoded outside the *mam* and *mms* operons might limit the number or size of magnetosomes in the overexpression strains as well as in the WT. For instance, the extracellular iron concentration is already known to be linked to crystal formation in *M. gryphiswaldense* [50]. However, incubation of the insertion mutants in medium supplemented with 500 µM ferric citrate (instead of 50 µM) did not result in a further increase in magnetosome numbers or size. Alternatively, insufficient expression of additional iron transport proteins encoded in the non-amplified genomic regions might limit further magnetosomal iron uptake. As mentioned in an earlier section, the *feoAB1* operon encoding a ferrous uptake system has been found to also play a role in magnetosome formation in *M. gryphiswaldense* (see 1.4.2). However, its chromosomal duplication in ΔRecA+*ABG6X* had only minor effects on the crystal size (see

Table S2). Therefore, it seems unlikely that the extracellular or magnetosomal iron supply limited a further increase in magnetosome numbers or size.

Alternatively, auxiliary factors encoded outside the MAI might limit magnetosome biosynthesis in *M. gryphiswaldense*. As mentioned in an earlier section (see 1.4.3), several enzymes participating in denitrification and aerobic respiration have been found to poise optimal redox conditions during magnetite biomineralization [63]. Consequently, the corresponding proteins could also indirectly limit the number or size of magnetite crystals. However, a more comprehensive genetic analysis will be necessary in the future to elucidate whether accessory, yet-unknown factors control magnetosome formation in the WT as well as in the overexpression strains.

Although the mode of action by which the overexpression of different *mam* and *mms* operons results in changes in magnetosome numbers or crystal sizes could not be fully unveiled, our approach nevertheless demonstrates that it is possible to specifically engineer *M. gryphiswaldense* for enhanced magnetosome production.

The constructed strains could be used for the high and stabilized production of magnetosomes, which are functionalized by genetic fusion with fluorescent markers or other recombinant proteins [28, 46] (see also 1.2). Furthermore, overexpression of selected magnetosome genes by chromosomal engineering might be exploited for the design of size-controlled nanocrystals that display altered magnetic properties. This could be of particular interest in applications, which depend on specific magnetic properties of the particles, such as magnetic resonance imaging [149] or hyperthermal treatment of tumors [150].

2.4 The *mam* and *mms* operons are sufficient for organelle formation in a non-magnetic host

Despite the increasing knowledge about the functions of single genes, prior to this work it remained elusive if the *mam* and *mms* operons are also sufficient for magnetosome formation in a heterologous system. Furthermore, it was not clear whether it is possible to reconstitute this structurally complex organelle in a foreign host.

For successful genetic transfer of magnetosome biosynthesis, an appropriate expression host had to be selected. In previous studies, *E. coli* was mostly used for expression of single magnetosome genes (see also 1.6). However, several problems in the genetic compatibility of *E. coli* such as inactivity of the native magnetosome operon promoters (see 1.6) [45], precluded the choice of this organism as expression host. Therefore, phylogenetically closely related alphaproteobacteria were selected for transfer of the constructed magnetosome expression cassettes. In addition, the physiochemical requirements for magnetosome biomineralization had to be taken into account. Magnetosome formation in *M. gryphiswaldense* does not occur under aerobic conditions [62]. Therefore, an organism capable of microoxic or anoxic growth was selected. Additionally, we hypothesized that the ability to form intracytoplasmic vesicles, which is present in several photosynthetic purple bacteria [151], could potentially facilitate magnetosome formation in a heterologous host.

The photosynthetic alphaproteobacterium *R. rubrum* shares a close phylogenetic relationship to *M. gryphiswaldense* (16S rRNA identity = 90%), has potential for various biotechnological applications (e.g. lycopene production), and can be grown to high cell densities at a large scale [23, 152-154]. Furthermore, this metabolically versatile organism efficiently expresses heterologous membrane proteins [155] and forms intracytoplasmic vesicles under low oxygen conditions [156]. In consideration of all these properties, we chose *R. rubrum* as heterologous host.

Although the *mamAB* operon alone has been shown to support some rudimentary biomineralization in *M. gryphiswaldense* [16], its genomic insertion alone, or in combination with the accessory *mamGFDC* genes (pTps_AB,

pTps_ABG), did not have any detectable phenotypic effect. Only after the genomic insertion of pTps_ABG6 (*mamAB*, *mamGFDC*, *mms6* operon), we were able to identify small, poorly crystalline hematite particles aligned in a chain-like structure within the cell. This clearly demonstrates that compared to the native host, additional genes are required for iron precipitation in *R. rubrum*. Genetic transfer of expression cassettes comprising all four major operons (pTps_ABG6 + pTps_XYZ) caused formation of membrane-bounded magnetite crystals in *R. rubrum*, which were aligned in short chains within the cell. As discussed in a previous section, *mamX* and *mamZ* located on the *mamXY* operon have key roles in magnetite biomineralization [55], which was further confirmed by our results in *R. rubrum*. However, additional insertion of an accessory MTB-specific *feoAB1* operon (Tet-pBam_feoAB1) [76] was required for production of donor-like magnetosomes, thereby emphasizing the important role of this recently identified ferrous transporter for magnetosomal iron uptake [52].

Overall, this finding is proof of principle that one of the most complex prokaryotic structures can be functionally reconstituted within a foreign host by transfer of a set of 29 genes. Furthermore, it also provides the first experimental evidence that the magnetotactic trait can be disseminated to a different species by only a single or few transfer events, which further suggests the wide phylogenetic distribution of magnetotaxis as a result of horizontal gene transfer events [11, 72, 74].

However, despite its first proof of feasibility several important questions regarding the genetic transfer of magnetosome biosynthesis still remain to be addressed and are discussed below.

Can the magnetosome organelle be reconstituted in additional heterologous hosts?

After transfer of the magnetosome expression cassettes into various additional alphaproteobacteria such as *Rhodobacter sphaeroides*, *Phaeospirillum molischianum*, *Azospirillum brasilense* and *Caulobacter crescentus* [157], we failed to detect additional magnetic hosts (see Table S3). One of the tested organisms, *P. molischianum*, is phylogenetically closer related to

M. gryphiswaldense (16S RNA identity = 94%) than *R. rubrum* (16S rRNA identity = 90%) [72]. Therefore, a close 16S rRNA relationship is not necessarily indicative for functional heterologous expression of magnetosome proteins, precluding straightforward predictions of further suitable recipient strains.

Noteworthy, except for *R. sphaeroides* and *A. brasilense,* the transconjugants did not express each of the tested magnetosome proteins (MamC, MamK and MamM). Therefore, the lack of expression of the transferred *mam* and *mms* genes might be one important reason for the inability to detect additional magnetic heterologous hosts. As another possibility, accessory genes required for magnetosome biomineralization might be conserved in *R. rubrum* and *M. gryphiswaldense*, but absent in the negatively tested hosts.

Is a core gene set encoded outside the *mam* and *mms* genes required for magnetosome biomineralization in different heterologous hosts?

In this thesis, I investigated the possibility to narrow down an accessory “core gene set” outside the *mam* and *mms* genes, which is required for magnetosome formation in different heterologous hosts. To this end, a genomic analysis based on *M. gryphiswaldense* and several tested foreign organisms was initiated. In a previous study, reciprocal best BLAST matches (RBMs) were used to find a core genome of MTB. For example, the so far overlooked *mamXY* operon and a set of 28 MTB-specific signature genes were identified [23]. Additionally, intercomparison of 3 magnetospirilla and *R. rubrum* yielded 41 conserved genes with no homologs in other organisms.

Using a similar setup, we found a set of 1765 genes, which is shared between *P. molischianum* and *M. gryphiswaldense* in contrast to 1611 for *R. rubrum* (see Fig. 7). This finding indicates that similar to the 16S rRNA gene identity, also the overall number of shared genes between *M. gryphiswaldense* and *P. molischianum* is higher compared to *R. rubrum*. To further narrow down a potential core gene set, I investigated, which of these RBMs are absent in the negatively tested hosts, such as *R. sphaeroides* and *A. brasilense*. For instance, 458 genes are shared between *M. gryphiswaldense* and *R. rubrum*, but absent in *R. sphaeroides* and *A. brasilense*. By contrast, when the RBMs from *P. molischianum* were excluded, 163 genes were found. Among these

candidates, numerous conserved hypothetical proteins (e.g. MGR2629, MGR4267), hemerythrin-like proteins (e.g. MGR0071), a NirT/NapC *c*-type cytochrome family protein TorC (MGR1306), and several proteins potentially involved in redox control, such as a ferredoxin protein (MGR0937) and oxidoreductases (MGR3182, MGR4270), were identified (Table S4). However, none of the *in silico* identified genes has been characterized in *M. gryphiswaldense* so far. Since the number of candidates playing a role in biomineralization is still too large for directed mutagenesis approaches in *M. gryphiswaldense*, at least one additional heterologous magnetic host would be necessary for a more comprehensive genomic comparison.

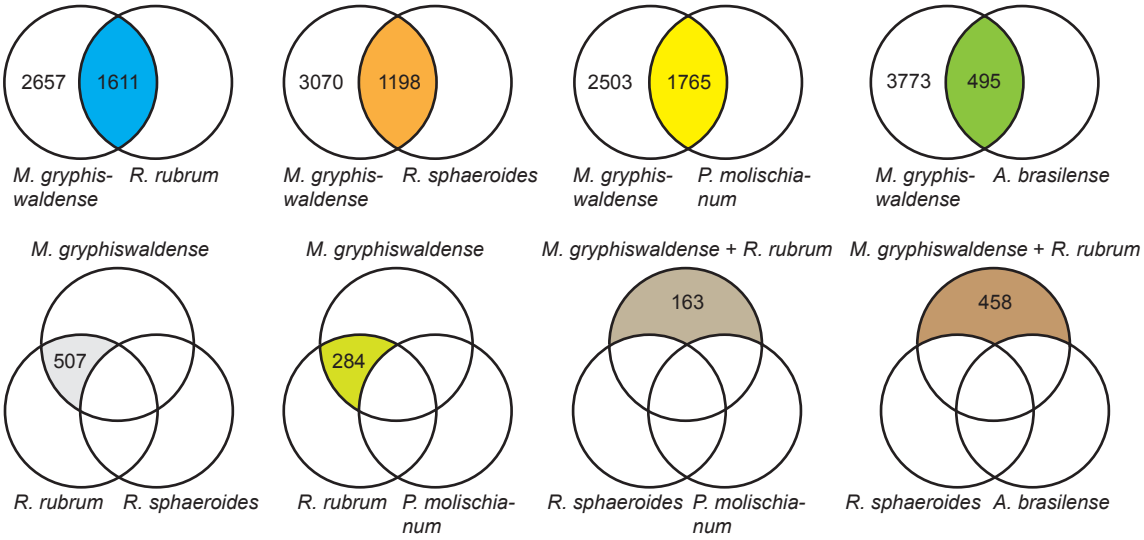

Figure 7: Comparative gene content analysis of different tested heterologous hosts based on reciprocal best matches (RBMs). Venn diagrams illustrate the (not) shared gene content between the different genomes.

2.5 Towards the construction of a synthetic magnetosome expression cassette

Despite the feasibility of constructing large expression cassettes based on native genes, only a limited number of sequence modifications can be introduced by recombinogenic cloning, such as exchange of the promoter sequences. By contrast, the design of synthetic gene clusters offers the possibility to freely combine a set of selected genes with well-characterized regulatory elements (ribosome binding sites, promoters), and restriction sites can be added or removed for interchangeability of different modules [158]. Furthermore, the CDS (coding sequences) can be optimized to the codon usage bias of a particular expression host to facilitate efficient translation elongation [159, 160].

Despite the potential of rationally optimizing the sequence parameters of gene clusters for expression in a heterologous system, only few studies so far reported the complete design of multigene cassettes. This is due to the regulatory and genetic complexity of gene clusters [1], as well as the costly synthesis of DNA sequences exceeding a few kb. For instance, Temme *et al.* described redesign of the 23.5 kb large nitrogen fixation (*nif*) gene cluster from *Klebsiella oxytoca* [158]. The "refactored" gene cluster contained only a minimal set of genes, which were as divergent from the WT as possible. Different synthetic constructs were transferred into a *K. oxytoca* mutant strain, lacking all *nif* genes. In a different study, a ~60 kb epothilone gene cluster from *Sorangium cellulosum* was successfully redesigned and assembled for expression in *E. coli* [161] or *M. xanthus* [160]. In contrast to the above-mentioned approach, the codons were optimized and not a minimal set, but all genes from the native cluster were synthesized. Each of the synthetic cassettes was functionally expressed after transfer into the respective host. However, the product yields were still significantly lower compared to that of the native organism, indicating the requirements for further systematic optimization approaches and careful evaluation of the most efficient expression strategy in the future. Nevertheless, these first studies demonstrate the feasibility to design and reassemble multigene clusters encoding complex functions.

The results are also promising for the rational design of magnetosome gene clusters for their subsequent transfer and expression in selected hosts. In this thesis, we rebuilt a synthetic cassette containing a minimal set of magnetosome genes as a first model. This approach has two central objectives. First, we want to investigate if a disruption of several magnetosome genes from their natural context, and their subsequent reorganization into synthetic building blocks still results in functional gene expression. Second, we aim to find the minimal gene set for magnetosome formation in *M. gryphiswaldense* and other hosts. Using deletion mutagenesis, 7 genes have been shown to be essential for magnetite formation in *M. gryphiswaldense* [80]. Specifically, *mamB*, *L* and *Q* were implicated to play a role in vesicle biogenesis, whereas *mamI, M, E* and *O* have been found to be essential for magnetite crystallization. However, it has not been demonstrated if these genes are also sufficient for magnetite formation in *M. gryphiswaldense*. Therefore, we designed an insertional plasmid with a *mamX* sequence (8.3 kb) consisting of two expression units, each controlled by a P_{mamH} promoter (ATG:biosynthetics). Whereas building block 1 harbors all known essential genes for vesicle biogenesis, building block 2 contains a minimal gene set for magnetite biomineralization (see Fig. S2).

The synthetic cassette will be tested for its functionality by reintegration into various single gene as well as operon deletion strains of *M. gryphiswaldense*. Furthermore, the modular design of the plasmid (see Fig. S2) allows easy exchange and cyclic addition of promoter sequences, single genes, or even complete building blocks. Therefore, it builds the foundation for the construction of large, synthetic cassettes for the transfer of magnetosome biosynthesis into various hosts.

2.6 Future directions

In this thesis, we enabled stable and enhanced production of magnetosomes in *M. gryphiswaldense*. Furthermore, we demonstrate the successful transplantation of magnetosome biosynthesis into a foreign host by autonomous expression of a set of *mam* and *mms* genes. Based on these findings, two different approaches could be applied in future studies.

Based on our results in engineering of *M. gryphiswaldense*, strain IK-1 could also serve as chassis for the heterologous expression of magnetosome genes from uncultivated or genetically non-accessible MTB. Ultimately, this could facilitate the synthesis of magnetosomes with different morphologies, such as elongated-prismatic or bullet-shaped, in *M. gryphiswaldense* (see Fig. 2A, 8A). This is interesting from two perspectives: First it allows the study of mechanisms underlying the formation of these crystals. Second, the production of e.g. bullet-shaped magnetosomes is also interesting from a biotechnological perspective, since these morphologies cannot be reconstructed by chemical synthesis so far. To this end, first the genes required for shape control of these crystals have to be elucidated by a bioinformatic analysis. Recently, a conserved set of *mad* genes (magnetosome associated deltaproteobacteria) has been identified in the genome of magnetotactic deltaproteobacteria, which is absent in MTB belonging to the *Alphaproteobacteria* [76]. Other genes, which are related to crystal growth and size control in *M. gryphiswaldense* and *M. magneticum* (*mamGFDC* operon, *mms6* and *mmsF*), are missing in these organisms. Therefore, some of these *mad* genes might be required for size control of bullet-shaped magnetosomes. In future studies, a comparative analysis of putative magnetosome genes from all MTB producing crystals of a specific morphology could narrow down potential candidates required for crystal shape control. Afterwards, a set of genes with optimized codons for efficient expression in *M. gryphiswaldense* could be synthesized. Ultimately, different expression cassettes could be transferred into strain IK-1 as well as different *M. gryphiswaldense* deletion mutants.

Another important challenge in future studies will be to facilitate the transplantation of the magnetosome biosynthesis pathway into additional hosts. To this end, a more detailed knowledge of the genes required for biomineralization will be important. We showed that 29 genes confer the ability to produce membrane-bounded nanocrystals in *R. rubrum*. However, it is still unknown if all of the transferred *mam* and *mms* genes are essential for magnetosome formation. Therefore, systematic reduction approaches in *R. rubrum* as surrogate host could be performed. This has been similarly applied in a different study by Parsons *et al.*, in which the minimal number of genes required for synthesis of pdu microcompartments was investigated in

the heterologous host *E. coli* [162]. As an alternative strategy to identify the number of genes required for magnetosome formation in *R. rubrum*, a bottom-up design based on the minimal synthetic expression cassette (see also 2.5) could be chosen.

To elucidate other factors influencing biomineralization in *M. gryphiswaldense*, which are encoded outside the *mam* and *mms* operons, a saturated transposon mutagenesis approach was recently initiated (K. Tavares, unpublished). The results from this study could be combined with our genomic comparison of *M. gryphiswaldense* and different heterologous hosts. This could narrow down the set of accessory genes required for magnetosome formation in different heterologous hosts. However, since we failed to detect protein expression in most of the tested heterologous hosts, further modifications in the regulatory sequences of the constructs will be necessary. Moderate changes in the already constructed cassettes (by e.g. exchange of promoters or insertion of accessory genes) might be sufficient for the successful transplantation of magnetosome biosynthesis in other representatives of the *Alphaproteobacteria,* such as *P. molischianum* or *R. sphaeroides.* However, a larger number of modifications in the coding and regulatory sequences will be necessary to eventually facilitate functional expression of magnetosome gene clusters in the more distantly related hosts, such as the well-characterized *E. coli*. To this end, the rational design of large magnetosome expression cassettes could allow to specifically adapt different sequence parameters. Additionally, further genetic engineering of *E. coli* could facilitate magnetosome formation in this particular host, for example by coexpression of a monotopic glycosyltransferase to trigger the formation of intracytoplasmic membranes [163].

As another possibility, expression cassettes could be constructed to endow eukaryotic organisms with magnetization by biomineralization of tailored magnetic nanostructures. Previous attempts to magnetize eukaryotic organisms resulted in only irregular and poorly crystalline iron deposits [164, 165]. The endogenously produced nanoparticles might be exploited for the expression of magnetic reporters for bioimaging [47] or for magnetogenetic manipulation of signaling pathways [166] or ion channels [167].

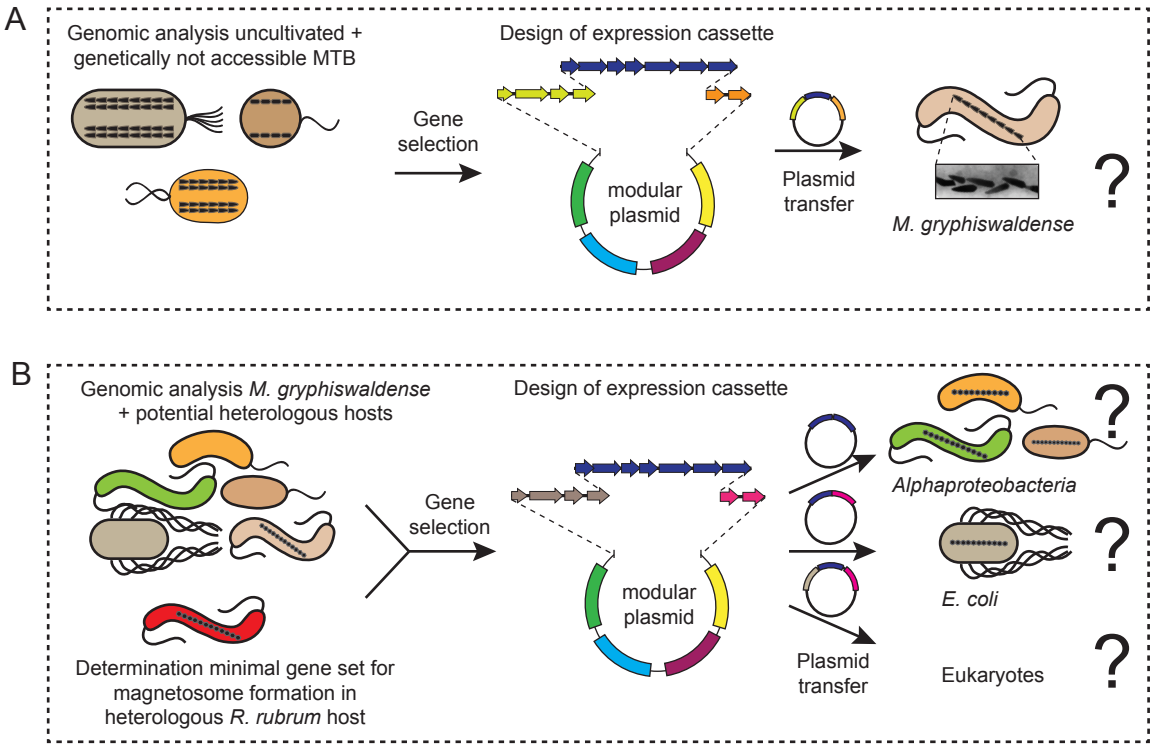

Figure 8: Future synthetic biology approaches based on the results of this thesis. A. Genetic engineering of *M. gryphiswaldense* by transfer of synthetic expression cassettes based on magnetosome genes from uncultivated or genetically not accessible MTB. B. Genetic transfer of the magnetosome biosynthesis pathway from *M. gryphiswaldense* into different hitherto non-magnetic hosts. The gene composition of the expression cassettes is adapted to different species by genomic analysis of the potential heterologous host and *M. gryphiswaldense*. Additionally, the minimal set of *mam* and *mms* genes is determined in the heterologous host *R. rubrum* for the construction of a compact cassette, which comprises only essential *mam* and *mms* genes.

3. References

1. Fischbach, M. and C.A. Voigt, *Prokaryotic gene clusters: a rich toolbox for synthetic biology.* Biotechnol J, 2010. **5**(12): p. 1277-96.
2. Hacker, J. and E. Carniel, *Ecological fitness, genomic islands and bacterial pathogenicity. A Darwinian view of the evolution of microbes.* EMBO Rep, 2001. **2**(5): p. 376-81.
3. Ullrich, S., et al., *A hypervariable 130-kilobase genomic region of Magnetospirillum gryphiswaldense comprises a magnetosome island which undergoes frequent rearrangements during stationary growth.* J Bacteriol, 2005. **187**(21): p. 7176-84.
4. Dubbels, B.L., et al., *Evidence for a copper-dependent iron transport system in the marine, magnetotactic bacterium strain MV-1.* Microbiology, 2004. **150**(9): p. 2931-45.
5. Fukuda, Y., et al., *Dynamic analysis of a genomic island in Magnetospirillum sp strain AMB-1 reveals how magnetosome synthesis developed.* FEBS Lett, 2006. **580**(3): p. 801-12.
6. Murat, D., *Magnetosomes: how do they stay in shape?* J. Mol Microbiol Biotechnol, 2013. **23**(1-2): p. 81-94.
7. Murat, D., et al., *The magnetosome membrane protein, MmsF, is a major regulator of magnetite biomineralization in Magnetospirillum magneticum AMB-1.* Mol Microbiol, 2012. **4**: p. 684-99.
8. Farina, M., D.M.S. Esquivel, and H.G.P.L. Debarros, *Magnetic Iron-Sulfur Crystals from a Magnetotactic Microorganism.* Nature, 1990. **343**(6255): p. 256-8.
9. Mann, S., et al., *Biomineralization of Ferrimagnetic Greigite (Fe_3S_4) and Iron Pyrite (FeS_2) in a Magnetotactic Bacterium.* Nature, 1990. **343**(6255): p. 258-61.
10. Frankel, R.B., R.P. Blakemore, and R.S. Wolfe, *Magnetite in freshwater magnetotactic bacteria.* Science, 1979. **203**(4387): p. 1355-6.
11. Lefèvre, C.T. and D.A. Bazylinski, *Ecology, diversity, and evolution of magnetotactic bacteria.* Microbiol Mol Biol Rev, 2013. **77**(3): p. 497-526.
12. Bazylinski, D.A. and R.B. Frankel, *Magnetosome formation in prokaryotes.* Nat Rev Microbiol, 2004. **2**(3): p. 217-30.

13. Blakemore, R., *Magnetotactic bacteria.* Science, 1975. **190**(4212): p. 377-9.
14. Amann, R., J. Peplies, and D. Schüler, *Diversity and taxonomy of magnetotactic bacteria*, in *Magnetoreception and magnetosomes in bacteria*, D. Schüler, Editor. 2006, Springer Verlag: Berlin, Heidelberg. p: 25-36.
15. Schüler, D. and M. Köhler, *The isolation of a new magnetic spirillum.* Zentralbl Mikrobiol, 1992. **147**: p. 150-1.
16. Lohsse, A., et al., *Functional analysis of the magnetosome island in Magnetospirillum gryphiswaldense: the mamAB operon is sufficient for magnetite biomineralization.* PLoS One, 2011. **6**(10): p. e25561.
17. Scheffel, A., et al., *The major magnetosome proteins MamGFDC are not essential for magnetite biomineralization in Magnetospirillum gryphiswaldense but regulate the size of magnetosome crystals.* J Bacteriol, 2008. **190**(1): p. 377-86.
18. Scheffel, A., et al., *An acidic protein aligns magnetosomes along a filamentous structure in magnetotactic bacteria.* Nature, 2006. **440**(7080): p. 110-4.
19. Katzmann, E., et al., *Loss of the actin-like protein MamK has pleiotropic effects on magnetosome formation and chain assembly in Magnetospirillum gryphiswaldense.* Mol Microbiol, 2010. **77**(1): p. 208-24.
20. Katzmann, E., et al., *Magnetosome chains are recruited to cellular division sites and split by asymmetric septation.* Mol Microbiol, 2011. **82**(6): p. 1316-29.
21. Schleifer, K.H., et al., *The Genus Magnetospirillum gen. nov. Description of Magnetospirillum gryphiswaldense sp. nov. and Transfer of Aquaspirillum magnetotacticum to Magnetospirillum magnetotacticum comb. nov.* System Appl Microbiol, 1991. **14**(4): p. 379–85.
22. Heyen, U. and D. Schüler, *Growth and magnetosome formation by microaerophilic Magnetospirillum strains in an oxygen-controlled fermentor.* Appl Microbiol Biotechnol, 2003. **61**(5-6): p. 536-44.
23. Richter, M., et al., *Comparative genome analysis of four magnetotactic bacteria reveals a complex set of group-specific genes implicated in magnetosome biomineralization and function.* J Bacteriol, 2007. **189**(13): p. 4899-910.
24. Wang, X., et al., *Complete Genome Sequence of Magnetospirillum gryphiswaldense MSR-1.* Genome Announc, 2014. **2**(2): p. e00171-14.

25. Schultheiss, D. and D. Schüler, *Development of a genetic system for Magnetospirillum gryphiswaldense.* Arch Microbiol, 2002. **179**: p. 89-94.
26. Ullrich, S. and D. Schüler, *Cre-lox-based method for generation of large deletions within the genomic magnetosome island of Magnetospirillum gryphiswaldense.* Appl Environ Microbiol, 2010. **76**(8): p. 2439-44.
27. Schultheiss, D., M. Kube, and D. Schüler, *Inactivation of the flagellin gene flaA in Magnetospirillum gryphiswaldense results in nonmagnetotactic mutants lacking flagellar filaments.* Appl Environ Microbiol, 2004. **70**(6): p. 3624-31.
28. Lang, C. and D. Schüler, *Biogenic nanoparticles: production, characterization, and application of bacterial magnetosomes.* J Phys: Condens Matter, 2006. **18**: p. 2815-28.
29. Frankel, R.B., D.A. Bazylinski, and D. Schüler, *Biomineralization of magnetic iron minerals in bacteria.* Supramol Sci, 1998. **5**(3-4): p. 383-90.
30. Devouard, B., et al., *Magnetite from magnetotactic bacteria: Size distributions and twinning.* Am Mineral, 1998. **83**(11-12): p. 1387-98.
31. Arató, B., et al., *Crystal-size and shape distributions of magnetite from uncultured magnetotactic bacteria as a potential biomarker* Am Mineral, 2005. **90**: p. 1233-341.
32. Faivre, D. and P. Zuddas, *Mineralogical and isotopic properties of biogenic nanocrystalline magnetites*, in *Magnetoreception and magnetosomes in bacteria*, D. Schüler, Editor. 2007, Springer-Verlag: Berlin, Heidelberg. p. 175-96.
33. Faivre, D. and D. Schüler, *Magnetotactic bacteria and magnetosomes.* Chem Rev, 2008. **108**(11): p. 4875-98.
34. Bazylinski, D.A., A.J. Garratt-Reed, and R.B. Frankel, *Electron microscopic studies of magnetosomes in magnetotactic bacteria.* Microsc Res Tech, 1994. **27**(5): p. 389-401.
35. Mann, S., R.B. Frankel, and R.P. Blakemore, *Structure, Morphology and Crystal-Growth of Bacterial Magnetite.* Nature, 1984. **310**(5976): p. 405-7.
36. Coker, V.S., et al., *Cation site occupancy of biogenic magnetite compared to polygenic ferrite spinels determined by X-ray magnetic circular dichroism.* Europ J Mineral, 2007. **19**(5): p. 707-16.
37. Matsuda, T., et al., *Morphology and Structure of Biogenic Magnetite Particles.* Nature, 1983. **302**(5907): p. 411-2.

38. Mann, S., N.H.C. Sparks, and R.P. Blakemore, *Structure, Morphology and Crystal-Growth of Anisotropic Magnetite Crystals in Magnetotactic Bacteria.* Proc R Soc Biol Sci, 1987. **231**(1265): p. 477-87.
39. Schüler, D., *Genetics and cell biology of magnetosome formation in magnetotactic bacteria.* FEMS Microbiol Rev, 2008. **32**(4): p. 654-72.
40. Lang, C., D. Schüler, and D. Faivre, *Synthesis of magnetite nanoparticles for bio- and nanotechnology: genetic engineering and biomimetics of bacterial magnetosomes.* Macromol Biosci, 2007. **7**(2): p. 144-51.
41. Grünberg, K., et al., *Biochemical and proteomic analysis of the magnetosome membrane in Magnetospirillum gryphiswaldense.* Appl Environ Microbiol, 2004. **70**(2): p. 1040-50.
42. Ghosh Chaudhuri, R. and S. Paria, *Core/shell nanoparticles: classes, properties, synthesis mechanisms, characterization, and applications.* Chem Rev, 2012. **112**(4): p. 2373-433.
43. Sun, J.B., et al., *Preparation and anti-tumor efficiency evaluation of doxorubicin-loaded bacterial magnetosomes: magnetic nanoparticles as drug carriers isolated from Magnetospirillum gryphiswaldense.* Biotechnol Bioeng, 2008. **101**(6): p. 1313-20.
44. Ohuchi, S. and D. Schüler, *In vivo display of a multisubunit enzyme complex on biogenic magnetic nanoparticles.* Appl Environ Microbiol, 2009. **75**(24): p. 7734-8.
45. Lang, C. and D. Schüler, *Expression of green fluorescent protein fused to magnetosome proteins in microaerophilic magnetotactic bacteria.* Appl Environ Microbiol, 2008. **74**(15): p. 4944-53.
46. Borg, S., et al., *New vectors for chromosomal integration enable high-level constitutive or inducible magnetosome expression of fusion proteins in Magnetospirillum gryphiswaldense.* Appl Environ Microbiol, 2014 (ahead of print).
47. Westmeyer, G.G. and A. Jasanoff, *Genetically controlled MRI contrast mechanisms and their prospects in systems neuroscience research.* Magnetic Resonance Imaging, 2007. **25**(6): p. 1004-10.
48. Komeili, A., et al., *Magnetosomes are cell membrane invaginations organized by the actin-like protein MamK.* Science, 2006. **311**(5758): p. 242-5.

49. Murat, D., et al., *Comprehensive genetic dissection of the magnetosome gene island reveals the step-wise assembly of a prokaryotic organelle.* Proc Natl Acad Sci U S A, 2010. **107**(12): p. 5593-8.
50. Schüler, D. and E. Bäuerlein, *Iron-limited growth and kinetics of iron uptake in Magnetospirillum gryphiswaldense.* Arch Microbiol, 1996. **166**(5): p. 301-7.
51. Uebe, R., *Mechanism and regulation of magnetosomal iron uptake and biomineralization in Magnetospirillum gryphiswaldense*, in *Department Biologie I.* 2011, Ludwig-Maximilians-Universität München.
52. Rong, C., et al., *Ferrous iron transport protein B gene (feoB1) plays an accessory role in magnetosome formation in Magnetospirillum gryphiswaldense strain MSR-1.* Res Microbiol, 2008. **159**(7-8): p. 530-6.
53. Rong, C., et al., *FeoB2 Functions in magnetosome formation and oxidative stress protection in Magnetospirillum gryphiswaldense strain MSR-1.* J Bacteriol, 2012. **194**(15): p. 3972-6.
54. Zhang, C., et al., *Two bifunctional enzymes with ferric reduction ability play complementary roles during magnetosome synthesis in Magnetospirillum gryphiswaldense MSR-1.* J Bacteriol, 2013. **195**(4): p. 876-85.
55. Raschdorf, O., et al., *The magnetosome proteins MamX, MamZ and MamH are involved in redox control of magnetite biomineralization in Magnetospirillum gryphiswaldense.* Mol Microbiol, 2013. **89**(5): p. 872-86.
56. Uebe, R., et al., *The cation diffusion facilitator proteins MamB and MamM of Magnetospirillum gryphiswaldense have distinct and complex functions, and are involved in magnetite biomineralization and magnetosome membrane assembly.* Mol Microbiol, 2011. **82**(4): p. 818-35.
57. Faivre, D., et al., *Intracellular magnetite biomineralization in bacteria proceeds by a distinct pathway involving membrane-bound ferritin and an iron(II) species.* Angew Chem Int Ed Engl, 2007. **46**(44): p. 8495-9.
58. Faivre, D., et al., *Mineralogical and isotopic properties of inorganic nanocrystalline magnetites.* Geochim Cosmochim Acta, 2004. **68**(21): p. 4395-403.
59. Baumgartner, J., et al., *Formation of Magnetite Nanoparticles at Low Temperature: From Superparamagnetic to Stable Single Domain Particles.* PLoS One, 2013. **8**(3): p. e57070.

60. Baumgartner, J., et al., *Magnetotactic bacteria form magnetite from a phosphate-rich ferric hydroxide via nanometric ferric (oxyhydr)oxide intermediates.* Proc Natl Acad Sci U S A, 2013. **110**(37): p. 14883-8.
61. Faivre, D., et al., *Development of cellular magnetic dipoles in magnetotactic bacteria.* Biophys J, 2010. **99**(4): p. 1268-73.
62. Schüler, D. and E. Bäuerlein, *Dynamics of iron uptake and Fe_3O_4 biomineralization during aerobic and microaerobic growth of Magnetospirillum gryphiswaldense.* J Bacteriol, 1998. **180**(1): p. 159-62.
63. Li, Y., *Oxygen regulation and redox control of magnetosome biomineralization in Magnetospirillum gryphiswaldense*, in *Department Biology I.* 2014, Ludwig-Maximilians-Universität München.
64. Katzmann, E., et al., *Analysis of magnetosome chains in magnetotactic bacteria by magnetic measurements and automated image analysis of electron micrographs.* Appl Environ Microbiol, 2013. **79**(24): p. 7755-62.
65. Grünberg, K., et al., *A large gene cluster encoding several magnetosome proteins is conserved in different species of magnetotactic bacteria.* Appl Environ Microbiol, 2001. **67**(10): p. 4573-82.
66. Okamura, Y., H. Takeyama, and T. Matsunaga, *A magnetosome-specific GTPase from the magnetic bacterium Magnetospirillum magneticum AMB-1.* J Biol Chem, 2001. **276**(51): p. 48183-8.
67. Dobrindt, U., et al., *Genomic islands in pathogenic and environmental microorganisms.* Nat Rev Microbiol, 2004. **2**(5): p. 414-24.
68. Juhas, M., et al., *Genomic islands: tools of bacterial horizontal gene transfer and evolution.* FEMS Microbiol Rev, 2009. **33**(2): p. 376-93.
69. Penn, K., et al., *Genomic islands link secondary metabolism to functional adaptation in marine Actinobacteria.* ISME J, 2009. **3**(10): p. 1193-203.
70. Ochman, H., J.G. Lawrence, and E.A. Groisman, *Lateral gene transfer and the nature of bacterial innovation.* Nature, 2000. **405**(6784): p. 299-304.
71. Schübbe, S., et al., *Characterization of a spontaneous nonmagnetic mutant of Magnetospirillum gryphiswaldense reveals a large deletion comprising a putative magnetosome island.* J Bacteriol, 2003. **185**(19): p. 5779-90.
72. Jogler, C., et al., *Comparative analysis of magnetosome gene clusters in magnetotactic bacteria provides further evidence for horizontal gene transfer.* Environ Microbiol, 2009. **11**(5): p. 1267-77.

73. Nakazawa, H., et al., *Whole genome sequence of Desulfovibrio magneticus strain RS-1 revealed common gene clusters in magnetotactic bacteria.* Genome Res, 2009. **19**(10): p. 1801-8.
74. Jogler, C., et al., *Conservation of proteobacterial magnetosome genes and structures in an uncultivated member of the deep-branching Nitrospira phylum.* Proc Natl Acad Sci U S A, 2011. **108**(3): p. 1134-9.
75. Schübbe, S., et al., *Complete genome sequence of the chemolithoautotrophic marine magnetotactic coccus strain MC-1.* Appl Environ Microbiol, 2009. **75**(14): p. 4835-52.
76. Lefèvre, C.T., et al., *Comparative genomic analysis of magnetotactic bacteria from the Deltaproteobacteria provides new insights into magnetite and greigite magnetosome genes required for magnetotaxis.* Environ Microbiol, 2013. **15**(10): p. 2712-35.
77. Lefèvre, C.T., et al., *Monophyletic origin of magnetotaxis and the first magnetosomes.* Environ Microbiol, 2013. **15**(8): p. 2267-74.
78. Schübbe, S., et al., *Transcriptional organization and regulation of magnetosome operons in Magnetospirillum gryphiswaldense.* Appl Environ Microbiol, 2006. **72**(9): p. 5757-65.
79. Tanaka, M., et al., *MMS6 protein regulates crystal morphology during nano-sized magnetite biomineralization in vivo.* J Biol Chem, 2011. **286**(8): p. 6386-92.
80. Lohsse, A., et al., *Genetic dissection of the mamAB and mms6 operons reveals a gene set essential for magnetosome biogenesis in Magnetospirillum gryphiswaldense.* J Bacteriol, 2014 (ahead of print).
81. Müller, F.D., et al., *The FtsZ-like protein FtsZm of Magnetospirillum gryphiswaldense likely interacts with its generic homolog and is required for biomineralization under nitrate deprivation.* J Bacteriol, 2014. **196**(3): p. 650-9.
82. Tanaka, M., A. Arakaki, and T. Matsunaga, *Identification and functional characterization of liposome tubulation protein from magnetotactic bacteria.* Mol Microbiol, 2010. **76**(2): p. 480-8.
83. Raschdorf, O., *Untersuchung der Funktion des mamXY Operons bei der Magnetosomenformation in Magnetospirillum gryphiswaldense*, in *Department Biologie I.* 2011, Ludwig-Maximilians-Universität München.

84. Komeili, A., *Molecular mechanisms of compartmentalization and biomineralization in magnetotactic bacteria.* FEMS Microbiol Rev, 2012. **36**(1): p. 232-55.
85. McMahon, H.T. and J.L. Gallop, *Membrane curvature and mechanisms of dynamic cell membrane remodelling.* Nature, 2005. **438**(7068): p. 590-6.
86. Komeili, A., et al., *Magnetosome vesicles are present before magnetite formation, and MamA is required for their activation.* Proc Natl Acad Sci U S A, 2004. **101**(11): p. 3839-44.
87. Yang, W., et al., *mamO and mamE genes are essential for magnetosome crystal biomineralization in Magnetospirillum gryphiswaldense MSR-1.* Res Microbiol, 2010. **161**(8): p. 701-5.
88. Zeytuni, N., et al., *Self-recognition mechanism of MamA, a magnetosome-associated TPR-containing protein, promotes complex assembly.* Proc Natl Acad Sci U S A, 2011. **108**(33): p. 480-7.
89. Siponen, M.I., et al., *Magnetochrome: a c-type cytochrome domain specific to magnetotatic bacteria.* Biochem Soc Trans, 2012. **40**(6): p. 1319-23.
90. Nudelman, H. and R. Zarivach, *Structure prediction of magnetosome-associated proteins.* Front Microbiol, 2014. **5**: p. 9.
91. Siponen, M.I., et al., *Structural insight into magnetochrome-mediated magnetite biomineralization.* Nature, 2013. **502**(7473): p. 681-4.
92. Scheffel, A. and D. Schüler, *The acidic repetitive domain of the Magnetospirillum gryphiswaldense MamJ protein displays hypervariability but is not required for magnetosome chain assembly.* J Bacteriol, 2007. **189**(17): p. 6437-46.
93. Draper, O., et al., *MamK, a bacterial actin, forms dynamic filaments in vivo that are regulated by the acidic proteins MamJ and LimJ.* Mol Microbiol, 2011. **82**(2): p. 342-54.
94. Uebe, R., et al., *Deletion of a fur-like gene affects iron homeostasis and magnetosome formation in Magnetospirillum gryphiswaldense.* J Bacteriol, 2010. **192**(16): p. 4192-204.
95. Li, Y.J., et al., *The Periplasmic Nitrate Reductase Nap Is Required for Anaerobic Growth and Involved in Redox Control of Magnetite Biomineralization in Magnetospirillum gryphiswaldense.* J Bacteriol, 2012. **194**(18): p. 4847-56.

96. Li, Y.J., et al., *Cytochrome cd_1 Nitrite Reductase NirS Is Involved in Anaerobic Magnetite Biomineralization in Magnetospirillum gryphiswaldense and Requires NirN for Proper d_1 Heme Assembly.* J Bacteriol, 2013. **195**(18): p. 4297-309.
97. Li, Y., et al., *The terminal oxidase cbb3 functions in redox control of magnetite biomineralization in Magnetospirillum gryphiswaldense.* J Bacteriol, 2014 (ahead of print).
98. Jogler, C. and D. Schüler, *Genetic analysis of magnetosome biomineralization*, in *Magnetoreception and magnetosomes in bacteria*, D. Schüler, Editor. 2006, Springer-Verlag: Heidelberg, Berlin. p. 134-61.
99. Okamura, Y., et al., *Design and application of a new cryptic-plasmid-based shuttle vector for Magnetospirillum magneticum.* Appl Environ Microbiol, 2003. **69**(7): p. 4274-7.
100. Matsunaga, T., et al., *Gene transfer in magnetic bacteria: transposon mutagenesis and cloning of genomic DNA fragments required for magnetosome synthesis.* J Bacteriol, 1992. **174**(9): p. 2748-53.
101. Raschdorf, O., et al., *A tailored galK counterselection system for efficient markerless gene deletion and chromosomal tagging in Magnetospirillum gryphiswaldense.* Appl Environ Microbiol, 2014 (ahead of print).
102. Kuzminov, A., *Recombinational repair of DNA damage in Escherichia coli and bacteriophage lambda.* Microbiol Mol Biol Rev, 1999. **63**(4): p. 751-813.
103. Karlin, S. and L. Brocchieri, *Evolutionary conservation of recA genes in relation to protein structure and function.* J Bacteriol, 1996. **178**(7): p. 1881-94.
104. Radman, M., *SOS repair hypothesis: phenomenology of an inducible DNA repair which is accompanied by mutagenesis.* Basic Life Sci, 1975. **5A**: p. 355-67.
105. Michel, B., *After 30 years of study, the bacterial SOS response still surprises us.* PLoS Biol, 2005. **3**(7): p. e255.
106. Makino, T., G. Skretas, and G. Georgiou, *Strain engineering for improved expression of recombinant proteins in bacteria.* Microb Cell Fact, 2011. **10**: p. 32.
107. Pradel, N., et al., *Biogenesis of actin-like bacterial cytoskeletal filaments destined for positioning prokaryotic magnetic organelles.* Proc Natl Acad Sci U S A, 2006. **103**(46): p. 17485-9.

108. Shaw, A.Z. and B. Miroux, *A general approach for heterologous membrane protein expression in Escherichia coli: the uncoupling protein, UCP1, as an example.* Methods Mol Biol, 2003. **228**: p. 23-35.
109. Ongley, S.E., et al., *Recent advances in the heterologous expression of microbial natural product biosynthetic pathways.* Nat Prod Rep, 2013. **30**(8): p. 1121-38.
110. Sharp, P.M. and W.H. Li, *The codon Adaptation Index--a measure of directional synonymous codon usage bias, and its potential applications.* Nucleic Acids Res, 1987. **15**(3): p. 1281-95.
111. Ikemura, T., *Codon usage and tRNA content in unicellular and multicellular organisms.* Mol Biol Evol, 1985. **2**(1): p. 13-34.
112. Dixon, R.A. and J.R. Postgate, *Genetic Transfer of Nitrogen Fixation from Klebsiella pneumoniae to Escherichia coli.* Nature, 1972. **237**(5350): p. 102-3.
113. Fu, J., et al., *Efficient transfer of two large secondary metabolite pathway gene clusters into heterologous hosts by transposition.* Nucleic Acids Res, 2008. **36**(17): p. e113.
114. Miao, V., et al., *Daptomycin biosynthesis in Streptomyces roseosporus: cloning and analysis of the gene cluster and revision of peptide stereochemistry.* Microbiology, 2005. **151**(5): p. 1507-23.
115. Bonacci, W., et al., *Modularity of a carbon-fixing protein organelle.* Proc Natl Acad Sci U S A, 2012. **109**(2): p. 478-83.
116. Chen, A.H. and P.A. Silver, *Designing biological compartmentalization.* Trends Cell Biol, 2012. **22**(12): p. 662-70.
117. Parsons, J.B., et al., *Biochemical and structural insights into bacterial organelle form and biogenesis.* J Biol Chem, 2008. **283**(21): p. 14366-375.
118. Choudhary, S., et al., *Engineered Protein Nano-Compartments for Targeted Enzyme Localization.* PLoS One, 2012. **7**(3).
119. Ramsay, J.P., et al., *A quorum-sensing molecule acts as a morphogen controlling gas vesicle organelle biogenesis and adaptive flotation in an enterobacterium.* Proc Natl Acad Sci U S A, 2011. **108**(36): p. 14932-37.
120. Bernaudat, F., et al., *Heterologous expression of membrane proteins: choosing the appropriate host.* PLoS One, 2011. **6**(12): p. e29191.

121. Tchamedeu Kameni, A.P., et al., *Inactivation of the spirochete recA gene results in a mutant with low viability and irregular nucleoid morphology.* J Bacteriol, 2002. **184**(2): p. 452-8.
122. Sander, P., et al., *A recA deletion mutant of Mycobacterium bovis BCG confers protection equivalent to that of wild-type BCG but shows increased genetic stability.* Vaccine, 2003. **21**(27-30): p. 4124-7.
123. Capaldo, F.N., G. Ramsey, and S.D. Barbour, *Analysis of the growth of recombination-deficient strains of Escherichia coli K-12.* J Bacteriol, 1974. **118**(1): p. 242-9.
124. Chen, I.P. and H. Michel, *Cloning, sequencing, and characterization of the recA gene from Rhodopseudomonas viridis and construction of a recA strain.* J Bacteriol, 1998. **180**(12): p. 3227-32.
125. Bo, T., et al., *Compromised DNA damage repair promotes genetic instability of the genomic magnetosome island in Magnetospirillum magneticum AMB-1.* Curr Microbiol, 2012. **65**(1): p. 98-107.
126. Gibson, D.G., et al., *Enzymatic assembly of DNA molecules up to several hundred kilobases.* Nat Methods, 2009. **6**(5): p. 343-41.
127. Weber, E., et al., *A modular cloning system for standardized assembly of multigene constructs.* PLoS One, 2011. **6**(2): p. e16765.
128. Shizuya, H., et al., *Cloning and stable maintenance of 300-kilobase-pair fragments of human DNA in Escherichia coli using an F-factor-based vector.* Proc Natl Acad Sci U S A, 1992. **89**(18): p. 8794-7.
129. Kim, U.J., et al., *Stable propagation of cosmid sized human DNA inserts in an F factor based vector.* Nucleic Acids Res, 1992. **20**(5): p. 1083-5.
130. Sternberg, N., *Bacteriophage-P1 Cloning System for the Isolation, Amplification, and Recovery of DNA Fragments as Large as 100 Kilobase Pairs.* Proc Natl Acad Sci U S A, 1990. **87**(1): p. 103-7.
131. Muyrers, J.P.P., et al., *Rapid modification of bacterial artificial chromosomes by ET-recombination.* Nucleic Acids Res, 1999. **27**(6): p. 1555-7.
132. Zhang, Y.M., et al., *A new logic for DNA engineering using recombination in Escherichia coli.* Nat Genet, 1998. **20**(2): p. 123-8.
133. Wang, J., et al., *An improved recombineering approach by adding RecA to lambda Red recombination.* Mol Biotechnol, 2006. **32**(1): p. 43-53.

134. Wenzel, S.C., et al., *Heterologous expression of a myxobacterial natural products assembly line in pseudomonads via red/ET recombineering.* Chemistry & Biology, 2005. **12**(3): p. 349-56.
135. Perlova, O., et al., *Reconstitution of the myxothiazol biosynthetic gene cluster by Red/ET recombination and heterologous expression in Myxococcus xanthus.* Appl Environ Microbiol, 2006. **72**(12): p. 7485-94.
136. Fu, J., et al., *Full-length RecE enhances linear-linear homologous recombination and facilitates direct cloning for bioprospecting.* Nat Biotechnol, 2012. **30**(5): p. 440-6.
137. Fu, J., et al., *Efficient transfer of two large secondary metabolite pathway gene clusters into heterologous hosts by transposition.* Nucleic Acids Res, 2008. **36**(17): p. e113.
138. Cheah, U.E., W.A. Weigand, and B.C. Stark, *Effects of recombinant plasmid size on cellular processes in Escherichia coli.* Plasmid, 1987. **18**(2): p. 127-34.
139. Pollithy, A., et al., *Magnetosome expression of functional camelid antibody fragments (nanobodies) in Magnetospirillum gryphiswaldense.* Appl Environ Microbiol, 2011. **77**(17): p. 6165-71.
140. Kolinko, I., *Untersuchungen zur heterologen Expression von Magnetosomengenclustern aus kultivierten und unkultivierten magnetotaktischen Bakterien*, in *Department Biology I.* 2009, Ludwig-Maximilians-Universität München.
141. Friehs, K., *Plasmid copy number and plasmid stability.* Adv Biochem Eng Biotechnol, 2004. **86**: p. 47-82.
142. Tyo, K.E., P.K. Ajikumar, and G. Stephanopoulos, *Stabilized gene duplication enables long-term selection-free heterologous pathway expression.* Nature Biotechnol, 2009. **27**(8): p. 760-5.
143. Bennett, P.M., *Genome plasticity: insertion sequence elements, transposons and integrons, and DNA rearrangement.* Methods Mol Biol, 2004. **266**: p. 71-113.
144. Martinez-Garcia, E., et al., *pBAM1: an all-synthetic genetic tool for analysis and construction of complex bacterial phenotypes.* BMC Microbiol, 2011. **11**: p. 38.
145. Plasterk, R.H., Z. Izsvak, and Z. Ivics, *Resident aliens: the Tc1/mariner superfamily of transposable elements.* Trends Genet, 1999. **15**(8): p. 326-32.

146. Berg, D.E. and C.M. Berg, *The Prokaryotic Transposable Element Tn5.* Bio-Technology, 1983. **1**(5): p. 417-35.
147. Nash, C.Z., *Mechanisms and evolution of magnetotactic bacteria*, 2008, California Institute of Technology. Pasadena, CA, USA.
148. Tang, Y., et al., *Duplication of partial spinosyn biosynthetic gene cluster in Saccharopolyspora spinosa enhances spinosyn production.* FEMS Microbiol Lett, 2011. **325**(1): p. 22-9.
149. Sun, C., J.S. Lee, and M. Zhang, *Magnetic nanoparticles in MR imaging and drug delivery.* Adv Drug Deliv Rev, 2008. **60**(11): p. 1252-65.
150. Hergt, R., et al., *Magnetic properties of bacterial magnetosomes as diagnostic and therapeutic tools.* J Magn Magn Mater, 2005. **293**: p. 80-6.
151. Imhoff, J.F., *The phototrophic Alpha-Proteobacteria*, in *The Prokaryotes*, M. Dworkin, et al., Editors. 2006, Springer: New York. p. 41-64.
152. Zeiger, L. and H. Grammel, *Model-based high cell density cultivation of Rhodospirillum rubrum under respiratory dark conditions.* Biotechnol Bioeng, 2010. **105**(4): p. 729-39.
153. Sasaki, K., et al., *Applications of photosynthetic bacteria for medical fields.* J Biosci Bioeng, 2005. **100**(5): p. 481-8.
154. Wang, G.S., et al., *High-level production of the industrial product lycopene by the photosynthetic bacterium Rhodospirillum rubrum.* Appl Environ Microbiol, 2012. **78**(20): p. 7205-15.
155. Butzin, N.C., H.A. Owen, and M.L. Collins, *A new system for heterologous expression of membrane proteins: Rhodospirillum rubrum.* Protein Expr Purif, 2010. **70**(1): p. 88-94.
156. Ghosh, R., et al., *Optimization of the Sistrom Culture Medium for Large-Scale Batch Cultivation of Rhodospirillum rubrum under Semiaerobic Conditions with Maximal Yield of Photosynthetic Membranes.* Appl Environ Microbiol, 1994. **60**(5): p. 1698-700.
157. Kiemer, F., *Untersuchungen zur heterologen Expression von Magnetosomenoperons aus Magnetospirillum gryphiswaldense*, in *Department Biology I.* 2013, Ludwig-Maximilians-Universität München.
158. Temme, K., D. Zhao, and C.A. Voigt, *Refactoring the nitrogen fixation gene cluster from Klebsiella oxytoca.* Proc Natl Acad Sci U S A, 2012. **109**(18): p. 7085-90.

159. Plotkin, J.B. and G. Kudla, *Synonymous but not the same: the causes and consequences of codon bias.* Nat Rev Genet, 2011. **12**(1): p. 32-42.
160. Osswald, C., et al., *Modular Construction of a Functional Artificial Epothilone Polyketide Pathway.* ACS Synth Biol, 2012 (ahead of print).
161. Mutka, S.C., et al., *Heterologous production of epothilone C and D in Escherichia coli.* Biochemistry, 2006. **45**(4): p. 1321-30.
162. Parsons, J.B., et al., *Synthesis of empty bacterial microcompartments, directed organelle protein incorporation, and evidence of filament-associated organelle movement.* Mol Cell, 2010. **38**(2): p. 305-15.
163. Eriksson, H.M., et al., *Massive formation of intracellular membrane vesicles in Escherichia coli by a monotopic membrane-bound lipid glycosyltransferase.* J Biol Chem, 2009. **284**(49): p. 33904-14.
164. Nishida, K. and P.A. Silver, *Induction of biogenic magnetization and redox control by a component of the target of rapamycin complex 1 signaling pathway.* PLoS Biol, 2012. **10**(2): p. e1001269.
165. Kim, T., D. Moore, and M. Fussenegger, *Genetically programmed superparamagnetic behavior of mammalian cells.* J Biotechnol, 2012. **162**(2-3): p. 237-45.
166. Etoc, F., et al., *Subcellular control of Rac-GTPase signalling by magnetogenetic manipulation inside living cells.* Nat Nanotechnol, 2013. **8**(3): p. 193-8.
167. Huang, H., et al., *Remote control of ion channels and neurons through magnetic-field heating of nanoparticles.* Nat Nanotechnol, 2010. **5**(8): p. 602-6.

4. Supplementary information

Table S1: Excerpt of plasmids that were constructed in this thesis. Respective promoters (P) are listed in parenthesis.

Plasmid	Description	Size (kb)
pTps_AB	MycoMar mariner transposon plasmid + (P_{mamH}) *mamAB* operon	23
pTps_ABG	MycoMar mariner transposon plasmid + (P_{mamH}) *mamAB* + (P_{mamDC}) *mamGFDC* operon	25
pTps_ABG6	MycoMar mariner transposon plasmid containing (P_{mamH}) *mamAB* + (P_{mamDC}) *mamGFDC* + (P_{mms}) *mms6* operon	29
pTps_XYZ	MycoMar mariner transposon plasmid + (P_{mamXY}) *mamX, mamY, mamZ*	9
Tet-pBam_feoAB1	Tn5 plasmid + (P_{mamH}) *feoAB1* operon	7

Table S2: Characteristics of generated overexpression strains compared to the parental strain *M. gryphiswaldense ΔrecA* (ΔRecA). Asterisks mark mutants, which were constructed and characterized by A. Lohße. n.d. = not determined

Strain	Genotype	Crystal Size	Increased size (%) compared to ΔRecA	Crystal number per cell	Increased number (%) compared to ΔRecA	Iron content (%) compared to ΔRecA
ΔRecA	1x MAI	36.2±11.0	-	33.9±10.3	-	-
WT	1x MAI	35.6±13.0	-1.7	34.3±8.4	1.2	n.d.
ΔRecA+ *mamGFDC**	2x *mamGFDC* operon	44.9±13.5	24.4	36.3±12.4	7.1	7.4±1.1
ΔRecA+ *mms6* 1x*	2x *mms6* operon	45.7±14.2	26.7	46.5±14.3	36.8	14.9±2.9
ΔRecA+ *GFDC/mms6**	2x *mms6* 2x *mamGFDC* operon	45.1±12.2	24.6	45.1±14.3	32.7	14.1±1.9
ΔRecA+ *mms6* 2x*	3x *mms6* operon	47.9±12.8	32.9	54.3±29.9	59.5	34.8±2.5
ΔRecA+ *mms6* 3x*	4x *mms6* operon	44.4±13.2	22.6	57.8±26.9	69.7	38.8±2.5
ΔRecA+ *mms6* 4x*	5x *mms6* operon	41.9±12.0	15.7	46.0±14.8	35.3	n.d.
ΔRecA+ *mamAB* 1x	2x *mamAB* operon	34.0±17.6	-6.2	73.4±43.1	115.2	0.4±0.5
ΔRecA+ *mamAB* 2x	3x *mamAB* operon	35.6±15.4	-1.0	68.8±13.2	102.9	9.4±0.5
ΔRecA+ *ABG6X*	2x *mamGFDC* 2x *mms6* 2x *mamAB* 2x *mamXY* operon	38.7±11.9	6.9	74.5±34.9	118.3	140.7±2.4
ΔRecA+ *ABG6X*+ *feo*	2x *mamGFDC* 2x *mms6* 2x *mamAB* 2x *mamXY* 2x *feoAB1* operon	41.1 ± 8.4	13.5	69.3±13.4	104.4	135.9±6.4

Table S3: Different hosts, which were chosen for conjugative transfer of the 4 major operons (*mamAB*, *mamGFDC*, *mms6*, *mamXYZ)*. Successful transfer of the magnetosome genes was verified by PCR of single magnetosome genes from the 4 operons. Protein expression was investigated by Western Blot analysis.

Acceptor strain	Genetic transfer expression cassettes	MamM expression	MamK expression	MamC expression
Rhodobacter sphaeroides	+	+	+	+
Phaeospirillum molischianum	+	-	-	-
Aquaspirillum polymorphum	+	-	-	-
Phaeospirillum fulvum	-			
Agrobacterium tumefaciens	+	+	+	-
Caulobacter crescentus	+	-	-	+
Bradyrhizobium japonicum	+	-	-	-
Sinorhizobium meliloti	-			
Mesorhizobium loti	-			
Methylobacterium extorquens	+	-	-	+
Rhodobacter capsulatus	+	+	+	-
Azospirillum brasilense	+	+	+	+

Table S4: Selected genes from the comparative gene content analysis of *M. gryphiswaldense*, *R. rubrum*, *P. molischianum*, *R. sphaeroides*, *A. brasilense* based on RBMs (expectation value E <1E-5, subject coverage >65%). Grey: genes that are present in *M. gryphiswaldense* and *R. rubrum*, but absent in *P. molischianum*, *R. sphaeroides*, *A. brasilense*. Green: Shared genes between *M. gryphiswaldense*, *R. rubrum* and *P. molischianum*, which are absent in *R. sphaeroides* and *A. brasilense*.

M. gryphiswaldense			**Best protein BLAST hit other MTB**				***R. rubrum***		
Gene	Gene product	Protein Accession number	Organism	Accession number	E-value	Identity (%)	Accession number	E-value	Identity (%)
MGR0027	Conserved hypothetical protein	CAM74798	*M. magneticum*	YP_422727	0E+00	59	YP_427286	4E-77	35
MGR0071	Hemerythrin-like protein	CAM74635	*M. magneticum*	YP_419589	2E-24	44	YP_426742	6E-17	40
MGR0112	Heme iron utilization protein	CAM76883	*M. magneticum*	YP_420146	4E-48	63	YP_428501	1E-29	37
MGR0257	Thioredoxin	CAM74218	*M. magneticum*	YP_422277	2E-44	61	YP_427887	9E-17	31
MGR0518	TPR repeat	CAM75609	*M. magneticum*	YP_420120	8E-41	45	YP_426619	2E-24	35
MGR0532	Putative bacterioferritin	CAM75623	*M. magneticum*	YP_421026	5E-56	67	YP_428555	3E-36	50
MGR0578	Conserved hypothetical protein	CAM75408	*M. magneticum*	YP_421164	4E-39	71	YP_426834	4E-17	50
MGR0652	Rieske 2Fe-2S protein	CAM75155	*M. magneticum*	YP_423539	2E-23	53	YP_428655	3E-16	48
MGR0655	Conserved hypothetical protein	CAM75158	*M. magneticum*	YP_423541	4E-66	55	YP_427126	8E-29	40
MGR0729	Hemerythrin	CAM75096	*M. magnetotacticum*	ZP_00056025	4E-49	67	YP_427730	3E-22	45
MGR0906	Cation efflux protein	CAM76906	*M. magneticum*	YP_420376	4E-152	95	YP_426785	2E-95	62
MGR0937	Ferredoxin	CAM74601	*M. magneticum*	YP_421500	1E-27	77	YP_427804	1E-16	55
MGR1288	Conserved hypothetical protein	CAM76396	-	-	-	-	YP_426061	8E-27	64

MGR1306	Cytochrome c-type protein TorC	CAM76414	-	-	-	-	YP_426371	9E-77	42
MGR2506	Conserved hypothetical protein, membrane	CAM77320	*M. magnetotacticum*	ZP_00055414	1E-19	61	YP_425483	1E-08	43
MGR2629	Conserved hypothetical protein	CAM77683	-	-	-	-	YP_427393	2E-10	73
MGR3182	Fe-S Oxidoreductase	CAM76455	*M. magnetotacticum*	YP_421030	3E-106	68	YP_428128	2E-76	52
MGR4267	Conserved hypothetical protein	CAM78199	*M. magneticum*	YP_423492	7E-103	71	YP_426501	1E-84	66
MGR4268	Iron sulfur protein	CAM78200	*M. magnetotacticum*	ZP_00055262	0E+00	75	YP_426500	2E-173	71
MGR4270	Oxidoreductase	CAM78202	*M. magneticum*	YP_423495	0E+00	64	YP_426498	0E+00	62

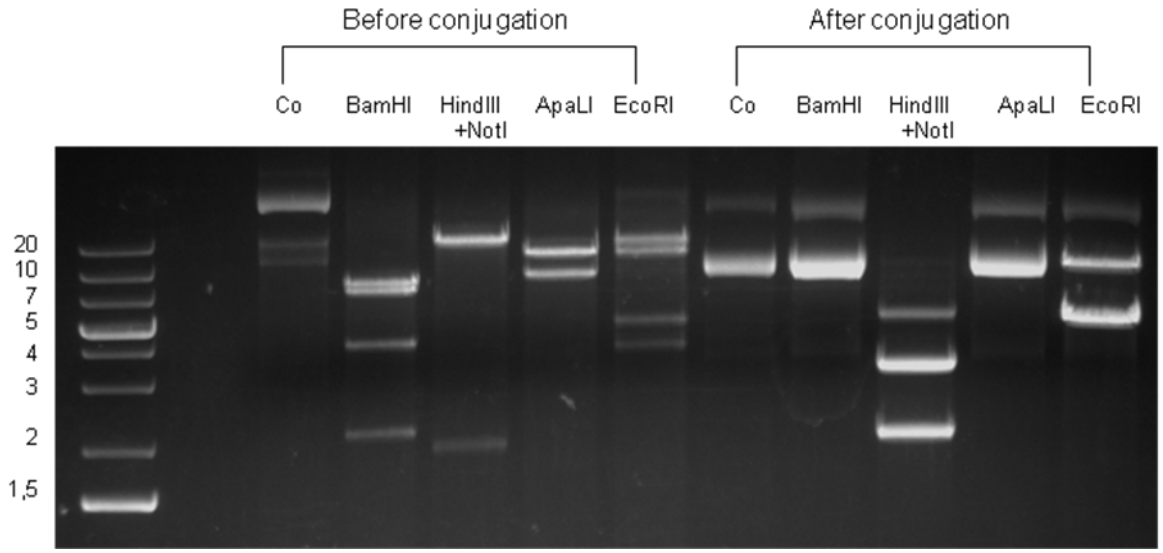

Figure S1: Results of the stability analysis of a reisolated *mamAB*-pBBR1 plasmid from *M. gryphiswaldense* Δ*mamB*. On the left side restriction analysis of the plasmid before conjugation is shown, on the right side after conjugative transfer. For size comparison a 1 kb Plus DNA-ladder was plotted on the Agarose gel. Co = unrestricted Control.

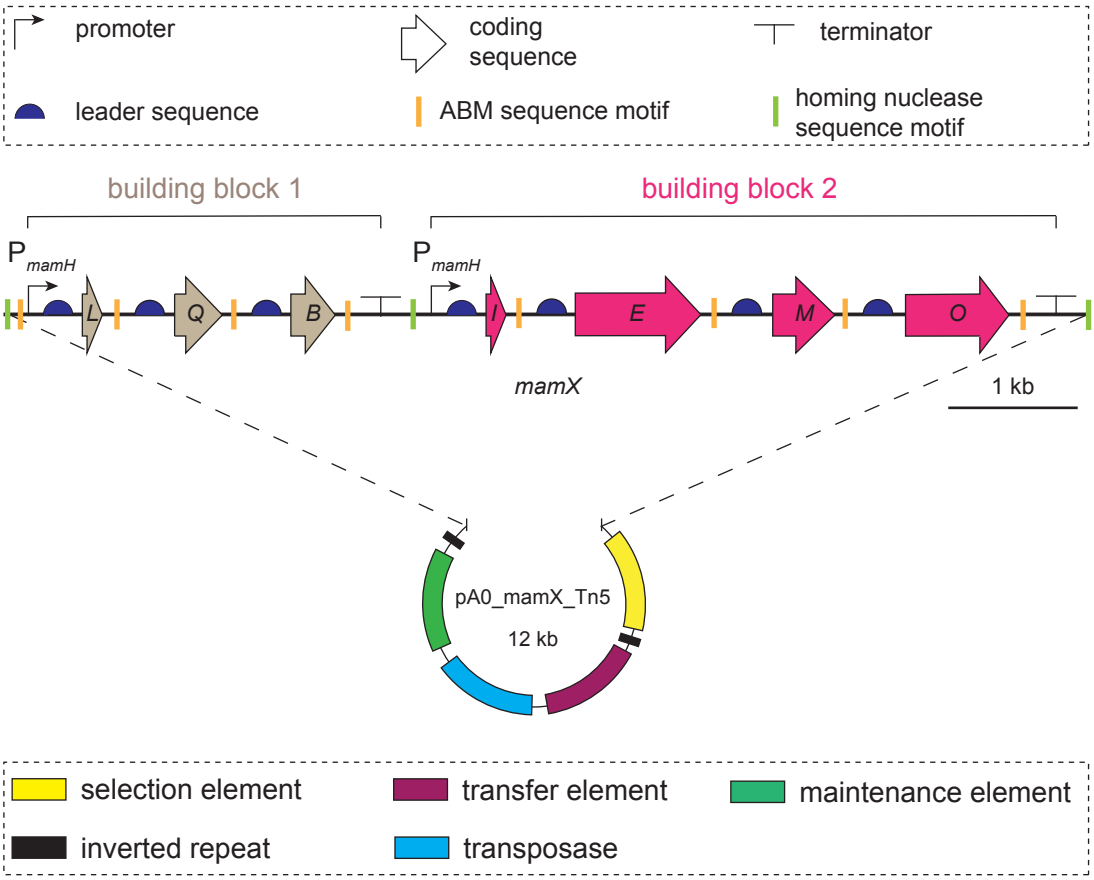

Figure S2: Organizational scheme of the synthetic plasmid pA0-mamX-Tn5. Grey and pink colors of the coding sequences indicate affiliations to building block 1 or 2. Each expression unit is under transcriptional control of a P_{mamH} promoter. Artificial Shine-Dalgarno (SD) sequences with calculated free accessibility on the messenger RNA (mRNA) were designed according to different computational models [1-3]. The coding sequences were not further optimized except for removal of disruptive endonuclease restriction sites. To allow complete de-assembly, recovery as well as recycling of all genes, individual coding sequences are each separated by an ABM (AscI-BssHII-MauBI) restriction site (orange lines). Homing endonuclease motifs (green lines) allow removal of building block 1 or 2, thereby facilitating transposition of only one expression unit. The vector backbone contains exchangeable elements for selection (kanamycin resistance cassette), maintenance in *E. coli* (p15A origin of replication) and transfer (RK2 mobilization system). A codon optimized Tn5 mobile element for high gene expression (K. Tavares, unpublished), and 2 IR repeat sequences facilitate random insertion of the *mamX* cassette.

References

1. Salis, H.M., E.A. Mirsky, and C.A. Voigt, *Automated design of synthetic ribosome binding sites to control protein expression.* Nat Biotechnol, 2009. **27**(10): p. 946-50.
2. Andronescu, M., et al., *Computational approaches for RNA energy parameter estimation.* Public RNA Soc, 2010. **16**(12): p. 2304-18.
3. Mathews, D.H., *Using an RNA secondary structure partition function to determine confidence in base pairs predicted by free energy minimization.* Public RNA Soc, 2004. **10**(8): p. 1178-90.

Chapter II

Manuscripts and publications

Manuscript 1:

Frequent mutations within the genomic magnetosome island of *Magnetospirillum gryphiswaldense* are mediated by RecA

Isabel Kolinko, Christian Jogler[†], Emanuel Katzmann, and Dirk Schüler[1]

Journal of Bacteriology (2011), 19: 5328-34

[1] Ludwig-Maximilians-Universität München, Department Biologie I, Biozentrum der LMU, Großhaderner Str. 4, 82152 Planegg-Martinsried, Germany

[†] Present address: Leibniz Institute DSMZ, Department of Microbial Cell Biology and Genetics, Inhoffenstraße 7B, 38124 Braunschweig, Germany

JOURNAL OF BACTERIOLOGY, Oct. 2011, p. 5328–5334 Vol. 193, No. 19
0021-9193/11/$12.00 doi:10.1128/JB.05491-11

Frequent Mutations within the Genomic Magnetosome Island of *Magnetospirillum gryphiswaldense* Are Mediated by RecA▽†

Isabel Kolinko, Christian Jogler,‡ Emanuel Katzmann, and Dirk Schüler*

Ludwig-Maximilians-Universität München, Department Biologie I, Bereich Mikrobiologie, Biozentrum der LMU, Großhaderner Str. 4, 82152 Planegg-Martinsried, Germany

Received 8 June 2011/Accepted 29 July 2011

Genes for magnetosome formation in magnetotactic bacteria are clustered in large genomic magnetosome islands (MAI). Spontaneous deletions and rearrangements were frequently observed within these regions upon metabolic stress. This instability was speculated to be due to RecA-dependent homologous recombination between the numerous sequence repeats present within the MAI. Here we show that a RecA-deficient strain of *Magnetospirillum gryphiswaldense* (IK-1) no longer exhibits genetic instability of magnetosome formation. Strain IK-1 displayed higher sensitivity to oxygen and UV irradiation. Furthermore, the lack of RecA abolished allelic exchange in the mutant. Cells of strain IK-1 displayed a slightly altered (i.e., more elongated) morphology, whereas the absence of RecA did not affect the ability to synthesize wild-type-like magnetosomes. Our data provide evidence that the observed genetic instability of magnetosome formation in the wild type is due predominantly to RecA-mediated recombination. In addition, increased genetic stability could make strain IK-1 a useful tool for the expression of genes and further genetic engineering, as well as for biotechnological production of bacterial magnetosomes.

The magnetotactic alphaproteobacterium *Magnetospirillum gryphiswaldense* synthesizes magnetosomes, which consist of magnetite (Fe_3O_4) crystals enclosed within intracytoplasmatic vesicles of the magnetosome membrane (MM) (35). All of the genes known to be responsible for magnetosome formation were found clustered within a conspicuous genomic "magnetosome island" (MAI) which comprises the *mamAB*, *mamGFDC*, *mms6*, and *mamXY* operons (33, 40, 41). Genes of these operons are involved in MM vesicle formation, magnetite biomineralization, and chain assembly (22, 30, 32, 34). The presence of conserved MAI-like structures in other cultivated (15, 16, 24, 27, 40) and uncultivated magnetotactic bacteria (MTB) (17, 18) suggests that the MAI was horizontally transferred between distantly related bacteria (15). In addition to all of the identified magnetosome genes, the MAI harbors numerous transposase genes, as well as hypothetical genes with unknown functions. It was shown in previous studies that the MAI undergoes frequent rearrangements during subcultivation in the laboratory (32, 40). Spontaneous mutants affected in magnetosome formation accumulated with a frequency of up to 10^{-2} after prolonged storage or exposure to oxidative stress and had all lost partial or complete *mms* and *mam* gene clusters encoding magnetosome proteins, as well as various copies of sequence repeats (40). This led to the hypothesis that the observed instability was caused by RecA-mediated homologous recombination, as also observed in other organisms like *Mycobacterium bovis* (29).

RecA is a ubiquitous and highly conserved protein. In *Escherichia coli*, RecA catalyzes strand exchanges between homologous DNA molecules via RecA–single-stranded DNA (ssDNA) complexes. Furthermore, it also plays a key role in signal transduction following DNA damage. Therefore, RecA binds ssDNA generated by DNA damage. The activated RecA complex then induces the SOS repair functions (25). Loss of RecA is associated with higher sensitivity to DNA damage and severe growth and recombination deficiency phenotypes (6–8, 23, 39). In two early studies, the *recA* gene of *M. magnetotacticum* MS-1 was shown to complement a *recA*-deficient *E. coli* strain with respect to recombination and DNA repair deficiency (2, 3). However, nothing is known about the physiological function of RecA in MTB and its involvement in the observed genetic rearrangements.

In this study, we constructed a RecA-deficient mutant strain of *M. gryphiswaldense*. Compared to the wild type (WT), strain IK-1 displays increased UV and oxygen sensitivity and decreased homologous recombination ability. Furthermore, the mutant no longer exhibits spontaneous mutations within MAI genes, indicating that the genetic instability of the WT depends on RecA activity. Its increased genetic stability may render the *recA* mutant strain a useful tool for gene expression and genetic engineering of *M. gryphiswaldense*.

MATERIALS AND METHODS

Bacterial strains, media, and growth conditions. The bacterial strains and plasmids used in this study are shown in Table 1. *E. coli* strains were cultivated in lysogeny broth (4) supplemented with 25 μg/ml kanamycin (Km), 12 μg/ml tetracycline (Tet), and 15 μg/ml gentamicin as previously described (16). For growth of *E. coli* BW29427 (kindly provided by B. Wanner, Purdue University, West Lafayette, IN), LB was supplemented with DL-α,ε-diaminopimelic acid (Sigma-Aldrich, Steinheim, Germany) to a final concentration of 1 mM. Liquid cultures and single colonies of *Magnetospirillum* strains were cultivated in FSM

* Corresponding author. Mailing address: Ludwig-Maximilians-Universität München, Department Biologie I, Bereich Mikrobiologie, Biozentrum der LMU, Großhaderner Str. 4, 82152 Planegg-Martinsried, Germany. Phone: 4989218074502. Fax: 4989218074515. E-mail: dirk.schueler@lmu.de.

‡ Present address: Harvard Medical School, 200 Longwood Avenue, Boston, MA.

† Supplemental material for this article may be found at http://jb.asm.org/.

▽ Published ahead of print on 5 August 2011.

TABLE 1. Bacterial strains and plasmids used in this study

Strain or plasmid	Characteristic(s)	Reference(s) or source
Strains		
M. gryphiswaldense		
MSR-1 R3/S1	WT (spontaneous Rif^r Sm^r mutant)	37
MSR-1 IK-1	R3/S1 Δ*recA*	This study
E. coli		
DH5α	F^- ϕ80*lacZ*ΔM15 Δ(*lacZYA-argF*)*U169 recA1 endA1 hsdR17* (r_K^- m_K^+) *phoA supE44* λ^- *thi-1 gyrA96 relA1*	Invitrogen
BW29427	*dap* mutant auxotrophic derivative of *E. coli* strain B2155	K. Datsenko and B. L. Wanner, unpublished data
Plasmids		
pJet 1.2/blunt	Ap^r, *eco47IR* (lethal restriction enzyme gene), *rep* (pMB-1)	Fermentas
pJetIB013+014	pJet containing the upstream fragment of the *recA* gene	This study
pJetIB015+016	pJet containing the downstream fragment of the *recA* gene	This study
pCM184	Ap^r Km^r Tet^r; broad-host-range allelic exchange vector	20
pCM184+*recAflank*	pCM184 with 1.6- and 1.8-kb up- and downstream fragments of *recA*	This study
pCM157	Tet^r; Cre recombinase expression vector	20
pBBR1MCS5	Km^r; mobilizable broad-host-range vector	19
pBBR1MCS5*recA*	pBBR1MCS5 containing *recA*	This study
pAL01	Km^r; pK19mobGII vector (Km^r, pMB-1 replicon, *gusA*, *lacZ*) containing a 2-kb fragment upstream of *mgr4019*	A. Lohße, unpublished data

medium (13) or on agar plates incubated at 30°C under aerobic, microaerobic, or anaerobic conditions. For aerobic growth, cells were cultivated in free gas exchange with air. For microaerobic and anaerobic conditions, flasks were sealed with butyl rubber stoppers and flushed before autoclaving with an atmosphere of 1% O_2-99% N_2 (microaerobic conditions) or N_2 (anaerobic conditions). Liquid cultures were agitated at 130 rpm under aerobic and microaerobic conditions. Agar plates were incubated in anaerobic jars in a 1% O_2-99% N_2 or N_2 atmosphere. For growth from single colonies, cells were transferred into 100 μl FSM medium in 96-deep-well plates (Eppendorf, Hamburg, Germany). Plates were incubated in anaerobic jars for 5 to 6 days. The volume was gradually increased by the addition of 200 μl to a final volume of 800 μl.

Molecular, biological, and genetic techniques. Unless specified otherwise, standard protocols were used as described previously (28). DNA was sequenced using BigDye Terminator v3.1 chemistry on an in-house ABI 3700 capillary sequencer. Sequences were analyzed with the Vector NTI (Invitrogen) program. Primers (see Table S1 in the supplemental material) were purchased from Sigma-Aldrich (Steinheim, Germany). Conjugation experiments were performed as described before (37, 38), with the following modifications. MSR-1 cells (2×10^9) were mixed with strain BW29427 cells and incubated microaerobically for 12 h on activated charcoal agar medium. Cells were rinsed from the agar surface, and a 1:5 dilution was plated on FSM agar supplemented with appropriate antibiotics. Transconjugants were screened after incubation for 7 to 10 days in anaerobic jars under microaerobic conditions.

Analytical methods. The optical density at 565 nm (OD_{565}) and magnetic response (C_{mag}) of *M. gryphiswaldense* cultures were measured turbidimetrically as previously described (36, 47). Intracellular iron concentrations were measured after incubation under anaerobic conditions using a modified version of the ferrozine assay (42). One-milliliter cultures were centrifuged for 1 min at 11,000 rpm and resuspended in 90 μl HNO_3 (65%) for 3 h at 99°C. Afterwards, the lysate was cleared by centrifugation and resuspended in 50 μl ammonium acetate.

Transmission electron microscopy (TEM) was performed as previously described (16). For differential interference contrast (DIC) microscopy using an Olympus IX81 inverted microscope, 5 μl of liquid culture was fixed on an agar pad.

Generation of *recA* deletion strain IK-1. A *cre-lox*-based method was used (20, 30, 41) to generate an unmarked Δ*recA* mutant strain as described elsewhere (see Fig. S1 in the supplemental material). First, 1.8- and 1.6-kb fragments up- and downstream of the *recA* gene (*mgr2512*) were amplified, respectively, with Phusion polymerase (NEB GmbH, Frankfurt am Main, Germany) and cloned into the pJet 1.2/blunt vector (Fermentas GmbH, St. Leon-Rot, Germany) to yield pJetIB013+014 (pJet containing the upstream fragment) and pJetIB015+016 (pJet carrying the downstream fragment). Plasmid pJetIB013+014 was digested with BglII and NcoI, and the 1.8-kb upstream fragment was inserted into suicide plasmid pCM184. The resulting plasmid, pCM184+IB013+014, and pJetIB015+016 similarly digested with MluI and AgeI were religated to yield pCM184*recAflank*. After verification by PCR (primers IB013 and IB014 and primers IB016 and IB017), the plasmid was transferred into *M. gryphiswaldense* R3/S1 (WT) by conjugation. Correct insertion was verified via PCR using primers IB017 and IB018, IB013 and 54rv, or IB014 and 61fw, respectively. In the last step, putative deletions were checked via Southern blot analysis (see Fig. S1E in the supplemental material). For Southern blot analysis, 5 μg of KpnI-digested genomic WT or Δ*recA* DNA was hybridized with a [α-^{32}P]dATP-labeled *recA* probe (primers IB017 and IB018) and excision of the Km resistance cassette was performed by transferring plasmid pCM157 expressing Cre recombinases. One positive clone was cured of plasmid pCM157 by passaging the cells 10 times in FSM medium in the absence of Km selection. Loss of the Km resistance cassette was verified via PCR and spotting on FSM-Km agar. The mutant strain was named *M. gryphiswaldense* IK-1.

UV irradiation assay. At an OD_{565} of 0.15, 20-ml volumes of *M. gryphiswaldense* cultures were harvested and washed twice in 10 ml $MgSO_4$ (0.1 M). A 5-ml volume of the suspension were transferred into sterile petri dishes (lids removed). After empirical testing of different irradiation intensities in a Biolink DNA cross-linker (Biometra GmbH, Göttingen, Germany), a dose of 15 mJ/cm^2 was considered to be most appropriate. After UV irradiation, cells were harvested, resuspended in 10 ml FSM medium, and incubated for 12 h at 30°C. The OD_{565} was adjusted to 0.04, and 1-ml aliquots were plated on FSM agar. Colonies were counted after 7 days of microaerobic incubation.

Induction and screening of MAI mutants. Twelve clones each of the WT and strain IK-1 were incubated in 100 μl FSM within the microwells of a 96-well plate (Sigma-Aldrich, Steinheim, Germany) at 4°C under microaerobic conditions for 1 week (see Fig. S2 in the supplemental material). This was followed by six cycles of growth to saturation for 48 h per cycle (without shaking) at 30°C under microaerobic conditions. Subsequently, 5 μl of each of the 12 cultures was spotted onto FSM agar (250 μM Fe) in several dilutions (1/10 to 1/100,000), incubated at 30°C under anaerobic conditions, and then visually screened for the appearance of white colonies. Twenty-four white colonies were randomly picked and cultured for further investigations.

Recombination assay. The suicide plasmid pAL01, carrying a region homologous to a 2-kb sequence within the MAI (upstream of *mgr4019*), was transferred into the WT, strain IK-1, and transcomplemented strain IK-1+/pBBR1MCS5*recA* via conjugation. We used 4×10^8 recipient cells per conjugation experiment. Colonies were counted after 7 days of incubation, and recombination efficiency was calculated.

RESULTS

Construction and characterization of Δ*recA* mutant *M. gryphiswaldense* strain IK-1. The *recA* gene from *M. gryphiswaldense* (NCBI accession no. CU459003) is located on contig1066 of the partial genome sequence (27). The predicted protein sequence (358 amino acids; molecular mass, 38 kDa) is 91% identical to that of *M. magneticum* AMB-1 and 68% identical to that of *E. coli*. Downstream, *recA* is adjacent to a gene encoding a putative sensor histidine kinase (*mgr2511*), and upstream, it is adjacent to *secA* (*mgr2513*), encoding a putative translocator protein (see Fig. S1A in the supplemental material). Similar to the organization in other bacteria like *E. coli* (14), *recA* of *M. gryphiswaldense* is likely to be monocistronic.

To analyze the function of RecA, deletion mutant strain *M. gryphiswaldense* IK-1 was constructed by allelic exchange. IK-1 showed growth characteristics similar to those of the WT under microaerobic and anaerobic conditions (Fig. 1), whereas its doubling time was increased under aerobic incubation conditions (WT doubling time, 5.0 h; IK-1 doubling time, 7.4 h). The C_{mag} values of IK-1 were lower than those of the WT under microaerobic and anaerobic conditions (WT microaerobic C_{mag}, 1.4; IK-1 microaerobic C_{mag}, 0.9; WT anaerobic C_{mag}, 1.5, IK-1 anaerobic C_{mag}, 0.9). However, strain IK-1 had an intracellular iron content similar to that of the WT (WT, 3.5% of dry weight; IK-1, 3.9% of dry weight) and similar sizes (Mann-Whitney *P* value, ≥0.05) and numbers (WT, 29; IK-1, 27) of crystals per cell (Fig. 2A and D). TEM (Fig. 2D) and DIC (Fig. 2B and C) analyses revealed a variable proportion of elongated and small vibrioid cells. Fifty-eight percent of the cells of the mutant were smaller than 3 μm, 38% of the larger cells (3 to 10 μm) were spiral shaped, and 2% of the cells were aberrantly elongated (≥10 μm) under microaerobic conditions after 24 h of incubation. In contrast, WT cultures contained 41% short vibrioid cells, 58% larger spiral-shaped cells, and 0.16% aberrantly long cells. Under aerobic conditions, the numbers of elongated cells of both IK-1 (13%) and WT (2%) were increased, consistent with a decreased number of short vibrioid cells (IK-1, 6.4%; WT, 2%). Also, if the bacteria were incubated under anaerobic conditions at 25°C, i.e., in the absence of oxidative and temperature stress, the percentage of elongated cells was still higher in the mutant (4% and 1%, respectively).

IK-1 is more sensitive to UV light. Since *recA* deletion mutants of other bacteria were shown to be more sensitive to UV light exposure (1, 26, 44) due to their inability to induce an SOS response (21, 43), we performed irradiation assays. UV sensitivity, measured by determining the number of surviving CFU/ml, was 28-fold higher in the mutant than in the WT (Fig. 3B). Whereas the WT count was 1.38×10^3 CFU/ml (survival rate, 7.8×10^{-5}) after irradiation, that of the mutant under the same conditions was 49.7 CFU/ml (survival rate, 4.1×10^{-6}). Increased UV sensitivity could be partially restored by providing the WT *recA* gene in *trans* on plasmid pBBR1MCS5*recA* (survival rate, 1.78×10^{-5}; 2.13×10^2 CFU/ml).

IK-1 is impaired in homologous recombination. To test whether homologous recombination was impaired in IK-1, the chromosomal integration of a suicide plasmid (pAL01) carrying a region homologous to a 2-kb chromosomal fragment was investigated (Fig. 3A). Kan^r transconjugants were counted, and recombination efficiency was calculated by considering the number of recipient cells per conjugation. Whereas only very few Km^r colonies (a total of four clones) were obtained in the Δ*recA* background (efficiency, 3.3×10^{-9}), the efficiency of the WT strain was 80-fold higher (2.7×10^{-7}). Recombination efficiency was restored to the WT level in the transcomplemented mutant strain IK-1+/pBBR1MCS5*recA* (3×10^{-7}).

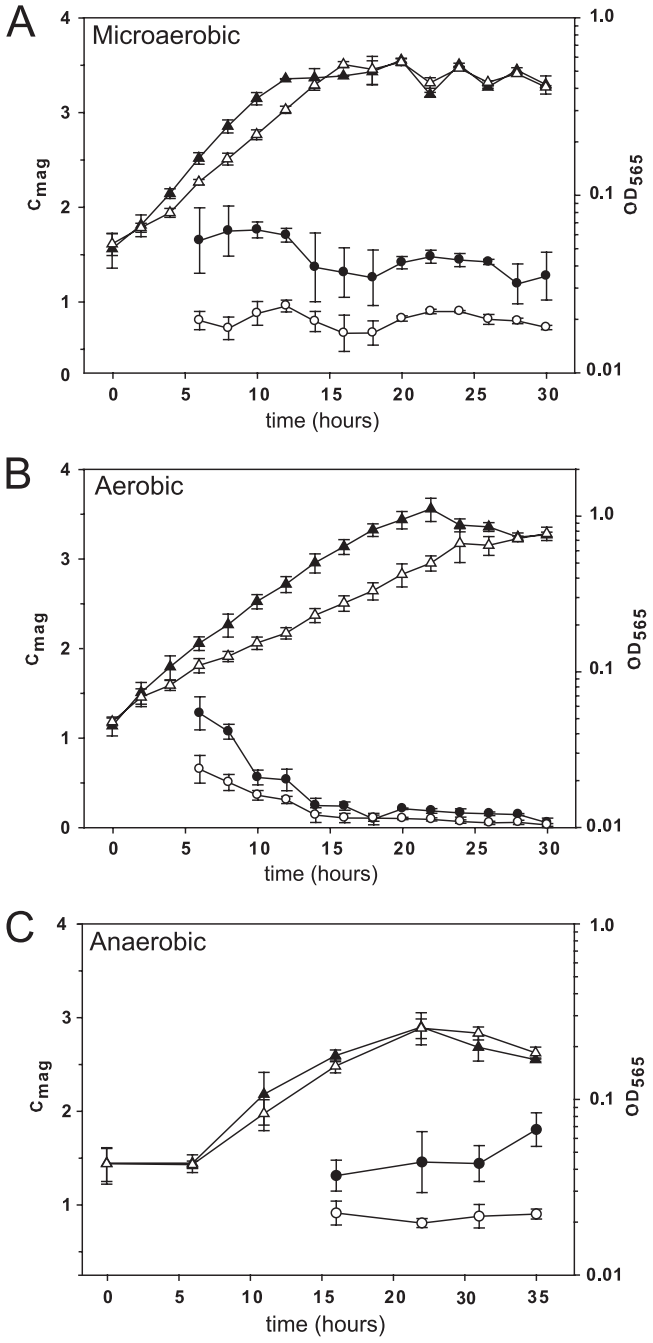

FIG. 1. Growth (OD_{565}) and C_{mag} of *M. gryphiswaldense* IK-1 and the WT (●, WT C_{mag}; ○, IK-1 C_{mag}; ▲, WT OD_{565}; Δ, IK-1 OD_{565}) during incubation for 30 h under microaerobic (A), aerobic (B), and anaerobic (C) conditions.

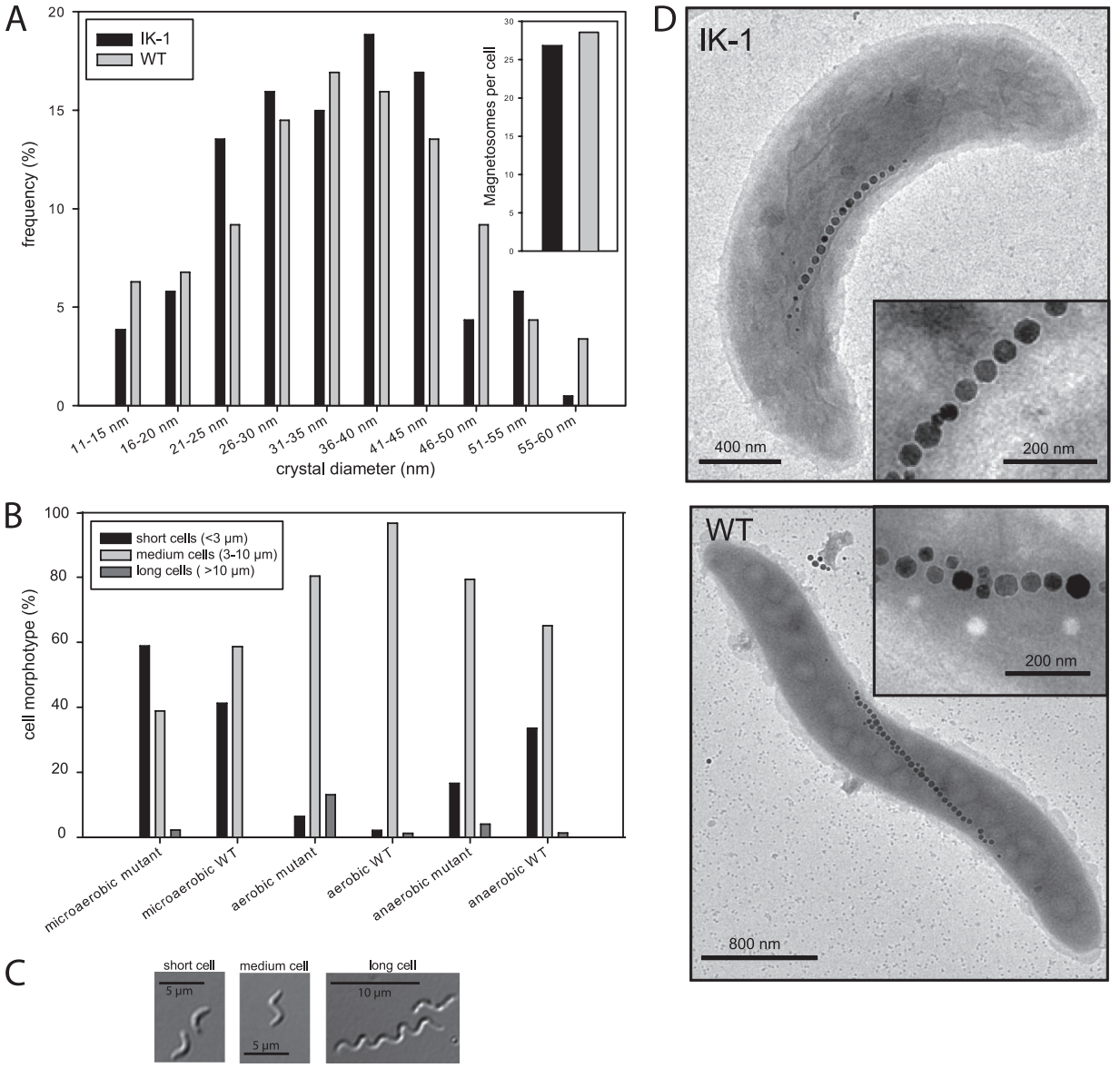

FIG. 2. (A) Magnetosome size distributions under anaerobic conditions (Mann-Whitney *P* value, ≥0.05) in IK-1 and the WT. (B) Distributions of different cell sizes of strain IK-1 and the WT were estimated. Morphotypes were investigated under aerobic, microaerobic, and anaerobic conditions. (C) DIC micrographs showing representative short, medium, and long cells. (D) TEM of the WT and strain IK-1. For TEM pictures, cells were incubated at 30°C under microaerobic conditions.

***M. gryphiswaldense* IK-1 displays increased genetic stability of the MAI under physiological stress conditions.** To assess the occurrence of spontaneous mutants in the WT and strain IK-1, we established an incubation regime for the efficient induction and isolation of mutants with either a weakly magnetic or a nonmagnetic phenotype (see Fig. S2 in the supplemental material). Cells were stored at 4°C for 1 week under microaerobic conditions. Afterwards, aliquots were spotted onto plates and colonies of the mutant strain and the WT were enumerated. Under oxygen-limited or anaerobic conditions, magnetite-synthesizing colonies of *M. gryphiswaldense* are dark brown (Mag^+), whereas clones which have lost the ability to produce magnetite (Mag^-) can be clearly distinguished by their whiteness (32) (see Fig. S2B). While no white clones were detectable among >10,000 clones of strain IK-1, 22% (60 out of 267) clones of the WT were white and thus seemed to be weakly magnetic or nonmagnetic. Of 24 randomly picked white clones, 18 proved to be completely nonmagnetic (Mag^-) upon subcultivation, whereas the C_{mag} of 5 clones was decreased (0.01 to 0.4) and 1 clone had a WT-like C_{mag} of 1.7 (Mag^+). All 18 Mag^- mutants were screened by PCR for deletions or rearrangements within the *mamAB* operon, which was previously shown to be essential for magnetosome formation in *Magnetospirillum* (22, 41). We failed to amplify fragments of the expected size from 11 Mag^- clones for at least one of the following gene regions: *mamH-mamE*, *mamM-mamN*, *mamO-mamA*, *mamQ-mamS*, *mamT-mamU*, and *mamJ-mamL*.

In six clones, the *mamH-mamE* region was absent, whereas

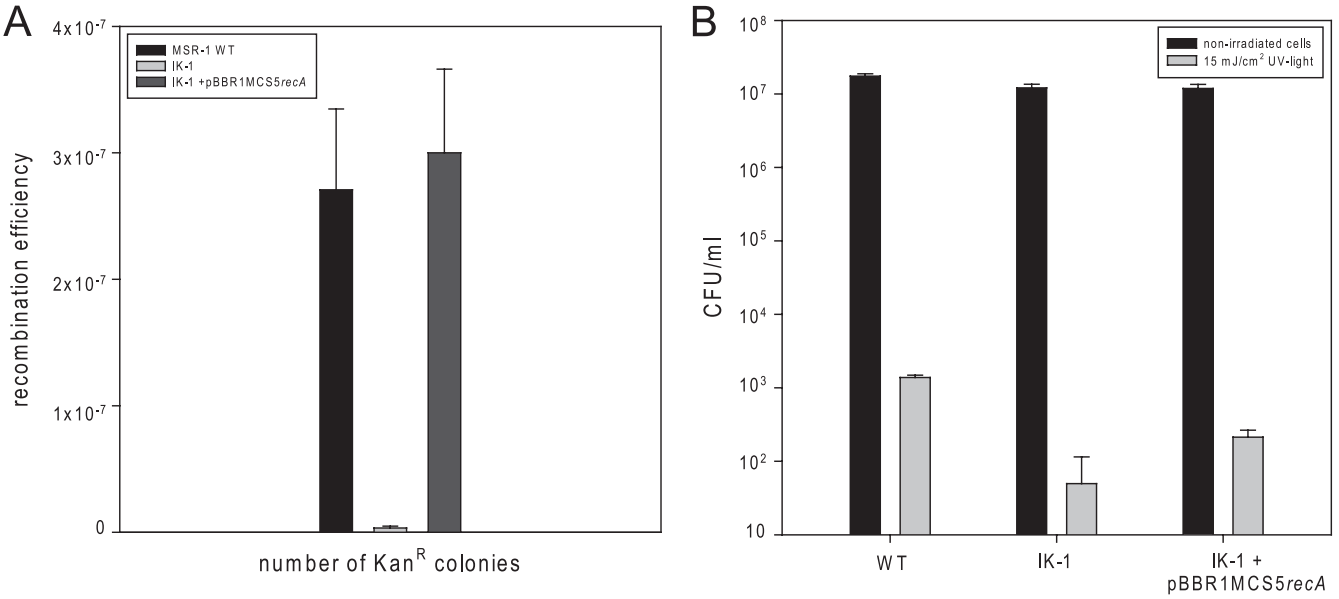

FIG. 3. (A) Recombination assay results. A suicide vector carrying a 2-kb insert homologous to a partial region of the MAI was transferred into the WT and the *recA* mutant. The frequency of cells with genomic insertions was estimated by the number of Km-resistant clones after 7 days of microaerobic incubation (4×10^8 recipient cells per conjugation). (B) UV irradiation assay results. Cells were irradiated with 15 mJ/cm^2 UV light. Both assays were performed in triplicates. Survival rates (CFU/ml) after irradiation were estimated after 7 days of microaerobic incubation.

in clones 8 and 15, a product 1 kb larger than expected was amplified. We failed to amplify a product of the expected size for *mamJ-mamL* from five clones, whereas in two of them (clones 10 and 12), the size of the PCR product was about 2 kb larger than that obtained from the WT, which is consistent with previous observations that *mamJ*, which harbors a repetitive and hypervariable domain, undergoes frequent rearrangements (32). The *mamO-mamA* region was absent from six clones, and *mamQ-mamS* was absent from five clones (Table 2; see Fig. S3 in the supplemental material). The *mamT-mamU* region was not detectable in two clones, whereas *mamM-mamN* seemed to be present in all of the spontaneous mutants. No modifications within the *mamAB* operon of seven Mag$^-$ mutants could be detected via PCR.

DISCUSSION

Analysis of RecA in MTB has so far been limited to the complementation of an *E. coli recA* mutant by the *M. magnetotacticum* gene (2). In this study, we generated and analyzed

TABLE 2. Results of PCR amplification of various regions within the *mamAB* operon from the spontaneous Mag$^-$ mutants of the WT strain[a]

Clone	Presence of following amplification product:					
	mamH-mamE (3.8 kb)	*mamJ-mamL* (2.7 kb)	*mamM-mamN* (2.2 kb)	*mamO-mamA* (3.4 kb)	*mamQ-mamS* (2.5 kb)	*mamT-mamU* (1.4 kb)
1	−	−	+	−	−	−
3	−	−	+	−	−	+
4	−	+	+	−	−	−
6	−	+	+	−	−	+
7	+	−	+	+	+	+
8	0	+	+	+	+	+
9	−	+	+	−	−	+
10	+	0	+	+	+	+
11	−	+	+	+	+	+
12	+	0	+	+	+	+
13	+	+	+	+	+	+
14	+	+	+	+	+	+
15	0	+	+	−	+	+
16	+	+	+	+	+	+
19	+	+	+	+	+	+
20	+	+	+	+	+	+
22	+	+	+	+	+	+
23	+	+	+	+	+	+

[a] Six regions were probed by PCR. The presence of bands was detected by agarose gel electrophoresis (see Fig. S2 in the supplemental material). −, no product detectable; +, product detectable; 0, product of aberrant size detectable.

the first *recA* mutant of a magnetotactic bacterium. Deletion of *recA* had only moderate effects on the growth rates of *M. gryphiswaldense* under aerobic conditions, indicating that *recA* is not essential for growth and magnetosome formation. This is in contrast to other bacteria like *Streptomyces lividans*, where difficulties due to essentiality in generating a full-length *recA* deletion have been suspected (23). As previously described for *E. coli*, deletions of *recA* resulted in growth defects and decreased viability (6). Under aerobic but not microaerobic and anaerobic conditions, exponential growth of *M. gryphiswaldense* IK-1 was delayed. A similar effect was also described for a *Lactococcus lactis recA* mutant and attributed to damage by hydroxyl radicals (OH^-) produced in the Fenton reaction during aerobic growth (10). In *M. gryphiswaldense*, a growth delay under aerobic conditions thus may also result from the inability to induce DNA repair mechanisms after damage via reactive oxygen species.

Although decreased C_{mag} values were measured for the mutant, a comparison of the size and number of magnetosomes and the intracellular iron content revealed no differences from the WT, which argues against a direct effect on magnetosome formation. Instead, the observed changes in cell dimensions and shapes likely account for the reduced magnetic response of the mutant. Measurement of the C_{mag} value is based on an optical method whereby cells are aligned parallel to the lines in a magnetic field, resulting in a change in light scattering (36). Therefore, slight deviations in cell shape might lead to differences in absorbance. An effect on cell shape and size (i.e., an increased proportion of elongated cells) was reported in a *recA*-deficient *Leptospira biflexa* strain, which was attributed to DNA segregation problems (39) and may also explain the phenotype of IK-1.

The survival rate of the IK-1 mutant strain was 28-fold lower than that of the WT, suggesting a role for the *recA* gene in stress response activation in *M. gryphiswaldense*. After transfer of the *recA* gene, partial restoration of UV sensitivity was observed. Nevertheless, the transcomplemented mutant still showed a survival rate lower than that of the WT. However, an intermediate rate of transcomplementation was also shown for other genes of *M. gryphiswaldense* (31, 46). Most notably, homologous recombination was decreased 80-fold in IK-1. Compared to other recombination-deficient mutants, such as *Rhodopseudomonas viridis* (7), *Agrobacterium tumefaciens* (11), or *E. coli* (8), where the difference in recombination efficiency was at least 10^3, the 80-fold decrease in *M. gryphiswaldense* is relatively small. However, even in the WT, the activity of RecA seems to be relatively low, as the observed frequencies of plasmid insertion were also significantly lower (2.7×10^{-7}) than those reported for other bacteria, e.g., 10^{-5} to 10^{-6} in *E. coli* (45).

Very few Km^r clones (4 transconjugants out of 1.2×10^9 recipients) were observed after conjugation of the suicide plasmids into the *recA* mutant strain. These mutants might have arisen by genomic insertion via RecA-independent recombination events, which are known to occur at low frequencies and are less responsive to the extent of homology (9). Transcomplementation of the mutant strain resulted in a frequency of homologous recombination slightly higher than that of the WT (WT, 2.7×10^{-7}; transcomplemented mutant, 3×10^{-7}). As allelic replacement in MTB has remained tedious due to poor recombination efficiency, transient overexpression of the *recA* gene thus might provide a way to enforce the construction of mutants in future approaches.

It was shown in previous studies that spontaneous MAI mutants affected in magnetosome formation might occur at a high frequency upon subcultivation and storage in the laboratory (32, 40). The mutations were polymorphic with respect to the sites and extents of deletions, but all mutations were found to be associated with the loss of various copies of insertion elements, most of which correspond to similar copies of transposase genes. In *M. gryphiswaldense*, 42 transposase genes were identified, which indicates that the MAI has been a genomic hot spot for multiple transposition events, which may account for its genetic instability (15). The rearrangements and deletions within the MAI hamper the analysis of magnetosome formation and may obscure genetic analysis results. A mechanism was postulated in which deletions are caused by homologous recombination between two identical insertion sequence repeat copies by a RecA-dependent mechanism. The incubation scheme used proved to be more efficient than previous approaches (10^{-2}) (40) in yielding a range of Mag^- phenotypes, which could be explained by the combination of different physiological stress conditions (temperature, starvation during stationary growth, and oxidative stress). Similar approaches were used before to isolate spontaneous pleiotropic mutants of several *Pseudomonas* species after stationary growth in nutrient-rich liquid medium for several days and correlate with a selective advantage for the cells (5, 12). We found up to 22% of the WT colonies to have pleiotropic magnetosome phenotypes, with 61% of the Mag^- clones harboring gene deletions. Furthermore, from 4 clones (8, 10, 12, and 15), PCR products with sizes differing from those expected were obtained, which might be due to rearrangement events within parts of the *mamAB* operon. Nevertheless, in 7 Mag^- mutants, no modifications within the *mamAB* operon could be detected via PCR. The residual Mag^- clones might be due to point mutations or rearrangements in genes or outside the *mamAB* operon. In contrast, we were unable to identify any white colonies among the >10,000 visually screened clones of the *recA* mutant strain. This supports the conclusion that the observed genetic instability within the MAI is, in fact, due to the activity of the RecA protein. Its significantly increased genetic stability in the absence of RecA also makes strain IK-1 a promising tool for the expression of genes and further genetic engineering, as well as the biotechnological production of bacterial magnetosomes.

REFERENCES

1. **Bender, R. A.** 1984. Ultraviolet mutagenesis and inducible DNA repair in *Caulobacter crescentus*. Mol. Gen. Genet. **197:**399–402.
2. **Berson, A. E., D. V. Hudson, and N. S. Waleh.** 1989. Cloning and characterization of the *recA* gene of *Aquaspirillum magnetotacticum*. Arch. Microbiol. **152:**567–571.
3. **Berson, A. E., M. R. Peters, and N. S. Waleh.** 1990. Nucleotide sequence of *recA* gene of *Aquaspirillum magnetotacticum*. Nucleic Acids Res. **18:**675.
4. **Bertani, G.** 2004. Lysogeny at mid-twentieth century: P1, P2, and other experimental systems. J. Bacteriol. **186:**595–600.
5. **Bull, C. T., et al.** 2001. Characterization of spontaneous *gacS* and *gacA* regulatory mutants of *Pseudomonas fluorescens* biocontrol strain CHAO. Antonie Van Leeuwenhoek **79:**327–336.
6. **Capaldo, F. N., G. Ramsey, and S. D. Barbour.** 1974. Analysis of the growth of recombination-deficient strains of *Escherichia coli* K-12. J. Bacteriol. **118:** 242–249.
7. **Cheng, P., and H. Michel.** 1998. Cloning, sequencing, and characterization of

the *recA* gene from *Rhodopseudomonas viridis* and construction of a *recA* strain. J. Bacteriol. **180:**3227–3232.
8. **Clark, A. J., and A. D. Margulies.** 1965. Isolation and characterization of recombination-deficient mutants of *Escherichia coli* K12. Proc. Natl. Acad. Sci. U. S. A. **53:**451–459.
9. **Dutra, B. E., V. A. Sutera, Jr., and S. T. Lovett.** 2007. RecA-independent recombination is efficient but limited by exonucleases. Proc. Natl. Acad. Sci. U. S. A. **104:**216–221.
10. **Duwat, P., S. D. Ehrlich, and A. Gruss.** 1995. The *recA* gene of *Lactococcus lactis*: characterization and involvement in oxidative and thermal stress. Mol. Microbiol. **17:**1121–1131.
11. **Farrand, S. K., S. P. O'Morchoe, and J. McCutchan.** 1989. Construction of an *Agrobacterium tumefaciens* C58 *recA* mutant. J. Bacteriol. **171:**5314–5321.
12. **Fox, A., et al.** 2008. Emergence of secretion-defective sublines of *Pseudomonas aeruginosa* PAO1 resulting from spontaneous mutations in the *vfr* global regulatory gene. Appl. Environ. Microbiol. **74:**1902–1908.
13. **Heyen, U., and D. Schüler.** 2003. Growth and magnetosome formation by microaerophilic *Magnetospirillum* strains in an oxygen-controlled fermentor. Appl. Microbiol. Biotechnol. **61:**536–544.
14. **Horii, T., T. Ogawa, and H. Ogawa.** 1980. Organization of the *recA* gene of *Escherichia coli*. Proc. Natl. Acad. Sci. U. S. A. **77:**313–317.
15. **Jogler, C., et al.** 2009. Comparative analysis of magnetosome gene clusters in magnetotactic bacteria provides further evidence for horizontal gene transfer. Environ. Microbiol. **11:**1267–1277.
16. **Jogler, C., et al.** 2009. Toward cloning of the magnetotactic metagenome: identification of magnetosome island gene clusters in uncultivated magnetotactic bacteria from different aquatic sediments. Appl. Environ. Microbiol. **75:**3972–3979.
17. **Jogler, C., et al.** 2010. Cultivation-independent characterization of '*Candidatus* Magnetobacterium bavaricum' via ultrastructural, geochemical, ecological and metagenomic methods. Environ. Microbiol. **12:**2466–2478.
18. **Jogler, C., et al.** 2011. Conservation of proteobacterial magnetosome genes and structures in an uncultivated member of the deep-branching Nitrospira phylum. Proc. Natl. Acad. Sci. U. S. A. **108:**1134–1139.
19. **Kovach, M. E., et al.** 1995. Four new derivatives of the broad-host-range cloning vector pBBR1MCS, carrying different antibiotic-resistance cassettes. Gene **166:**175–176.
20. **Marx, C. J., and M. E. Lidstrom.** 2002. Broad-host-range cre-lox system for antibiotic marker recycling in gram-negative bacteria. Biotechniques **33:** 1062–1067.
21. **Michel, B.** 2005. After 30 years of study, the bacterial SOS response still surprises us. PLoS Biol. **3:**e255.
22. **Murat, D., A. Quinlan, H. Vali, and A. Komeili.** 2010. Comprehensive genetic dissection of the magnetosome gene island reveals the step-wise assembly of a prokaryotic organelle. Proc. Natl. Acad. Sci. U. S. A. **107:**5593–5598.
23. **Muth, G., D. Frese, A. Kleber, and W. Wohlleben.** 1997. Mutational analysis of the *Streptomyces lividans recA* gene suggests that only mutants with residual activity remain viable. Mol. Gen. Genet. **255:**420–428.
24. **Nakazawa, H., et al.** 2009. Whole genome sequence of *Desulfovibrio magneticus* strain RS-1 revealed common gene clusters in magnetotactic bacteria. Genome Res. **19:**1801–1808.
25. **Neidhardt, F. C., et al. (ed.).** 1996. *Escherichia coli* and *Salmonella*: cellular and molecular biology, 2nd ed., vol. 2. ASM Press, Washington, DC.
26. **O'Neill, E. A., R. H. Hynes, and R. A. Bender.** 1985. Recombination deficient mutant of *Caulobacter crescentus*. Mol. Gen. Genet. **198:**275–278.
27. **Richter, M., et al.** 2007. Comparative genome analysis of four magnetotactic bacteria reveals a complex set of group-specific genes implicated in magnetosome biomineralization and function. J. Bacteriol. **189:**4899–4910.
28. **Sambrook, J., and D. W. Russell.** 2001. Molecular cloning: a laboratory manual, 3rd ed. Cold Spring Harbor Laboratory Press, Cold Spring Harbor, NY.
29. **Sander, P., et al.** 2003. A *recA* deletion mutant of *Mycobacterium bovis* BCG confers protection equivalent to that of wild-type BCG but shows increased genetic stability. Vaccine **21:**4124–4127.
30. **Scheffel, A., A. Gardes, K. Grünberg, G. Wanner, and D. Schüler.** 2008. The major magnetosome proteins MamGFDC are not essential for magnetite biomineralization in *Magnetospirillum gryphiswaldense* but regulate the size of magnetosome crystals. J. Bacteriol. **190:**377–386.
31. **Scheffel, A., and D. Schüler.** 2007. The acidic repetitive domain of the *Magnetospirillum gryphiswaldense* MamJ protein displays hypervariability but is not required for magnetosome chain assembly. J. Bacteriol. **189:**6437–6446.
32. **Schübbe, S., et al.** 2003. Characterization of a spontaneous nonmagnetic mutant of *Magnetospirillum gryphiswaldense* reveals a large deletion comprising a putative magnetosome island. J. Bacteriol. **185:**5779–5790.
33. **Schübbe, S., et al.** 2006. Transcriptional organization and regulation of magnetosome operons in *Magnetospirillum gryphiswaldense*. Appl. Environ. Microbiol. **72:**5757–5765.
34. **Schüler, D.** 2008. Genetics and cell biology of magnetosome formation in magnetotactic bacteria. FEMS Microbiol. Rev. **32:**654–672.
35. **Schüler, D.** 2004. Molecular analysis of a subcellular compartment: the magnetosome membrane in *Magnetospirillum gryphiswaldense*. Arch. Microbiol. **181:**1–7.
36. **Schüler, D., R. R. Uhl, and E. Bäuerlein.** 1995. A simple light scattering method to assay magnetism in *Magnetospirillum gryphiswaldense*. FEMS Microbiol. Ecol. **132:**139–145.
37. **Schultheiss, D., M. Kube, and D. Schüler.** 2004. Inactivation of the flagellin gene *flaA* in *Magnetospirillum gryphiswaldense* results in nonmagnetotactic mutants lacking flagellar filaments. Appl. Environ. Microbiol. **70:**3624–3631.
38. **Schultheiss, D., and D. Schüler.** 2002. Development of a genetic system for *Magnetospirillum gryphiswaldense*. Arch. Microbiol. **179:**89–94.
39. **Tchamedeu Kameni, A. P., E. Couture-Tosi, I. Saint-Girons, and M. Picardeau.** 2002. Inactivation of the spirochete *recA* gene results in a mutant with low viability and irregular nucleoid morphology. J. Bacteriol. **184:**452–458.
40. **Ullrich, S., M. Kube, S. Schübbe, R. Reinhardt, and D. Schüler.** 2005. A hypervariable 130-kilobase genomic region of *Magnetospirillum gryphiswaldense* comprises a magnetosome island which undergoes frequent rearrangements during stationary growth. J. Bacteriol. **187:**7176–7184.
41. **Ullrich, S., and D. Schüler.** 2010. Cre-lox-based method for generation of large deletions within the genomic magnetosome island of *Magnetospirillum gryphiswaldense*. Appl. Environ. Microbiol. **76:**2439–2444.
42. **Viollier, E., P. W. Inglett, K. Hunter, A. N. Roychoudhury, and P. Van Cappellen.** 2000. The ferrozine method revisited: Fe(II)/Fe(III) determination in natural waters. Appl. Geochem. **15:**785–790.
43. **Walker, G. C.** 1984. Mutagenesis and inducible responses to deoxyribonucleic acid damage in *Escherichia coli*. Microbiol. Rev. **48:**60–93.
44. **Witkin, E. M.** 1976. Ultraviolet mutagenesis and inducible DNA repair in *Escherichia coli*. Bacteriol. Rev. **40:**869–907.
45. **Wollman, E. L., F. Jacob, and W. Hayes.** 1956. Conjugation and genetic recombination in *Escherichia coli* K-12. Cold Spring Harb. Symp. Quant. Biol. **21:**141–162.
46. **Yang, W., et al.** 2010. *mamO* and *mamE* genes are essential for magnetosome crystal biomineralization in *Magnetospirillum gryphiswaldense* MSR-1. Res. Microbiol. **161:**701–705.
47. **Zhao, L., D. Wu, L. F. Wu, and T. Song.** 2007. A simple and accurate method for quantification of magnetosomes in magnetotactic bacteria by common spectrophotometer. J. Biochem. Biophys. Methods **70:**377–383.

Supplementary material

Table S1: Oligonucleotides used in this study. Underlined sequences indicate restriction sites.

Primer	Nucleotide sequence (5´-3´)[a]	Product
IB009-for	CGCACAAGCTGTTCACCAAGG	flanking region of the *recA* gene
IB010-rev	TCATCATCAATCTGGCGGTCA	
IB011-for	CGCACCGAGGCATAGAACT	flanking region of the *recA* gene
IB012-rev	TCGAGGAAACGCTCAGACG	
IB013-for	GACGTCGGCGTCGATCACCTTCCAGAA	upstream fragment of the *recA* gene
IB014-rev	AGATCTTGCCAATCCCGCTCGGTC	
IB015-for	ACGCGTCATCCCAAGGTACATGAT	downstream fragment of the *recA* gene
IB016-rev	GAGCTCGATTCCGACGGTATCATC	
IB017-for	TCAATCCTCGGCGGCGTT	*recA* gene
IB018-rev	ATGTCTCAGGCTGCGTTGCG	
IB056-fw	ATGGAACCTGGCAGATCAGAAGT	*mamH-mamE*
IB057-rev	TCAAAGAACAATCCAGAACTCTTGG	
IB058-fw	ATGAGGAAGAGCGGTTGCGC	*mamM-mamN*
IB059-rv	TCATCCTGCGAGAACGGCGA	
IB060-fw	ATGATTGAAATTGGCGAGACCA	*mamO-mamA*
IB061-rv	CTCAATGAGACCTTCTACATCGACTG	
IB062-fw	ATGGCAGTAAGCGATGCGG	*mamQ-mamS*
IB063-rv	TCACTGCACGGTCATCCACA	
IB064-fw	ATGGGTACGCCAGGGGG	*mamT-mamU*
IB065-rv	TTATTTCGGAACCAGTATGGAAAGC	
IB072-for	GGTACCTCAATCCTCGGCGGCGT	*recA* fragment containing the native promoter
IB073-rev	CTCGAGCTACCCACCGCCCCCGA	
pJet 1.2-for	CGACTCACTCACTATAGGGAGAGCGGC	sequencing primers (Fermentas)
pJet 1.2-rev	AAGAACATCGATTTTCCAATGGCAG	
EK_JKL_f	CGAGACTTTTATGGCTCCG	*mamJ-mamL* (kindly provided by E. Katzmann)
EF_JKL_r	ACTTCAACCTCGGCATCC	
61 fw	GCAACACCTTCTTCACG	pCM184 *loxP* sites (kindly provided by René Uebe)
54 rv	GAGATTTTGAGACACAACGTG	

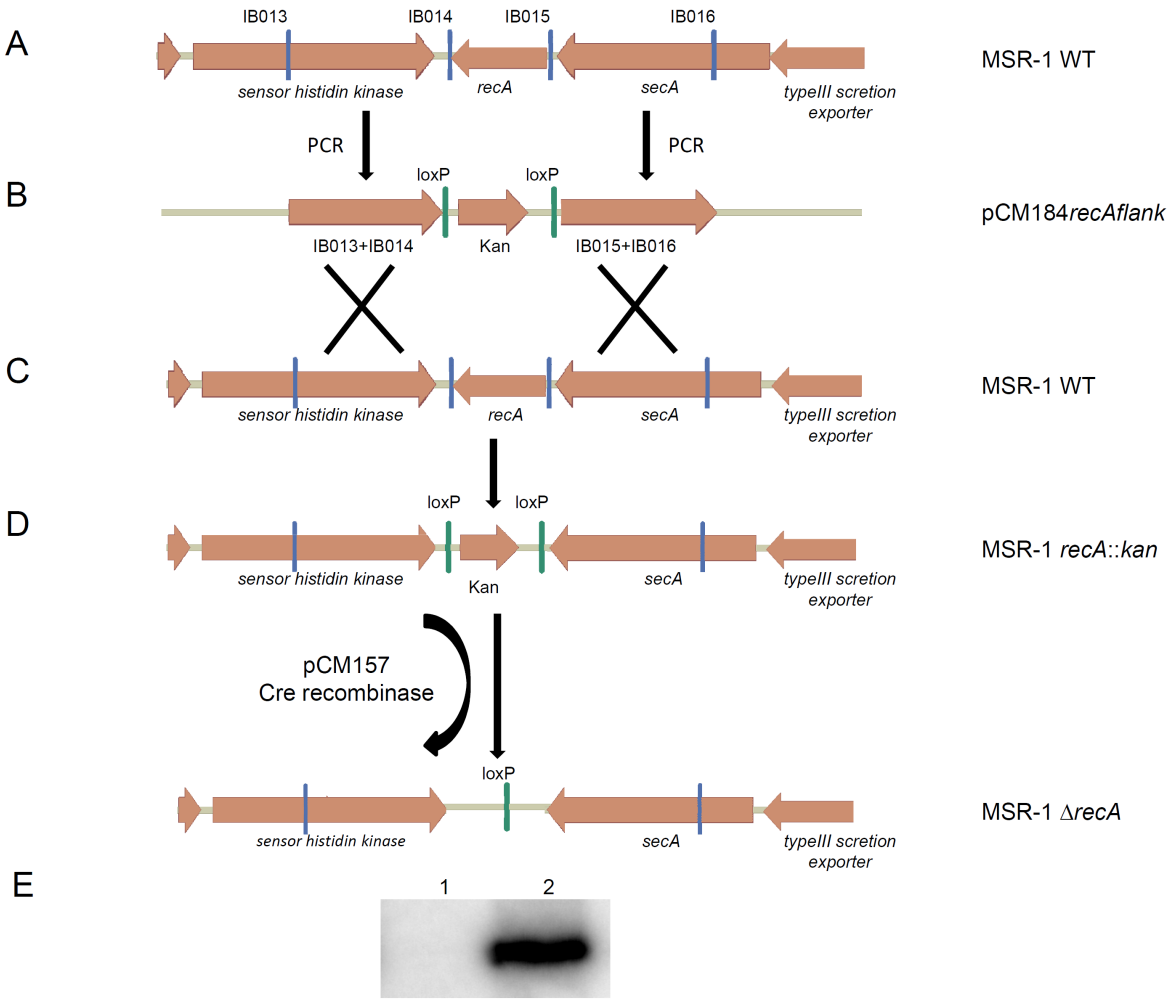

Figure S1. Genomic neighborhood of *recA* in *M. gryphiswaldense* and scheme for construction of a *recA* mutant. A. Amplification of the flanking regions and construction of the suicide vector pCM184*recAflank*. B. Conjugative transfer and double crossover C. Generation of a *recA* mutant containing a kanamycin resistance cassette. D. Removal of the cassette via Cre recombinases encoded on the plasmid pCM157, and generation of an unmarked deletion mutant. E. Confirmation of the *recA* deletion by Southern blot of KpnI-digested genomic WT (lane 2) and *ΔrecA* DNA (lane 1). The blot was hybridized with α-32P-dATP labeled *recA* probe (primers IB017, IB018; product size 1077 bp). The fragment indicates presence of the *recA* gene, whereas no signal verifies the deletion mutant. IB013, IB014, IB015, IB016: primer binding sites. IB013+IB014, IB015+IB016: flanking regions of *recA*. Kan: *kanamycin resistance cassette*. loxP: *loxP sites*.

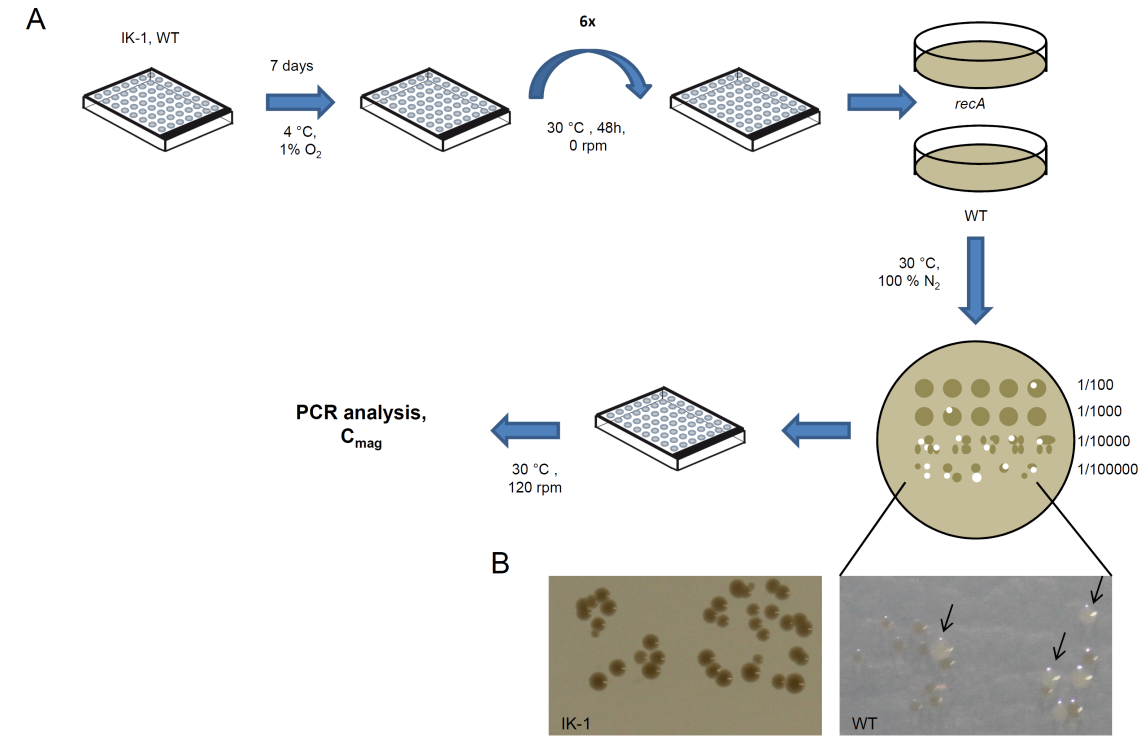

Figure S2: A. Experimental scheme for the induced mutagenesis of IK-1 and the WT. Cells were incubated for 7 days at 4 °C under microaerobic conditions. Afterwards, cultures were passaged every 48 hours six times without shaking. Cells were spotted in different dilutions on Agar plates. Colonies were visually screened and white colonies were picked and further screened via PCR and C_{mag} measurements. B. Visual screening for spontaneous non-magnetic mutants: (→) indicate abberant white colonies.

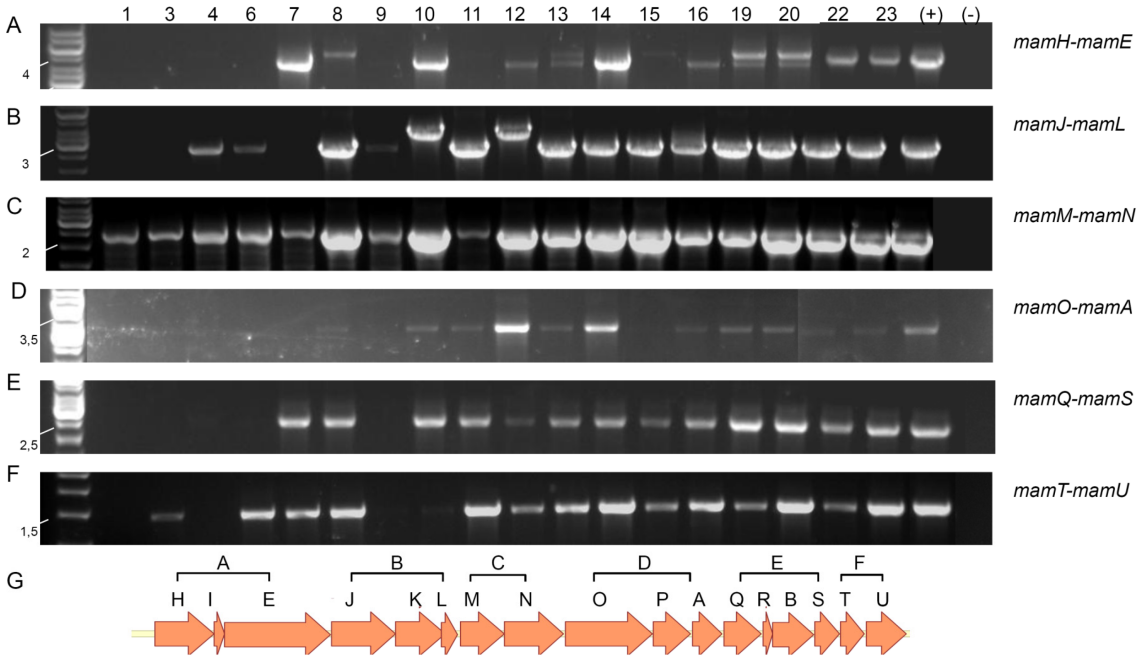

Figure S3: PCR analysis of the spontaneous nonmagnetic mutants (mutants: 1-23, (+): WT, (-): negative control) via PCR. Several regions within the *mamAB*-operon were tested. After amplification, PCR products were loaded on a 1% agarose gel. A. Results for amplification of

the region *mamH-mamE* (primers IB056, IB057); expected PCR product: 3.8 kb. B. Results for amplification of the region *mamJ-mamL* (primers EK_mamJKL_f, EK_mamJKL_r), expected product: 2.7 kb. C. Results for amplification of the region *mamM-mamN* (primers: IB058, IB059); product: 2.2 kb. D. Results for amplification of the region *mamO-mamA* (primers: IB060, IB061); product: 3.4 kb. E. Results for amplification of the region *mamQ-mamS* (primers IB062, IB063); expected product: 2.5 kb. F. Results for amplification of the region *mamT-mamU* (primers IB064, IB065); expected product: 1.4 kb. G. Overview of the *mamAB* operon (A-F: amplified regions)

Manuscript 2:

Chromosomal multiplication of the *mam* and *mms* operons enables enhanced magnetosome biosynthesis in *Magnetospirillum gryphiswaldense*

Anna Lohße[1*], Isabel Kolinko[1*], René Uebe[1], Oliver Raschdorf[1,2], Jürgen Plitzko[2,3], Sarah Borg[1], Andreas Brachmann[1], and Dirk Schüler[1]

In preparation

[*] both authors contributed equally to this work

[1]Ludwig-Maximilians-Universität München, Department Biologie I, Biozentrum der LMU, Großhaderner Str. 4, 82152 Planegg-Martinsried, Germany

[2]Max Planck Institute of Biochemistry, Department of Molecular Structural Biology, Am Klopferspitz 18, 82152 Martinsried, Germany

[3]Bijvoet Center for Biomolecular Research, Utrecht University, 3584 CH Utrecht, Netherlands

Introduction

The ability of magnetotactic bacteria (MTB) to orient along the earth's magnetic field is based on specific organelles, the magnetosomes, which are membrane-enveloped crystals of an iron mineral [1]. The model organism *Magnetospirillum gryphiswaldense* (in the following referred to as MSR) synthesizes cuboctahedral magnetite (Fe_3O_4) particles, which are assembled to a chain-like structure within the cell. Magnetosome crystals have uniform morphologies [2], a high chemical purity [3], and structural perfection [4], which are mostly unknown from inorganic systems. The unusual characteristics of the crystals as well as the inherent biocompatibility provided by the magnetosome membrane (MM) inspired numerous ideas for their biotechnological application [5], such as magnetic drug targeting, immunoassays and magnetic resonance imaging [6-11].

The biomineralization of magnetite crystals in MTB proceeds in sequential steps including MM vesicle formation, sorting of MM-specific proteins, magnetosomal iron uptake, magnetite crystallization and chain assembly along a cytoskeletal filament [3, 12-15]. We recently discovered genes controlling magnetosome synthesis in MSR to be clustered within a larger (115 kb) genomic magnetosome island, in which they are interspersed by numerous genes of unrelated or unknown functions [16, 17]. While the smaller *mamGFDC*, *mms6* and *mamXY* operons have accessory roles in the biomineralization of properly sized and shaped crystals [17-19], only the large *mamAB* operon is necessary and sufficient for magnetite biomineralization [17]. In contrast, at least the *mamGFDC*, *mms6,* and *mamAB* operons are needed for formation of poorly crystalline hematite particles in the heterologous host *Rhodospirillum rubrum*, and all 4 major operons are required for biomineralization of magnetite crystals [20].

Previous studies in MSR and the genetically closely related *Magnetospirillum magneticum* AMB-1 (referred to as AMB) so far focused on genetic dissection of the MAI and the *mam* and *mms* operons by deletion mutagenesis. For instance, a comprehensive analysis of the *mamAB* operon recently revealed that eight proteins (MamI, E, L, M, N, O, B, Q) are essential for magnetosome biomineralization in AMB, whereas in MSR only six proteins (MamE, L, M, O, B, Q) are required for at least some rudimentary iron

biomineralization and, if including MamI, seven proteins for the biosynthesis of magnetite-containing magnetosomes [21, 22]. The major magnetosome proteins MamG, F, D, and C, which account for over 35% of all magnetosome-associated proteins, have been shown to be involved in size control, since mutant cells formed smaller and less regular magnetite crystals [23, 24]. Deletion of the 3.7 kb *mms6* operon resulted in significantly smaller crystals which are aligned in short chains or loosely scattered within the cell [17]. Consistent with this finding, the MTB-specific MmsF and Mms6 proteins are predicted to be major regulators of crystal size and shape in AMB [25, 26]. In MSR, elimination of two additional genes of the *mms6* operon, *mms36* and *mms48* caused the synthesis of fewer, but larger magnetite crystals compared that of the WT [22]. Therefore, a cumulative effect on biomineralization by various proteins encoded by the *mms6* operon has been suggested [22]. The proteins mamX and MamZ encoded by the *mamXY* operon were shown to be major redox regulators for magnetite biomineralization in MSR [19]. Deletion of the whole operon resulted in size reduction of the crystals as well as in the coexistence of various distinct magnetosome morphologies, including cuboctahedral magnetite particles flanked by flake-like hematite crystals [17].

But while previous studies mainly focused on the effects of gene deletions on magnetosome formation, the potential to enhance the biomineralization by a gene dosage increase of selected *mam* and *mms* genes has been poorly investigated so far. For instance, Scheffel *et al.* showed that *in trans* expression of additional copies of the entire *mamGFDC* operon in the wild type caused the formation of enlarged magnetite particles (by a few nm) compared to those produced by the wild type without additional copies [18]. Recently, overexpression of *mms48* also resulted in a slight increase in the particle numbers per cell (40 instead of 36 for the WT) [22]. Both studies showed that selective overexpression of single or few magnetosome genes resulted in the synthesis of weakly larger crystals or increased magnetosome numbers in *M gryphiswaldense*. However, the effects of a further gene dosage increase of single operons or even multiplication of all *mam* and *mms* genes on magnetosome formation have not be systematically investigated so far.

Here we show that it is possible to stably enhance magnetite biomineralization in MSR by multiplication of single, as well as all major magnetosome operons

via transposition. A higher gene dosage of the *mms6* operon resulted in the formation of larger crystals as well as moderately increased magnetosome numbers per cell. In contrast, overexpression of all major operons specifically enhanced the number of particles by about 118%. This indicates that the expression level of different *mam* and *mms* proteins seems to be an important factor in the regulation of crystal formation. Furthermore, the findings show that genetic engineering by a gene dosage increase of the *mam* and *mms* genes provides a powerful strategy for the precise control of the particle size or numbers in MSR.

Methods

Bacterial strains, plasmids, and culture conditions

MSR and its mutant strains (Table S1) were grown in liquid modified flask standard medium (FSM) or low iron medium (LIM) at 30°C under microaerobic condition if not otherwise specified [27]. Therefore, cells were cultivated in gased flasks with a mixture of 2% O_2 and 98% N_2 or in purged jars. For anaerobic cultivation, O_2 was excluded from the gas mixture, while aerobic conditions were generated by free gas exchange to air. Single colonies were transferred into 100 µl FSM medium in 96-deep-well plates (Eppendorf, Hamburg, Germany and incubated in anaerobic jars for 5 to 6 days. The liquid cultures were scaled up to an final volume of 10 ml. Culture conditions for *Escherichia coli* strains (Table S1) were as previously described [28]. For strains BW29427 and WM3064 lysogeny broth medium was supplemented with 1 mM DL-α, ε-diaminopimelic acid (DAP). For selection of antibiotic resistant strains the following antibiotics concentrations were used: 25 µg/ml kanamycin (Km), 12 µg/ml tetracycline (Tet), and 15 µg/ml gentamicin (Gm) for *E. coli* strains, and 5 µg/ml kanamycin, 5 µg/ml tetracycline, and 20 µg/ml gentamicin for MSR strains, respectively. Magnetosomes were isolated as described in Grünberg *et al*. (2004) after microaerobic cultivation of 5 liter cultures [24]. Optical density and magnetic response (C_{mag}) were analyzed photometrical at 565 nm [29].

Molecular and genetic techniques

Oligonucleotide sequences for amplification of DNA fragments (Tabel S2) were deduced from the working draft genome sequence of *M. gryphiswaldense* (GenBank accession number No. CU459003) and were purchased from Sigma-Aldrich (Steinheim, Germany). Standard polymerase chain reaction (PCR) procedures were used to amplify genetic fragments, and plasmids were sequenced using BigDye Terminator v3.1 chemistry on an in-house ABI 3700 capillary sequencer (Applied Biosystems, Darmstadt, Germany). Sequences were analyzed with Software Vector NTI Advance® 11.5 (Invitrogen, Darmstadt, Germany). For genomic sequencing of over expression strains tagged libraries (about 200-300 bp insert size) were constructed from 1 ng of genomic DNA with

the Nextera XT DNA kit (Illumina) according to the manufacturer's protocol. The eight libraries were sequenced in multiplex format using the Illumina MiSeq technology. The obtained sequences were assembled *de novo* as well as to the reference genome with a commercial software, CLC Genomics Workbench 5.5.

Analytical methods

Iron content of magnetosomes or whole cells was measured three times in triplicates by ferrozine assay [30]. After 16 hours of cultivation cells were washed with 20 mM Tris-HCl, 5 mM EDTA, pH 7.4 to remove extracellular iron. 1ml cultures were centrifuged for 1 min at 11,000 rpm and resuspended in 90 µl HNO_3 (65%) for 3 h at 99°C. Afterwards, the lysate was cleared by centrifugation and resuspended in 1 ml H_2O and ferrozine assay was performed as previously described [30, 31].

Construction of plasmids for overexpression and conjugative transfer

Plasmids pTps_AB and pTps_XYZ were constructed in a previous study by Kolinko et al., 2014 [20]. For cloning of plasmid Gm-pTps_AB, the Km resistance gene on plasmid pTps_AB was exchanged by gentamicin via recombinogenic cloning [32, 33]. To this end a cloning cassette comprising the gentamicin gene and the respective promoter was PCR-amplified (oligonucleotides IB173/IB174) and transferred into electrocompetent *E. coli* cells (DH10b+pTps_AB) expressing phage derived recombinases from a circular plasmid (pSC101-BAD-gbaA). After transfer of the cassette, recombination between homologous regions on the linear fragment and the plasmid pTps_AB occurred.

For overexpression of the *mms6* and *mamGFDC* operon, a modified pBam-1 vector was designed. To this end e*gfp* (enhanced green fluorescent protein) was amplified with oligonucleotides IB102 and IB103 and integrated into pBam-1 after digestion with KpnI and EcoRI, resulting in pBam-gfp The *mamGFDC* and *mms6* operons were amplified by PCR from the genome of MSR (AL179/AL301) and were inserted into the XbaI+KpnI digested pBam-gfp, resulting in pBam_*mamGFDC* and pBam_*mms6* 1x, respectively with a c-terminal fusion to *mamC* or *mgr4070* of e*gfp*. For generation of pBam_*mms6* 2x and pBam_*GFDC*/*mms6*, the *mms6* operon of pBam_*mms6* 1x was amplified

with oligonucleotides AL377/AL379 and integrated into pBam_*mamGFDC* as well as pBam_*mms6* 1x after digestion with EcoRI. The gentamicin gene, flanked by a *lox71* and *lox66* sequence was generated by amplification with oligonucleotides AL300/AL303 from pBBR-MCS5 and cloned into the SanDI/AatII side of pBam_*mamGFDC*, resulting in pBam_GFDC/*Gm*. The *mms6* operon was inserted after digestion of pBam_GFDC/*Gm* with XbaI+KpnI, generating pBam_*mms6*/*Gm*. Generated plasmids were examined by restriction analysis with a set of different enzymes or PCR and transferred into different recipients via conjugation as described elsewhere [31].

Fluorescence microscopy

For localization studies of the EGFP-fusion proteins and cell length measurement, generated mutant strains of *M. gryphiswaldense* were immobilized on agarose pads (FSM salts in H2O, supplemented with 1% agarose), and analysed with an Olympus BX81 microscope provided with a 100 UPLSAPO100XO objective (numerical aperture of 1.40) and a Hamamatsu Orca AG camera. Data were evaluated with the Olympus cell software.

TEM and CET

Cells or magnetosomes were concentrated and adsorbed onto carbon-coated copper grids for TEM analyses. Isolated magnetosomes were treated with 1% v/v uranyl acetate for staining of magnetosome membrane. Cells and vesicles were imaged with a FEI Morgagni 268 (FEI, Eindhoven, Netherlands) at an accelerating voltage of 200 kV.

For CET analysis, cells were cultivated anaerobically in FSM or aerobically in LIM and treated with formaldehyde (Fluka, Switzerland) to a final concentration of 0.1% v/v after 16h of cultivation. A FEI Tecnai F30 Polara transmission electron microscope (FEI; Eindhoven, the Netherlands), equipped with a 300 kV field emission gun, a Gatan GIF 2002 Post-Column Energy Filter, and a 2048 ¥ 2048 pixel Gatan CCDCamera (Gatan; Pleasanton, CA) was used for data generation, whereby all measurements were performed at 300 kV, with the energy filter operated in the zero-loss mode (slit width of 20 eV). Tilt series were processed with the Serial EM (Mastronarde, 2005) and FEI's Explore 3D

software. Sample preparation and tilt record was implemented as described previously [13].

Cell fractionation

Mutant strain ΔRecA, ΔRecA+*mms6* 3x and ΔRecA+*ABG6X* were grown in 5 liter FSM under microaerobic conditions. After centrifugation at 9,200 g, cells were resuspended in 20 mM Tris-HCl, pH 7.4, 5 mMEDTA and stored at 4°C. Procedures for cell fractionation and magnetosomes isolation was executed as described elsewhere [34].

Gel electrophoresis and Western blot experiments

The BCA-Protein Micro assay kit (Pierce) was used for determination of protein concentrations, according to the manufacturer's recommendation. Protein samples from the magnetosome membrane fraction was resuspended in electrophoresis sample buffer and denatured at 98 °C for 5 min. Polyacrylamide gels were prepared according to the procedure of Laemmli [35]. 10 µg of protein extracts were separated on a 15% SDS-polyacrylamide gel. Protein bands were visualized by Coomassie brilliant blue staining. Western blot analysis for detection of MamM, MamA and MamC was performed as previously described [24]. The intensity of the protein bands of MamM, MamA and MamC was compared via the ImageJ software.

Results

Overexpression of the *mms6* and *mamGFDC* operons

For controlled overexpression of different magnetosome operons, MSR was engineered by mariner or Tn5 transposon driven random chromosomal insertion. This technique has recently also been successfully applied for genetic transfer of the magnetosome biosynthesis pathway into *R. rubrum* [20], expression of recombinant proteins on the magnetosome surface [10], and chromosomal insertion of single magnetosome genes [22].

Transconjugants were obtained at frequencies between 2-5x10^{-7} and chromosomal insertions were stably inherited as indicated by the ability of transformed strains to grow in the presence of kanamycin after 120 generations without antibiotic selection. All insertants essentially displayed WT-like growth (data not shown). Chromosomal duplication of the *mms6* operon resulted in strain ΔRecA+*mms6* 1x that possesses one native and one inserted *mms6* operon, and remarkably increased magnetosome biomineralization. The merodiploid mutant strain synthesized 37% more crystals per cell (47 compared to 34 magnetosomes per cell within ΔRecA (Table 1) with an increased size of 46 nm (ΔRecA= 36 nm) and formed a high proportion of multiple chains that were less frequently observed in ΔRecA. Intracellular iron content of ΔRecA+*mms6* 1x was increased by about 14.9±2.9% (Table 1).

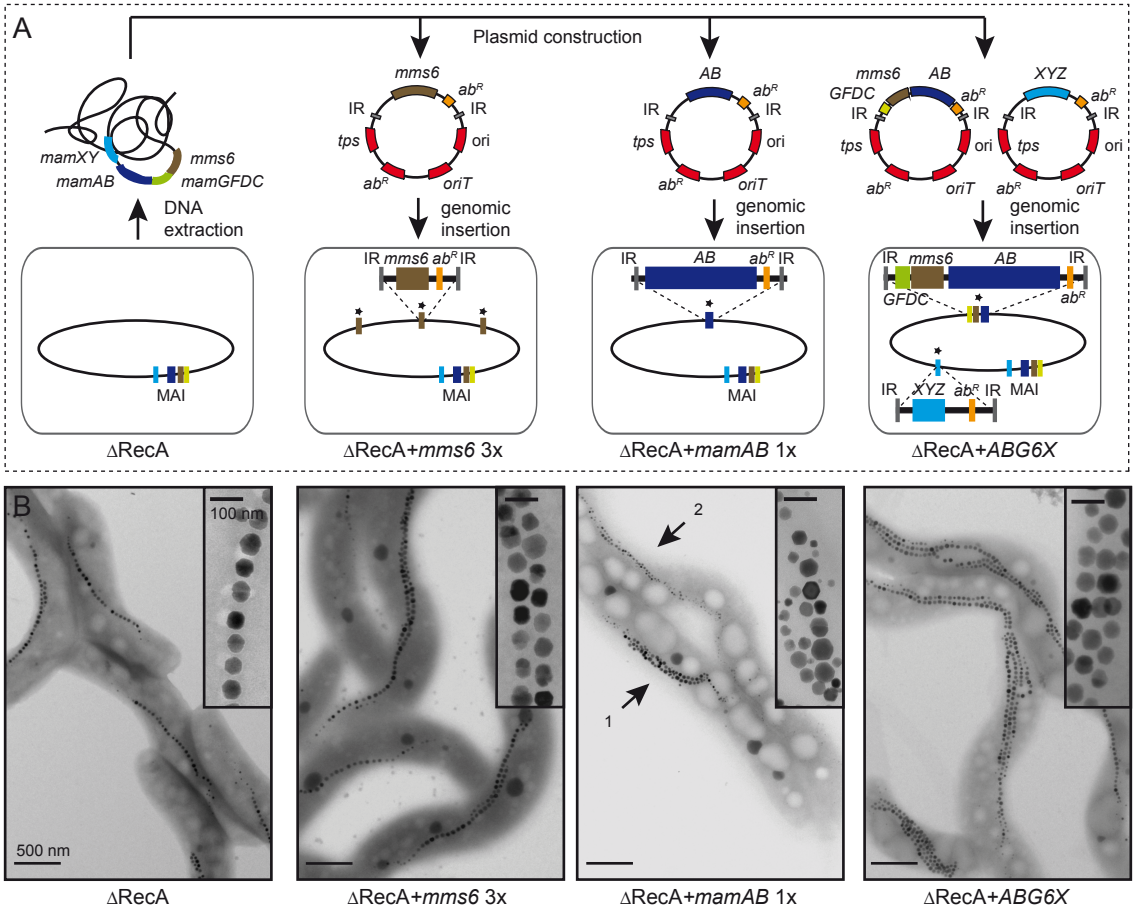

Fig 1: A. Strategy for construction of overexpression strains by amplification of different magnetosome operons. Insertional plasmids were constructed based on genomic DNA from *M. gryphiswaldense*. Plasmids contain the magnetosome operons *mamAB* (blue, *AB*), *mamGFDC* (green, GFDC), *mms6* (brown) and the *mamXY* operon lacking *ftsZm* (pale blue, *XYZ*). The vector backbone (genes are indicated in red) contains a transposase gene (*tps*), inverted repeats (IR), origin of transfer (*oriT*), an R6K or p15A origin of replication (*ori*) and antibiotic resistance cassette (ab^R). After conjugative transfer of the plasmids, the transposase recognizes IR sequences and catalyzes chromosomal insertion of the target sequence. Additional copies of respective magnetosome operons in the chromosome (oval shape) are marked with asterisks. B. TEM analysis of overexpression strains compared to the parental strain IK-1 (ΔRecA). 1 and 2 illustrate the different morphotypes found for ΔRecA+*mamAB* 1x.

Insertion of two further *mms6* operons (one native and two inserted *mms6* operons) in strains ΔRecA+*mms6* 2x led in average (n=1183) to 54 magnetite particles per cell with a size of 48 nm that corresponds to an increase in number by 60%, size by 33%, and intracellular iron content of 34.8±2.5% compared to ΔRecA (Table 1, Figure S1). ΔRecA+*mms6* 3x carrying four copies of *mms6* operon produced 58 magnetite crystals per cell with a diameter of 44 nm and an

intracellular iron content increased from 2.68% to 3.73% iron per dry weight, which represents only a slight further increase compared to ΔRecA+ *mms6* 2x (increase by 38.8±2.5% compared to ΔRecA (Table 1, Figure S1)). Cultivation under anaerobic conditions with 50 µM or 500 µM iron did not significantly increase iron uptake or magnetosome numbers of ΔRecA+*mms6* 3x compared to cultivation under microaerobic conditions with 50µM iron (data not shown). Insertion of four additional copies of the *mms6* operon in ΔRecA+*mms6* 4x (5 *mms6* operons in total) did not further increase biomineralization, but on the contrary caused a size reduction of 16% and 7% compared to ΔRecA+*mms6* 2x and ΔRecA+*mms6* 3x, respectively (Table 1).

Table 1: Characteristics of generated overexpression strains compared to the parental strain ΔRecA (n.d. = not determined).

Strain	Genotype	Crystal Size	Increased size (%) compared to ΔRecA	Crystal number per cell	Increased number (%) compared to ΔRecA	Iron content (%) compared to ΔRecA	Cell length (µm)
ΔRecA	1x MAI	36.2±11.0	-	33.9±10.3	-	-	4.4± 1.3
WT	1x MAI	35.6±13.0	-1.7	34.3±8.4	1.2	n.d.	n.d.
ΔRecA+ *mamGFDC**	2x *mamGFDC* operon	44.9±13.5	24.4	36.3±12.4	7.1	7.4±1.1	n.d.
ΔRecA+ *mms6* 1x*	2x *mms6* operon	45.7±14.2	26.7	46.5±14.3	36.8	14.9±2.9	4.5±1.6
ΔRecA+ *GFDC/mms6**	2x *mms6* 2x *mamGFDC* operon	45.1±12.2	24.6	45.1±14.3	32.7	14.1±1.9	n.d.
ΔRecA+ *mms6* 2x*	3x *mms6* operon	47.9±12.8	32.9	54.3±29.9	59.5	34.8±2.5	4.6 ±1.5
ΔRecA+ *mms6* 3x*	4x *mms6* operon	44.4±13.2	22.6	57.8±26.9	69.7	38.8±2.5	5.1 ±1.9
ΔRecA+ *mms6* 4x*	5x *mms6* operon	41.9±12.0	15.7	46.0±14.8	35.3	n.d.	5.3±1.7
ΔRecA+ *mamAB* 1x	2x *mamAB* operon	34.0±17.6	-6.2	73.4±43.1	115.2	0.4±0.5	4.8± 1.8
ΔRecA+ *mamAB* 2x	3x *mamAB* operon	35.6±15.4	-1.0	68.8±13.2	102.9	9.4±0.5	6.0± 2.6
ΔRecA+ *ABG6X*	2x *mamGFDC* 2x *mms6* 2x *mamAB* 2x *mamXY* operon	38.7±11.9	6.9	74.5±34.9	118.3	140.7±2.4	n.d.
ΔRecA+ *ABG6X+ feo*	2x *mamGFDC* 2x *mms6* 2x *mamAB* 2x *mamXY* Operon 2x *feoAB1*x	41.1 ± 8.4	13.5	69.3±13.4	104.4	135.9±6.4	n.d.

Within anaerobically grown cells of ΔRecA+*mms6* 2x and ΔRecA+*mms6* 3x a variable proportion of enlarged vesicles were visible in cryo electron tomograms (Figure 2A). These “giant” vesicles appeared as regularly shaped as in the wild type (WT), but their size was increased up to 119 nm (ΔRecA+*mms6* 2x) whereas WT vesicles had a maximum size of 54 nm. However, the ratio between the size of the vesicle and the particle sizes measured from CET tomograms was similar and not significantly increased (ΔRecA+*mms6* 2x: 2.8±0.8, ΔRecA+*mms6* 3x: 2.3±0.9; WT: 2.1±1.4).

As reported for the parental strain ΔRecA, all overexpression strains had a variable proportion of small vibrioid and elongated cells [31] and cells on average became more elongated with increasing copy number of inserted *mms6* operons (4.5±1.6 µm, 4.6 ±1.5 µm, 5.1 ±1.9 µm, and 5.3±1.7 µm for ΔRecA+*mms6* 1x, 2x, 3x, and 4x, respectively versus 4.4± 1.3 µm for ΔRecA (Figure 2A). Shorter cells (<10µm) of ΔRecA+*mms6* 2x contained fewer 43 and smaller 43 nm particles, whereas highly elongated cells (>10 µm) had significantly more (53-138 particles, mean: 104; n=572, equivalent to a 206% increase) and larger magnetite crystals (49 nm) with a maximum size of 80 nm (Table 1).

As observed by TEM in ΔRecA+*mms6* 2x and 3x cells, the magnetosome chains were persistently located at midcell and split into two subchains during cell division, similar as in the WT [36]. However, we frequently observed that cells of ΔRecA+*mms6* 2x and 3x remained connected by tubular extensions at advanced stages of constriction, which kept the daughter cells attached to each other and hampered their separation immediately after septation before the cells eventually became disconnected. Within these tubular extensions always few (2-10) magnetosome particles were encapsulated and separated from daughter chains (Figure 3B).

Next, we explored overexpression of the *mamGFDC* operon, which is adjacent to the *mms6* operon and was previously described to be involved in size control of magnetosomes [18]. While duplication of *mamGFDC* alone had only a weak effect on crystal number per cell (36; n=419), the duplication of both the *mms6* and *mamGFDC* operons (RecA+ *mms6/GFDC*) caused the synthesis of 32% more crystals per cell (45; n=483) (Table 1). Intracellular iron content of ΔRecA+*mamGFDC* was increased by about 7.4%±1.1% and even

further 14.1%±1.9% in RecA+*mms6/GFDC* (Table 1). ΔRecA+*mamGFDC* and ΔRecA+*mms6/GFDC* produced 24%, and 25% larger crystals, respectively, compared to ΔRecA (Table 1).

In summary, the genomic insertion of up to additional three *mms6* operons enhanced the biosynthesis of magnetosomes with increased sizes and numbers. However, the introduction of either additional *mms6* operon copies or the combined overexpression of *mamGFDC* did not further increase biomineralization, suggesting that magnetosome synthesis was likely limited by different factors encoded elsewhere, which control growth of magnetite particles other than by vesicle sizes, such as iron transport, activation and nucleation of crystals. Therefore, we next attempted to overexpress the large *mamAB* operon that encodes most magnetosome proteins essential and crucial for magnetosome formation.

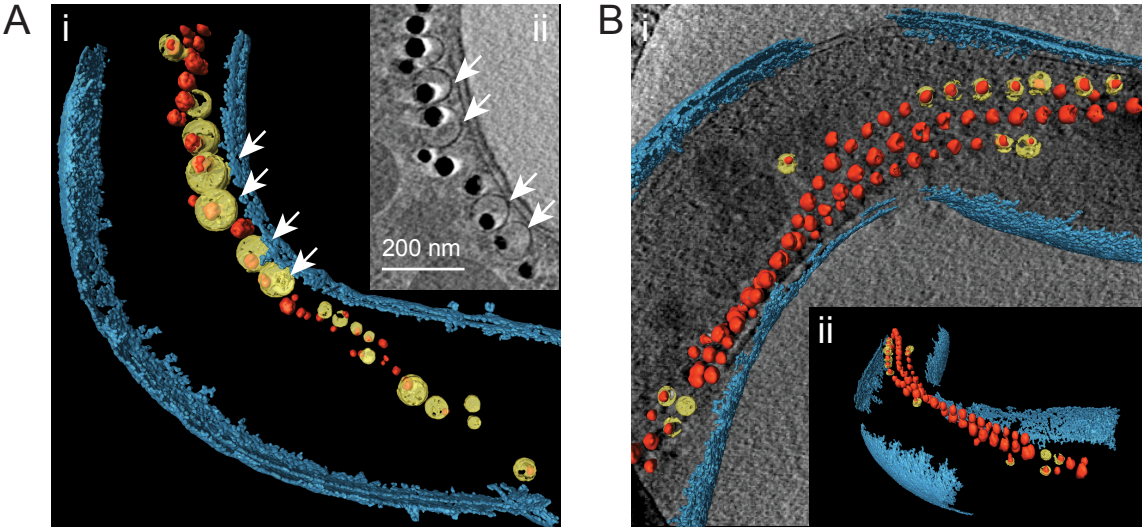

Fig. 2: Cryo-electron tomography of ΔRecA+*mms6* 2x and ΔRecA+*ABG6X*. Ai. Segmented tomogram of a ΔRecA+*mms6* cell, illustrating the intracellular position of the magnetosome chain as well as the membrane vesicles. White arrows indicate enlarged vesicles that were observed within the cell. ii. Tomogram section of the same ΔRecA+*mms6* 2x cell with enlarged vesicles (white arrows). B. Segmented tomograms (i and ii) of a ΔRecA+*ABG6X* cell shown from different angles, which contains 3 magnetosome chains, and regularly sized vesicles. Different colors indicate the outer and inner membrane (blue), magnetosome vesicels (yellow), and magnetite crystals (red).

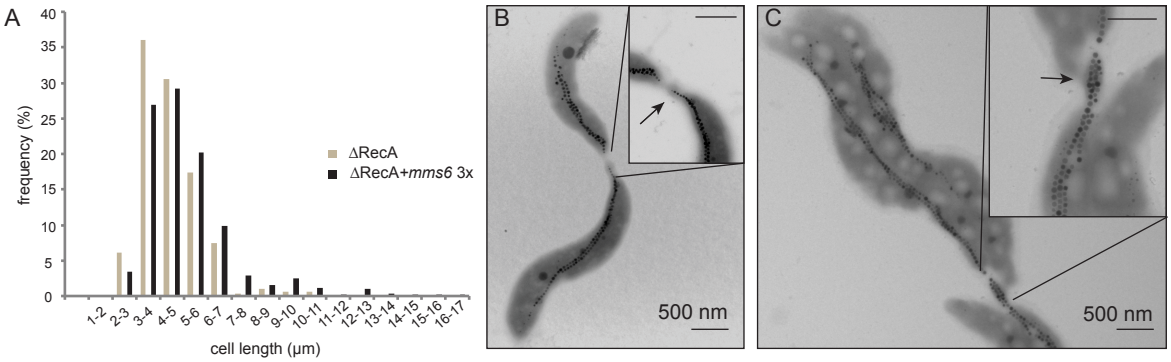

Fig. 3: A. Results of cell length measurements of ΔRecA+*mms6* 3x and the parental strain ΔRecA. The size distribution of strain ΔRecA+*mms6* 3x cells was slightly shifted towards longer cells compared to ΔRecA. B. TEM micrographs of dividing cells of ΔRecA+*mms6* 3x and ΔRecA+*ABG6X+feo* (C), which remained connected by tubular extensions with enclosed magnetosomes (arrows). Scale bar = 500 nm.

Genomic multicopy insertion of the *mamAB* operon

Transfer and single-copy chromosomal insertion of the *mamAB* operon was achieved by mariner transposon based gene delivery into random sites with a conjugational efficiency of 10^{-7}-10^{-8} [20]. As with the smaller *mms6* and *mamGFDC* operons, also the *mamAB* operon was stable for 40 generations, after repeated passaging under metabolic stress (cold storage, oxidative stress). ΔRecA+*mamAB* 1x (one native and one inserted *mamAB* operon) showed a similar magnetic response like the parental strain (Cmag=0.8±0.2; [31]) and the iron content was not significantly increased (+0.4±0.5%; Table 1). Cells were slightly elongated (4.8± 1.8 µm; ΔRecA: 4.4± 1.3 µm) and displayed no obvious morphological abnormalities. However, TEM analyses revealed phenotypic heterogeneity with respect to magnetosome formation with two distinct morphotypes present in variable proportions comprising i) about 47% cells in which the number of regular-sized magnetosomes was increased to 77, ii) 42% cells increased number of magnetosomes (68) with aberrant crystal sizes and intracellular localization, and iii) 10% WT-like cells (Figure 1, Figure S2).

We next constructed the merotriploid insertion mutant ΔRecA+*mamAB* 2x by transfer of pTps_*mamAB-Gm* into the insertion mutant ΔRecA+*mamAB* 1x. The mutant showed a similar phenotype as observed for ΔRecA+*mamAB* 1x, and the number of magnetosomes (68.8±13.2) did not further increase, despite of a slightly increased (by 9.4±0.5%) intracellular iron content. The C_{mag} value of

ΔRecA+*mamAB* 2x was even lower than that of the parent strain (C_{mag}= 0.5±0.2), possibly caused by altered cell dimensions (6.0± 2.6 µm compared to 4.4± 1.3 µm of ΔRecA (Table 1).

The magnetosome membrane of magnetosome particles isolated from strain ΔRecA+*mamAB* 1x had the same appearance and thickness of (5.4±1.8) nm as ΔRecA *(*5.2±1.9) nm. Coomassie-stained SDS-PAGE profiles of MM from strains ΔRecA+*mamAB* 1x revealed similar patterns compared to ΔRecA. However in strain ΔRecA+*mamAB* 1x several bands including magnetosome proteins MamA, and MamM, showed higher intensities between 51% and 145%. Western Blot analysis of selected proteins confirmed that MamM and MamA were more abundant within ΔRecA+*mamAB* 1x by about 128% and 145%, respectively, whereas the abundance of MamC was not significantly increased (9%), although the Coomassie-stained MamC band appeared more intense in ΔRecA (Figure S3).

In summary, the overexpression of all magnetosome proteins, encoded by the *mamAB* operon, alone did not consistently enhance magnetosome formation and therefore we suggested that further regulators for biogenesis are needed to increase magnetosome yield.

Overexpression of the *mamGFDC*, *mms6*, *mamAB*, and *mamXY* operon

Since all individual four major operons (*mms6, mamGFDC, mamAB* and *mamXY*) were shown to be implicated in regulation of magnetosome size and number, we next tested whether their combined overexpression may enhance biomineralization even further. Therefore, the *mamAB*, *mms6*, and *mamGFDC* operon were simultaneously integrated into the genome of ΔRecA that was further modified by insertion of the *mamXY* operon using mariner transposon based gene delivery, resulting in strain ΔRecA+*AB6GX*. The intracellular iron content was enormously increased to 3.77% iron per dry weight, which is an increase of about 140.7%±2.4% compared to ΔRecA. TEM revealed that the number of magnetosomes per cell was increased by 118% compared to the parental strain (Table 1; Figure 1, Figure S4). About 28% of the cells contained more than 100 magnetosomes whereas ΔRecA did not produce more than 58 particles per cell within the analyzed TEM micrographs. Most cells formed multiple magnetosome chains (2-4), whereas the parental strain exhibited not

more than 2 chains per cell. Beside cells with proper chains localized at the inner convex curvature of the cell, we frequently observed cells with one chain located at the inner convex cell curvature and up to three magnetosome chains at the concave curvature (Figure S4 B). Additionally, the plentiful particles in some cells lacked a clearly ordered chain-like alignment, but were “stuffed” into compact bundles or clusters (Figure 1, Figure S4 C). Interestingly, the mean size of crystals was only slightly increased to 39 nm (Table 1, Figure S5).

Whereas cells, which were merodiploid for *mamAB* (strain ΔRecA+*mamAB* 1x), showed two distinct magnetosome morphotypes, within strain ΔRecA+*ABG6X* only 12% cells had scattered magnetosomes and aberrant crystal sizes (ΔRecA+*mamAB* 1x: 42%). The magnetic response of ΔRecA+*AB6GX* was not affected by the altered biomineralization phenotype and consistent with the C_{mag} of the parent strain ΔRecA ($C_{magABG6X}$=0.7). In dividing cells we did also observe tubular extensions during or after cell division. In contrast to the giant MM vesicles observed by CET in strain ΔRecA+*mms6* 2x and ΔRecA+*mms6* 3x, MM vesicles were not significantly enlarged in relation to the crystals and ~55 nm in size (Fig. 2B).

The expression of the FeoAB proteins increased particle size in a heterologous host [20] suggesting that overexpression of these proteins also enhances particle synthesis in MSR. Therefore, the genes *feoA* and *feoB* were inserted into ΔRecA+*AB6GX* by Tn5 transposition. However, crystal sizes were only slightly increased (41 nm instead of 39 nm in RecA+AB6GX) in strain ΔRecA+*ABG6X+feo*, whereas crystal numbers per cell even slightly decreased (69 particles instead of 74 in strain for ΔRecA+*AB6GX*) (Table 1, Figure 2C).

Discussion

In this work, we investigated to what extent magnetosome production in MSR can be enhanced by a gene dosage increase of the *mam* and *mms* operons. In general, overexpression of genes is achieved by cloning of the target sequence into high copy number plasmids, as well as placing the genes under control of strong promoters for efficient RNA polymerase binding [37]. However, no stronger promoters than the native magnetosome operon promoters have been identified for MSR so far. Furthermore, a replicative plasmid harboring the large *mamAB* operon was unstable in MSR (unpublished data).

As an alternative strategy to achieve higher product yields, gene cluster amplification via chromosomal insertion has been applied in several studies. For instance, Tang *et al.* recently increased production of the secondary metabolite spinosyn in the native host by partial gene cluster duplication [38]. Using a chemically inducible chromosomal evolution approach, 40 consecutive copies of a poly-3-hydroxybutyrate gene cluster were inserted into the chromosome of *E. coli*, thereby causing a significant increase in the productivity of this biopolymer [39].

In our approach we found that dupli-or triplication of the *mms6* operon alone caused formation of larger crystals and a moderate increase in crystal numbers. In contrast, amplification of all *mam* and *mms* gene clusters specifically enhanced magnetosome numbers per cell.

While the changes in magnetosome production varied depending on the inserted genes, we found that cells were longer in all overexpression strains, potentially related to a minor cell division phenotype. Additionally, cells often remained connected by tubular extensions at advanced stages of constriction, which kept the daughter cells attached to each other. One explanation why cells remained connected after constriction in the overexpression strains could be the magnetostatic interactions within the chains, which are significantly higher in a two stranded chain as well as for larger crystals [36]. Consequently, the cells might not the able to split magnetosome chains after constriction due to the magnetic attraction forces in the magnetosome chains. On top of this, also the presence of 2-3 stranded MamK filaments itself might hinder splitting of the

daughter cells by the lack of additional mechanical forces for cleavage of the cytoskeletal filaments [36].

Despite the weak cell division phenotype in the overexpression mutants, this study demonstrates the feasibility to increase the number as well as size of the magnetosome particles by a gene dosage increase of the *mam* and *mms* operons. In the mutants that overexpressed single magnetosome operons, the biomineralization seemed to be limited by the lack of accessory factors encoded in the non-amplified magnetosome operons. In contrast, chromosomal duplication of all major operons resulted in the strongest increase in magnetosome production.

However, several questions regarding the regulation of the magnetosome numbers as well as size in the different overexpression still remain elusive. For instance it is unknown, to what extent overexpression of the *mms6* operon alone causes formation of larger crystals. One important factor spatially constraining growth of the crystals is the size of the magnetosome vesicles. We sometimes found significantly enlarged vesicles in the *mms6* insertion strains by CET (119 nm instead of up to 54 nm in the parental strain). This finding indicates that overexpression of a set of genes might also directly influence the vesicle diameter prior to crystallization, thereby defining the increase in crystal size. This could be caused by accumulation of proteins encoded by the *mms6* operon in the MM, thereby having a marked effect on the vesicle size. In strain ΔRecA+*mamAB 1x*, we observed that MamM and MamA were enriched in the MM compared to that of strain IK-1 (by 128% and 145%, respectively). As expected, no changes in the expression level of MamC were detectable in ΔRecA+*mamAB 1x*. This finding demonstrates that the protein composition of the MM changes by overexpression of only a set of genes. However, besides the formation of larger crystals in the *mms6* overexpression strains, also the numbers of magnetosomes were increased. This observation suggests that overexpression of a set of magnetosome genes influences the expression or the recruitment of accessory proteins controlling other processes during magnetosome formation, such as magnetosomal iron transport, vesicle biogenesis, or magnetosome chain assembly.

Altogether, our findings indicate that the expression level of magnetosome proteins seems to be one important factor determining the number and size of

magnetite crystals. However, we did not compare the transcript or protein levels of all expressed magnetosome genes in the insertional mutants with that of the ΔRecA control. Therefore, it is unknown whether a gene dosage increase of the *mam* and *mms* operons results in uniform overexpression of all amplified magnetosome genes.

Our findings also raise the question, which accessory factors encoded outside the *mam* and *mms* operons might limit the number or size of magnetosomes in the overexpression strains as well as in the WT. For instance, the extracellular iron concentration is already known to be linked to crystal formation in MSR [40]. In the WT, iron concentrations of 100 µM have been shown to support highest cell yield and magnetism [40]. Since the intracellular iron content was enhanced in the overexpression strains (by up to 141%), we wondered whether magnetosome biosynthesis could be further increased by higher iron concentrations in the medium. However, incubation of the insertion mutants in medium supplemented with 500 µM ferric citrate (instead of 50 µM) did not result in a further increase in magnetosome numbers or size. This might indicate that the intracellular iron supply was already saturated for lower iron concentrations in the medium. Alternatively, this finding could also hint towards an insufficient expression of additional iron transport proteins encoded in the non-amplified genomic regions, which might limit further magnetosomal iron uptake. For instance, deletion of *feoB1* encoding a constituent of a specific ferrous iron transport system specific for magnetotactic bacteria caused fewer and smaller magnetosomes in MSR [41]. However, chromosomal duplication of the *feoAB1* operon in ΔRecA+*ABG6X* had only minor effects on the crystal size (see Table 1). Therefore, it seems unlikely that the extracellular or magnetosomal iron supply limited a further increase in magnetosome numbers or size.

The regulator protein Fur is involved in global iron homeostasis in MSR [15], and has been found to control expression of all identified iron uptake proteins, such as components of ferrous (FeoAB) and ABC ferric ion transport systems. Therefore, this protein could also be indirectly involved in limiting the numbers and size of magnetosomes by regulating the transcription of genes encoding constituents of iron uptake systems. However, deletion of *fur* had only minor effects on biomineralization in MSR [15]. Therefore, this protein likely

plays only a minor role in controlling magnetosome formation in the WT as well as in the overexpression strains.

Besides the intracellular iron supply, which spatially constrains magnetosome formation, other factors encoded outside the *mam* and *mms* operons might limit magnetosome biosynthesis in MSR. Several enzymes participating in denitrification (nitrate reductase Nap, nitrite reductase NirS [42, 43]), aerobic respiration (cytochrome c oxidase cbb_3 [44, 45]), and the oxygen sensor Fnr [44] have been found to poise optimal redox conditions during magnetite biomineralization. Consequently, the corresponding proteins could also indirectly limit the number or size of magnetite crystals by regulation of the intracellular redox balance. However, a more comprehensive genetic analysis will be necessary in the future to elucidate whether accessory, yet-unknown factors control magnetosome formation in the WT as well as in the overexpression strains.

Although the mode of action by which the overexpression of different *mam* and *mms* operons results in changes in magnetosome numbers or crystal sizes could not be fully unveiled, our approach nevertheless demonstrates that it is possible to specifically engineer MSR for enhanced magnetosome production.

The constructed strains could be used for the high and stabilized production of magnetosomes, which are functionalized by genetic fusion with fluorescent markers or other recombinant proteins [5, 10]. Furthermore, overexpression of selected magnetosome genes by chromosomal engineering might be exploited for the design of size-controlled nanocrystals that display altered magnetic properties. This could be of particular interest in applications, which depend on specific magnetic properties of the particles such as magnetic resonance imaging [46] or hyperthermal treatment of tumors [47].

References

1. Bazylinski, D.A. and R.B. Frankel, *Magnetosome formation in prokaryotes.* Nat Rev Microbiol, 2004. **2**(3): p. 217-30.
2. Faivre, D. and P. Zuddas, *Mineralogical and isotopic properties of biogenic nanocrystalline magnetites*, in *Magnetoreception and magnetosomes in bacteria*, D. Schüler, Editor. 2007, Springer-Verlag: Berlin, Heidelberg. p. 175-96.
3. Faivre, D. and D. Schüler, *Magnetotactic bacteria and magnetosomes.* Chem Rev, 2008. **108**(11): p. 4875-98.
4. Coker, V.S., et al., *Cation site occupancy of biogenic magnetite compared to polygenic ferrite spinels determined by X-ray magnetic circular dichroism.* Europ J Mineral, 2007. **19**(5): p. 707-16.
5. Lang, C. and D. Schüler, *Biogenic nanoparticles: production, characterization, and application of bacterial magnetosomes.* J Phys: Condens Matter, 2006. **18**: p. 2815-28.
6. Sun, J.B., et al., *Preparation and anti-tumor efficiency evaluation of doxorubicin-loaded bacterial magnetosomes: magnetic nanoparticles as drug carriers isolated from Magnetospirillum gryphiswaldense.* Biotechnol Bioeng, 2008. **101**(6): p. 1313-20.
7. Lang, C., D. Schüler, and D. Faivre, *Synthesis of magnetite nanoparticles for bio- and nanotechnology: genetic engineering and biomimetics of bacterial magnetosomes.* Macromol Biosci, 2007. **7**(2): p. 144-51.
8. Ohuchi, S. and D. Schüler, *In vivo display of a multisubunit enzyme complex on biogenic magnetic nanoparticles.* Appl Environ Microbiol, 2009. **75**(24): p. 7734-8.
9. Lang, C. and D. Schüler, *Expression of green fluorescent protein fused to magnetosome proteins in microaerophilic magnetotactic bacteria.* Appl Environ Microbiol, 2008. **74**(15): p. 4944-53.
10. Borg, S., et al., *New vectors for chromosomal integration enable high-level constitutive or inducible magnetosome expression of fusion proteins in Magnetospirillum gryphiswaldense.* Appl Environ Microbiol, 2014 (ahead of print).

11. Westmeyer, G.G. and A. Jasanoff, *Genetically controlled MRI contrast mechanisms and their prospects in systems neuroscience research.* Magn Resonance Imag, 2007. **25**(6): p. 1004-10.
12. Schüler, D., *Genetics and cell biology of magnetosome formation in magnetotactic bacteria.* FEMS Microbiol Rev, 2008. **32**(4): p. 654-72.
13. Katzmann, E., et al., *Loss of the actin-like protein MamK has pleiotropic effects on magnetosome formation and chain assembly in Magnetospirillum gryphiswaldense.* Mol Microbiol, 2010. **77**(1): p. 208-24.
14. Scheffel, A., et al., *An acidic protein aligns magnetosomes along a filamentous structure in magnetotactic bacteria.* Nature, 2006. **440**(7080): p. 110-4.
15. Uebe, R., et al., *Deletion of a fur-like gene affects iron homeostasis and magnetosome formation in Magnetospirillum gryphiswaldense.* J Bacteriol, 2010. **192**(16): p. 4192-204.
16. Ullrich, S., et al., *A hypervariable 130-kilobase genomic region of Magnetospirillum gryphiswaldense comprises a magnetosome island which undergoes frequent rearrangements during stationary growth.* J Bacteriol, 2005. **187**(21): p. 7176-84.
17. Lohsse, A., et al., *Functional analysis of the magnetosome island in Magnetospirillum gryphiswaldense: the mamAB operon is sufficient for magnetite biomineralization.* PLoS One, 2011. **6**(10): p. e25561.
18. Scheffel, A., et al., *The major magnetosome proteins MamGFDC are not essential for magnetite biomineralization in Magnetospirillum gryphiswaldense but regulate the size of magnetosome crystals.* J Bacteriol, 2008. **190**(1): p. 377-86.
19. Raschdorf, O., et al., *The magnetosome proteins MamX, MamZ and MamH are involved in redox control of magnetite biomineralization in Magnetospirillum gryphiswaldense.* Mol Microbiol, 2013. **89**(5): p. 872-86.
20. Kolinko, I., et al., *Biosynthesis of magnetic nanostructures in a foreign organism by transfer of bacterial magnetosome gene clusters.* Nat Nanotechnol, 2014. **9**(3): p. 193-7.

21. Murat, D., et al., *Comprehensive genetic dissection of the magnetosome gene island reveals the step-wise assembly of a prokaryotic organelle.* Proc Natl Acad Sci U S A, 2010. **107**(12): p. 5593-8.
22. Lohsse, A., et al., *Genetic dissection of the mamAB and mms6 operons reveals a gene set essential for magnetosome biogenesis in Magnetospirillum gryphiswaldense.* J Bacteriol, 2014 (ahead of print).
23. Scheffel, A. and D. Schüler, *The acidic repetitive domain of the Magnetospirillum gryphiswaldense MamJ protein displays hypervariability but is not required for magnetosome chain assembly.* J Bacteriol, 2007. **189**(17): p. 6437-46.
24. Grünberg, K., et al., *Biochemical and proteomic analysis of the magnetosome membrane in Magnetospirillum gryphiswaldense.* Appl Environ Microbiol, 2004. **70**(2): p. 1040-50.
25. Tanaka, M., et al., *MMS6 protein regulates crystal morphology during nano-sized magnetite biomineralization in vivo.* J Biol Chem, 2011. **286**(8): p. 6386-92.
26. Murat, D., et al., *The magnetosome membrane protein, MmsF, is a major regulator of magnetite biomineralization in Magnetospirillum magneticum AMB-1.* Mol Microbiol, 2012. **4**: p. 684-99.
27. Heyen, U. and D. Schüler, *Growth and magnetosome formation by microaerophilic Magnetospirillum strains in an oxygen-controlled fermentor.* Appl Microbiol Biotechnol, 2003. **61**(5-6): p. 536-44.
28. Sambrook, J. and D. Russell, *Molecular cloning:a laboratory manual*. Vol. 3. 2001, Cold Spring Harbor NY: Cold Spring Harbor Laboratory Press.
29. Schüler, D., R. Uhl, and E. Bäuerlein, *A simple light-scattering method to assay magnetism in Magnetospirillum gryphiswaldense* FEMS Microbiol. Lett. , 1995. **132**: p. 139-45.
30. Viollier, E., et al., *The ferrozine method revisited: Fe(II)/Fe(III) determination in natural waters.* Appl. Geochemistry, 2000. **15**: p. 785-90.
31. Kolinko, I., et al., *Frequent mutations within the genomic magnetosome island of Magnetospirillum gryphiswaldense are mediated by RecA.* J Bacteriol, 2011. **193**(19): p. 5328-34.

32. Wang, J., et al., *An improved recombineering approach by adding RecA to lambda Red recombination.* Mol Biotechnol, 2006. **32**(1): p. 43-53.
33. Zhang, Y.M., et al., *A new logic for DNA engineering using recombination in Escherichia coli.* Nat Genet, 1998. **20**(2): p. 123-28.
34. Uebe, R., et al., *The cation diffusion facilitator proteins MamB and MamM of Magnetospirillum gryphiswaldense have distinct and complex functions, and are involved in magnetite biomineralization and magnetosome membrane assembly.* Mol Microbiol, 2011. **82**(4): p. 818-35.
35. Laemmli, U.K., *Cleavage of structural proteins during the assembly of the head of bacteriophage T4.* Nature, 1970. **227**(5259): p. 680-5.
36. Katzmann, E., et al., *Magnetosome chains are recruited to cellular division sites and split by asymmetric septation.* Mol Microbiol, 2011. **82**(6): p. 1316-29.
37. Cebolla, A., et al., *Improvement of recombinant protein yield by a combination of transcriptional amplification and stabilization of gene expression.* Appl Environ Microbiol, 2002. **68**(10): p. 5034-41.
38. Tang, Y., et al., *Duplication of partial spinosyn biosynthetic gene cluster in Saccharopolyspora spinosa enhances spinosyn production.* FEMS Microbiol Lett, 2011. **325**(1): p. 22-9.
39. Tyo, K.E., P.K. Ajikumar, and G. Stephanopoulos, *Stabilized gene duplication enables long-term selection-free heterologous pathway expression.* Nat Biotechnol, 2009. **27**(8): p. 760-5.
40. Schüler, D. and E. Bäuerlein, *Iron-limited growth and kinetics of iron uptake in Magnetospirillum gryphiswaldense.* Arch Microbiol, 1996. **166**(5): p. 301-7.
41. Rong, C., et al., *Ferrous iron transport protein B gene (feoB1) plays an accessory role in magnetosome formation in Magnetospirillum gryphiswaldense strain MSR-1.* Res. Microbiol., 2008. **159**(7-8): p. 530-6.
42. Li, Y.J., et al., *The Periplasmic Nitrate Reductase Nap Is Required for Anaerobic Growth and Involved in Redox Control of Magnetite Biomineralization in Magnetospirillum gryphiswaldense.* J Bacteriol, 2012. **194**(18): p. 4847-56.

43. Li, Y.J., et al., *Cytochrome cd_1 Nitrite Reductase NirS Is Involved in Anaerobic Magnetite Biomineralization in Magnetospirillum gryphiswaldense and Requires NirN for Proper d_1 Heme Assembly.* J Bacteriol, 2013. **195**(18): p. 4297-309.
44. Li, Y., *Oxygen regulation and redox control of magnetosome biomineralization in Magnetospirillum gryphiswaldense*, in *Department Biology I.* 2014, Ludwig-Maximilians-Universität: München.
45. Li, Y., et al., *The terminal oxidase cbb3 functions in redox control of magnetite biomineralization in Magnetospirillum gryphiswaldense.* J Bacteriol, 2014 (ahead of print).
46. Sun, C., J.S. Lee, and M. Zhang, *Magnetic nanoparticles in MR imaging and drug delivery.* Adv Drug Deliv Rev, 2008. **60**(11): p. 1252-65.
47. Hergt, R., et al., *Magnetic properties of bacterial magnetosomes as diagnostic and therapeutic tools.* J Magn Magn Mater, 2005. **293**: p. 80-6.

Supplementary information

Table S1: Strains and plasmids used in this study.

Strains and plasmids	Description	References
***M. gryphiswaldense* strains**		
MSR-1 R3/S1	Rif^R Sm^R, spontaneous mutant	[1]
MSR-1B	R3/S1 Spontaneous mutant, lacking 40,385 kb genomic region	[2]
ΔRecA	R3/S1 Δ*recA*	[3]
ΔRecA+*mamGFDC*	ΔRecA with two copies of the *mamGFDC* operon, Km^R	This study
ΔRecA+*mms6* 1x	ΔRecA with two copies of the *mms6* operon, Km^R	This study
ΔRecA+GFDC/*mms6*	ΔRecA with two copies of the *mms6* and *mamGFDC* operon, Km^R	This study
ΔRecA+*mms6* 2x	ΔRecA with three copies of the *mms6* operons, Km^R	This study
ΔRecA+*mms6* 3x/Gm	ΔRecA with four copies of the *mms6* operons, Km^R, Gm^R	This study
ΔRecA+*mms6* 3x	ΔRecA with four copies of the *mms6* operons, Km^R, Gm^S	This study
ΔRecA+*mms6* 4x	ΔRecA with five copies of the *mms6* operons, Km^R, Gm^S	This study
ΔRecA+*mamAB*	ΔRecA with two copies of the *mamAB* operon, Km^R	This study
ΔRecA+*mamAB* 2x	ΔRecA with three copies of the *mamAB* operon, Km^R, Gm^R	This study
ΔRecA+ABG6X	ΔRecA with two copies of the *mamAB*, *mamGFDC*, *mms6* operon and *mamXYZ* genes	This study
ΔRecA+ABG6X+feo	ΔRecA with two copies of the *mamAB*, *mamGFDC*, *mms6* operon and *mamXYZ* genes and operon *feoAB1*	This study
***E. coli* strain**		
BW29427	*thrB1004 pro thi rpsL hsdS lacZDM15 RP4-1360D(araBAD)567DdapA*	Datsenko and Wanner (unpublished)
DH5a	*1341::[erm pir(wildtype)]trahsdR17 recA1-endA1gyrA96thi-1relA1*	Invitrogen
DH10b	*F¯ endA1 recA1 galE15 galK16 nupG rpsL ΔlacX74 Φ80lacZΔM15 araD139 Δ(ara,leu)7697 mcrA*	Invitrogen

	Δ(mrr-hsdRMS-mcrBC) λ⁻	
S17-1*λpir*	RPA-2, Tc::Mu-Km::Tn7 (λpir)	[4]
WM3064	*thrB1004 pro thi rpsL hsdS lacZDM15 RP4-1360D(araBAD) 567DdapA*::[*erm pir*]	W. Metcalf, kindly provided by J. Gescher, KIT Karlsruhe
Plasmids		
pJet1.2	Ap^r, *eco47IR*, *rep* (pMB-1)	Fermentas
pCM157	Tet^R, Cre expression vector	[5]
pBBR-MCS5	Gm^r, *lacZa*	[6]
pBam-1	*ori*R6K, Km^R, Ap^R	[7]
pTps_AB	Km^R, BSD^R, mariner tps vector containing *mamAB* operon	[8]
Gm- pTps_AB	Gm^R, BSD^R, mariner tps vector containing *mamAB* operon	This study
pTps_ABG6	Cm^R, Km^R, BSD^R, mariner tps vector with *mamAB*, *mamGFDC*, and *mms6* operon	[8]
pTps_XYZ	Gm^R, BSD^R, mariner Tps vector with *mamY*, *mamX* and *mamZ*	[8]
Tet-pBam_feoAB1	Tc^R, Ap^R, *feoAB1* operon under the control of P_{mamH}, Tn5 vector	[8]
pBam_*mamGFDC*	pBam-1, *mamGFDC* operon	This study
pBam_*mms6* 1x	pBam-1, *mms6* operon	This study
pBam_GFDC/*mms6*	pBam_*mamGFDC*, *mms6* operon	This study
pBam_*mms6* 2x	pBam_*mms6* 1x , *mms6* operon (two *mms6* operons)	This study
pBam_GFDC/*Gm*	pBam_*mamGFDC, lox71*_Gm^r_*lox66*	This study
pBam_*mms6*/Gm	pBam_*mms6* 1x, *lox71*_Gm^r_*lox66*	This study

Table S2. DNA oligonucleotides used in this work.

Name	Sequence
IB102	GGCGGTACCGGAGGCGGAGGCGGT
IB103	GGCGAATTCTTACTTGTACAGCTCGTCCATG
IB173	CCGGAATTGCCAGCTGGGGCGCCCTCTGGTAAGGTTGGGAAGCCCTGCAACG TATAATATTTGCCCATG
IB174	AGGCGATAGAAGGCGATGCGCTGCGAATCGGGAGCGGCGATACCGTAAAGCG ATCTCGGCTTGAA
AL179	CATATGTTGGGCTTGTGGTTTTGGCGG
AL301	GGTACCTGTACTGCGGAACAGTCGCG
AL377	GAATTCCAACTTTTTCGCTTTACTAG
AL379	GAATTCTCATGTACTGCGGAACAGTC
AL300	TATGGGACCCTACCGTTCGTATAATGTATGCTATACGAAGTTATCGATCTCGGC TTGAA
AL303	AATGACGTCTACCGTTCGTATAGCATACATTATACGAAGTTATCGTATAATATTT GCCCATG

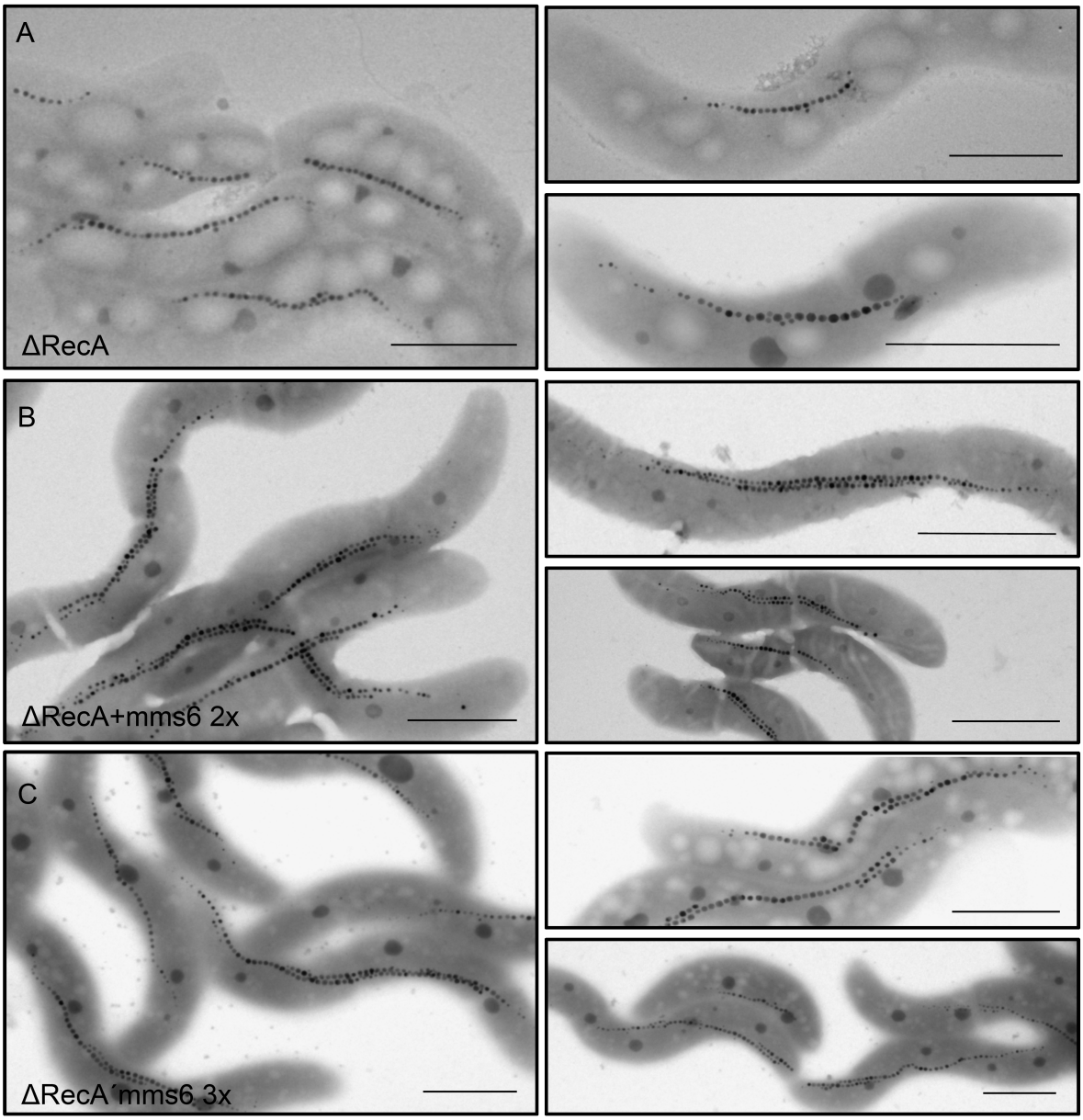

Figure S1: Transmission electron micrographs of mutants ΔRecA+*mms6* 2x and ΔRecA+*mms6* 3x compared to ΔRecA. Scale bar = 1 µm.

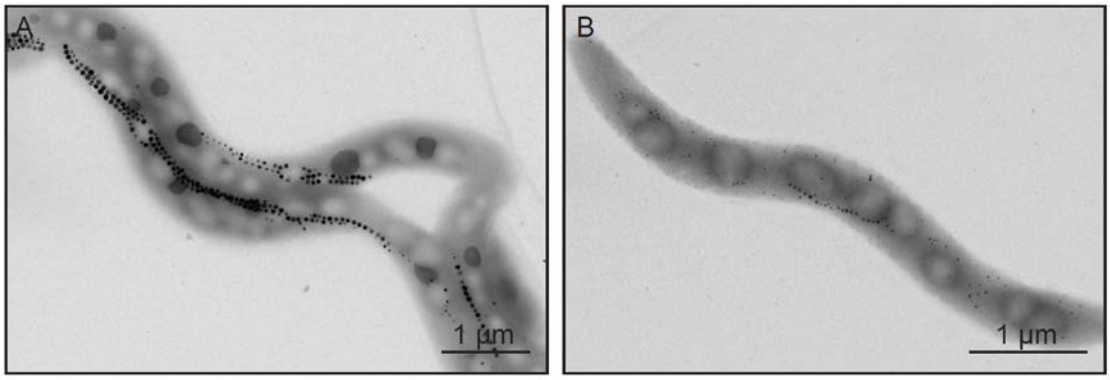

Figure S2: Transmission electron micrographs of ΔRecA+*mamAB* 1x, illustrating the phenotypic heterogeneity with respect to magnetosome formation found in this mutant. A. Cell with increased regular-sized magnetosomes. B. Cell with increased number of magnetosomes with aberrant crystal sizes and intracellular localization.

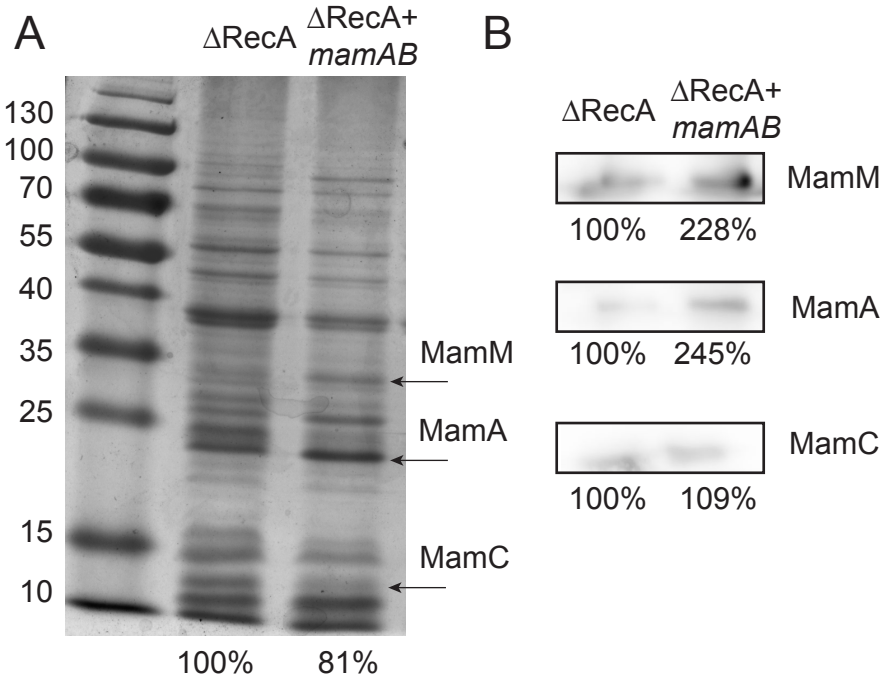

Figure S3: Proteomic analysis of magnetosomes from ΔRecA+*mamAB*. A. 1D SDS-PAGE of Coomassie blue stained proteins, which were solubilized from isolated magnetosome particles of *M. gryphiswaldense* ΔRecA and ΔRecA+*mamAB*. Bands of size of MamM (34 kDa), MamA (24 kDa) and MamC (12 kDa) are indicated (arrows). B. Immnuodetection of MamM, MamA and MamC in blotted magnetosome membrane fractions from ΔRecA and ΔRecA+*mamAB*. Respective protein bands of strain ΔRecA were assigned to 100%.

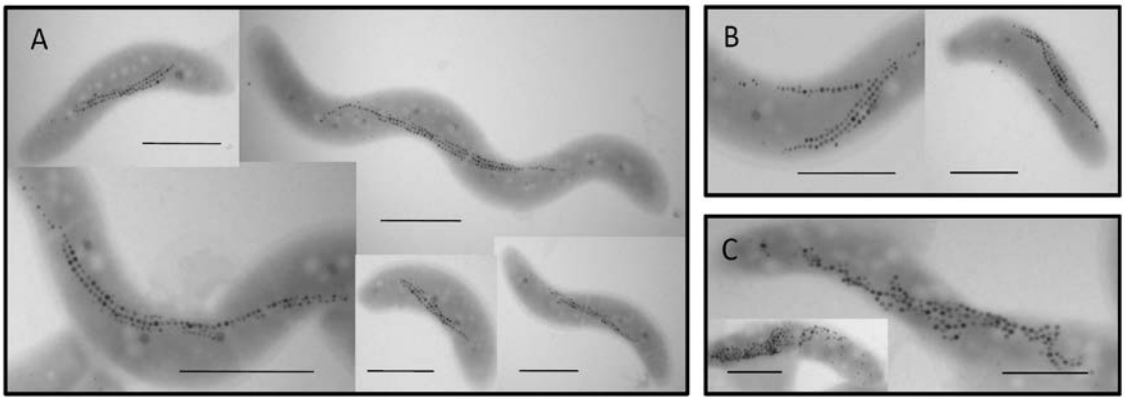

Figure S4: Transmission electron micrographs of ΔRecA+*ABG6X*. A. Cells with one chain located at the inner convex cell curvature and up to three magnetosome chains at the concave curvature. C. Cells that lack a clearly ordered chain-like alignment of the produced particles. Scale bar = 1 µm.

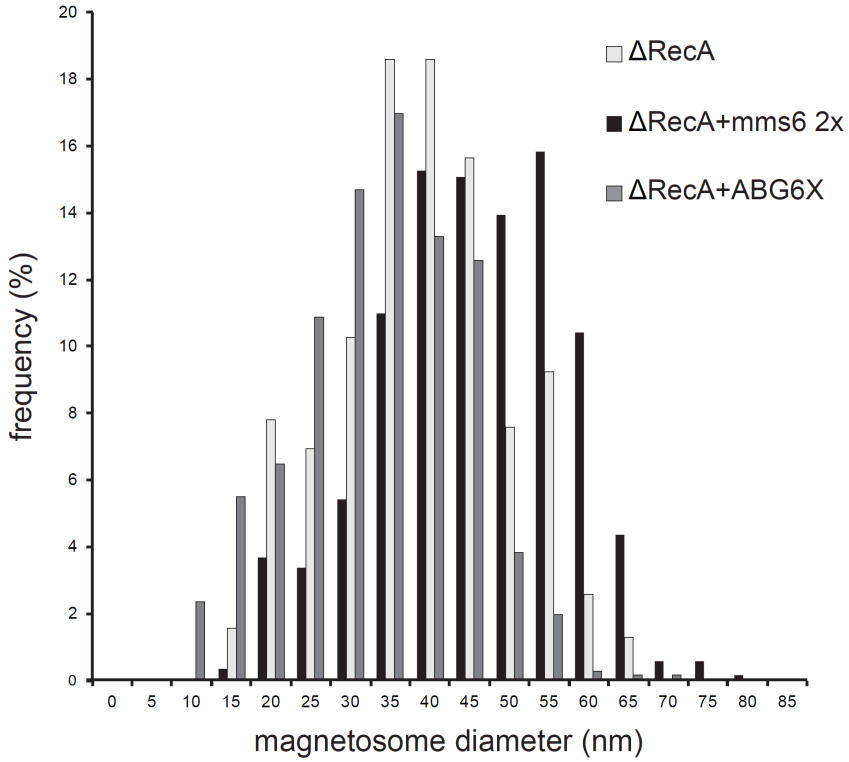

Figure S5: Magnetosome size distributions of the insertion mutant ΔRecA+*mms6* 2x, ΔRecA+*ABG6X* and the parental strain ΔRecA.

References

1. Schultheiss, D. and D. Schüler, *Development of a genetic system for Magnetospirillum gryphiswaldense.* Arch Microbiol, 2002. **179**: p. 89-94.
2. Schübbe, S., et al., *Characterization of a spontaneous nonmagnetic mutant of Magnetospirillum gryphiswaldense reveals a large deletion comprising a putative magnetosome island.* J Bacteriol, 2003. **185**(19): p. 5779-90.
3. Kolinko, I., et al., *Frequent mutations within the genomic magnetosome island of Magnetospirillum gryphiswaldense are mediated by RecA.* J Bacteriol, 2011. **193**(19): p. 5328-34.
4. Simon R, Priefer U, and A. Puhler, *A Broad Host Range Mobilization System for In Vivo Genetic Engineering: Transposon Mutagenesis in Gram Negative Bacteria.* Nat Biotech, 1983(1): p.784-791.
5. Marx, C.J. and M.E. Lidstrom, *Broad-host-range cre-lox system for antibiotic marker recycling in gram-negative bacteria.* Biotechniques, 2002. **33**(5): p. 1062-7.
6. Kovach, M.E., et al., *Four new derivatives of the broad-host-range cloning vector pBBR1MCS, carrying different antibiotic-resistance cassettes.* Gene, 1995. **166**(1): p. 175-6.
7. Martinez-Garcia, E., et al., *pBAM1: an all-synthetic genetic tool for analysis and construction of complex bacterial phenotypes.* BMC Microbiol, 2011. **11**: p. 38.
8. Kolinko, I., et al., *Biosynthesis of magnetic nanostructures in a foreign organism by transfer of bacterial magnetosome gene clusters.* Nat Nanotechnol, 2014. **9**(3): p. 193-7.

Manuscript 3:

Biosynthesis of magnetic nanostructures in a foreign organism by transfer of bacterial magnetosome gene clusters

Isabel Kolinko[1], Anna Lohße[1], Sarah Borg[1], Oliver Raschdorf[1,2], Christian Jogler[1†], Qiang Tu[3,4], Mihály Pósfai[5], Éva Tompa[5], Jürgen M. Plitzko[2,6], Andreas Brachmann[1], Gerhard Wanner[1], Rolf Müller[3], Youming Zhang[4*] and Dirk Schüler[1*]

Nature Nanotechnology (2014), 3: 193-7

[1]Ludwig-Maximilians-Universität München, Department of Biology I, Großhaderner Straße 2-4, 82152 Martinsried, Germany

[2]Max Planck Institute of Biochemistry, Department of Molecular Structural Biology, Am Klopferspitz 18, 82152 Martinsried, Germany

[3]Helmholtz Institute for Pharmaceutical Research Saarland, Helmholtz Centre for Infection Research and Department of Pharmaceutical Biotechnology, Saarland University, PO Box 151150, 66041 Saarbrücken, Germany

[4]Shandong University – Helmholtz Joint Institute of Biotechnology, State Key Laboratory of Microbial Technology, Life Science College, Shandong University, Jinan 250100, China

[5]University of Pannonia, Department of Earth and Environmental Sciences, Veszprem, H-8200 Hungary

[6]Bijvoet Center for Biomolecular Research, Utrecht University, 3584 CH Utrecht, Netherlands

[†]Present address: Leibniz Institute DSMZ, Department of Microbial Cell Biology and Genetics, Inhoffenstraße 7B, 38124 Braunschweig

nature nanotechnology

LETTERS

PUBLISHED ONLINE: 23 FEBRUARY 2014 | DOI: 10.1038/NNANO.2014.13

Biosynthesis of magnetic nanostructures in a foreign organism by transfer of bacterial magnetosome gene clusters

Isabel Kolinko[1], Anna Lohße[1], Sarah Borg[1], Oliver Raschdorf[1,2], Christian Jogler[1†], Qiang Tu[3,4], Mihály Pósfai[5], Éva Tompa[5], Jürgen M. Plitzko[2,6], Andreas Brachmann[1], Gerhard Wanner[1], Rolf Müller[3], Youming Zhang[4]* and Dirk Schüler[1]*

The synthetic production of monodisperse single magnetic domain nanoparticles at ambient temperature is challenging[1,2]. In nature, magnetosomes—membrane-bound magnetic nanocrystals with unprecedented magnetic properties—can be biomineralized by magnetotactic bacteria[3]. However, these microbes are difficult to handle. Expression of the underlying biosynthetic pathway from these fastidious microorganisms within other organisms could therefore greatly expand their nanotechnological and biomedical applications[4,5]. So far, this has been hindered by the structural and genetic complexity of the magnetosome organelle and insufficient knowledge of the biosynthetic functions involved. Here, we show that the ability to biomineralize highly ordered magnetic nanostructures can be transferred to a foreign recipient. Expression of a minimal set of genes from the magnetotactic bacterium *Magnetospirillum gryphiswaldense* resulted in magnetosome biosynthesis within the photosynthetic model organism *Rhodospirillum rubrum*. Our findings will enable the sustainable production of tailored magnetic nanostructures in biotechnologically relevant hosts and represent a step towards the endogenous magnetization of various organisms by synthetic biology.

The alphaproteobacterium *M. gryphiswaldense* produces uniform nanosized crystals of magnetite (Fe_3O_4), which can be engineered by genetic[6,7] and metabolic means[8] and are inherently biocompatible. The stepwise biogenesis of magnetosomes involves the invagination of vesicles from the cytoplasmic membrane, magnetosomal uptake of iron, and redox-controlled biomineralization of magnetite crystals, as well as their self-assembly into nanochains along a dedicated cytoskeletal structure to achieve one of the highest structural levels in a prokaryotic cell[3,9].

We recently discovered genes controlling magnetosome synthesis to be clustered within a larger (115 kb) genomic magnetosome island, in which they are interspersed by numerous genes of unrelated or unknown functions[6,10]. Although the smaller *mamGFDC*, *mms6* and *mamXY* operons have accessory roles in the biomineralization of properly sized and shaped crystals[6,11], only the large *mamAB* operon encodes factors essential for iron transport, magnetosome membrane (MM) biogenesis, and crystallization of magnetite particles, as well as their chain-like organization and intracellular positioning[6,10,12]. However, it has been unknown whether this gene set is sufficient for autonomous expression of magnetosome biosynthesis.

Using recombineering (recombinogenic engineering) based on phage-derived Red/ET homologous recombination, we stitched together several modular expression cassettes comprising all 29 genes (26 kb in total) of the four operons in various combinations (Supplementary Fig. 1), but lacking the tubulin-like *ftsZm*. This gene was omitted from its native *mamXY* operon because of its known interference with cell division during cloning. Regions 200–400 bp upstream of all operons were retained to ensure transcription from native promoters[13]. Transposable expression cassettes comprising the MycoMar (*tps*) or Tn5 transposase gene, two corresponding inverted repeats, the origin of transfer *oriT*, and an antibiotic resistance gene were utilized to enable transfer and random chromosomal integration in single copy[14,15] (Supplementary Tables 3 and 4). Chromosomal reintegration of all cassettes into different non-magnetic single-gene and operon deletion strains of *M. gryphiswaldense* resulted in stable wild type-like restoration of magnetosome biomineralization, indicating that transferred operons maintained functionality upon cloning and transfer (Supplementary Fig. 2).

We next attempted the transfer of expression cassettes to a foreign non-magnetic host organism (Fig. 1). We chose the photosynthetic alphaproteobacterium *R. rubrum* as a first model because of its biotechnological relevance and relatively close relationship to *M. gryphiswaldense*[16–18] (16S rRNA similarity to *M. gryphiwaldense* = 90%). Although the *mamAB* operon alone has been shown to support some rudimentary biomineralization in *M. gryphiswaldense*[6], neither genomic insertion of the *mamAB* operon alone (pTps_AB) nor in combination with the accessory *mamGFDC* genes (pTps_ABG) had any detectable phenotypic effect (Supplementary Table 1). We also failed to detect a magnetic response (C_{mag}) in the classical light scattering assay[19] after insertion of pTps_ABG6 (*mamAB* + *mamGFDC* + *mms6*). However, the cellular iron content of *R. rubrum_ABG6* increased 2.4-fold compared with the untransformed wild type (Supplementary Table 1). Transmission electron microscopy (TEM) revealed a loose chain

[1]Ludwig-Maximilians-Universität München, Department of Biology I, Großhaderner Straße 2-4, 82152 Martinsried, Germany, [2]Max Planck Institute of Biochemistry, Department of Molecular Structural Biology, Am Klopferspitz 18, 82152 Martinsried, Germany, [3]Helmholtz Institute for Pharmaceutical Research Saarland, Helmholtz Centre for Infection Research and Department of Pharmaceutical Biotechnology, Saarland University, PO Box 151150, 66041 Saarbrücken, Germany, [4]Shandong University – Helmholtz Joint Institute of Biotechnology, State Key Laboratory of Microbial Technology, Life Science College, Shandong University, Jinan 250100, China, [5]University of Pannonia, Department of Earth and Environmental Sciences, Veszprém, H-8200 Hungary, [6]Bijvoet Center for Biomolecular Research, Utrecht University, 3584 CH Utrecht, The Netherlands, [†]Present address: Leibniz Institute DSMZ, Department of Microbial Cell Biology and Genetics, Inhoffenstraße 7B, 38124 Braunschweig, Germany. *e-mail: dirk.schueler@lmu.de; zhangyouming@sdu.edu.cn

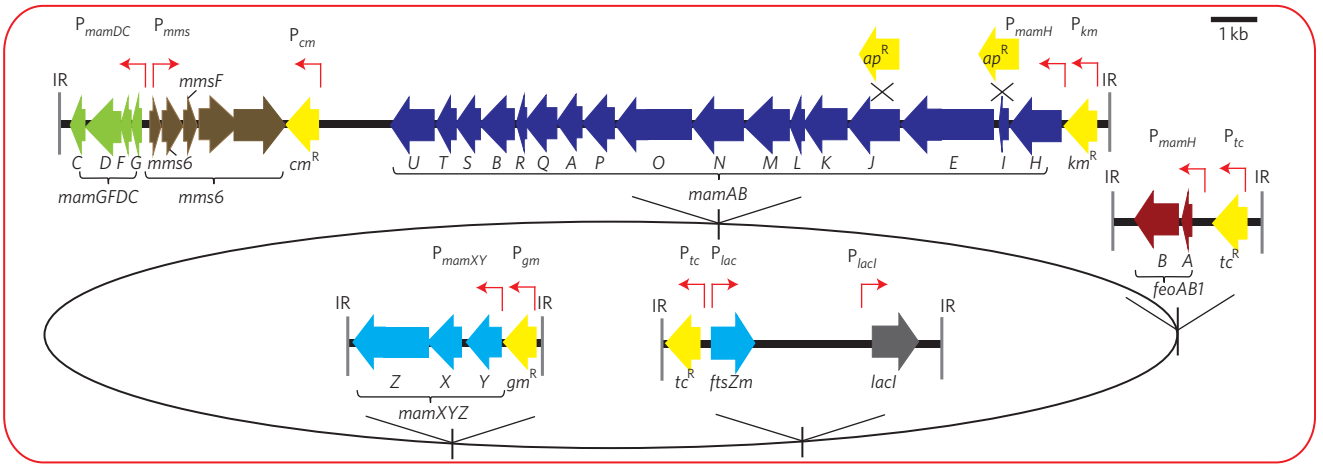

Figure 1 | Schematic representation of molecular organization of gene cassettes inserted into the chromosome of *R. rubrum* in a stepwise manner. Broad arrows indicate the extensions and transcriptional directions of individual genes. Different colours illustrate the cassettes inserted into the chromosome (oval shape, not to scale) as indicated by their gene names in the figure. Shown in yellow are antibiotic resistance genes (km^R, kanamycin resistance; tc^R, tetracycline resistance; ap^R, ampicillin resistance; gm^R, gentamicin resistance). Thin red arrows indicate different promoters (P) driving transcription of inserted genes (P_{km}, P_{gm}, P_{tc}, promoters of antibiotic resistance cassettes; P_{lacI}, promoter lac repressor; P_{mms}, P_{mamDC}, P_{mamH}, P_{mamXY}, native promoters of the respective gene clusters from *M. gryphiswaldense*; P_{lac}, *lac* promoter). Crossed lines indicate sites of gene deletions of *mamI* and *mamJ* in strains *R. rubrum_ABG6X_dI* and *R. rubrum_ABG6X_dJ*, respectively. IR, inverted repeat defining the boundaries of the sequence inserted by the transposase.

of small (~12 nm) irregularly shaped electron-dense particles (Fig. 2a,ii), identified as poorly crystalline hematite (Fe_2O_3) by analysis of the lattice spacings in high-resolution TEM images (Supplementary Fig. 3), much as in the hematite particles previously identified in *M. gryphiswaldense* mutants affected in crystal formation[11,20]. To further enhance biomineralization, we next transferred pTps_XYZ, an insertional plasmid harbouring *mamX*, *Y* and *Z* from the *mamXY* operon, into *R. rubrum_ABG6* (Supplementary Fig. 1). The resulting strain *ABG6X* encompassed all 29 relevant genes of the magnetosome island except *ftsZm*. Intriguingly, cells of *ABG6X* exhibited a significant magnetic response (Supplementary Table 1) and were 'magnetotactic', that is, within several hours accumulated as a visible pellet near a magnet at the edge of a culture flask (Fig. 2b). TEM micrographs revealed the presence of electron-dense particles identified as magnetite (Fe_3O_4) (Fig. 2d, Supplementary Fig. 8 and Table 1), which were aligned in short, fragmented chains loosely dispersed within the cell (Fig. 2a,iii). Despite their smaller sizes (average, 24 nm) the particles strongly resembled the magnetosomes of the donor strain in terms of their projected outlines and thickness contrast, suggestive of cubooctahedral or octahedral crystal morphologies (Fig. 2d). Additional insertion of the *ftsZm* gene under control of the inducible *lac* promoter had no effect on the cellular iron content and the number and size of magnetite crystals in the resulting *R. rubrum_ABG6X_ftsZm* (Fig. 2a,iv, Supplementary Table 1). Magnetite biomineralization occurred during microoxic chemotrophic as well anoxic photoheterotrophic cultivation. Medium light intensity, 50 μM iron and 23 °C supported the highest magnetic response (C_{mag}) and robust growth of the metabolically versatile *R. rubrum_ABG6X*, which was indistinguishable from the untransformed wild type (Supplementary Figs 4 and 5). The magnetic phenotype remained stable for at least 40 generations under non-selective conditions, with no obvious phenotypic changes.

To test whether known mutation phenotypes from *M. gryphiswaldense* could be replicated in *R. rubrum*, we constructed variants of expression cassettes in which single genes were omitted from the *mamAB* operon by deletion within the cloning host *Escherichia coli*. The small (77 amino acids) MamI protein was previously implicated in MM vesicle formation and found to be essential for magnetosome synthesis[12]. *R. rubrum_ABG6X-dI* failed to express magnetosome particles (Supplementary Fig. 10), which phenocopied a *mamI* deletion in the related *M. magneticum*[12]. Another tested example was MamJ, which is assumed to connect magnetosome particles to the cytoskeletal magnetosome filament formed by the actin-like MamK[21]. Much as in *M. gryphiswaldense*, deletion of *mamJ* caused agglomeration of magnetosome crystals in ~65% of *R. rubrum_ABG6X-dJ* cells (Fig. 2a,v, Supplementary Fig. 10 and Table 1). Together, these observations indicate that magnetosome biogenesis and assembly within the foreign host are governed by very similar mechanisms and structures as in the donor, which are conferred by the transferred genes.

As magnetosomes in *R. rubrum_ABG6X* were still smaller than those of *M. gryphiswaldense*, we wondered whether full expression of biomineralization may depend on the presence of further auxiliary functions, possibly encoded outside the canonical magnetosome operons. For instance, deletion of *feoB1* encoding a constituent of a ferrous iron transport system specific for magnetotactic bacteria caused fewer and smaller magnetosomes in *M. gryphiswaldense*[22]. Strikingly, insertion of *feoAB1* into *R. rubrum* strain *ABG6X* resulted in even larger, single-crystalline and twinned magnetosomes and longer chains (440 nm) (Fig. 2a,vi, Supplementary Table 1). The size (37 nm) of the crystals approached that of the donor, and cellular iron content was substantially increased (0.28% of dry weight) compared with *R. rubrum_ABG6X* (0.18%), although still lower than in *M. gryphiswaldense* (3.5%), partly because of the considerably larger volume of *R. rubrum* cells (Fig. 2c).

Magnetosome particles could be purified from disrupted cells by magnetic separation and centrifugation[23] and formed stable suspensions (Fig. 3). Isolated crystals were clearly enclosed by a layer of organic material resembling the MM attached to magnetosomes of *M. gryphiswaldense*. Smaller, immature crystals were surrounded by partially empty vesicles (Fig. 3c, inset), which were also seen in thin-sectioned cells (Supplementary Fig. 8) and on average were smaller (66 ± 6 nm) than the abundant photosynthetic intracytoplasmic membranes (ICMs) (93 ± 34 nm; Fig. 3a, Supplementary Fig. 8).

Organic material of the putative MM could be solubilized from isolated magnetite crystals of *R. rubrum_ABG6X* by various detergents (Fig. 3d), in a similar manner to that reported for MM of

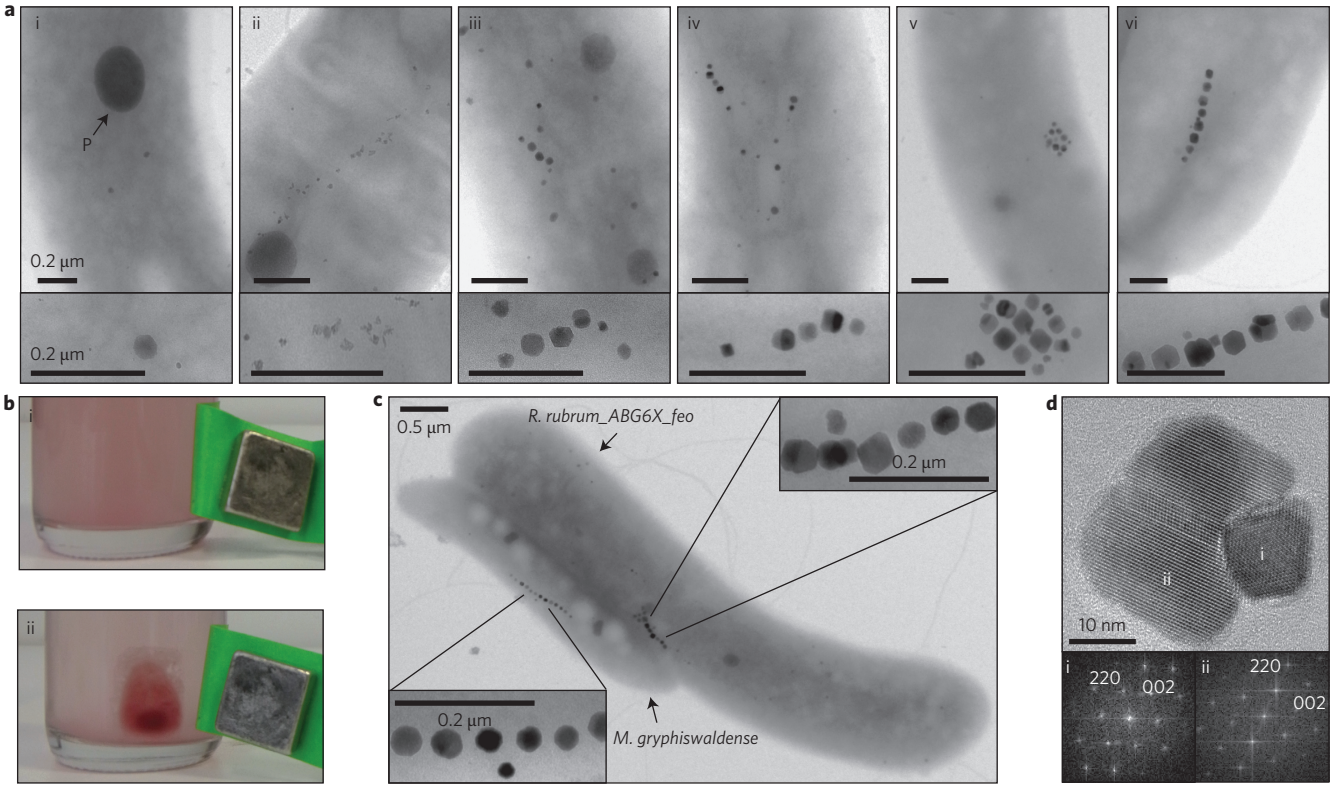

Figure 2 | Phenotypes of *R. rubrum* strains expressing different magnetosome gene clusters and auxiliary genes. a, TEM images: *R. rubrum* wild type (i), containing a larger phosphate inclusion (P) and some small, non-crystalline, electron-dense particles; *R. rubrum_ABG6* (ii); *R. rubrum_ABG6X* (iii); *R. rubrum_ABG6X_ftsZm* (iv); *R. rubrum_ABG6X_dJ* (v); *R. rubrum_ABG6X_feo* (vi). Insets: Magnifications of non-crystalline electron-dense particles (i) or heterologously expressed nanocrystals (ii–vi). All insets are of the same particles/crystals as in their respective main images, except for (v). For further TEM micrographs see Supplementary Fig. 10. **b**, Unlike the untransformed *R. rubrum* wild type, cells of *R. rubrum_ABG6X* accumulated as a visible red spot near the pole of a permanent magnet at the edge of a culture flask. **c**, TEM micrograph of a mixed culture of the donor *M. gryphiswaldense* and the recipient *R. rubrum_ABG6X_feo*, illustrating characteristic cell properties and magnetosome organization. Insets: Magnifications of magnetosomes from *M. gryphiswaldense* and *R. rubrum_ABG6X_feo*. **d**, High-resolution TEM lattice image of a twinned crystal from *R. rubrum_ABG6X*, with Fourier transforms (i) and (ii) showing intensity maxima consistent with the structure of magnetite.

M. gryphiswaldense[23]. Proteomic analysis of the SDS-solubilized MM revealed a complex composition (Supplementary Fig. 6), and several genuine magnetosome proteins (MamKCJAFDMBYOE, Mms6, MmsF) were detected among the most abundant polypeptides (Supplementary Table 2). An antibody against MamC, the most abundant protein in the MM of *M. gryphiswaldense*[23], also recognized a prominent band with the expected mass (12.4 kDa) in the MM of *R. rubrum_ABG6X* (Supplementary Fig. 6).

The subcellular localization of selected magnetosome proteins in *R. rubrum* depended on the presence of further determinants encoded by the transferred genes. For example, MamC tagged with a green fluorescent protein, which is commonly used as magnetosome chain marker in *M. gryphiswaldense*[24] displayed a punctuate pattern in the *R. rubrum* wild type background. In contrast, a filamentous fluorescent signal became apparent in the majority of cells (79%) of the *R. rubrum_ABG6X* background, in which the full complement of magnetosome genes is present (Supplementary Fig. 7), reminiscent of the magnetosome-chain localization of these proteins in *M. gryphiswaldense*[24].

Our findings demonstrate that one of the most complex prokaryotic structures can be functionally reconstituted within a foreign, hitherto non-magnetic host by balanced expression of a multitude of structural and catalytic membrane-associated factors. This also provides the first experimental evidence that the magnetotactic trait can be disseminated to different species by only a single event, or a few events, of transfer, which are likely to occur also under natural conditions by horizontal gene transfer as speculated before[18,25,26].

The precise functions of many of the transferred genes have remained elusive in native magnetotactic bacteria, but our results will now enable the dissection and engineering of the entire pathway in genetically more amenable hosts. The approximately 30 transferred magnetosome genes constitute an autonomous expression unit that is sufficient to transplant controlled synthesis of magnetite nanocrystals and their self-assembly within a foreign organism. However, further auxiliary functions encoded outside the *mam* and *mms* operons are necessary for biomineralization of donor-like magnetosomes. Nevertheless, this minimal gene set is likely to shrink further as a result of systematic reduction approaches in different hosts.

Importantly, the results are promising for the sustainable production of magnetic nanoparticles in biotechnologically relevant photosynthetic hosts. Previous attempts to magnetize both prokaryotic and eukaryotic cells by genetic and metabolic means (for example, refs 27,28) resulted in only irregular and poorly crystalline iron deposits. This prompted ideas to borrow genetic parts of the bacterial magnetosome pathway for the synthesis of magnetic nanoparticles within cells of other organisms[4,29]. Our results now set the stage for synthetic biology approaches to genetically endow both uni- and multicellular organisms with magnetization by biomineralization of tailored magnetic nanostructures. This might be exploited for instance in nanomagnetic actuators or *in situ* heat

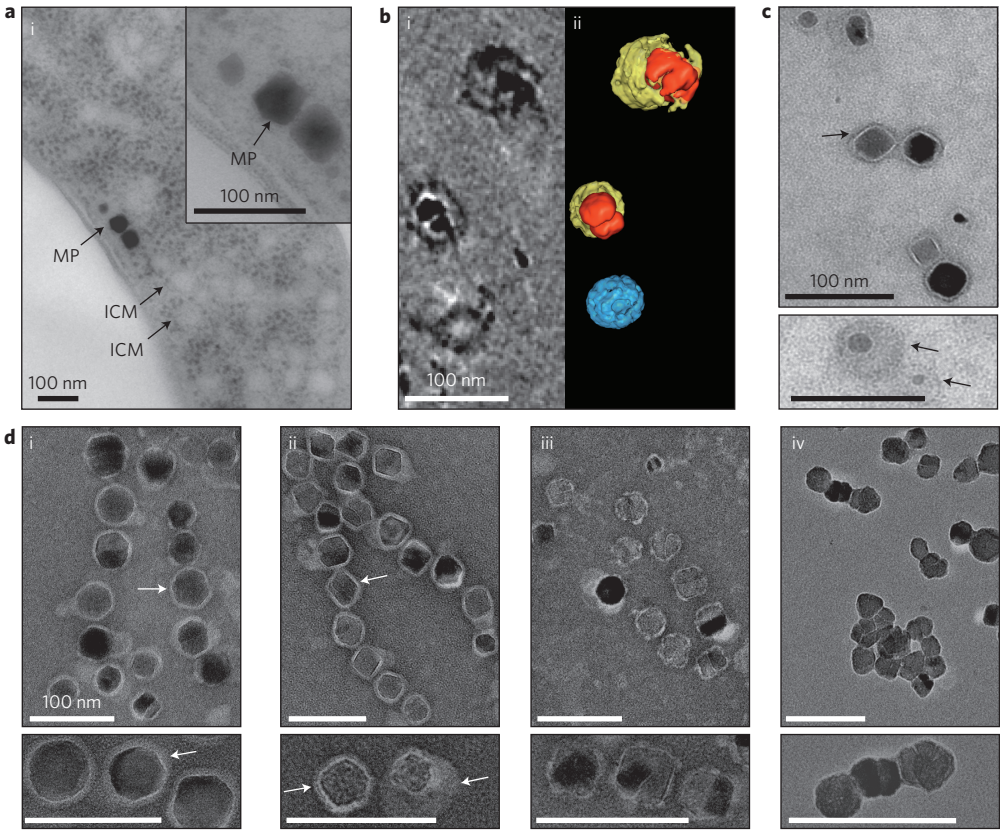

Figure 3 | Ultrastructural analysis of *R. rubrum_ABG6X* and isolated crystals. a, Cryo-fixed, thin-sectioned *R. rubrum_ABG6X* contained intracytoplasmic membranes (ICMs) (93±34 nm, $n=95$) and magnetic particles (MP). Inset: Magnification of the magnetite crystals. **b**, Cryo-electron tomography of isolated magnetic particles of *R. rubrum_ABG6X*: *x*–*y* slice of a reconstructed tomogram (i) and surface-rendered three-dimensional representation (ii). A membrane-like structure (yellow, thickness 3.4±1.0 nm, $n=6$) surrounds the magnetic particles (red). (Blue, empty vesicle.) **c**,**d**, TEM images of isolated magnetosomes from *R. rubrum_ABG6X* (**c** and **d**,ii, iii, iv) and *M. gryphiswaldense* (**d**,i) negatively stained by uranyl acetate (**c**) or phosphotungstic acid (**d**). Insets: Higher-magnification images of magnetic particles; these are of different particles to those shown in the main images, except for (iv). Scale bars, 100 nm. Arrows indicate the magnetosome membrane, which encloses magnetic crystals of *M. gryphiswaldense* (thickness 3.2±1.0 nm, $n=103$) and *R. rubrum_ABG6X* (thickness 3.6±1.2 nm, $n=100$). Organic material could be solubilized from magnetite crystals of *R. rubrum_ABG6X* with SDS (sodium dodecyl sulfate, iv) and less effectively also with Triton X-100 (iii).

generators in the emerging field of magnetogenetics[30], or for endogenous expression of magnetic reporters for bioimaging[31].

Methods

Bacterial strains, media and cultivation. The bacterial strains are described in Supplementary Table 4. *E. coli* strains were cultivated as previously described[32]. A volume of 1 mM DL-α,ε-diaminopimelic acid was added for the growth of auxotrophic strains BW29427 and WM3064. *M. gryphiswaldense* strains were cultivated in flask standard medium (FSM), in liquid or on plates solidified by 1.5% agar, and incubated at 30 °C under microoxic (1% O_2) conditions[33]. Cultures of *R. rubrum* strains were grown as specified (Supplementary Fig. 3).

Construction of magnetosome gene cluster plasmids and conjugative transfer. The oligonucleotides and plasmids used in this study are listed in Supplementary Tables 4 and 5. Red/ET (Lambda red and RecET) recombination was performed as described previously[14]. Briefly, a cloning cassette was amplified by polymerase chain reaction (PCR) and transferred into electrocompetent *E. coli* cells (DH10b) expressing phage-derived recombinases from a circular plasmid (pSC101-BAD-gbaA). After transfer of the cassette, recombination occurred between homologous regions on the linear fragment and the plasmid.

To stitch the magnetosome gene clusters together into a transposon plasmid (Supplementary Fig. 1) we used triple recombination[14] and co-transformed two linear fragments, which recombined with a circular plasmid. Recombinants harbouring the correct plasmids were selected by restriction analysis[32].

Conjugations into *M. gryphiswaldense* were performed as described before[33]. For conjugation of *R. rubrum*, cultures were incubated in ATCC medium 112. Approximately 2×10^9 cells were mixed with 1×10^9 *E. coli* cells, spotted on American Type Culture Collection (ATCC) 112 agar medium and incubated for 15 h. Cells were flushed from the plates and incubated on ATCC 112 agar medium supplemented with appropriate antibiotics for 7–10 days (Tc = 10 μg ml^{-1}; Km = 20 μg ml^{-1}; Gm = 10 μg ml^{-1}, where Tc, tetracycline; Km, kanamycin; Gm, gentamicin). Sequential transfer of the plasmids resulted in 1×10^{-6} to 1×10^{-8} antibiotic-resistant insertants per recipient, respectively. Two clones from each conjugation experiments were chosen for further analyses. Characterized insertants were indistinguishable from wild type with respect to motility, cell morphology or growth (Supplementary Fig. 5).

Analytical methods. The optical density of *M. gryphiswaldense* cultures was measured turbidimetrically at 565 nm as described previously[19]. The optical density of *R. rubrum* cultures was measured at 660 nm and 880 nm. The ratio of 880/660 nm was used to determine yields of chromatophores within intact cells (Supplementary Fig. 4). Furthermore, *bacteriochlorophyll a* was extracted from cultures with methanol. Absorption spectra (measured in an Ultrospec 3000 photometer, GE Healthcare) of photoheterotrophically cultivated *R. rubrum_ABG6X* cells were indistinguishable from that of the wild type (Supplementary Fig. 4). The average magnetic orientation of cell suspensions (C_{mag}) was assayed with a light scattering assay as described previously[19]. Briefly, cells were aligned at different angles to a light beam by application of an external magnetic field.

Microscopy. For TEM of whole cells and isolated magnetosomes, specimens were directly deposited onto carbon-coated copper grids. Magnetosomes were stained with 1% phosphotungstic acid or 2% uranyl acetate. Samples were viewed and recorded with a Morgagni 268 microscope. Sizes of crystals and vesicles were measured with ImageJ software.

Chemical fixation, high-pressure freezing and thin sectioning of cells were performed as described previously[17]. Processed samples were viewed with an EM 912 electron microscope (Zeiss) equipped with an integrated OMEGA energy filter operated at 80 kV in the zero loss mode. Vesicle sizes were measured with ImageJ software. High-resolution TEM was performed with a JEOL 3010 microscope,

operated at 297 kV and equipped with a Gatan Imaging Filter for the acquisition of energy-filtered compositional maps. For TEM data processing and interpretation, DigitalMicrograph and SingleCrystal software were used[20]. Cryo-electron tomography was performed as described previously[21]. Fluorescence microscopy was performed with an Olympus IX81 microscope equipped with a Hamamatsu Orca AG camera using exposure times of 0.12–0.25 s. Image rescaling and cropping were performed with Photoshop 9.0 software.

Received 9 September 2013; accepted 16 January 2014; published online 23 February 2014

References

1. Prozorov, T., Bazylinski, D. A., Mallapragada, S. K. & Prozorov, R. Novel magnetic nanomaterials inspired by magnetotactic bacteria: topical review. *Mater. Sci. Eng. R* **74,** 133–172 (2013).
2. Baumgartner, J., Bertinetti, L., Widdrat, M., Hirt, A. M. & Faivre, D. Formation of magnetite nanoparticles at low temperature: from superparamagnetic to stable single domain particles. *PLoS ONE* **8,** e57070 (2013).
3. Bazylinski, D. A. & Frankel, R. B. Magnetosome formation in prokaryotes. *Nature Rev. Microbiol.* **2,** 217–230 (2004).
4. Goldhawk, D. E., Rohani, R., Sengupta, A., Gelman, N. & Prato, F. S. Using the magnetosome to model effective gene-based contrast for magnetic resonance imaging. *Wiley Interdiscip. Rev. Nanomed. Nanobiotechnol.* **4,** 378–388 (2012).
5. Murat, D. Magnetosomes: how do they stay in shape? *J. Mol. Microbiol. Biotechnol.* **23,** 81–94 (2013).
6. Lohsse, A. *et al.* Functional analysis of the magnetosome island in *Magnetospirillum gryphiswaldense*: the *mamAB* operon is sufficient for magnetite biomineralization. *PLoS ONE* **6,** e25561 (2011).
7. Pollithy, A. *et al.* Magnetosome expression of functional camelid antibody fragments (nanobodies) in *Magnetospirillum gryphiswaldense*. *Appl. Environ. Microbiol.* **77,** 6165–6171 (2011).
8. Staniland, S. *et al.* Controlled cobalt doping of magnetosomes *in vivo*. *Nature Nanotech.* **3,** 158–162 (2008).
9. Jogler, C. & Schüler, D. Genomics, genetics, and cell biology of magnetosome formation. *Annu. Rev. Microbiol.* **63,** 501–521 (2009).
10. Ullrich, S., Kube, M., Schübbe, S., Reinhardt, R. & Schüler, D. A hypervariable 130-kilobase genomic region of *Magnetospirillum gryphiswaldense* comprises a magnetosome island which undergoes frequent rearrangements during stationary growth. *J. Bacteriol.* **187,** 7176–7184 (2005).
11. Raschdorf, O., Müller, F. D., Pósfai, M., Plitzko, J. M. & Schüler, D. The magnetosome proteins MamX, MamZ and MamH are involved in redox control of magnetite biomineralization in *Magnetospirillum gryphiswaldense*. *Mol. Microbiol.* **89,** 872–886 (2013).
12. Murat, D., Quinlan, A., Vali, H. & Komeili, A. Comprehensive genetic dissection of the magnetosome gene island reveals the step-wise assembly of a prokaryotic organelle. *Proc. Natl Acad. Sci. USA* **107,** 5593–5598 (2010).
13. Schübbe, S. *et al.* Transcriptional organization and regulation of magnetosome operons in *Magnetospirillum gryphiswaldense*. *Appl. Environ. Microbiol.* **72,** 5757–5765 (2006).
14. Fu, J. *et al.* Efficient transfer of two large secondary metabolite pathway gene clusters into heterologous hosts by transposition. *Nucleic Acids Res.* **36,** e113 (2008).
15. Martinez-Garcia, E., Calles, B., Arevalo-Rodriguez, M. & de Lorenzo, V. pBAM1: an all-synthetic genetic tool for analysis and construction of complex bacterial phenotypes. *BMC Microbiol.* **11,** 38 (2011).
16. Richter, M. *et al.* Comparative genome analysis of four magnetotactic bacteria reveals a complex set of group-specific genes implicated in magnetosome biomineralization and function. *J. Bacteriol.* **189,** 4899–4910 (2007).
17. Jogler, C. *et al.* Conservation of proteobacterial magnetosome genes and structures in an uncultivated member of the deep-branching *Nitrospira phylum*. *Proc. Natl Acad. Sci. USA* **108,** 1134–1139 (2011).
18. Lefèvre, C. T. *et al.* Monophyletic origin of magnetotaxis and the first magnetosomes. *Environ. Microbiol.* **15,** 2267–2274 (2013).
19. Schüler, D. R., Uhl, R. & Bäuerlein, E. A simple light scattering method to assay magnetism in *Magnetospirillum gryphiswaldense*. *FEMS Microbiol. Ecol.* **132,** 139–145 (1995).
20. Uebe, R. *et al.* The cation diffusion facilitator proteins MamB and MamM of *Magnetospirillum gryphiswaldense* have distinct and complex functions, and are involved in magnetite biomineralization and magnetosome membrane assembly. *Mol. Microbiol.* **82,** 818–835 (2011).
21. Scheffel, A. *et al.* An acidic protein aligns magnetosomes along a filamentous structure in magnetotactic bacteria. *Nature* **440,** 110–114 (2006).
22. Rong, C. *et al.* Ferrous iron transport protein B gene (feoB1) plays an accessory role in magnetosome formation in *Magnetospirillum gryphiswaldense* strain MSR-1. *Res. Microbiol.* **159,** 530–536 (2008).
23. Grünberg, K. *et al.* Biochemical and proteomic analysis of the magnetosome membrane in *Magnetospirillum gryphiswaldense*. *Appl. Environ. Microbiol.* **70,** 1040–1050 (2004).
24. Lang, C. & Schüler, D. Expression of green fluorescent protein fused to magnetosome proteins in microaerophilic magnetotactic bacteria. *Appl. Environ. Microbiol.* **74,** 4944–4953 (2008).
25. Jogler, C. *et al.* Comparative analysis of magnetosome gene clusters in magnetotactic bacteria provides further evidence for horizontal gene transfer. *Environ. Microbiol.* **11,** 1267–1277 (2009).
26. Jogler, C. *et al.* Toward cloning of the magnetotactic metagenome: identification of magnetosome island gene clusters in uncultivated magnetotactic bacteria from different aquatic sediments. *Appl. Environ. Microbiol.* **75,** 3972–3979 (2009).
27. Nishida, K. & Silver, P. A. Induction of biogenic magnetization and redox control by a component of the target of rapamycin complex 1 signaling pathway. *PLoS Biol.* **10,** e1001269 (2012).
28. Kim, T., Moore, D. & Fussenegger, M. Genetically programmed superparamagnetic behavior of mammalian cells. *J. Biotechnol.* **162,** 237–245 (2012).
29. Murat, D. *et al.* The magnetosome membrane protein, MmsF, is a major regulator of magnetite biomineralization in *Magnetospirillum magneticum* AMB-1. *Mol. Microbiol.* **85,** 684–699 (2012).
30. Huang, H., Delikanli, S., Zeng, H., Ferkey, D. M. & Pralle, A. Remote control of ion channels and neurons through magnetic-field heating of nanoparticles. *Nature Nanotech.* **5,** 602–606 (2010).
31. Westmeyer, G. G. & Jasanoff, A. Genetically controlled MRI contrast mechanisms and their prospects in systems neuroscience research. *Magn. Reson. Imaging* **25,** 1004–1010 (2007).
32. Sambrook, J. & Russell, D. *Molecular Cloning: A Laboratory Manual* Vol. 3 (Cold Spring Harbor Laboratory Press, 2001).
33. Kolinko, I., Jogler, C., Katzmann, E. & Schüler, D. Frequent mutations within the genomic magnetosome island of *Magnetospirillum gryphiswaldense* are mediated by RecA. *J. Bacteriol.* **193,** 5328–5334 (2011).

Acknowledgements

This work was supported by the Human Frontier Science Foundation (grant RGP0052/2012), the Deutsche Forschungsgemeinschaft (grants SCHU 1080/12-1 and 15-1) and the European Union (Bio2MaN4MRI). The authors thank F. Kiemer for expert help with iron measurements and cultivation experiments.

Author contributions

I.K., D.S., Y.Z., Q.T., C.J. and R.M. planned and performed cloning experiments. I.K. and A.L. performed genetic transfers and cultivation experiments. G.W. prepared cryo- and chemically fixed cells. S.B., O.R. and G.W. performed TEM and I.K. analysed the data. J.P. and O.R. performed cryo-electron tomography experiments. E.T. and M.P. took high-resolution TEM micrographs and analysed the data. I.K. and A.L. took fluorescence micrographs and performed phenotypization experiments. I.K. performed western blot experiments and analysed proteomic data. A.B. performed Illumina genome sequencing and I.K. analysed the data. I.K. and D.S. designed the study and wrote the paper. All authors discussed the results and commented on the manuscript.

Additional information

Supplementary information is available in the online version of the paper. Reprints and permissions information is available online at www.nature.com/reprints. Correspondence and requests for materials should be addressed to Y.Z. and D.S.

Competing financial interests

I.K. and D.S. (LMU Munich) have filed a patent application on the process described in this work (Production of magnetic nanoparticles in recombinant host cells, EP13193478).

Supplementary material

Supplementary methods

Construction of Tn5 transposon plasmids

For construction of translational (C-terminal) gene fusions, the *mamDC* promoter (XbaI, BamHI restriction sites added) was cloned in front of either the *mamGFDC* operon or the *mamJ* gene (NdeI, KpnI), which were followed by the *egfp* gene (KpnI, EcoRI). The resulting construct was cloned into pBAM1[1] modified by a tetracycline resistance cassette (exchange of km^R against tc^R with SanDI and AatII). The replicative plasmid pFM211 (Frank Müller, unpublished) harboring *ftsZm* with a *mCherry* fusion under control of an inducible lac promoter was recombined with pBAM1 to construct pBAM-ftsZm_mcherry. The resident km^R was replaced by tc^R using ET-recombination. For construction of pBAM_feoAB1, a fragment with P_{mamH} and *feoAB1* was amplified by PCR from pRU1feoAB (XbaI, EcoRI) and cloned into Tet-pBAM1.

Intracellular iron measurements

Cellular iron contents were determined after incubation under photoheterotrophic conditions in 10 ml Hungate tubes using a modified version of the ferrozine assay[2]. To this end, 4 ml cultures were centrifuged for 1 min at 11.000 rpm, resuspended in 90 µl HNO_3 (65%) and incubated for 3 h at 99 °C.

Sequencing

For whole genome sequencing of strain *R. rubrum_ABG6X* a genomic DNA library was generated with the Nextera Kit (Illumina). Sequencing (1.25 Mio clusters, 2x 250 bp) was performed with a MiSeq sequencer (Illumina). Data analysis with CLC Genomics Workbench (CLCbio) confirmed single-site integration of both expression cassettes without mutations, except for a spontaneous deletion (aa 169-247) within the hypervariable non-essential CAR domain of *mamJ* which was shown to be irrelevant for protein function[3].

Magnetosome isolation, electrophoresis and immuno-chemical detection

For magnetosome isolation and expression analysis, cultures of *R. rubrum* were grown photoheterotrophically in sealed 5 liter flasks illuminated by white light, 1000 lux intensity. Cells were harvested, washed and resuspended into HEPES buffer[4]. Cell suspensions were lysed by sonication and cellular debris was removed by low-speed centrifugation. Magnetic separation of magnetosome particles, solubilization of the enclosing organic layer and fractionation of non-magnetic membrane fraction and soluble proteins were performed as previously described[5,6]. Polyacrylamide gels were prepared according to the procedure of Laemmli[7]. Protein samples from different cellular fractions (magnetosome membrane, soluble fraction, non-magnetic membrane fraction) were resuspended in electrophoresis sample buffer and denatured at 98 °C for 5 min[8]. 10 µg of protein extracts were separated on a 15% SDS-polyacrylamide gel. Protein bands were visualized by Coomassie brilliant blue staining. Western blot analysis for detection of MamC was performed as previously described[6].

Mass spectrometry

For mass spectrometry 25 µg solubilised proteins were tryptically in-gel digested as described previously[9]. The resulting fragments were separated on a C18 reversed-phase column and analyzed by nano-electrospray ionization-LC tandem MS (ESI-LC-MS/MS), recorded on an Orbitrap mass spectrometer[9]. Spectra were analyzed via Mascot™ software using the NCBI nr Protein Database and a database from *M. gryphiswaldense*[10].

Supplementary tables & figures

Table S1: Summary of magnetic responses (C_{mag}), intracellular iron content and crystal size and number of various strains (median values, ± = standard deviation). If not indicated otherwise, cells were grown in the presence of 50 µM ferric citrate. Magnetic response and total iron content measurements were performed with (n) biological replicates under identical conditions (see also material & methods). For determination of crystal size and number per cell, cells of one clone were analyzed by TEM (n=sample size). The Mann-Whitney test (http://elegans.som.vcu.edu/~leon/stats/utest.html) was performed for crystal size comparison of *R. rubrum_ABG6X* and *R. rubrum_ABG6X_feo*: the difference was highly significant (p<0.001, two tailed test). Crystal size comparison of *R. rubrum_ABG6X_feo* and *M. gryphiswaldense* revealed no significant difference (p≥0.05, two tailed test).

Strain	Magnetic response ("C_{mag}")	Iron content (% dry weight)	Crystal size (nm)	Crystal number per cell
M. gryphiswaldense MSR-1	1.4 ± 0.2 (n=3)	3.5 (n=3)	36 ± 9 (n=310)	24 ± 8 (n=52)
M. gryphiswaldense Δ*mamAB_AB*	1.2 ± 0.2 (n=3)	n.d.	37 ± 10 (n=112)	23 ± 7 (n=24)
M. gryphiswaldense MSR-1B_*AB*	0.2 (n=3)	n.d.	17 ± 6 (n=112)	16 ± 6 (n=20)
M. gryphiswaldense MSR-1B_*ABG*	0.6 ± 0.1, (n=3)	n.d.	25 ± 6 (n=104)	13 ± 6 (n=20)
M. gryphiswaldense MSR-1B_*ABG6*	0.9± 0.2 (n=3)	n.d.	35 ± 8 (n=103)	18 ± 8 (n=22)
R. rubrum ATCC 11170	-	0.07 ± 0.04 (n=3)	-	-
R. rubrum_AB	-	0.08 (n=3)	-	-
R. rubrum_ABG	-	0.10 ± 0.01 (n=3)	-	-
R. rubrum_ABG6	-	0.17 (n=4)	12 ± 6 (n=304)	26 ± 10 (n=50)
R. rubrum_ABG6X	0.3 ± 0.2 (n=3)	0.17 ± 0.02 (n=4)	24 ± 7 (n=307)	10 ± 4 (n=50)
R. rubrum_ABG6X 500 µM ferric citrate	0.3 (n=4)	n. d.	25 ± 7 (n=301)	11 ± 5 (n=51)
R. rubrum_ABG6X 100 µM ferrous sulfate	0.2 (n=4)	n.d.	24 ± 8 (n=312)	10 ± 5 (n=52)
R. rubrum_ABG6X_ftsZm	0.6 ± 0.1* (n=3)	0.18 ± 0.03 (n=3)	26 ± 9 (n=300)	11 ± 4 (n=51)
R. rubrum_ABG6X_dJ	0.2 (n=3)	0.18 ± 0.01 (n=3)	27 ± 9 (n=300)	9 ± 4 (n=50)**

R. rubrum_ABG6X_dI	-	0.09 ± 0.07 (n=3)	-	-
R. rubrum_ABG6X_feo	0.8 ± 0.1 (n=3)	0.28 ± 0.07 (n=3)	37 ± 10 (n=300)	10 ± 4 (n=52)

*The slightly increased C_{mag} is likely due to effects of the genuine cell division protein FtsZm on cell morphology, as no difference in iron content and crystal size or number per cell was detectable.
**64% of mutant cells (n=32) harbored clustered magnetosomes, whereas 36% still showed a chain-like alignment of magnetosomes (n=18).

Table S2: Magnetosome proteins identified in the MM of strain *R. rubrum_ABG6X* by nano-electrospray ionization-LC tandem MS (ESI-LC-MS/MS). Spectra were analyzed via Mascot™ software using the NCBI nr Protein Database and a database from *M. gryphiswaldense*[10] (asterisks). Proteins are listed in the order of their exponentially modified protein abundance index (emPAI). The data have been deposited to ProteomeXchange with identifier PXD000348 (DOI 10.6019/PXD000348).

Protein	Accession number	Coverage (%)	No. of spectrum matches	No. of sequence peptides	Molecular weight (kDa)	Calculated pI	emPAI	Putative function
MamK	MGR_4093	57	9	9	39.6	5.4	1.51	Magnetosome chain assembly/positioning [11,12]
MamC	MGR_4078	32	4	3	12.4	5.1	1.01	Crystal size and shape control [13]
MamJ	MGR_4092	32	10	6	48.6	4.0	0.76	Magnetosome chain assembly [14]
MamA	MGR_4099	37	1	1	23.9	5.7	0.65	TPR-like protein associated with the magnetosome membrane [15,16]
MamF	MGR_4076	17	1	1	12.4	9.1	0.60	Magnetosome size and shape control [13]
Mms6	MGR_4073	19	1	1	12.7	9.5	0.58	Magnetosome crystallization [17,18]
MamD	MGR_4077	20	3	3	30.2	9.8	0.49	Crystal size and shape control [13]
MamM*	MGR_4095	15	3	3	34.7	5.8	0.42	Iron transport/MM assembly [4]
MmsF*	MGR_4072	8	2	1	13.9	9.3	0.23	Crystal size and shape control [19]
MamB*	MGR_4102	7	1	1	32.1	5.4	0.21	Iron transport/MM assembly [4]
MamY*	MGR_4150	18	2	2	40.9	4.8	0.16	Tubulation and magnetosome membrane formation [20]
MamO*	MGR_4097	6	3	3	65.3	6.5	0.15	Magnetosome crystallization [21,22]
MamE	MGR_4091	4	2	2	78.3	8.1	0.08	Magnetosome crystallization [21,22]

Table S3: Strains and plasmids used in this study. Km^R= kanamycin resistance, Tc^R= tetracycline resistance, Ap^R= ampicillin resistance, BSD^R= blasticidin S resistance, Cm^R= chloramphenicol resistance, Gm^R= gentamicin resistance, $Spec^R$= spectinomycin resistance.

Strain or plasmid	Characteristics	Reference(s) or source
Magnetospirillum gryphiswaldense strains		
M. gryphiswaldense MSR-1	Wild-type (wt)	DSM-6361[23]
M. gryphiswaldense MSR-1B	spontaneous unmagnetic mutant lacking parts of the MAI	[24]
M. gryphiswaldense ∆*mamAB*	*mamAB* deletion mutant	[25]
M. gryphiswaldense ∆*mamAB _AB*	Km^R, transposon mutant with inserted *mamAB* operon	This study
M. gryphiswaldense MSR-1B*_AB*	Km^R, transposon mutant with inserted *mamAB* operon	This study
M. gryphiswaldense MSR-1B*_ABG*	Km^R, $Spec^R$, transposon mutant with inserted *mamAB and mamGFDC* operon	This study
M. gryphiswaldense MSR-1B*_ABG6*	Km^R, Cm^R, transposon mutant with inserted *mamAB, mamGFDC* and *mms6* operon	This study
Rhodospirillum rubrum strains		
R. rubrum ATCC 11170	wt	[26] (kindly provided by H. Grammel, Magdeburg)
R. rubrum_AB	Km^R, transposon mutant with inserted *mamAB* operon	This study
R. rubrum_ABG	Km^R, $Spec^R$, transposon mutant with inserted *mamAB and mamGFDC* operon	This study
R. rubrum _ABG6	Km^R, Cm^R, transposon mutant with inserted *mamAB, mamGFDC* and *mms6* operon	This study
R. rubrum_ABG6X	Km^R, Cm^R, Gm^R transposon mutant with inserted *mamAB, mamGFDC, mms6* and *mamXY* operon (without *ftsZm*)	This study
R. rubrum_ABG6X_dJ	Km^R, Cm^R, Gm^R, Ap^R transposon mutant with inserted *mamAB* (*mamJ* deletion), *mamGFDC, mms6* and *mamXY* operon (without *ftsZm*)	This study
R. rubrum_ABG6X_dI	Km^R, Cm^R, Gm^R, Ap^R transposon mutant with inserted *mamAB* (*mamI* deletion), *mamGFDC, mms6* and *mamXY* operon (without *ftsZm*)	This study

R. rubrum_ABG6X_ftsZm	Km^R, Cm^R, Gm^R, Tc^R transposon mutant with inserted *mamAB, mamGFDC, mms6* and *mamXY* operon (without *ftsZm*) and *ftsZm* under control of an inducible lac promoter	This study
R. rubrum_ABG6X_feo	Km^R, Cm^R, Gm^R, Tc^R transposon mutant with inserted with inserted *mamAB, mamGFDC, mms6, mamXY* and *feoAB1* operon	This study
R.rubrum_GFDC-EGFP	Tc^R transposon mutant with inserted *mamGFDC-EGFP*	This study
R.rubrum_ABG6X_GFDC-EGFP	Km^R, Cm^R, Gm^R, Tc^R transposon mutant with inserted *mamAB, mamGFDC, mms6* and *mamXY* operon (without *ftsZm*) and *mamGFDC-EGFP*	This study
R. rubrum_J-EGFP	Tc^R transposon mutant with inserted *mamGFDC-EGFP*	This study
R. rubrum_ABG6X_J-EGFP	Km^R, Cm^R, Gm^R, Tc^R transposon mutant with inserted *mamAB, mamGFDC, mms6* and *mamXY* operon (without *ftsZm*) and *mamJ-EGFP*	This study
Escherichia coli strains		
DH10b	*F– mcrA Δ(mrr-hsdRMS-mcrBC) Φ80lacZΔM15 ΔlacX74 recA1 endA1 araD139 Δ(ara leu) 7697 galU galK rpsL nupG λ–*	Invitrogen
BW29427	*dap* auxotroph derivative of *E. coli* strain B2155	K. Datsenko and B. L. Wanner, unpublished
WM3064	*thrB1004 pro thi rpsL hsdS lacZΔM15 RP4-1360 Δ(araBAD)567 ΔdapA1341::[erm pir]*	W. Metcalf, kindly provided by J. Gescher, KIT Karlsruhe
Plasmids		
pSC101-BAD-gbaA	Tc^R, replicative plasmid containing redα/redβ recombinases under the control of a L-Arabinose inducible promoter, temperature sensitive origin of replication	[27]
p15A-Tps-oriT-Km	Km^R, BSD^R, oriT, p15A origin of replication, mariner tps, cloning cassette	[28]
pSSK18 (BAC_*mamAB*)	BAC containing the *mamAB* operon from *M. gryphiswaldense*	[24]
pTps_AB	Km^R, BSD^R, mariner tps vector containing *mamAB* operon	This study
pTps_ABG	$Spec^R$, Km^R, BSD^R, mariner tps vector with *mamAB* and *mamGFDC* operon	This study

pTps_ABG6	Cm^R, Km^R, BSD^R, mariner tps vector with *mamAB*, *mamGFDC*, and *mms6* operon	This study
pTps_XYZ	Gm^R, BSD^R, mariner Tps vector with *mamY*, *mamX* and *mamZ*	This study
pTps_ABG6_dJ	Cm^R, Km^R, BSD^R, Ap^R, mariner tps vector with *mamAB*, *mamGFDC*, and *mms6* operon, (*mamJ* deletion)	This study
pTps_ABG6_dI	Cm^R, Km^R, BSD^R, Ap^R, mariner tps vector with *mamAB*, *mamGFDC*, and *mms6* operon, (*mamI* deletion)	This study
pBAM1	Km^R, Ap^R, γR6K origin of replication, oriT, Tn5 vector	[1]
Tet-pBAM1	Tc^R, Ap^R, γR6K origin of replication, oriT, Tn5 vector	This study
Tet-pBam_mamGFDC-EGFP	Tc^R, Ap^R, *mamGFDC* operon under control of $P_{mamDC}$with a C-terminal EGFP fusion, Tn5 vector	This study
Tet-pBam_MamJ-EGFP	Tc^R, Ap^R, *mamJ* under control of P_{mamDC} with a C-terminal EGFP fusion, Tn5 vector	This study
pRU-1feoAB	Km^R, broad host range pBBRMCS2, *feoAB1* operon under the control of P_{mamH}	R. Uebe, unpublished
Tet-pBam_feoAB1	Tc^R, Ap^R, *feoAB1* operon under the control of P_{mamH}, Tn5 vector	This study
Tet-pBam-ftsZm_mCherry	Tc^R, Ap^R, *ftsZm, lacI* with a C-terminal mCherry fusion under control of inducible P_{lac}, Tn5 vector	This study
pFM211	Km^R, broad host range pBBRMCS2, lacI, *ftsZm* with C-terminal *mCherry* fusion, *mamK* with N-terminal EGFP fusion	F. Müller, unpublished

Table S4: Oligonucleotides used in this study.

Primer	Nucleotide sequence (5'-3')[a]	Product
Mam-tps5	AATTCGCACGGACTATAGCAACGAATCGAGGTCGGTTGACAAGC CATAAATCAGAAGAACTCGTCAAGAAGGC	p15A-Tps-oriT-Km, ET-recombination with BAC_*mamAB,* pTps_AB
Mam-tps3	GAACGAAGATGAGACAGAAATCCGTGGCGCCGAGCGTAAGCAT CCGGTGAGAACCTCATTCCCTCATGATACAG	
mamGFC3	TATCATGAGGGAATGAGGTTCTCACCGGATGCTTACGCTCGGCG CCAGAGCACATCGGGGTGAATGACGAC	*mamGFDC* operon, ET-recombination with pTps_AB
mamGFC5	CGCTAGCTGCGGGTTATTCGCATTTGC	
spectMam3	TCAAAACCCGCGCAGAGGCAAATGCGAATAACCCGCAGCTAGC GTTATAATTTTTTTAATCTGTTATT	Spectinomycin resistance cassette, ET-recombination with pTps_AB
spectMam5	TGATCCGCTATGGTAAGCGCATCATGTCCGGATCCCATGGCGTT CCGCTCGTAACGTGACTGGCAAGAGATATT	
mms6cm5	TACTGCGATGAGTGGCAGGGCGGGGCGTAAGCTTACAATTTCCA TTCGCCATTC	*mms6* operon, ET-recombination with pTps_ABG
mms6mam3	GTGCTTCGCTGTGTCCACAAGAACC	
cm-mms6-3	TGGCGAATGGAAATTGTAAGCTTACGCCCCGCCCTGCCACTC	Chloramphenicol resistance cassette, ET-recombination with pTps_ABG
cm-mms6-5	TGATCCGCTATGGTAAGCGCATCATGTCCGGATCCCATGGCGTT CCGCTCGTCCTGGTGTCCCTGTTGATACC	
IK097	TCTAGAGGGCCCCAACTTTTTCGCTTTACTAGCTCTTAGTTCTCC AATAAATTCCCTGCGTCGA	P_{mamDC} in pBAM1
IK098	CATATGCTGATCTCCGGCAAGTGTATGCACGATTCCCTCTCTGC CCCTTAAAATCGACGCAGGGAAT	
IK107	CATATGATCAAGGGCATCGCGGG	*mamGFDC* operon in pBAM1
IK101	GGTACCGGCCAATTCTTCCCTCAGAA	
IK102	GGTACCGGAGGCGGAGGCGGT	*egfp* in pBAM1
IK103	GAATTCTTACTTGTACAGCTCGTCCATG	
IK163	GAATTCTTAGCCGATTCGCAG	*mamXY*-operon (without ftsZm), ET-recombination with p15A-Tps-oriT-Gm
IK164	GAGCTCGGCAGCCTCATTTAAA	
IK173	CCGGAATTGCCAGCTGGGGCGCCCTCTGGTAAGGTTGGGAAGC CCTGCAACGTATAATATTTGCCCATG	Gentamicin resistance cassette, ET-Recombination with p15A-Tps-oriT-Km
IK174	AGGCGATAGAAGGCGATGCGCTGCGAATCGGGAGCGGCGATAC CGTAAAGCGATCTCGGCTTGAA	
IK208	CCCGGTACCCAGCTTTTGTTCCCTTTAGTGAGGGTTAATTGCGC GCTTGGCCTCATTCCCTCATGATACAGAGAC	p15A-Tps-oriT-Gm, ET-recombination with *mamXY*
IK209	GGCGTTACCCAACTTAATCGCCTTGCAGCACATCCCCCTTTCGC CAGCTGTCTCGGCTTGAACGAATTG	
IK213	GACGTCGAGCCACGGCGG	Tetracycline resistance cassette in pBAM1
IK214	GGGTCCCTCAGGTCGAGGTGGC	
IK215	TCTAGACTACAAGAATGTCCCGC	*feoAB1* operon+P_{mamH} in pBAM1
IK216	GAATTCGGCATCCTGATCGGT	
IK217	CATATGATGGCAAAAAACCGG	*mamJ* in pBAM1
IK218	GGCGGTACCTTTATTCTTATCTTCAGCATCAC	
IK235	GGGTGGAGCGGGATAATGGCAAAAAACCGGCGTGATCGCGGCA CGGCTAAATACATTCAAATATGTATCC	Ampicillin resistance cassette insertion into *mamJ* of pTps_ABG6
IK236	CTATTTATTCTTATCTTCAGCATCACATTTCGGCGATGAACAACTA CCTTACCAATGCTTAATCAGTG	
IK239	CGCCGCTTGTGTTCTGTATCAAGACTGGAGAACGTTTATGCCAA CTAAATACATTCAAATATGTATCC	Ampicillin resistance cassette Insertion into *mamI* of pTps_ABG6
IK240	TCAACCATCGATGTTAGGGTCTGAGTTCGCCCTCTTACCGGCAG GTTACCAATGCTTAATCAGTG	
IK251	AAACCGCCCAGTCTAGCTATCGCCATGTAAGCCCACTGCAAGCT ACCTGCCCTCATTCCCTCATGATACA	Tet-pBAM1, ET-recombination with recombination with pFM211
IK252	CAGCACATCCCCCTTTCGCCAGCTGGCGTAATAGCGAAGAGGCC CGCACCGGATTTTGAGACACAAGACGTC	

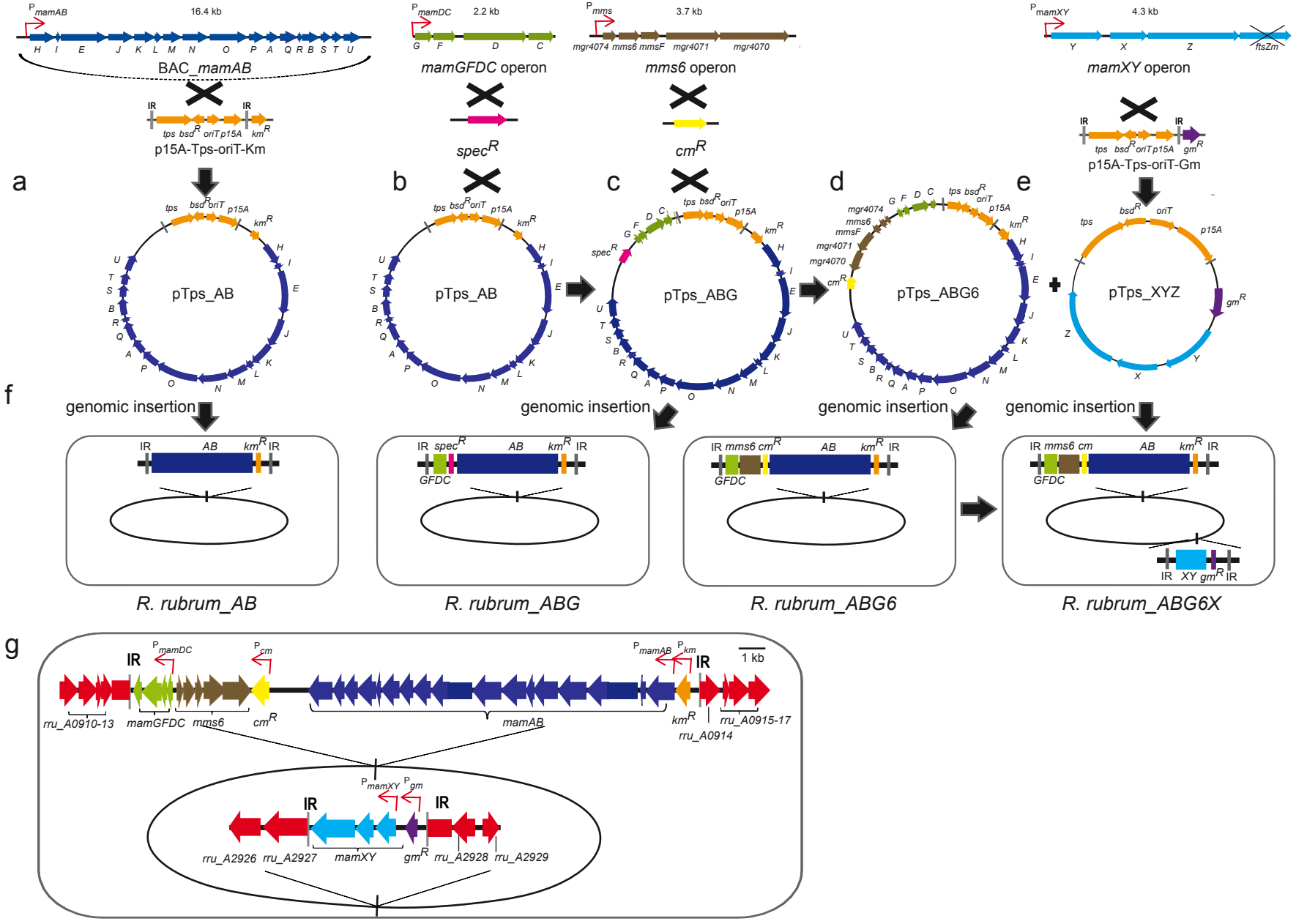
BAC_mamAB
16.4 kb
mamGFDC operon
2.2 kb
mms6 operon
3.7 kb
mamXY operon
4.3 kb
p15A-Tps-oriT-Km
p15A-Tps-oriT-Gm
specR
cmR
a
b
c
d
e
pTps_AB
pTps_ABG
pTps_ABG6
pTps_XYZ
f
genomic insertion
R. rubrum_AB
R. rubrum_ABG
R. rubrum_ABG6
R. rubrum_ABG6X
g
1 kb
rru_A0910-13
mamGFDC
mms6
cmR
mamAB
kmR
rru_A0914
rru_A0915-17
rru_A2926
rru_A2927
mamXY
gmR
rru_A2928
rru_A2929

Fig. S1: Construction scheme of insertion cassettes for modular expression of the *mam* and *mms* operons. (**a**) Recombineering of a BAC containing the *mamAB* operon (blue) and a vector backbone (Km-p15A-Tps-oriT-Km, orange) harboring a MycoMar transposase gene (*tps*), inverted repeats (IR), origin of transfer (*oriT*), p15A origin of replication (*p15A*) and a *kanamycin*^{R} cassette (*km*^{R}, orange). (**b**) Insertion of a *spectinomycin*^{R} cassette (*spec*^{R}, pink) and the *mamGFDC* operon (green) into pTps_AB by triple recombination. (**c & d**) Stitching of pTps_ABG by insertion of the *mms6* operon and a *chloramphenicol*^{R} cassette. (**e**) pTps_XYZ consisting of a Tps vector backbone (orange), *mamXYZ* (pale blue) and a *gentamicin*^{R} gene (*gm*^{R}, purple) was constructed. (**f**) Plasmids were transferred by conjugation into *R. rubrum*. Transposition of the DNA-fragments within the IR sequences occurred at random positions at TA dinucleotide insertion sites by a “cut and paste” mechanism[29]. (**g**) Chromosomal insertion sites of the transposed constructs in *R. rubrum_ABG6X* are shown with adjacent genes (red) as revealed by whole genome sequencing performed with a MiSeq sequencer (Illumina) (accession number of *R. rubrum* ATCC 11170: NC_007643). pTps_ABG6 inserted within a gene encoding a putative aldehyd dehydrogenase (YP_426002), and pTps_XYZ inserted within rru_A2927, encoding a putative acriflavin resistance protein (protein accession number YP_428011). Sequences of inserted magnetosome operons matched those of the donor (*M. gryphiswaldens*e) with no detectable mutations, except for a deletion (aa 169-247) within the hypervariable non-essential CAR domain of *mamJ,* which was shown to be irrelevant for protein function[30].

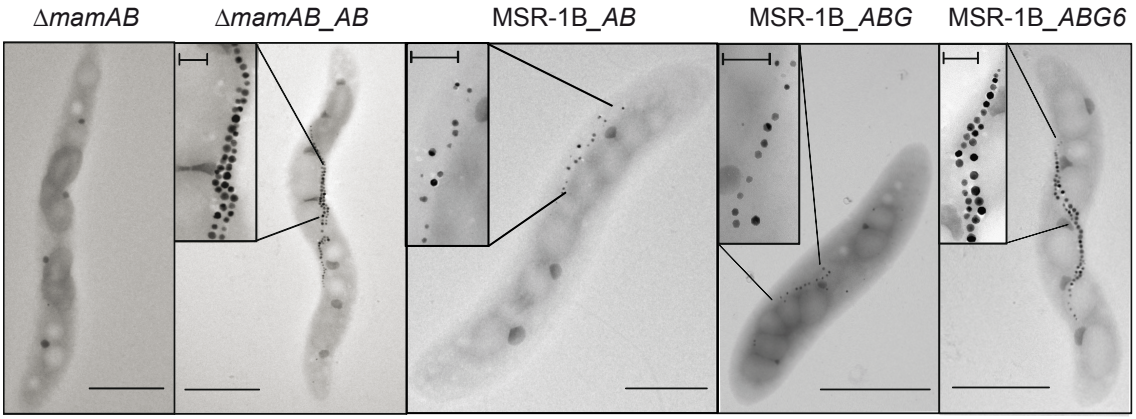

Fig. S2: Transmission electron micrographs of MSR mutants expressing various insertional transposon constructs. The plasmids pTps_AB, pTps_ABG and pTps_ABG6 were transferred into the non-magnetic *M. gryphiswaldense* mutants Δ*mamAB*[25] and MSR-1B, the latter lacking most of the magnetosome genes except of the *mamXY* operon[24,25]. After transfer of pTps_AB, a wt-like phenotype was restored in *ΔmamAB_AB* as revealed by C_{mag} (1.2 ± 0.2) and measured crystal sizes (37 ± 10 nm) in comparison with *M. gryphiswaldense* wt (36 ± 9 nm, C_{mag}=1.4 ± 0.2) (see also Table S1). Mutant MSR-1B was only partly complemented after insertion of pTps_AB and pTps_ABG, that is, C_{mag} and crystal sizes were still lower than in the wt (Table S1). Transfer of pTps_ABG6 restored nearly wt-like magnetosome formation in MSR-1B (35 ± 8 nm, C_{mag}=0.9± 0.1). ±= s.d. Scale bar: 1 µm, insets: 0.2 µm.

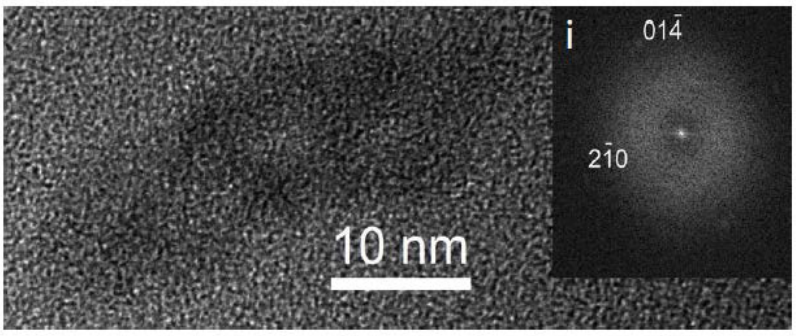

Fig. S3: HRTEM image of a poorly crystalline iron oxide particle from *R. rubrum_ABG6* with the corresponding Fourier transform (i) that shows diffuse, faint intensity maxima consistent with the structure of hematite.

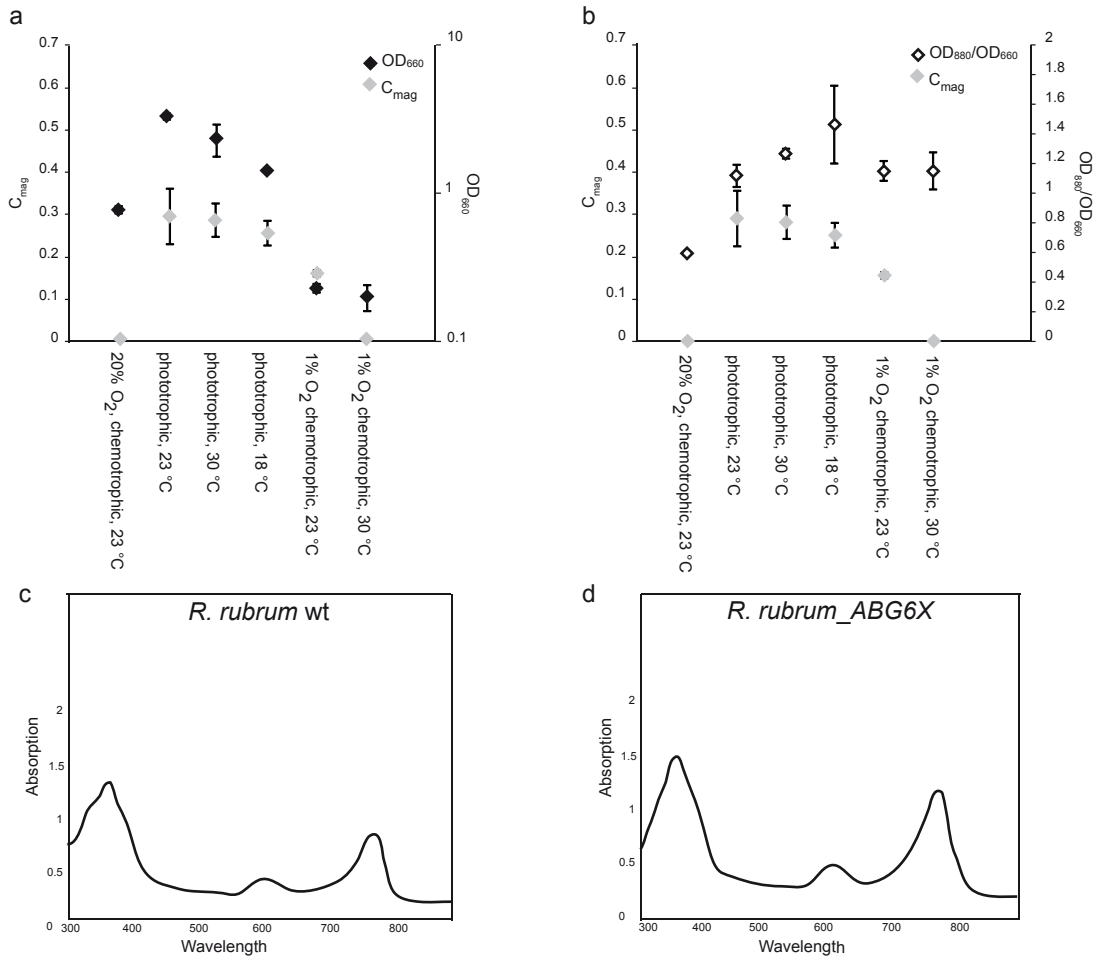

Fig. S4: Growth, magnetic response and ICM/Bchl a production of *R. rubrum_AGB6X*. (**a & b**) Cells were grown in ATCC 112 (chemotrophic, 20% O_2), Sistrom A (phototrophic, anoxygenic) and M2SF (chemotrophic, 1%O_2) medium for 3 (30 °C), 4 (23 °C) or 10 (18 °C) days. Optical density at 660 nm (minimal Bchl a absorption, black diamonds), 880 nm (maximal Bchl a absorption) and magnetic response (grey diamonds) were measured. The ratio OD_{880}/OD_{660} (white diamonds) correlates with the amount of chromatophores produced in the cells[31] (median values n=3, error bars indicate s.d.). No C_{mag} was detectable under aerobic and microaerobic conditions at 30 °C. (**c & d**) Absorption spectra of extracted bacteriochlorophylls from *R. rubrum* wt (**c**) and *R. rubrum_ABG6X* (**d**) (phototrophic growth, 30 °C).

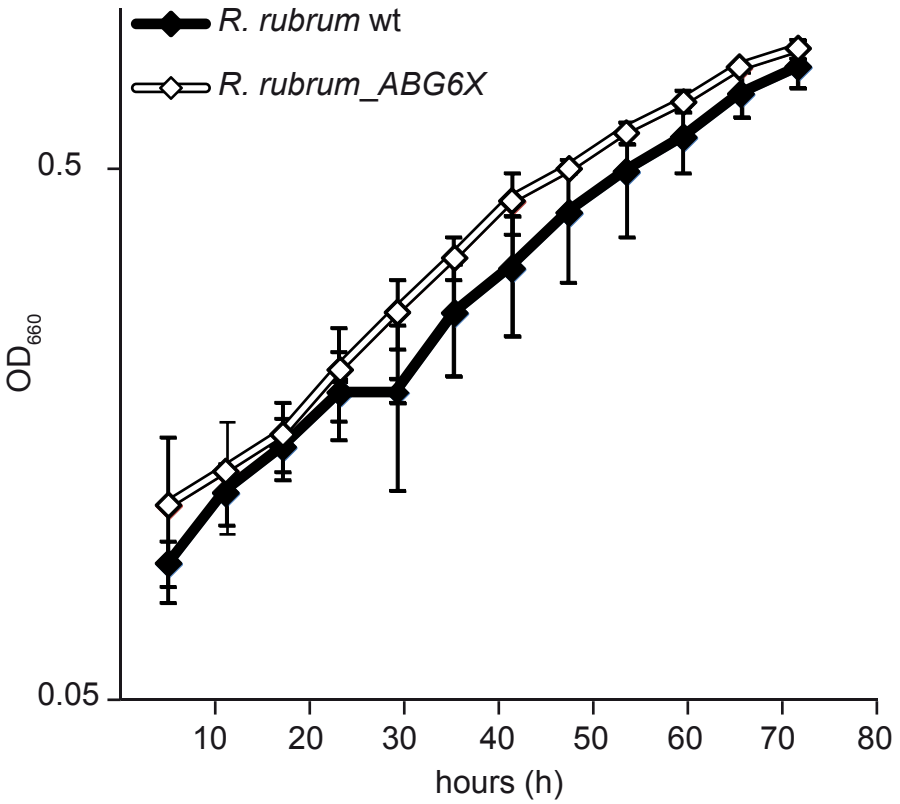

Fig. S5: Growth of *R. rubrum* wt and *R. rubrum_ABG6X* (OD_{660}). Cells of *R. rubrum* (Sistrom A medium, 1000 lux) were incubated in Sistrom A medium (1000 lux) for 3 days at 23 °C under anaerobic conditions. No major growth differences between wt (n=3) and mutant strain *ABG6X* (median values n=3, error bars indicate s.d.) were detectable .

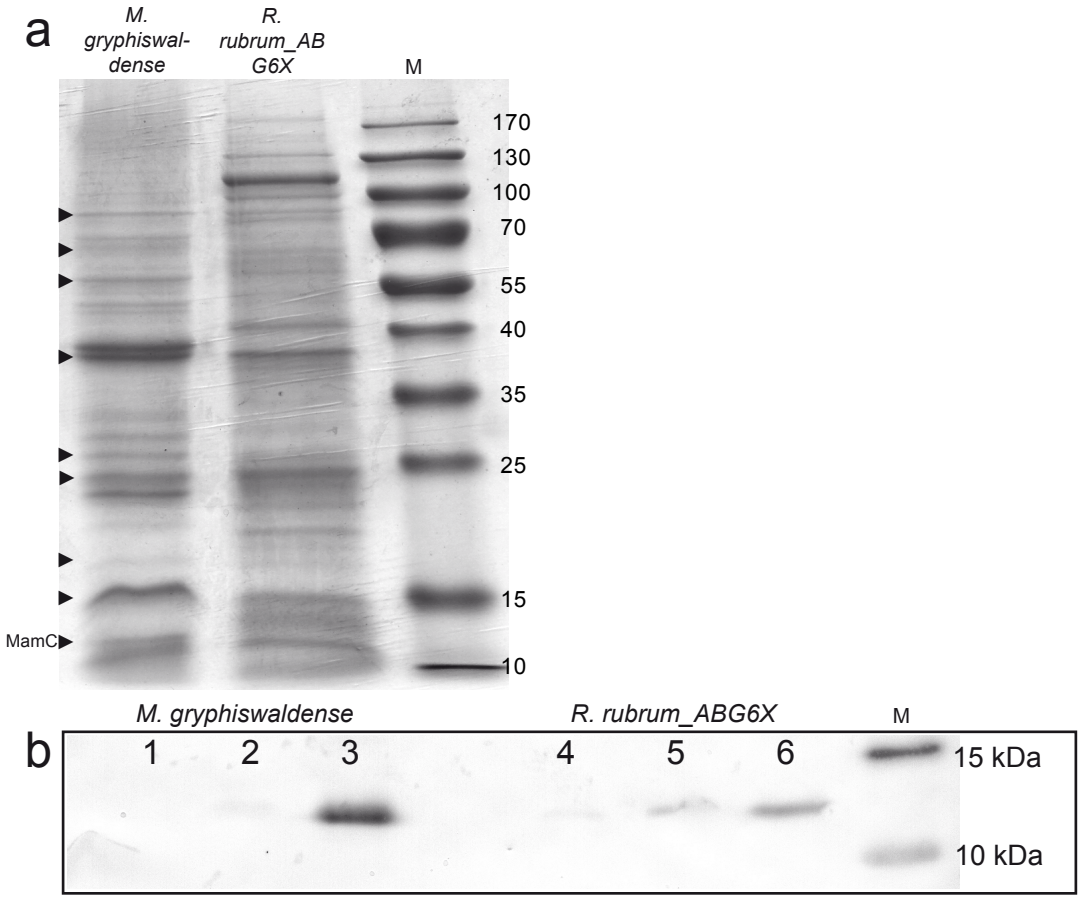

Fig. S6: Proteomic analysis of magnetosomes from *R. rubrum_ABG6X*. (**a**) 1D SDS-PAGE of Coomassie blue stained proteins solubilized from isolated magnetosome particles of *M. gryphiswaldense* and *R. rubrum_ABG6X*. Bands of the same size are indicated (arrowheads). (**b**) Immunodetection of MamC (12.4 kDa) in blotted fractions of *M. gryphiswaldense* and *R. rubrum_ABG6X* using an anti-MamC antibody[6]. A signal for MamC was detectable in the magnetic membrane fraction of *R. rubrum_ABG6X* (6), which was absent from the soluble fraction, but faintly present also in the non-magnetic membrane fraction (5), possibly originating from empty membrane vesicles or incomplete magnetic separation during isolation. Protein extracts from *M. gryphiswaldense*: 1. soluble fraction, 2. non-magnetic membrane fraction, 3. magnetosome membrane. Protein extracts from *R. rubrum_ABG6X*: 4. soluble fraction, 5. non-magnetic membrane fraction, 6. magnetic ("magnetosome") membrane fraction. M: Marker.

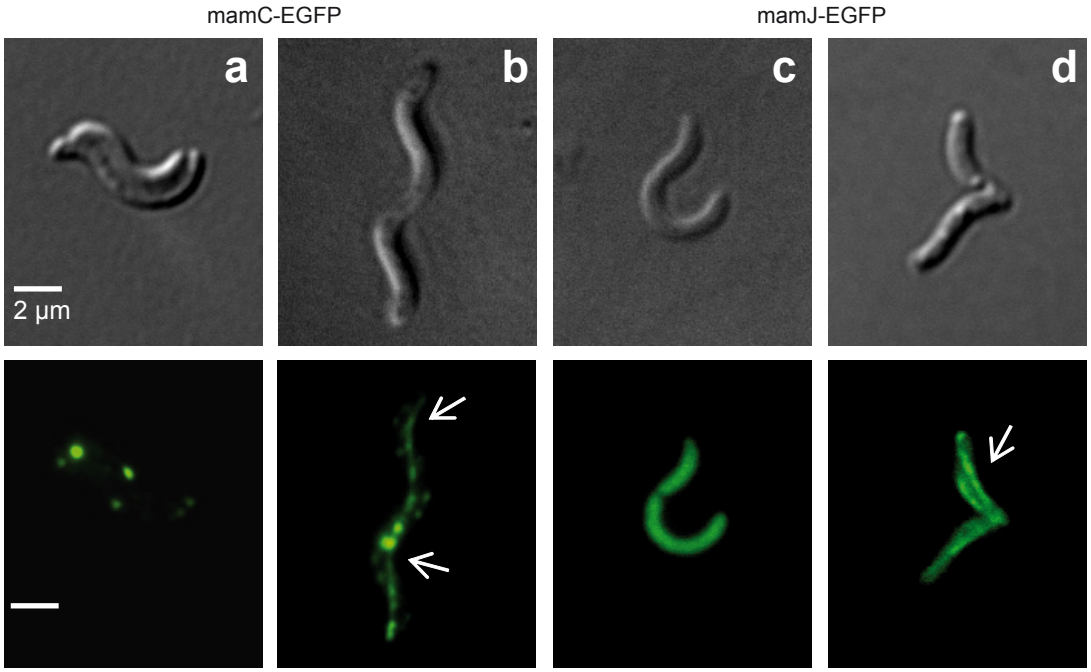

Fig. S7: Fluorescence microscopy of *R. rubrum* wt and *R. rubrum_ABG6X* cells expressing different EGFP-tagged magnetosome proteins. For localization studies of fluorescently labeled magnetosome proteins, strains were cultivated in ATCC medium overnight at 30 °C with appropriate antibiotics (Table S3). (**a & b**) MamGFDC with a C-terminal MamC-EGFP fusion expressed in *R. rubrum* wt (n=151) (**a**), and *R. rubrum_ABG6X* (n=112) (**b**). In the transformed strain, a filamentous structure is visible for 79% of the cells (n=89). **c & d**, MamJ-EGFP expressed in *R. rubrum* wt (n=109) (**c**), and in *R. rubrum_ABG6X* (n=89) displaying a chain-like fluorescence signal in 63% of the cells (n=56) (**d**). Scale bar: 2 µm.

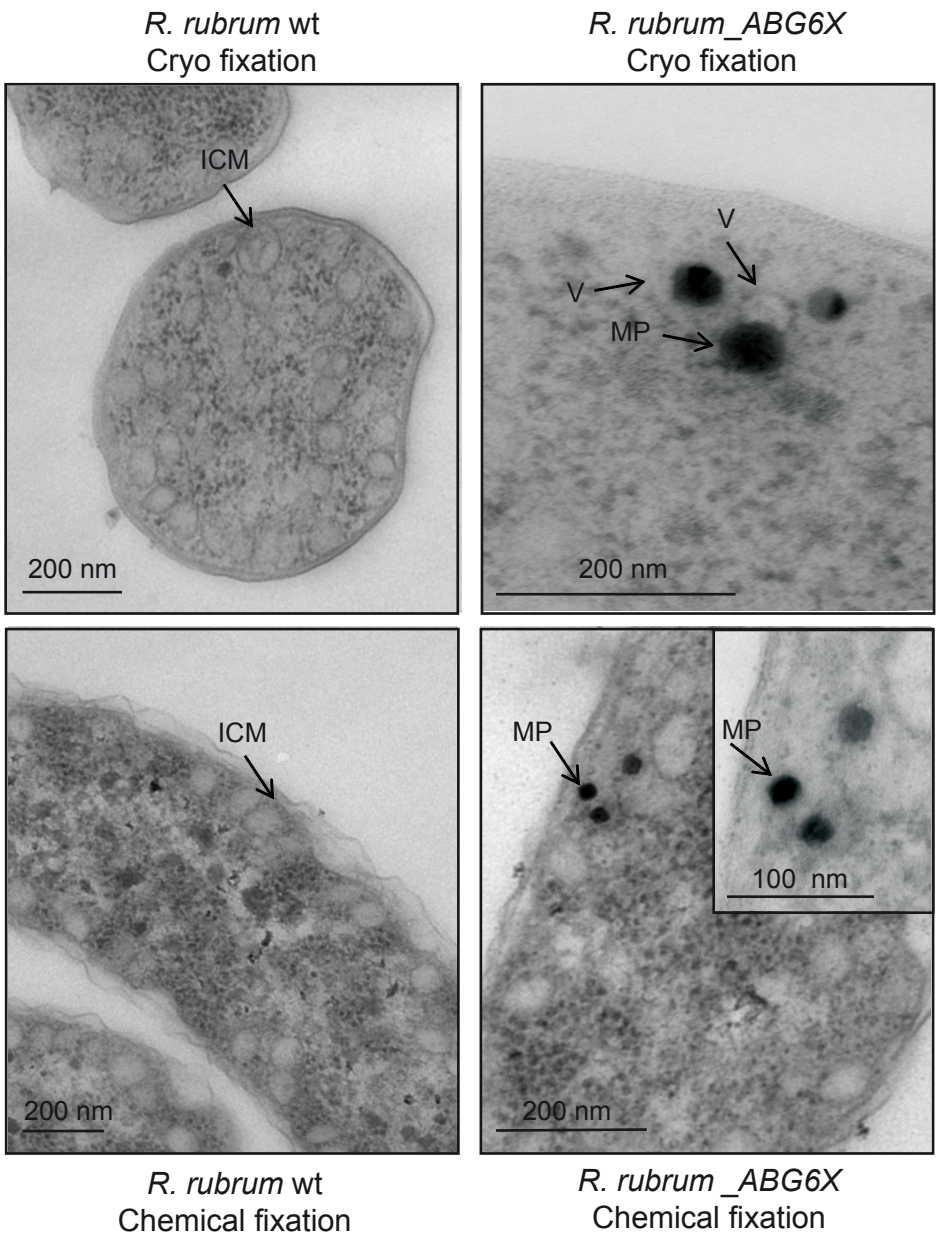

Fig. S8: TEM of cryo- or chemically fixed, thin sectioned *R. rubrum* strains. Cells were cultivated under photo-heterotrophic conditions. ICM sizes of cryo-fixed *R. rubrum* wt (93 ± 34 nm, n=95) and vesicles surrounding immature magnetosomes of cryo-fixed *R. rubrum_ABG6X* (66 ± 6 nm, n=6) were measured.

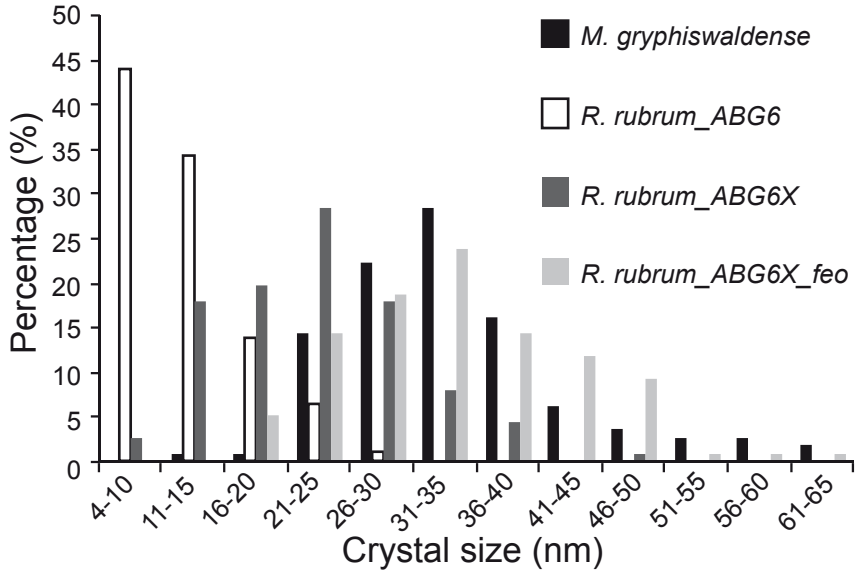

Fig. S9: Size distribution of magnetosome crystals in *M. gryphiswaldense* and different *R. rubrum* strains. Whereas crystals of *R. rubrum_ABG6* (n=303) and *R. rubrum_ABG6X* (n=306) were smaller than those of the donor *M. gryphiswaldense* (n=310), crystal sizes of *R. rubrum_ABG6X_feo* (n=301) were significantly larger, approaching those of the donor strain (see also Supplementary Table 1).

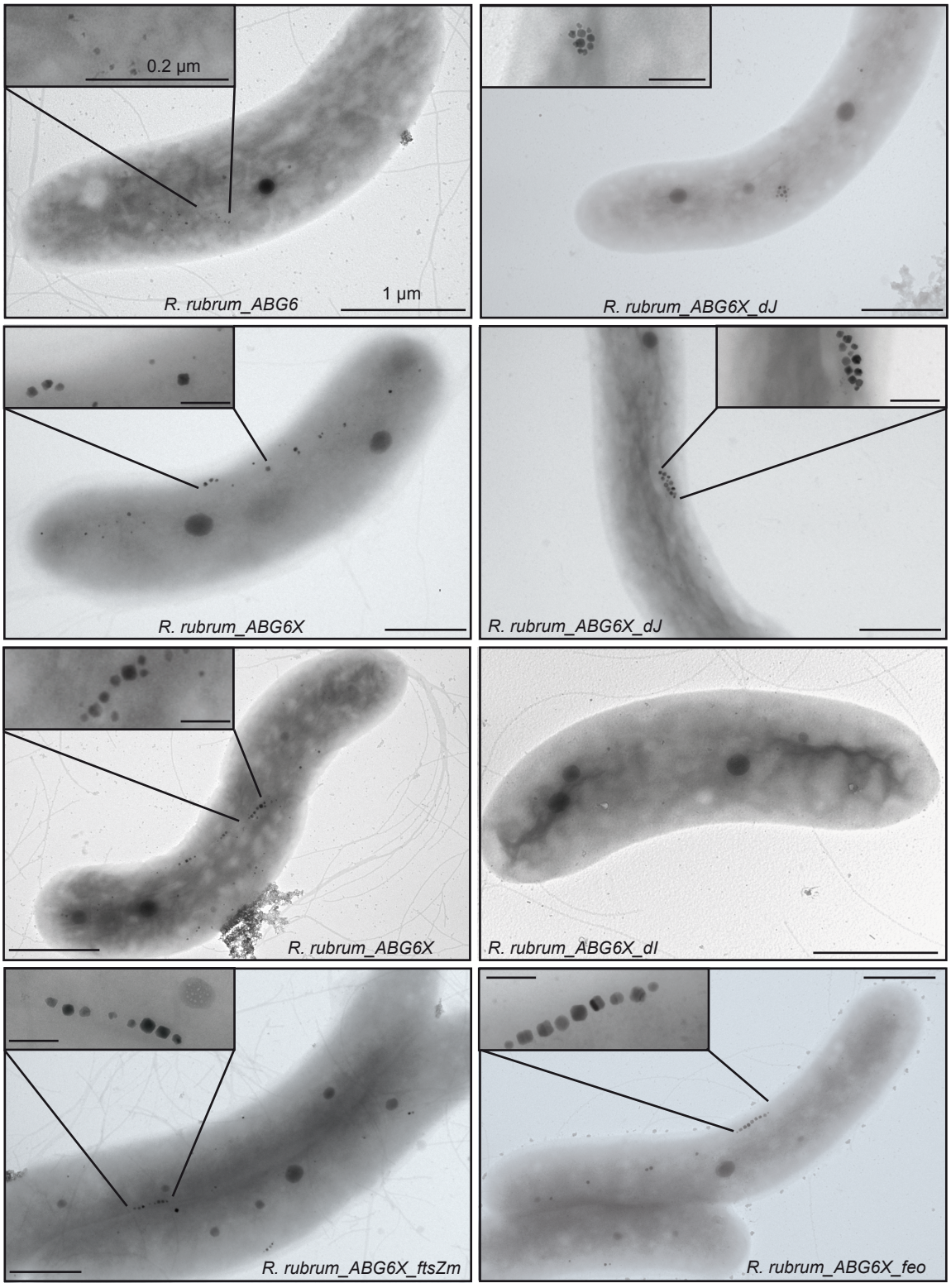

Figure S10: Transmission electron micrographs of whole cells of different *R. rubrum* strains expressing magnetosome gene clusters. Scale bar: 1 µm, inset: 0.2 µm.

References

1 Martinez-Garcia, E., Calles, B., Arevalo-Rodriguez, M. & de Lorenzo, V. pBAM1: an all-synthetic genetic tool for analysis and construction of complex bacterial phenotypes. *BMC Microbiol.* **11**, 38 (2011).

2 Viollier, E., Inglett, P. W., Hunter, K., Roychoudhury, A. N. & Van Cappellen, P. The ferrozine method revisited: Fe(II)/Fe(III) determination in natural waters. *Appl. Geochemistry* **15**, 785-790 (2000).

3 Scheffel, A. & Schüler, D. The acidic repetitive domain of the *Magnetospirillum gryphiswaldense* MamJ protein displays hypervariability but is not required for magnetosome chain assembly. *J. Bacteriol.* **189**, 6437-6446 (2007).

4 Uebe, R. *et al.* The cation diffusion facilitator proteins MamB and MamM of *Magnetospirillum gryphiswaldense* have distinct and complex functions, and are involved in magnetite biomineralization and magnetosome membrane assembly. *Mol. Microbiol.* **82**, 818-835 (2011).

5 Grünberg, K. *et al.* Biochemical and proteomic analysis of the magnetosome membrane in *Magnetospirillum gryphiswaldense*. *Appl. Environ. Microbiol.* **70**, 1040-1050 (2004).

6 Lang, C. & Schüler, D. Expression of green fluorescent protein fused to magnetosome proteins in microaerophilic magnetotactic bacteria. *Appl. Environ. Microbiol.* **74**, 4944-4953 (2008).

7 Laemmli, U. K. Cleavage of structural proteins during the assembly of the head of bacteriophage T4. *Nature* **227**, 680-685 (1970).

8 Uebe, R. *et al.* The cation diffusion facilitator proteins MamB and MamM of *Magnetospirillum gryphiswaldense* have distinct and complex functions, and are involved in magnetite biomineralization and magnetosome membrane assembly. *Mol. Microbiol.* **82**, 818-835 (2011).

9 Klein, A. *et al.* Characterization of the insertase for beta-barrel proteins of the outer mitochondrial membrane. *J. Cell Biol.* **199**, 599-611 (2012).

10 Richter, M. *et al.* Comparative genome analysis of four magnetotactic bacteria reveals a complex set of group-specific genes implicated in magnetosome biomineralization and function. *J. Bacteriol.* **189**, 4899-4910 (2007).

11 Katzmann, E. *et al.* Magnetosome chains are recruited to cellular division sites and split by asymmetric septation. *Mol. Microbiol.* **82**, 1316-1329 (2011).

12 Draper, O. *et al.* MamK, a bacterial actin, forms dynamic filaments *in vivo* that are regulated by the acidic proteins MamJ and LimJ. *Mol. Microbiol.* **82**, 342-354 (2011).

13 Scheffel, A., Gardes, A., Grünberg, K., Wanner, G. & Schüler, D. The major magnetosome proteins MamGFDC are not essential for magnetite biomineralization in *Magnetospirillum gryphiswaldense* but regulate the size of magnetosome crystals. *J. Bacteriol.* **190**, 377-386 (2008).

14 Scheffel, A. *et al.* An acidic protein aligns magnetosomes along a filamentous structure in magnetotactic bacteria. *Nature* **440**, 110-114 (2006).

15 Zeytuni, N. *et al.* Self-recognition mechanism of MamA, a magnetosome-associated TPR-containing protein, promotes complex assembly. *Proc. Natl Acad. Sci.USA* **108**, E480-487 (2011).

16 Komeili, A., Vali, H., Beveridge, T. J. & Newman, D. K. Magnetosome vesicles are present before magnetite formation, and MamA is required for their activation. *Proc. Natl Acad. Sci.USA* **101**, 3839-3844, doi:10.1073/pnas.0400391101 (2004).

17 Arakaki, A., Webb, J. & Matsunaga, T. A novel protein tightly bound to bacterial magnetic particles in *Magnetospirillum magneticum* strain AMB-1. *J. Biol. Chem.* **278**, 8745-8750 (2003).

18 Prozorov, T. *et al.* Protein-Mediated Synthesis of Uniform Superparamagnetic Magnetite Nanocrystals. *Adv. Funct. Mater.* **17**, 951–957 (2007).

19 Murat, D. *et al.* The magnetosome membrane protein, MmsF, is a major regulator of magnetite biomineralization in *Magnetospirillum magneticum* AMB-1. *Mol. Microbiol.*, 684-699 (2012).

20 Tanaka, M., Arakaki, A. & Matsunaga, T. Identification and functional characterization of liposome tubulation protein from magnetotactic bacteria. *Mol. Microbiol.* **76**, 480-488 (2010).

21 Yang, W. *et al. mamO* and *mamE* genes are essential for magnetosome crystal biomineralization in *Magnetospirillum gryphiswaldense* MSR-1. *Res. Microbiol.* **161**, 701-705 (2010).

22 Quinlan, A., Murat, D., Vali, H. & Komeili, A. The HtrA/DegP family protease MamE is a bifunctional protein with roles in magnetosome protein localization and magnetite biomineralization. *Mol. Microbiol.* **80**, 1075-1087 (2011).

23 Schleifer, K. *et al.* The genus *Magnetospirillum* gen. nov., description of *Magnetospirillum gryphiswaldense* sp. nov. and transfer of *Aquaspirillum magnetotacticum* to *Magnetospirillum magnetotacticum c*omb. nov. *Syst. Appl. Microbiol.* **14**, 379–385 (1991).

24 Schübbe, S. *et al.* Characterization of a spontaneous nonmagnetic mutant of *Magnetospirillum gryphiswaldense* reveals a large deletion comprising a putative magnetosome island. *J. Bacteriol.* **185**, 5779-5790 (2003).

25 Lohsse, A. *et al.* Functional analysis of the magnetosome island in *Magnetospirillum gryphiswaldense*: the *mamAB* operon is sufficient for magnetite biomineralization. *PloS one* **6**, e25561 (2011).

26 Pfenning, N. & Trüper, H. G. Type and Neotype Strains of the Species of Phototrophic Bacteria Maintained in Pure Culture. *Internatl.J. System. Bacteriol.* **21**, 19-24 (1971).

27 Wang, J. *et al.* An improved recombineering approach by adding RecA to lambda Red recombination. *Mol. Biotechnol.* **32**, 43-53 (2006).

28 Fu, J. *et al.* Efficient transfer of two large secondary metabolite pathway gene clusters into heterologous hosts by transposition. *Nucleic Acids Res.* **36**, e113 (2008).

29 Rubin, E. J. *et al. In vivo* transposition of *mariner*-based elements in enteric bacteria and mycobacteria. *Proc. Natl Acad. Sci.USA* **96**, 1645-1650 (1999).

30 Scheffel, A. & Schüler, D. The acidic repetitive domain of the *Magnetospirillum gryphiswaldense* MamJ protein displays hypervariability but is not required for magnetosome chain assembly. *J. Bacteriol.* **189**, 6437-6446 (2007).

31 Ghosh, R., Hardmeyer, A., Thoenen, I. & Bachofen, R. Optimization of the Sistrom Culture Medium for Large-Scale Batch Cultivation of *Rhodospirillum rubrum* under Semiaerobic Conditions with Maximal Yield of Photosynthetic Membranes. *Appl. Environ. Microbiol.* **60**, 1698-1700 (1994).

Manuscript 4:

Genetic dissection of the *mamAB* and *mms6* operons reveals a gene set essential for magnetosome biogenesis in *Magnetospirillum gryphiswaldense*

Anna Lohße[1], Sarah Borg[1], Oliver Raschdorf[1], Isabel Kolinko[1], Éva Tompa[2], Mihály Pósfai[2], Damien Faivre[3], Jens Baumgartner[3], and Dirk Schüler*[1]

Journal of Bacteriology, (2014), doi: 10.1128/JB.01716-14, ahead of print.

[1]Ludwig-Maximilians-Universität München, Dept. Biologie I, Mikrobiologie, LMU Biozentrum, Großhaderner Str. 4, D-82152 Planegg Martinsried, Germany
[2]University of Pannonia, Dept. of Earth and Environmental Sciences, Veszprém, POB 158, H-8200, Hungary
[3]Max-Planck-Institut für Kolloid- und Grenzflächenforschung, Am Mühlenberg 1,14476 Potsdam, Germany

Abstract

Biosynthesis of bacterial magnetosomes, which are intracellular membrane-enclosed, nano-sized magnetic crystals, is controlled by a set of >30 specific genes. In *Magnetospirillum gryphiswaldense* these are clustered mostly within a large conserved genomic magnetosome island (MAI) comprising the *mms6, mamGFDC*, *mamAB* and *mamXY* operons. Here, we demonstrate that the five previously uncharacterized genes of the *mms6* operon have crucial functions in the regulation of magnetosome biomineralization that partially overlap with MamF and other proteins encoded by the adjacent *mamGFDC* operon. While all other deletions resulted in size reduction, elimination of either *mms36* or *mms48* caused the synthesis of magnetite crystals larger than those in the WT. Whereas the *mms6* operon encodes accessory factors for crystal maturation, the large *mamAB* operon contains several essential and non-essential genes involved in various other steps of magnetosome biosynthesis, as shown by single deletions of all *mamAB* genes. While single deletions of *mamL, P, Q, R, B, S, T* and *mamU* showed phenotypes similar to those of their orthologs in a previous study in the related *M. magneticum*, we found *mamI* and *mamN* to be not required for at least rudimentary iron biomineralization in *M. gryphiswaldense*. Thus, only *mamE, L, M, O, Q*, and *mamB* were essential for formation of magnetite, whereas a *mamI* mutant still biomineralized tiny particles which, however, consisted of the non-magnetic iron oxide hematite as shown by HRTEM and XANES. Based on this and previous studies we propose an extended model for magnetosome biosynthesis in MSR.

Introduction

Magnetotactic bacteria (MTB) orient along the Earth magnetic field lines to navigate to their growth-favoring microoxic habitats within stratified aquatic sediments (1). This behavior is enabled by the synthesis of ferrimagnetic intracellular organelles termed magnetosomes (2). In the α-proteobacterium *Magnetospirillum gryphiswaldense* (in the following referred to as MSR) and related MTB, magnetosomes consist of crystals of the magnetic iron oxide magnetite (Fe_3O_4) enclosed by the magnetosome membrane (MM) that contains a specific set of about 30 proteins (3, 4). The biosynthesis of magnetosomes is a complex process that comprises the (i) invagination of vesicles from the inner membrane (5, 6), (ii) sorting of magnetosome proteins to the MM (7), (iii) iron transport and crystallization of magnetite crystals (8), (iv) crystal maturation (7) and (v) assembly as well as positioning of mature crystals into a linear chain along a filamentous cytoskeletal structure (6, 9). Each step is under strict genetic control and responsible genes were found to be located mostly within a genomic magnetosome island (MAI) (10, 11), comprising the *mms6 (*in the following referred to as *mms6op)*, *mamGFDC (mamGFDCop)*, *mamAB* (*mamABop*), and *mamXY (mamXYop)* operons (10-12). These operons were found to be highly conserved also in the closely related *M. magneticum* (in the following referred to as AMB) (13-17). It has been shown that the regions between and flanking the identified magnetosome operons have no functional relevance for magnetosome biosynthesis in MSR and AMB (7, 18) . In MSR the *mms6, mamGFDC, mamAB* and *mamXY* operons are transcribed as single polycistronic messengers under control of the P_{mms6}, P_{mamDC}, P_{mamH}, and P_{mamXY} promoters, respectively (19, 20). A deletion mutant of *mamGFDCop* encoding the most abundant magnetosome proteins retained the ability to form magnetic, although smaller and less regular magnetosomes, while plasmidal overexpression of the entire *mamGFDCop* yielded magnetite particles even larger than those produced by the WT (21). Elimination of the corresponding region R3 in AMB, comprising in addition parts of *mms6op*, caused a severe biomineralization defect, resulting in cells with reduced magnetosome sizes and numbers (7). Deletion of the entire *mamXYop* resulted in smaller and misshaped magnetosome particles in MSR (18), whereas no obvious phenotype was observed for Δ*mamXYop* in AMB (7).

The *mms6op* of MSR comprises the genes *mgr4074*, *mms6*, *mmsF*, *mgr4071* (in the following renamed into *mms36)* and *mgr4070* (renamed into *mms48*; Fig. S1*)*, which was previously predicted to encode a TPR-like protein (18). A mutant, in which the entire *mms6op* was deleted (ΔA10), was also severely impaired in the biomineralization of magnetite crystals, which exhibited defects in crystal morphology, size and organization. However, the individual functions of *mgr4074*, *mms6*, *mmsF*, *mms36* and *mms48* as well as their contribution to the strong phenotype of Δ*mms6op* have remained unknown. In AMB, the *mms6* cluster was described to comprise only *amb0955* (*mgr4074*), *amb0956* (*mms6*), *amb0967* (*mmsF*), but to lack homologs of *mms48* and *mms36* (22). Single gene deletions of *mms6* in AMB by different groups revealed inconsistent phenotypes. Whereas Tanaka (23), reported an important regulatory function of Mms6 for magnetosome morphology, Murat *et al*., observed only minor effects on magnetosome biosynthesis after deletion of *mms6 in vivo* (22, 24). *In vitro*, the small (12.76 kDa in MSR and 14.69 in AMB) Mms6 protein was shown to be tightly bound to isolated bacterial magnetite crystals as visualized by atomic force microscopy and TEM (25, 26). *In vitro* crystallization experiments suggested that Mms6 and peptides mimicking it have iron-binding activity and affected the formation of cubo-octahedral crystal morphologies (27, 28).

In contrast to the smaller accessory operons, *mamABop* was found to contain genes absolutely essential for magnetosome biosynthesis in MSR and AMB (18, 22).Whereas *mamABop* was found to be sufficient to support at least some rudimentary biomineralization of small magnetite crystals even in the absence of all other magnetosme operons in both strains (18, 22), the *mamXY*, *mamGFDC*, *mms6,* and *mamAB* operons were required altogether for magnetite biomineralization upon their transfer into the foreign host *Rhodospirillum rubrum* (29).

A recent comprehensive genetic dissection of *mamABop* in AMB revealed that *mamH, P, R, S*, and *mamT* encode accessory functions for magnetosome synthesis, since mutants display various biomineralization defects, whereas *mamU* and *V* had no obvious magnetosome phenotype (7). As in MSR (see below), *mamK* and *mamJ* were implicated in magnetosome chain assembly, but their loss did not affect biomineralization (30, 31). However, gene deletions of *mamI, E, L, M, N, O,* and *mamQ* as well as *mamB (*co-deleted with their

respective orthologs) fully abolished magnetosome synthesis in AMB (7, 32). Whereas MamI, L, Q and B were suggested to be essential for vesicle genesis, MamE, O, M, and N were classified to be mainly required only for magnetite crystallization (7). The discovery of a small “magnetosome islet” in the genome of AMB with further copies of *mamE, J, K, L, M, F* as well as *mamD* suggested genetic redundancy that has to be clarified with respect to determination of the minimal essential gene set (33).

In MSR the 16.4 kb *mamABop* contains 17 genes (*mamH, I, E, J, K, L, M, N, O, P, A, Q, R, B, S, T* and *mamU*) (Fig. 3). Only a few genes of *mamABop* so far were analyzed individually in this organism. The actin-like protein MamK forms a filamentous structure for magnetosome assembly and interacts with the acidic protein MamJ that is involved in connecting magnetosomes to the filament. Both proteins, however, have no or only minor effects on biomineralization (9, 34). Deletion of *mamH* caused a moderate decrease of magnetosome number and size, whereas co-deletion of *mamH* and its partial homologue *mamZ* had a considerably stronger effect with only very few or no regular crystals detectable in the cells (20). Deletion of *mamE, O, M* and *mamB* resulted in either a total inhibition of crystal nucleation or prevented MM vesicle synthesis (18, 35, 36). However, *mamI, L, N, P, A, Q, R, S, T*, and *mamU* were not yet analyzed individually by mutagenesis, and it has remained unknown whether they have functions similar or distinct from those of their corresponding orthologs in AMB. Finally, it is not clear, which genes constitute the minimal set of essential determinants for magnetosome biomineralization in MSR.

Here, we analyzed the functional relevance of proteins encoded by *mms6op* and *mamABop* for the biosynthesis of magnetic minerals in MSR. We demonstrate that besides Mms6 and MmsF, *mms6op* of MSR encodes two further important regulators (Mms36 and Mms48) for magnetosome biomineralization. Whereas deletions of *mamA, R, S, T*, and *mamU* resulted in similar phenotypes as those observed for deletion of homologous genes in AMB, we show that other than in AMB, Δ*mamN*
and Δ*mamI* still synthesize particles in MSR, thus further shrinking the minimal gene set for iron biomineralization to *mamE, L, M, O, Q* and *mamB.* Finally, we propose an extended model for magnetosome biosynthesis.

Material and Methods

Bacterial strains, plasmids, and culture conditions

Bacterial strains and plasmids used in this study are listed in Table S1. WT and mutant strains of MSR were grown in liquid modified flask standard medium (FSM) at 30°C under microaerobic conditions if not otherwise specified (37, 38). Therefore, cells were cultivated in flasks, closed with butyl-rubber stoppers after incubation with a gas mixture of 2% O_2 and 98% N_2 or in purged jars. For anaerobic requirements, O_2 was excluded from the gas mixture, while aerobic conditions were generated through free gas exchange with air. *Escherichia coli* strains were cultivated as previously described (39) and lysogeny broth medium was supplemented with 1 mM DL-α, ε-diaminopimelic acid (DAP) for cultivation of *E. coli* strain BW29427 as well as WM3064. For selection of antibiotic resistant cells, media were supplemented with 25 g/ml kanamycin (Km), 12 g/ml tetracycline (Tet), and 15 g/ml gentamicin (Gm) for *E. coli* strains, and 5 g/ml Km, 5 g/ml Tet, and 20 g/ml Gm for MSR strains, respectively.

Molecular and genetic techniques

Oligonucleotide sequences (Table S2) were deduced from the working draft genome sequence of MSR (GenBank accession number No. CU459003) and purchased from Sigma-Aldrich (Steinheim, Germany). Genetic fragments were amplified by standard polymerase chain reaction (PCR) procedures with Phusion polymerase (NEB GmbH, Frankfurt am Main, Germany) and generated plasmids were sequenced with an ABI 3700 capillary sequencer (Applied Biosystems, Darmstadt, Germany), utilizing BigDye Terminator v3.1. Data were analyzed with Software Vector NTI Advance® 11.5 (Invitrogen, Darmstadt, Germany) or MacVector 7.2.3 (Oxford Molecular, Oxford, UK).

Generation of unmarked deletion mutants

Markerless single gene deletions within the *mamAB*, *mms6*, and *mamGFDC* operon were partially realized with the pORFM*_galK* plasmid. The vector was digested with *BamHI* and *KpnI* to insert the approximately 1 kb downstream and upstream fragments of *mamI, L, N, P, Q, R, S, T, U, mms36, mms48,* and *mmsF_mms6.* For integration of homologous regions of *mamA* and *mamL* the plasmid was digested with *BamHI/NotI* and *Nsi/SpeI,* respectivaly. Oligonucleotides, used to amplify the 5' and 3' flanking sequence from MSR by PCR are listed in Table 3. Both fragments were linked by an overlap PCR with the first and last listed corresponding oligonucleotide, subcloned into pJet1.2/blunt, sequenced and ligated into the digested pORFM*_galK* vectors. Generated plasmids were termed: pAL_ Δ*mamI*, pORΔ*mamL*, pAL_ Δ*mamN*, pAL_ Δ*mamP*, pAL_ Δ*mamA*, pAL_ Δm*amQ*, pAL_ Δ*mamR*, pAL_ Δ*mamS*, pAL_ Δ*mamT*, pAL_ Δ*mamU*, pAL_ Δ*mms36*, pAL_ Δ*mms48*, and pAL_ Δ*mmsF_mms6.* Deletion of *mms6, mmsF, mamF* and double deletion of *mmsF_mamF* was accomplished by double cross over method. Oligonucleotides for amplification of flanking sections are listed in Table S3. Regions were cloned into pJet1.2/blunt and sequenced. Plasmid pCM184 was digested with *ApaI/SacI* and 3' end regions were inserted for deletion of *mms6, mmsF* and *mamF*. Generated plasmids were digested with *EcoRI/NdeI* and 5' flanking sequence was inserted, resulting in pCM184*_mms6* 3'5', pCM184*_mmsF* 3'5' and pCM184*_mamF* 3'5'. The generated plasmids were examined by restriction analysis with a set of different enzymes or PCR and transferred into MSR WT by conjugation using *E. coli* BW29427 as donor strain as described elsewhere (18). Genomic insertion mutants were selected on Km plates, cultivated in 100 µl FSM medium over night at 30 °C and scaled up to 1 ml. Proper plasmid integration was verified by PCR and if necessary counter selection was implemented. Positive excision strains were verified by PCR and mutants were termed as: *ΔmamI*, *ΔmamL, ΔmamN*, *ΔmamP*, *ΔmamA*, *ΔmamQ*, *ΔmamR*, *ΔmamS*, *ΔmamT*, *ΔmamU, Δmms48, Δmms36*, and *ΔmmsF_mms6*. Mutants generated by double cross over were cultivated in 10 ml MSR medium and excision of the Km resistance gene was induced after conjugation with the *Cre* expression plasmid pCM157. Generated strains were termed: *ΔmmsF* and *Δmms6.* For double deletion of *mmsF* and *mamF*, the plasmid pCM184*_mamF*

3’5’ was introduced into *ΔmmsF*, and deletion was verified as described above, resulting in strain *ΔmmsF_mamF*.

Complementation of generated mutants and GFP localization

For MamC-GFP localization experiments the plasmid pFM323 was integrated into the genome of *ΔmamI*, *ΔmamL, ΔmamN*, *ΔmamP*, *ΔmamA*, *ΔmamQ*, *ΔmamR*, *ΔmamS*, and *ΔmamT*. For construction of pAL*_mamIg, mamI* was amplified with oligonucleotides AL394/AL395 and inserted into pCL6 after digestion with *NdeI/EcoRI*. Plasmids for complementation of the other mutant strains were derivatives of pBAM1 and labeled pBAM*_mamL, P, S, T, R, A*, *N*, *mms48*, *mms36*, and *mgr4074* respectively. Oligonucleotides for amplification of the genes are listed in Table S3. Genes were cloned between the *NdeI/EcoRI* or *NdeI/PacI* sites (for *mamN*) of pBAM*_GFDC* under control of the P_{mamDC} promoter. Plasmids pBam*_mms36* and pBam*_mms48* were also used for overexpression studies in WT. For complementation of Δ*mmsF*, Δ*mms6*, Δ*mmsF_mamF*, Δ*mmsF_mms6*, or ΔA10, corresponding genes were amplified with oligonucleotides listed in Table S3. Genes were inserted into pAP150 after digestion with *BamHI/NdeI,* resulting in pAL*_mmsF*, pAL*_mms6,* pAL_P_{mamDC}*_mms6op.*, and pAL_P_{mamDC}*_mms6,F,4074*. The plasmid pBBRMCS2 was digested with *NsiI/EcoRI* for integration of genes *mms6, mmsF* and *mgr4074* after amplification with AL125/AL136, generating pAL_P_{mms6}*_mms6,F,4074.* For transcomplementation assays, the plasmids were transferred to the respective deletion mutant by conjugation. Δ*mmsF_mms6* and Δ*mmsF_mamF* were complemented with pAL*_mms6* and pAL*_mmsF*, respectively. Plasmids pBam*_mgr4074*; pAL_ P_{mamDC} *_mms6op*; pAL_ P_{mms6}*_mms6,F,4074*; pAL_P_{mamDC}*_mms6,F,4074* were used for complementation studies in ΔA10.

Analytic methods

Optical density and magnetic response (C_{mag}) were analyzed photometrically at 565 nm (40). The applied magnetic field for C_{mag} measurements was about 70 mT, which is able to magnetize very small or irregular magnetosomes within the superparamagnetic state. Intracellular iron concentrations were measured after incubation under anaerobic conditions as described (41).

Phase Contrast and Fluorescence Microscopy

MSR strains with genomic egfp were grown in 5 ml FSM in six-well plates for 16 h at 30°C and 2% O_2 without agitation. Cells were immobilized on agarose pads (FSM salts in H_2O, supplemented with 1% agarose), and imaged with an Olympus BX81 microscope equipped with a 100 UPLSAPO100XO objective (numerical aperture of 1.40) and a Hamamatsu Orca AG camera. The Olympus cell software was used to capture and analyze images.

TEM and HRTEM

Magnetosome phenotypes of cells with respect to size, shape and number per cell were examined by transmission electron microscopy (42), for which cells were concentrated and adsorbed onto carbon-coated copper grids. Cells were imaged with a FEI Morgagni 268 (*FEI,* Eindhoven, Netherlands) electron microscope at an accelerating voltage of 80 kV. Bright-field TEM images and selected-area electron diffraction (SAED) patterns were recorded on image plates, using a Philips CM20 microscope operated at 200 kV and fitted with a Noran Voyager energy-dispersive X-ray detector. High-resolution transmission electron microscopy (HRTEM) was performed using a JEOL 3010 microscope, operated at 297 kV and equipped with a Gatan Imaging Filter (GIF) for the acquisition of electron energy-loss spectra and energy-filtered compositional maps. For TEM data processing and interpretation the softwares DigitalMicrograph and SingleCrystal were used.

X-ray Absorption Spectroscopy

Bacterial cultures (90–135 mL) were pelleted by centrifugation (5 min at 9,000 x g, 4 °C) and washed 3x by resuspension with 5 mL TBS (pH 7.6) and centrifugation. Pellets were then resuspended in 100 µL TBS + 25 µL glycerol and frozen in liquid nitrogen on sample holders with Kapton film support. Samples were shipped to the European Synchrotron Radiation Facility (ESRF) on dry ice, where they were stored at −80 °C until measurement. Fe K-edge X-ray absorption near edge structure (XANES) spectra were recorded at the undulator beamline ID26 of the ESRF. We used a Si (311) double-crystal monochromator and focusing mirrors giving a beam spot size of ~200x400 μm^2

on the samples. Data were recorded in fluorescence detection mode using a Rowland-type spectrometer equipped with 4 Ge (440) analyzer crystals and a Si-photodiode. During all measurements, samples were cooled to around 10 K using a liquid He cryostat. XANES spectra were recorded with 0.1 eV step from 7100 to 7200 eV. To improve data quality, 10 to 100 XANES scans were recorded for each sample. Samples were moved of few hundreds of microns between each scan in order to minimize radiation damage. Data were averaged using PyMca 4.6.2 after evaluation for iron photo-reduction. Averaged spectra were normalized and fitted using Demeter 0.9.16. As reference materials we used spinach ferredoxin (Sigma Aldrich), hematite (20-60 nm grain size, Alfa Aesar), magnetite, ferrihydrite and phosphate-enriched ferric oxyhydroxides (described earlier in (43)).

Results

Deletion mutagenesis of the *mms6* operon and *mamF*

After reassessment of annotation and correction of the MmsF N-terminus (Figure S1), we generated various unmarked *in frame* single and double deletions of all *mms6op* genes as well as of *mamF* (localized in the adjacent *mamGFDCop*), which is highly similar (61% aa identity) to *mmsF* (see Table 1 and Figure 1 for overview over deletions and resulting phenotypes). We found the hypothetical *mgr4074* to be poorly conserved, and its chromosomal reintegration into Δ*mms6op* (ΔA10, (18)) did not alleviate the severe biomineralization defects of the parent strain. We therefore consider *mgr4074* a pseudogene with no role in biomineralization, although further studies are needed to address the expression and putative localization of its gene product. Strain Δ*mms6* had slightly smaller crystals (30 nm; Wild-type (WT): 36 nm) that were scattered throughout the cell, either aligned in irregularly spaced ‘‘pseudo-chains’’ (i. e., with <10 crystals per chain) or approximating WT-like chain configurations (Table 1; Figure 1). Crystals between 30 and 35 nm were predominant (WT: 40-45 nm), but particles larger than 60 nm were absent (WT: <70 nm; Figure S2). The average crystal number per cell was reduced to 30 (WT: 34 particles per cell), and the magnetic response of a Δ*mms6* culture was slightly weaker than that of the WT ($C_{mag(\Delta mms6)}$: 1.7±0.1; $C_{mag(WT)}$: 2.0±0.1; Table 1).

C_{mag} of Δ*mmsF* cells was similar to those of Δ*mms6*. Magnetosomes displayed variable intracellular arrangements, such as one or more short chains, partially scattered crystals, or lacking any chain-like alignment (Figure 1). Mean crystal sizes were reduced to <30 nm, whereas the particle number was only slightly lower than in the WT (Table 1; Figure S2). Since the high similarity of 61% between MmsF and MamF suggested possible functional redundancy, *mamF* was eliminated both alone and in combination with *mmsF*. In Δ*mamF*, MamC encoded downstream of *mamF* in the same operon was found to be properly expressed by immunodetection, indicating that deletion of *mamF* had no polar effect (data not shown). Mean crystal size (34 nm) and number (34 per cell) were similar in Δ*mamF* to WT. However, the combined excision of both genes within Δ*mmsF*_Δ*mamF* resulted in a more drastic decrease in size (25 nm) and

number (27 crystals per cell, Figure 1; Table 1; Figure S2). Thus, loss of MmsF had a more pronounced effect on crystal size, number and alignment than MamF, and the additive effect of their combined deletion suggested that both proteins are involved in size control.

Double deletion of *mmsF* and *mms6* reduced size to 24 nm and number to 24 crystals per cell (Table 1). However, iron content, size and numbers of magnetite particles as well as C_{mag} (1.6±0.1) of Δ*mmsF*_Δ*mms6* were still higher than in the operon deletant ΔA10 (C_{mag}: 1.0±0.1), with particles of 20-25 nm prevailing in both strains (Figure 1; Table 1; Figure S2). HRTEM images of particles from ΔA12, in which the entire *mms6op* and *mamGFDCop* were deleted together (18), revealed fringes spacing corresponding to magnetite. This indicates that the deleted genes alone do not have a critical role in magnetite formation (Figure 2). In contrast to the strong size reduction observed in all other mutant strains, deletions of *mgr4070* and *mgr4071* (renamed into *mms48* und *mms36* according to their predicted protein masses of 48 and 36 kDa, respectively) unexpectedly caused a substantial increase in mean crystal size. Particles synthesized by both strains resembled WT crystals in shape, but were significantly larger in Δ*mms36* (39 nm) and Δ*mms48* (46 nm; Figure 1; Table 1; Figure S2). This is equivalent to a mean size increase of about 30% compared to WT for the latter strain, in which crystals between 50 and 60 nm were most abundant, with a maximum size of up to 85 nm (Figure S2). However, both strains synthesized fewer particles than the WT (Δ*mms36*: 22; Δ*mms48*: 16 per cell), and whereas in WT magnetosome chains of larger particles at midchain are usually flanked by numerous smaller crystals, those characteristic small crystals (15-25 nm) were less frequent at the chain ends in Δ*mms36* and Δ*mms48* (Figure 1; Table 1; Figure S2). Thus, the predominance of larger (>30 nm) particles partly accounted for the substantially increased mean crystal size. However, despite the reduced particle numbers per cell, overall magnetite biomineralization was increased as evident by the increased iron content of both deletion strains (21% more iron compared to WT). Genomic expression of additional copies of *mms48* and *mms36* did not significantly change mean particle size (WT::*mms36*: 35 nm; WT::*mms48*: 33 nm; Table 1) but the size distribution was shifted towards smaller crystals for both strains. Crystals between 30 and 45 nm were predominant in WT::*mms36* and

WT::*mms48*, whereas particles larger than 60 nm were not observed, unlike WT crystals that were most frequently between 40 and 45 nm with a maximum size up to 70 nm (data not shown). Whereas particle number was WT-like for overexpression of Mms36 (32 per cell), crystal number was increased for strain WT::*mms48* (40 per cell; Table 1). Interestingly, cells containing double chains were more abundant for WT::*mms48* (WT::*mms48*: 67%; WT::*mms36*: 28%; WT: 32%; Figure S3).

In summary, all proteins encoded by *mms6op* are involved in control of magnetosome size or/and number. The previously observed severe biomineralization defects in Δ*mms6op* are thus not due to loss of a single, but several genes, which points towards a cumulative effect on magnetosome synthesis by various proteins encoded by *mms6op*.

Deletion analysis of the *mamAB* operon: *mamE, L, M, O, Q* and *B* are essential for iron biomineralization

First, annotations of all 17 *mamABop* genes were re-assessed. N-termini that were conserved between all three closely related magnetospirilla MSR, AMB and *M. magnetotacticum* were considered the most likely translation starts. Annotations were corrected accordingly for *mamI* and *mamL* (Figure S4) and experimentally confirmed by the ability of genes to complement their respective gene deletions. In addition to the previous deletions of the *mamABop* genes, we constructed ten single *in frame* deletions comprising *mamI*, *L*, *N*, *P*, *A*, *Q*, *R*, *S*, *T*, and *mamU*, respectively. As expected, all resulting deletion strains displayed WT-like growth and morphologies. However, deletion mutants were impaired in magnetosome biomineralization to variable extents. Based on their magnetic response mutants either were i) magnetically responsive with variable but significant C_{mag} (Δ*mamN*, *P*, *A*, *R*, *S*, *T*, *U*) or ii) entirely non-magnetic without any detectable C_{mag} (Δ*mamI*, *Q, L*; Table 1). TEM analysis confirmed that group (i) strains were still able to synthesize magnetosome-like particles, but displayed various distinct phenotypes with respect to crystal morphology, size, and number per cell (Figure 3). Δ*mamU* was hardly distinguishable from WT cells and produced 32 cubo-octahedral crystals per cell with a size of 37 nm. All other mutants showed a drastically decreased magnetosome size, number and/or alignment. Magnetosomes of Δ*mamA* had a WT-like size of 35 nm, but

their number was substantially decreased to 10 per cell. Δ*mamS* particles exhibited a widely spaced linear chain-like arrangement within the cell. Whereas the crystal size was strongly decreased (22 nm), they were present in about same numbers as in the WT (35 particles per cell). Δ*mamT* also synthesized irregularly spaced magnetosome chains, whereas in some cells larger magnetosomes appeared at the chain center and formed condensed ‘‘pseudo-chains’’. Due to the prevalence of smaller crystals, the mean particle size was decreased to 29 nm, whereas their number was WT-like (32 particles per cell). Several Δ*mamR* cells showed scattered magnetosomes lacking any chain-like alignment, or short, densely spaced chains flanked by smaller particles with irregular morphologies, or WT chains (average size: 29 nm; number per cell: 34). Δ*mamP* cells at first glance seemed to contain only few (i. e., not more than six magnetosomes, mean three) larger than WT particles (59 nm on average). However, at closer inspection numerous very small and irregularly shaped crystals flanking the larger crystals became apparent with an average size of 16 nm (see arrows in Figure 3). In total, Δ*mamP* cells synthesized on average only 19 crystals with a mean size of 22 nm. HRTEM of the two distinct particle types revealed that the lattice fringes for the larger crystals corresponded clearly to magnetite, whereas by contrast the smaller and poorly crystalline particles produced lattice fringes characteristic for hematite (Figure 2). The Δ*mamN* mutant showed a very weak, but detectable magnetic response (C_{mag}: 0.1). TEM confirmed the presence of few (11 per cell) tiny, widely spaced crystals with a size of only 18 nm. HRTEM images of these particles and their Fourier-transforms indicated that crystals have the structure of magnetite.

Δ*mamI*, Δ*mamL and* Δ*mamQ* represent the second class of mutants with no detectable magnetic response (C_{mag}: 0). Δ*mamQ* and Δ*mamL* were entirely devoid of any visible crystalline electron dense structures (Figure 2). Careful analysis of Δ*mamI* cells, however, revealed the presence of a few (10 per cell) electron-dense particles with highly irregular or elongated morphologies and a size of 15 nm (Figure 3). As shown by HRTEM, the nuclei within Δ*mamI* were composed of several small grains that formed thin aggregates (Figure 2). Lattice fringes were observed in only two particles, and according to the Fourier transforms of the HRTEM images, the spacing between the fringes is very close to the d(012) and d(014) spacing in hematite. XANES (X-ray Absorption Near

Edge Structure) spectra obtained from whole Δ*mamI* and Δ*mamN* cells were clearly distinct from those of pure magnetite as in the WT and suggest that the ferrous compounds are predominantly Fe-S clusters (proteins) that account for around 40% of the total iron content in the cells (Figure S5). Magnetite was clearly present in Δ*mamN* cells (around 50% of total iron), whereas the low fit quality for Δ*mamI* did not allow us to reliable determine the structure of the Fe present in the bacteria apart from Fe-S (see supplements for more detailed information). However, the overall line shape appears most consistent with an amorphous or only poorly ordered Fe compound as suggested by HRTEM.

Intracellular localization of the magnetosome chain marker MamC-GFP

All mutant strains could be complemented by either genomic reintegration or plasmidal transfer (see supplements). We studied the ability of all mutants to properly localize the abundant MamC magnetosome protein, which served as a marker for magnetosome chain localization in previous studies (6, 36, 44). To this end, MamC was tagged by a chromosomal *in-frame* EGFP insertion on pFM236 that shows in WT cells a continuous straight-line fluorescence signal (Figure S6). Within Δ*mamN, P, S*, and *mamT* MamC-GFP localized as shorter structures, but still showed a linear localization running along the inner curvature of the cell. Within Δ*mamI* a short, but still elongated fluorescence signal at midcell was observed. Thus MamI, N, P, R, S, and T are not required for proper MamC localization. On the contrary, in Δ*mamA*, *Q* and *mamL* cells, no defined position of the MamC-GFP signal was detectable, but instead a diffuse spot like accumulation within the cell was predominant (Figure S6). In the deletion mutant Δ*mamA* the magnetosome formation was not inhibited, even though MamC is misplaced within this strain, which suggests that MamA may interact with MamC.

Discussion

The *mms6* operon encodes non-essential magnetosome proteins crucial for proper crystal growth

As in AMB (size reduction of crystals by 19% (22)), we observed only minor biomineralization defects upon deletion of *mms6* in MSR (15% size reduction). Only 20% size reduction was also seen after *mmsF* deletion in MSR, which, however, is weaker than its deletion phenotype in AMB (52% size reduction, (22)). However, double deletion of *mms6* and *mmsF* resulted in an almost 32% size reduction, which suggests a certain functional overlap between Mms6 and MmsF. We found functional redundancy between *mmsF and mamF* (encoded by the adjacent *mamGFDCop*), since their double deletion exacerbated defects in crystal maturation (30% size reduction). Hence, loss of several genes together contributed to the strong magnetosome defect (45% size reduction) observed after deletion of the entire *mms6op* (ΔA10), which indicates a cumulative regulation of magnetosome biomineralization.

Mms6op of MSR contains two additional genes named *mms36* (*mgr4071*) and *mms48* (*mgr4070*) that are expressed under magnetosome forming conditions (18), but had not yet been studied by deletion analysis in either MSR or AMB. Surprisingly, their deletion caused the synthesis of larger magnetite crystals instead of size reduction. Since no conserved domains or motifs are present in Mms36 and 48, apart from weak similarity to proteins involved in porphyrine synthesis (Mms36: 29% to uroporphyrinogen III synthase of *Rhodospirillum rubrum*; Mms48: 28% to HemY-like proteins, possibly involved in porphyrin biosynthesis (45, 46)), their precise *in vivo* functions are difficult to infer. They might be itself either inhibitors of crystal growth (32) or recruit other inhibitory proteins to the MM in order to prevent excessive crystal growth.

Genetic analyses of the *mamAB* operon: MamU, T, S, R, A, N and MamI are not essential for iron biomineralization in MSR

We found that deletion of several genes (*mamU, T, S, R, A, P, Q, L*) from *mamABop* of MSR essentially phenocopied the deletions of their orthologs in AMB (7). Loss of *mamU, T, S, R, A, P, and mamN* did not entirely abolish biomineralization of magnetite crystals. As in AMB, deletion of MamU did not have any detectable magnetosome phenotype in MSR. MamT of AMB as well as of MSR contains a double cytochrome c motif (CXXCH) referred to as magnetochrome domain necessary for heme-binding (47). It was speculated that MamT therefore transfers electrons to balance the ferric-to-ferrous iron ratio form required for magnetite formation (47). Deletion of *mamT* in MSR resulted in smaller magnetosome particles as in AMB, supporting its previously predicted function in crystal maturation. As in Δ*mamT*, deletion of *mamR* in MSR resulted in smaller crystals and partially modified chain formation similar to the phenotype observed for Δ*mamR* in AMB. Thus, MamR is involved in controlling particle number and size as also suggested for MamR of AMB (7). We also confirmed a key role of MamS in MSR, which has similarity to the putative serine proteases and magnetochrome domain containing proteins MamE and MamX (20, 32). However, MamS itself lacks a magnetochrome domain, which argues against its direct participation in redox control. The TPR domain-containing protein MamA was speculated to play a role in activation of biomineralization (5). It was suggested that MamA self-assembles through its putative TPR domain and concave site to form a large homooligomeric scaffold surrounding the magnetosomes (48, 49), whereas its convex site interacts with other magnetosome-associated proteins like MamC and several unidentified proteins (48, 49). However, as in AMB the deletion of *mamA* in MSR had only a weak effect (5), suggesting that these interactions are not essential or can be partly compensated by other proteins. In Δ*mamP* of MSR, particles larger than those synthesized by the WT were flanked by smaller and poorly crystalline particles similar to AMB (50). *MamP* contains two closely spaced magnetochrome domains and was speculated to interact with MamE, MamX and MamT through its PDZ domain and to somehow regulate the electron transport required for biomineralization of the mixed valence iron oxide

magnetite (20, 32, 50). Magnetosomes in Δ*mamP* of MSR show a similar crystallization defect (magnetite crystals flanked by flakes) like the *mamX* mutant of MSR (20) and thus might indicate the involvment in the same step of magnetosome biosynthesis. In contrast, phenotypes of MSR Δ*mamT* (smaller particles) and Δ*mamE* (total loss of electron dense particles) are distinct from the deletion phenotype of Δ*mamP,* suggesting that some or all of the magnetochrome proteins have different or additional functions. However, MamE also contains beside the magnetochrome domains, a protease and double PDZ domains, which might cause the differences between the generated mutants upon their deletion (32). Thus, further analyses are needed to explain the different observed mutant phenotypes, such as the specific deletion of the different magnetochrome domains. MamP from AMB catalyzed the formation of ferrihydrite and magnetite from iron solutions *in vitro,* indicating that MamP binds and oxidizes iron (50). However, this ability of MamP is not essential *in vivo*, as the Δ*mamP* mutant of MSR continued to biomineralize particles of magnetite. Potentially this might be due to unchecked mineral growth after deletion of a major redox regulator (51) or/and the ability of other magnetochrome proteins like MamX, MamE and MamT to partially compensate the loss of MamP.

In addition to the strong similarities between several AMB and MSR mutants, we also found several striking differences between the two species. MamN was described to be essential for magnetosome biosynthesis, as indicated by the absence of electron dense crystals in AMB (7). However, our TEM, HRTEM and XANES analyses revealed the presence of magnetite particles within Δ*mamN* of MSR. Because of its similarity to the human Permease P that is predicted to regulate the intraorganelle pH of melanosomes together with an ATP-driven proton pump (52), MamN was speculated to regulate pH conditions within the magnetosome vesicles by export of protons released by the precipitation of magnetite ($2Fe^{3+}+ Fe^{2+}+ 4H_2O \rightarrow Fe_3O_4+8H^+$ (38, 53)), and thus the observed phenotype of Δ*mamN* might be due to alteration of the intra-magnetosomal pH.

Another gene, which exhibited a strikingly distinct deletion phenotype between AMB and MSR is *mamI,* which encodes a small magnetospirilla-specific magnetosome protein (70 aa) with no significant homology to already characterized proteins. In AMB, MamI was found to be essential for the

biosynthesis of both magnetosome membrane vesicles, and consequently, iron biomineralization (7). In contrast, excision of *mamI* in MSR did not entirely abolish the biomineralization of electron dense iron-rich particles, but the mutant still synthesized tiny and poorly crystalline non-magnetic particles, which in some cases were shown to consist of hematite. Recent findings in MSR and AMB indicate that the observed poorly ordered iron (oxyhydr)oxide phases are precursors to the magnetite phase in bacteria (43, 54). In addition, the ability of MamP to precipitate ferrihydrite and magnetite *in vitro* suggests that magnetite may be formed through a stepwise phase transformation process (50). Such a biosynthetic phase transformation requires a precise control of iron supersaturation, pH, and redox potential levels (55), suggesting that MamI may be involved at an early stage of magnetite nucleation by regulation of proper conditions within the vesicles.

Only MamE, L, M, O, B and Q are essential for iron biomineralization in MSR

In addition to the previously identified *mamE* (35)*, mamM* (56), *mamO* (35) and *mamB* (56) we also demonstrated *mamQ* and *mamL* to be essential genes for magnetosome synthesis in MSR, since their deletions fully abolished the biomineralization of electron dense particles. MamQ shares homology with the LemA protein, which is conserved in several bacteria but whose function is uncertain (12, 57). MamQ has a high content of α-helices that are somewhat reminiscent to the EFC/BAR domain of Formin Binding Protein 17 (7). BAR domains have the ability to sense and stabilize membrane curvatures (58), and their weak similarity to MamQ might hint towards related functions in MM vesicle genesis of the protein. The small protein MamL has no predicted function, but was shown to be essential for magnetosome membrane genesis in AMB (7).

Despite the metabolic and genetic similarities between AMB and MSR, previous studies already suggested that the function of orthologous genes might be somewhat distinct in these organisms (6, 18, 59). Apart from the possibility that the tiny magnetite and hematite particles in Δ*mamN* and Δ*mamI* of MSR simply had escaped detection in the corresponding mutants of AMB (7), this might possibly due to the different genetic context, with only about 50% of all genes

shared by the genomes of these two strains (14). In fact, it can not be excluded that further genes outside of the MAI partially compensate the loss of deleted genes as observed in a recent study, in which a magnetosome islet outside the MAI compensated the deletion of *mamK* in AMB (6, 33).

In summary, whereas in AMB eight proteins (MamI, E, L, M, N, O, B, Q) were found to be essential for magnetosome biomineralization, in MSR only six proteins (MamE, L, M, O, B, Q) are essential for at least some rudimentary iron biomineralization and, if including MamI, seven proteins for the biosynthesis of magnetite-containing magnetosomes. This leads to an expanded model of magnetosome biosynthesis in MSR (Figure 4). However, it remains to be shown whether these essential magnetosome proteins are also sufficient for vesicle formation and crystallization even in the absence of the other factors encoded by the *mamAB* and other magnetosome operons.

Acknowledgement

This work was funded by the Deutsche Forschungsgemeinschaft (grants DFG Schu1080/13-1 and 15-1) and the European Union (Project Bio2MaN4MRI n°245542). AL was supported by the Konrad-Adenauer-Stiftung. We acknowledge the European Synchrotron Radiation Facility for provision of synchrotron radiation facilities. We thank J.-D. Cafun, P. Glatzel, and C. Lapras for assistance in using beamline ID26 at ESRF. We are thankful to R. Susen, A. Hähle, A. Singer, T. Perez Gonzalez and G. Morin for experimental support. The research was further supported by the Max Planck Society and the European Research Council through a Starting Grant to DF (Project MB² n°256915).

Figures

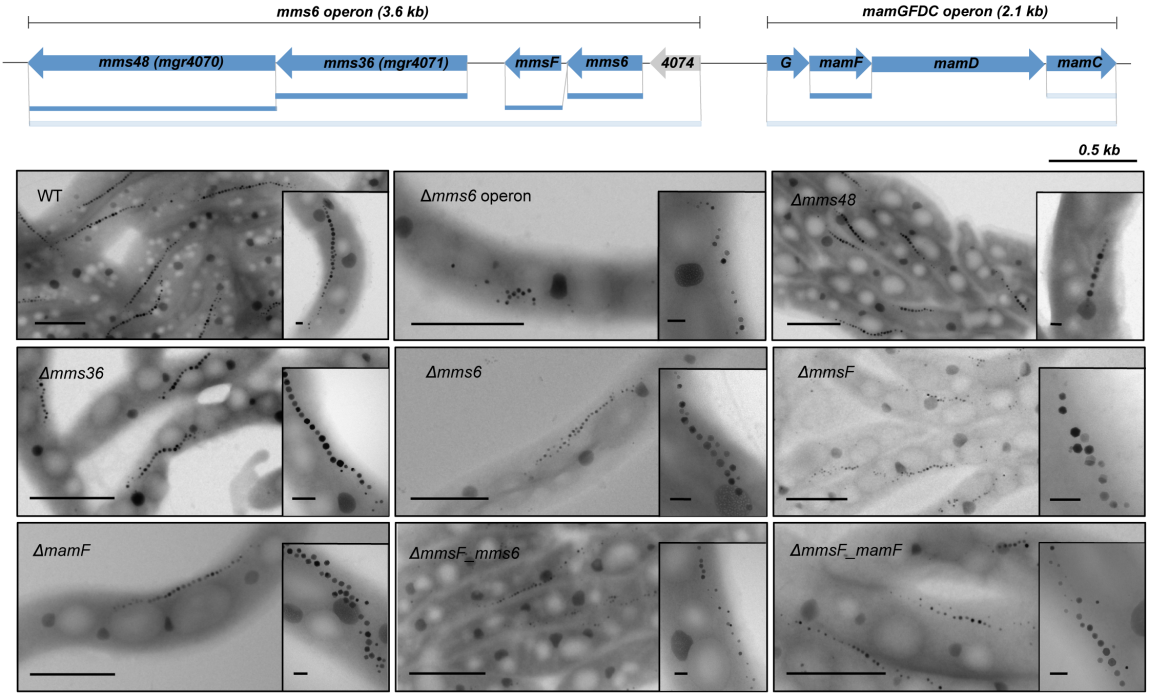

Figure 1. Molecular organization of the *mms6* and *mamGFDC* operons in MSR and TEM micrographs of generated deletion mutants. Scale bar: 1 µm. Dark blue bars: Indicate extent of gene deletions generated in this study. Light blue bars: Gene deletion mutants generated by (18, 21).

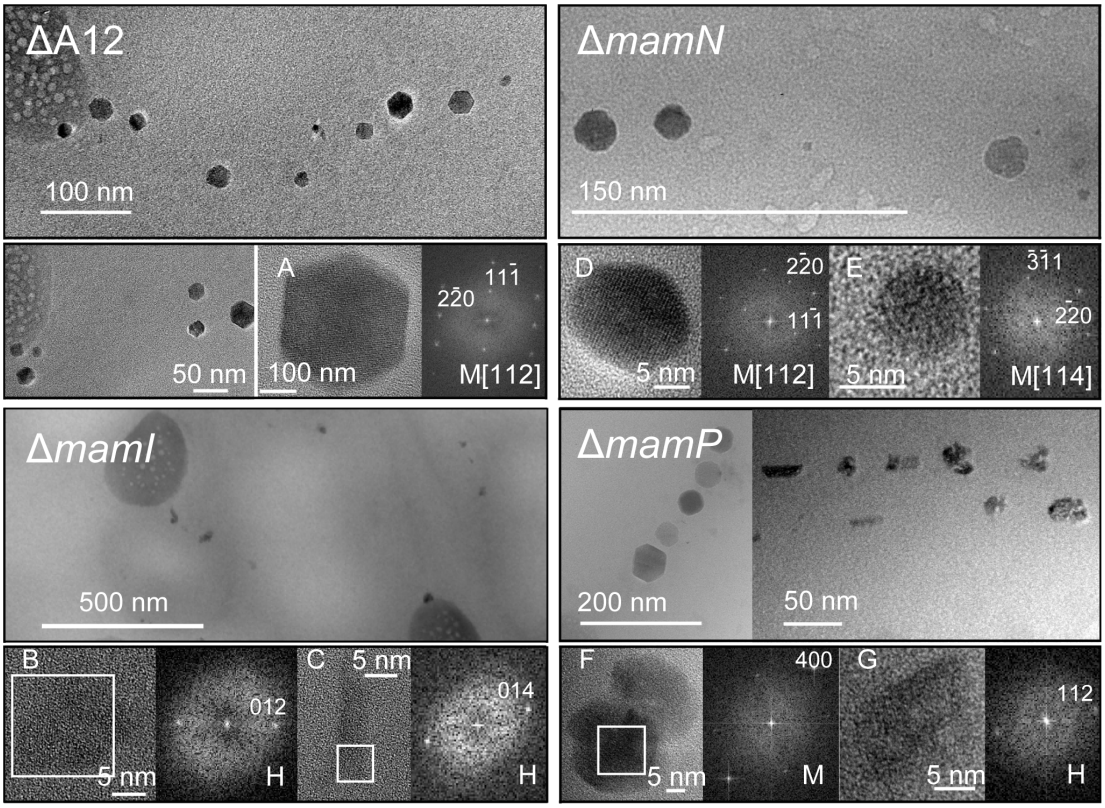

Figure 2. TEM and HRTEM micrographs and their corresponding Fourier transforms of electron dense particles in various generated deletion strains of MSR.

The Fourier transforms were obtained from the images of entire particles or from the boxed areas in each corresponding HRTEM image. The lattice fringe spacings correspond to the strucures of either magnetite (A, D, E, F, G) or hematite (B, C) in the mutants ΔA12, Δ*mamI*, Δ*mamN*, and Δ*mamP*.

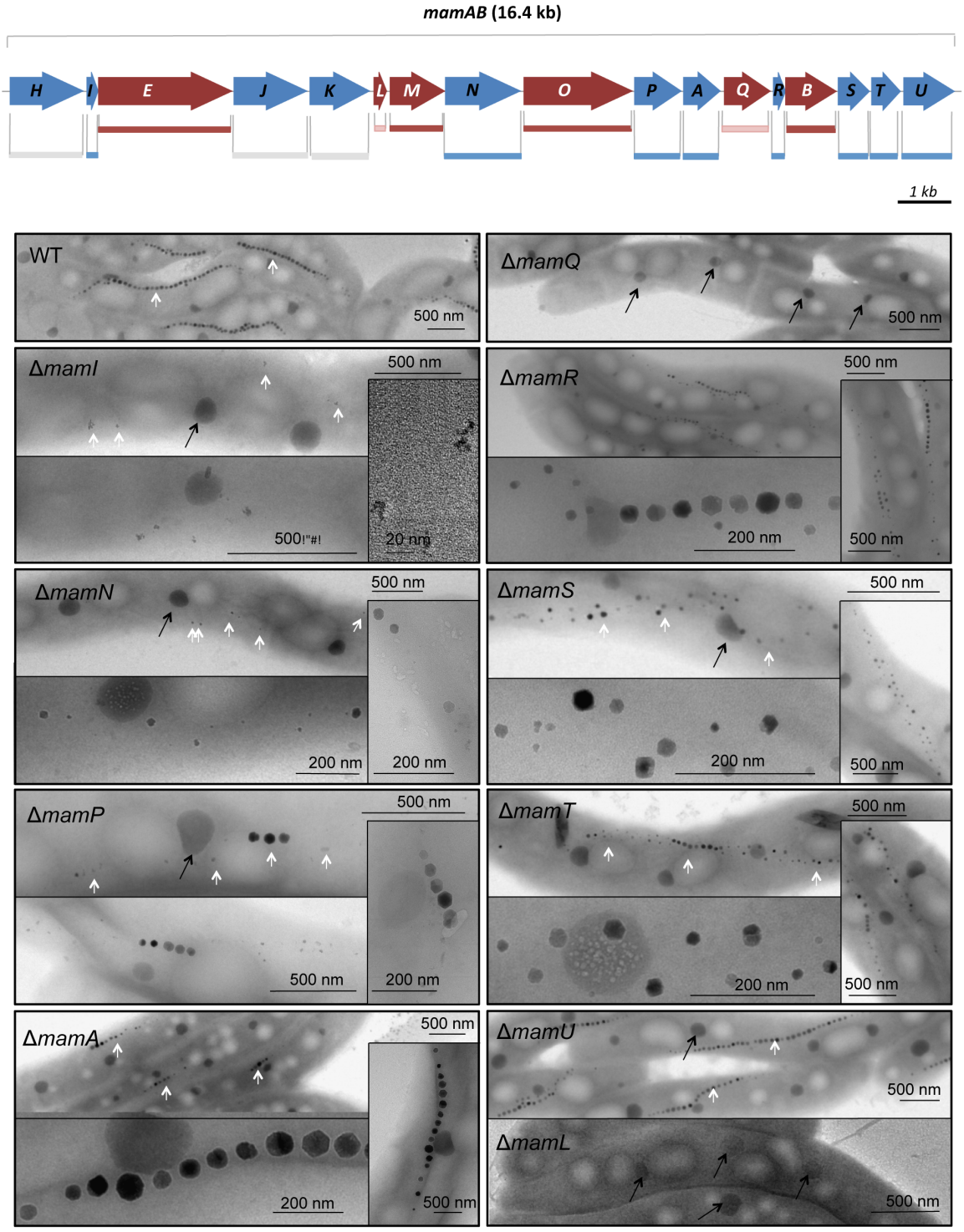

Figure 3. Molecular organization and deletion analysis of the *mamAB* operon of MSR as well as representative TEM micrographs of cells and magnetosome morphologies observed within the generated excision mutants. The highly conserved *mamAB* operons

encodes 17 magnetosome proteins (MamH, I, E, J, K, L, M, N, O, P, A, Q, R, B, S, T, and U) in MSR and was found to be essential and sufficient to maintain magnetite biogenesis (18, 22). Red arrows: Genes essential for magnetosome crystal formation. Blue arrows: Genes non-essential for particle formation. Grey bars: Non essential genes, for which deletion strains were previously generated (6, 9, 20). Blue bars: Non-essential genes, (deletions generated in this study). Dark red bars: Essential genes (deletions generated previously (35, 36)). Light red bar: Essential genes (deletions generated in this study). White arrows: magnetosome chains or particles; Black arrows: PHB granules.

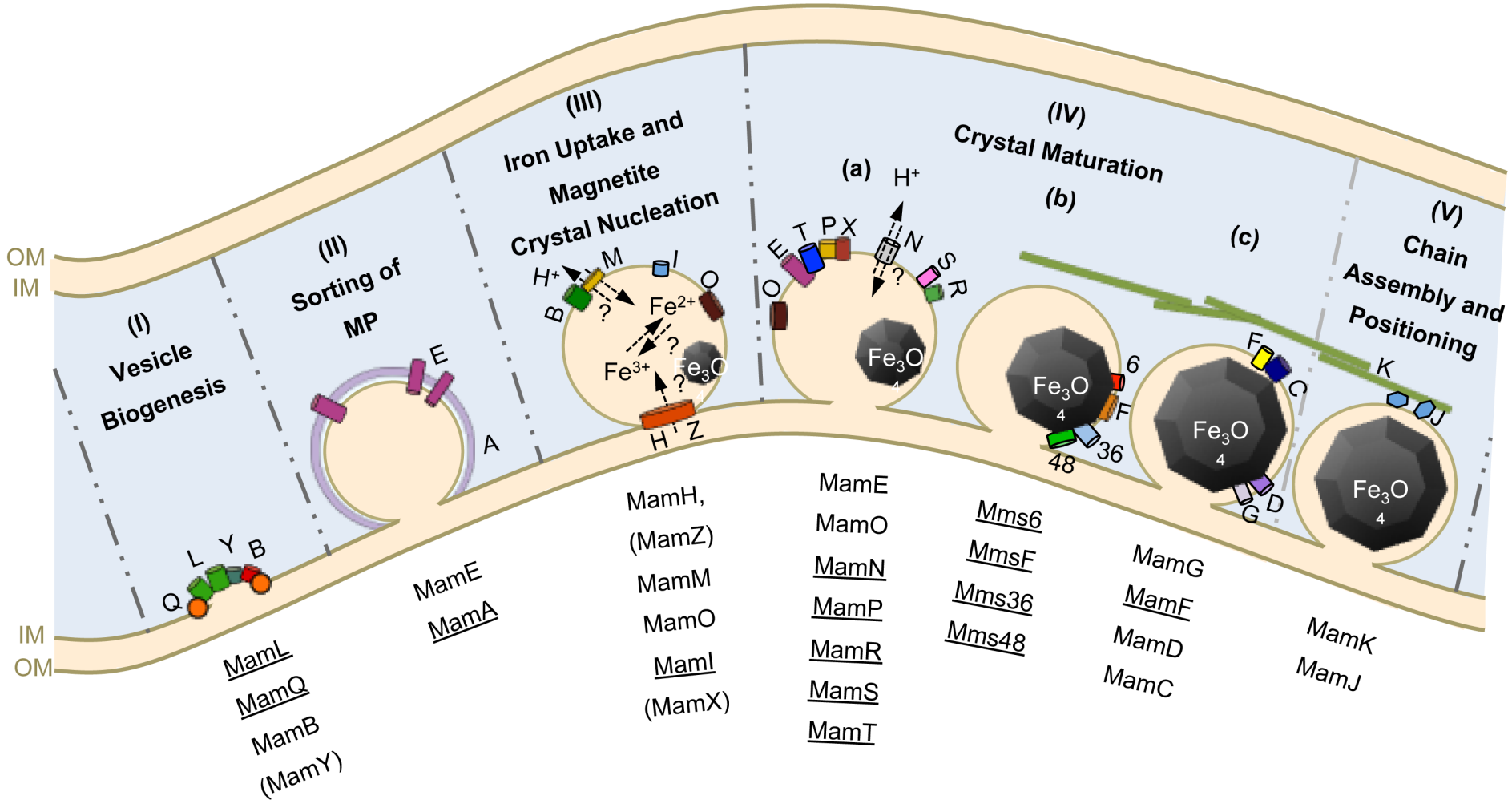
OM
IM
IM
OM
(I)
Vesicle
Biogenesis
(II)
Sorting of
MP
(III)
Iron Uptake and
Magnetite
Crystal Nucleation
(IV)
Crystal Maturation
(a)
(b)
(c)
(V)
Chain
Assembly and
Positioning
H+
Fe2+
Fe3+
Fe3O4
L
Y
B
Q
E
A
M
I
O
B
H
Z
T
P
X
E
O
N
S
R
6
F
36
48
F
C
G
D
K
J
MamL
MamQ
MamB
(MamY)
MamE
MamA
MamH,
(MamZ)
MamM
MamO
MamI
(MamX)
MamE
MamO
MamN
MamP
MamR
MamS
MamT
Mms6
MmsF
Mms36
Mms48
MamG
MamF
MamD
MamC
MamK
MamJ

Figure 4. Hypothetical model for magnetosome biosynthesis in MSR. Magnetosome biosynthesis depends on various steps including various magnetosome proteins. Magnetosome vesicle formation (I) is induced by the proteins MamQ, MamL, and MamB. MamY was found to regulate vesicle shape (23). MamA forms a multiprotein complex surrounding the magnetosome membrane (49) and MamE is involved in localization of magnetosome proteins by a protease independent process (32). The heterodimer of the CDF transporters MamB and MamM transports ferrous iron into the magnetosome vesicles (56) and ferric iron is taken up by MamH and MamZ (20) or formed by oxidation of ferrous iron within the vesicles. MamI is involved in magnetite nucleation. MamO was speculated to be directly involved in precipitation of iron oxide particles (32). The crystal growth is affected by several magnetosome proteins also including MamE that proteolytically remove a/an growth inhibitor/s or activate growth promoting proteins (32). Based on the conserved CXXCH heme-binding motifs within MamE, MamT, MamP and MamX it has been speculated that the proteins form a complex for electron transport to regulate electron flow (20, 47). MamS and MamR control crystal size by an unknown mechanism. MamN exhibits similarity to H^+-translocation proteins and might be involved in crystal growth by regulating intramagnetosomal pH (53). Mms6 is tightly bound to the magnetosome crystals (26, 28) and assembles into coherent micelles for templating crystal growth (60). *Mms48* (Mms48) and *mms36* (Mms36) act as inhibitors of crystal growth or recruit inhibiting proteins of particle growth by an unknown mechanism. The small, hydrophobic proteins MamG, MamF, MamD, and MamC control in a cumulative manner the growth of magnetite crystals (21). Magnetosomes were assembled into chains by the interaction of MamJ with the actin-like MamK filament that is also involved in chain positioning (6, 9, 61). OM: outer membrane; IM: inner membrane; MP: magnetosome protein; underlined proteins: analyzed proteins in this study, by single gene deletion of encoding genes. Proteins in brackets: non-essential proteins encoded by the *mamXYop*.

References

1. **Bazylinski D, Lefèvre C, Schüler D.** 2013. Magnetotactic Bacteria, p. 453-494. *In* Rosenberg E, DeLong E, Lory S, Stackebrandt E, Thompson F (ed.), The Prokaryotes. Springer Berlin Heidelberg.
2. **Blakemore R.** 1975. Magnetotactic bacteria. Science **190:**377-379.
3. **Schüler D.** 2004. Molecular analysis of a subcellular compartment: the magnetosome membrane in Magnetospirillum gryphiswaldense. Arch Microbiol **181:**1-7.
4. **Grünberg K, Müller EC, Otto A, Reszka R, Linder D, Kube M, Reinhardt R, Schüler D.** 2004. Biochemical and proteomic analysis of the magnetosome membrane in Magnetospirillum gryphiswaldense. Appl Environ Microbiol **70:**1040-1050.
5. **Komeili A, Vali H, Beveridge TJ, Newman DK.** 2004. Magnetosome vesicles are present before magnetite formation, and MamA is required for their activation. Proc Natl Acad Sci U S A **101:**3839-3844.
6. **Katzmann E, Scheffel A, Gruska M, Plitzko JM, Schüler D.** 2010. Loss of the actin-like protein MamK has pleiotropic effects on magnetosome formation and chain assembly in Magnetospirillum gryphiswaldense. Mol Microbiol **77:**208-224.
7. **Murat D, Quinlan A, Vali H, Komeili A.** 2010. Comprehensive genetic dissection of the magnetosome gene island reveals the step-wise assembly of a prokaryotic organelle. Proc Natl Acad Sci U S A **107:**5593-5598.
8. **Faivre D, Böttger LH, Matzanke BF, Schüler D.** 2007. Intracellular magnetite biomineralization in bacteria proceeds by a distinct pathway involving membrane-bound ferritin and an iron(II) species. Angew Chem Int Ed Engl **46:**8495-8499.
9. **Scheffel A, Gruska M, Faivre D, Linaroudis A, Plitzko JM, Schüler D.** 2006. An acidic protein aligns magnetosomes along a filamentous structure in magnetotactic bacteria. Nature **440:**110-114.
10. **Schübbe S, Kube M, Scheffel A, Wawer C, Heyen U, Meyerdierks A, Madkour MH, Mayer F, Reinhardt R, Schüler D.** 2003. Characterization of a spontaneous nonmagnetic mutant of Magnetospirillum

gryphiswaldense reveals a large deletion comprising a putative magnetosome island. J Bacteriol **185:**5779-5790.

11. **Ullrich S, Kube M, Schübbe S, Reinhardt R, Schüler D.** 2005. A hypervariable 130-kilobase genomic region of Magnetospirillum gryphiswaldense comprises a magnetosome island which undergoes frequent rearrangements during stationary growth. J Bacteriol **187:**7176-7184.
12. **Grünberg K, Wawer C, Tebo BM, Schüler D.** 2001. A large gene cluster encoding several magnetosome proteins is conserved in different species of magnetotactic bacteria. Appl Environ Microbiol **67:**4573-4582.
13. **Matsunaga T, Okamura Y, Fukuda Y, Wahyudi AT, Murase Y, Takeyama H.** 2005. Complete genome sequence of the facultative anaerobic magnetotactic bacterium Magnetospirillum sp. strain AMB-1. DNA Res **12:**157-166.
14. **Richter M, Kube M, Bazylinski DA, Lombardot T, Glöckner FO, Reinhardt R, Schüler D.** 2007. Comparative genome analysis of four magnetotactic bacteria reveals a complex set of group-specific genes implicated in magnetosome biomineralization and function. J Bacteriol **189:**4899-4910.
15. **Nakazawa H, Arakaki A, Narita-Yamada S, Yashiro I, Jinno K, Aoki N, Tsuruyama A, Okamura Y, Tanikawa S, Fujita N, Takeyama H, Matsunaga T.** 2009. Whole genome sequence of Desulfovibrio magneticus strain RS-1 revealed common gene clusters in magnetotactic bacteria. Genome Res **19:**1801-1808.
16. **Jogler C, Kube M, Schübbe S, Ullrich S, Teeling H, Bazylinski DA, Reinhardt R, Schüler D.** 2009. Comparative analysis of magnetosome gene clusters in magnetotactic bacteria provides further evidence for horizontal gene transfer. Environ Microbiol **11:**1267-1277.
17. **Schübbe S, Williams TJ, Xie G, Kiss HE, Brettin TS, Martinez D, Ross CA, Schüler D, Cox BL, Nealson KH, Bazylinski DA.** 2009. Complete genome sequence of the chemolithoautotrophic marine magnetotactic coccus strain MC-1. Appl Environ Microbiol **75:**4835-4852.
18. **Lohsse A, Ullrich S, Katzmann E, Borg S, Wanner G, Richter M, Voigt B, Schweder T, Schüler D.** 2011. Functional analysis of the

magnetosome island in Magnetospirillum gryphiswaldense: the mamAB operon is sufficient for magnetite biomineralization. PLoS One **6:**e25561.

19. **Schübbe S, Würdemann C, Peplies J, Heyen U, Wawer C, Glöckner FO, Schüler D.** 2006. Transcriptional organization and regulation of magnetosome operons in Magnetospirillum gryphiswaldense. Appl Environ Microbiol **72:**5757-5765.
20. **Raschdorf O, Müller FD, Posfai M, Plitzko JM, Schüler D.** 2013. The magnetosome proteins MamX, MamZ and MamH are involved in redox control of magnetite biomineralization in Magnetospirillum gryphiswaldense. Mol Microbiol **89:**872-886.
21. **Scheffel A, Gardes A, Grünberg K, Wanner G, Schüler D.** 2008. The major magnetosome proteins MamGFDC are not essential for magnetite biomineralization in Magnetospirillum gryphiswaldense but regulate the size of magnetosome crystals. J Bacteriol **190:**377-386.
22. **Murat D, Falahati V, Bertinetti L, Csencsits R, Körnig A, Downing K, Faivre D, Komeili A.** 2012. The magnetosome membrane protein, MmsF, is a major regulator of magnetite biomineralization in Magnetospirillum magneticum AMB-1. Molecular Microbiology **85:**684-699.
23. **Tanaka M, Arakaki A, Matsunaga T.** 2010. Identification and functional characterization of liposome tubulation protein from magnetotactic bacteria. Mol Microbiol **76:**480-488.
24. **Tanaka M, Mazuyama E, Arakaki A, Matsunaga T.** 2011. MMS6 protein regulates crystal morphology during nano-sized magnetite biomineralization in vivo. J Biol Chem **286:**6386-6392.
25. **Arakaki A, Webb J, Matsunaga T.** 2003. A novel protein tightly bound to bacterial magnetic particles in Magnetospirillum magneticum strain AMB-1. J Biol Chem **278:**8745-8750.
26. **Oestreicher Z, Valverde-Tercedor C, Chen L, Jimenez-Lopez C, Bazylinski DA, Casillas-Ituarte NN, Lower SK, Lower BH.** 2012. Magnetosomes and magnetite crystals produced by magnetotactic bacteria as resolved by atomic force microscopy and transmission electron microscopy. Micron **43:**1331-1335.

27. **Amemiya Y, Arakaki A, Staniland SS, Tanaka T, Matsunaga T.** 2007. Controlled formation of magnetite crystal by partial oxidation of ferrous hydroxide in the presence of recombinant magnetotactic bacterial protein Mms6. Biomaterials **28:**5381-5389.

28. **Arakaki A, Masuda F, Amemiya Y, Tanaka T, Matsunaga T.** 2010. Control of the morphology and size of magnetite particles with peptides mimicking the Mms6 protein from magnetotactic bacteria. J Colloid Interface Sci **343:**65-70.

29. **Kolinko I, Lohsse A, Borg S, Raschdorf O, Jogler C, Tu Q, Pósfai M, Tompa É, Plitzko JM, Brachmann A, Wanner G, Müller R, Zhang Y, Schüler D.** 2014. Biosynthesis of magnetic nanostructures in a foreign organism by transfer of bacterial magnetosome gene clusters. Nat Nanotechnol **9:**193-197.

30. **Komeili A, Li Z, Newman DK, Jensen GJ.** 2006. Magnetosomes are cell membrane invaginations organized by the actin-like protein MamK. Science **311:**242-245.

31. **Draper O, Byrne ME, Li Z, Keyhani S, Barrozo JC, Jensen G, Komeili A.** 2011. MamK, a bacterial actin, forms dynamic filaments in vivo that are regulated by the acidic proteins MamJ and LimJ. Molecular Microbiology **82:**342-354.

32. **Quinlan A, Murat D, Vali H, Komeili A.** 2011. The HtrA/DegP family protease MamE is a bifunctional protein with roles in magnetosome protein localization and magnetite biomineralization. Molecular Microbiology **80:**1075-1087.

33. **Rioux JB, Philippe N, Pereira S, Pignol D, Wu LF, Ginet N.** 2010. A second actin-like MamK protein in Magnetospirillum magneticum AMB-1 encoded outside the genomic magnetosome island. PLoS One **5:**e9151.

34. **Katzmann E, Scheffel A, Gruska M, Plitzko JM, Schüler D.** 2010. Loss of the actin-like protein MamK has pleiotropic effects on magnetosome formation and chain assembly in Magnetospirillum gryphiswaldense. Mol Microbiol **77:**208-224.

35. **Yang W, Li R, Peng T, Zhang Y, Jiang W, Li Y, Li J.** 2010. mamO and mamE genes are essential for magnetosome crystal biomineralization in Magnetospirillum gryphiswaldense MSR-1. Res Microbiol **161:**701-705.

36. **Uebe R, Junge K, Henn V, Poxleitner G, Katzmann E, Plitzko JM, Zarivach R, Kasama T, Wanner G, Posfai M, Böttger L, Matzanke B, Schüler D.** 2011. The cation diffusion facilitator proteins MamB and MamM of Magnetospirillum gryphiswaldense have distinct and complex functions, and are involved in magnetite biomineralization and magnetosome membrane assembly. Mol Microbiol **82:**818-835.

37. **Heyen U, Schüler D.** 2003. Growth and magnetosome formation by microaerophilic Magnetospirillum strains in an oxygen-controlled fermentor. Appl Microbiol Biotechnol **61:**536-544.

38. **Faivre D, Böttger LH, Matzanke BF, Schüler D.** 2007. Intracellular magnetite biomineralization in bacteria proceeds by a distinct pathway involving membrane-bound ferritin and an iron(II) species. Angew Chem Int Ed Engl **46:**8495-8499.

39. **Sambrook J, Russell DW.** 2001. Molecular cloning: a laboratory manual, vol. 2. Cold Spring Harbor Laboratory Press, New York.

40. **Schüler D, Uhl R, Baeuerlein E.** 1995. A simple light-scattering method to assay magnetism in Magnetospirillum gryphiswaldense FEMS Microbiol. Lett. **132:**139-145.

41. **Kolinko I, Jogler C, Katzmann E, Schüler D.** 2011. Frequent mutations within the genomic magnetosome island of Magnetospirillum gryphiswaldense are mediated by RecA. J Bacteriol **193:**5328-5334.

42. **Sodhi S, Banda H, Kathyola D, Burciul B, Thompson S, Joshua M, Bateman E, Fairall L, Martiniuk A, Cornick R, Faris G, Draper B, Mondiwa M, Katengeza E, Sanudi L, Zwarenstein M, Schull MJ.** 2011. Evaluating a streamlined clinical tool and educational outreach intervention for health care workers in Malawi: the PALM PLUS case study. BMC Int Health Hum Rights **11 Suppl 2:**S11.

43. **Baumgartner J, Morin G, Menguy N, Perez Gonzalez T, Widdrat M, Cosmidis J, Faivre D.** 2013. Magnetotactic bacteria form magnetite from a phosphate-rich ferric hydroxide via nanometric ferric (oxyhydr)oxide intermediates. Proc Natl Acad Sci U S A **110:**14883-14888.

44. **Lang C, Schüler D.** 2008. Expression of green fluorescent protein fused to magnetosome proteins in microaerophilic magnetotactic bacteria. Appl Environ Microbiol **74:**4944-4953.

45. **Frankenberg N, Moser J, Jahn D.** 2003. Bacterial heme biosynthesis and its biotechnological application. Applied Microbiology and Biotechnology **63:**115-127.

46. **Panek H, O'Brian MR.** 2002. A whole genome view of prokaryotic haem biosynthesis. Microbiology **148:**2273-2282.

47. **Siponen MI, Adryanczyk G, Ginet N, Arnoux P, Pignol D.** 2012. Magnetochrome: a c-type cytochrome domain specific to magnetotatic bacteria. Biochem Soc Trans **40:**1319-1323.

48. **Yamamoto D, Taoka A, Uchihashi T, Sasaki H, Watanabe H, Ando T, Fukumori Y.** 2010. Visualization and structural analysis of the bacterial magnetic organelle magnetosome using atomic force microscopy. Proceedings of the National Academy of Sciences **107:**9382-9387.

49. **Zeytuni N, Ozyamak E, Ben-Harush K, Davidov G, Levin M, Gat Y, Moyal T, Brik A, Komeili A, Zarivach R.** 2011. Self-recognition mechanism of MamA, a magnetosome-associated TPR-containing protein, promotes complex assembly. Proceedings of the National Academy of Sciences **108:**E480-E487.

50. **Siponen MI, Legrand P, Widdrat M, Jones SR, Zhang W-J, Chang MCY, Faivre D, Arnoux P, Pignol D.** 2013. Structural insight into magnetochrome-mediated magnetite biomineralization. Nature **502:**681-684.

51. **Rahn-Lee L, Komeili A.** 2013. The magnetosome model: insights into the mechanisms of bacterial biomineralization. Front Microbiol **4:**352.

52. **Brilliant MH.** 2001. The mouse p (pink-eyed dilution) and human P genes, oculocutaneous albinism type 2 (OCA2), and melanosomal pH. Pigment Cell Res **14:**86-93.

53. **Schüler D.** 2008. Genetics and cell biology of magnetosome formation in magnetotactic bacteria. FEMS Microbiol Rev **32:**654-672.

54. **Fdez-Gubieda ML, Muela A, Alonso J, Garcia-Prieto A, Olivi L, Fernandez-Pacheco R, Barandiaran JM.** 2013. Magnetite

biomineralization in Magnetospirillum gryphiswaldense: time-resolved magnetic and structural studies. ACS Nano **7:**3297-3305.

55. **Bell PE, Mills AL, Herman JS.** 1987. Biogeochemical Conditions Favoring Magnetite Formation during Anaerobic Iron Reduction. Appl Environ Microbiol **53:**2610-2616.
56. **Uebe RJ, K. Henn, V. Poxleitner, G. Katzmann, E. Plitzko, J.M. Zarivach, R. Kasama, T. Wanner, G. Pósfai, M. Böttger, L. Matzanke, B. Schüler, D.** 2011. The cation diffusion facilitator proteins MamB and MamM of Magnetospirillum gryphiswaldense have distinct and complex functions, and are involved in magnetite biomineralization and magnetosome membrane assembly. Molecular Microbiology **82:**818–835.
57. **Lenz LL, Dere B, Bevan MJ.** 1996. Identification of an H2-M3-restricted Listeria epitope: implications for antigen presentation by M3. Immunity **5:**63-72.
58. **McMahon HT, Gallop JL.** 2005. Membrane curvature and mechanisms of dynamic cell membrane remodelling. Nature **438:**590-596.
59. **Richter M, Kube M, Bazylinski DA, Lombardot T, Glöckner FO, Reinhardt R, Schüler D.** 2007. Comparative genome analysis of four magnetotactic bacteria reveals a complex set of group-specific genes implicated in magnetosome biomineralization and function. J Bacteriol **189:**4899-4910.
60. **Wang W, Bu W, Wang L, Palo PE, Mallapragada S, Nilsen-Hamilton M, Vaknin D.** 2012. Interfacial Properties and Iron Binding to Bacterial Proteins That Promote the Growth of Magnetite Nanocrystals: X-ray Reflectivity and Surface Spectroscopy Studies. Langmuir **28:**4274-4282.
61. **Katzmann E, Müller FD, Lang C, Messerer M, Winklhofer M, Plitzko JM, Schüler D.** 2011. Magnetosome chains are recruited to cellular division sites and split by asymmetric septation. Mol Microbiol **82:**1316-1329.

Supplementary material

HRTEM of mutants Δ*mamI* and Δ*mamN*

As shown by HRTEM, the nuclei within Δ*mamI* were composed of several small grains that formed thin aggregates (Figure 2). In most particles, the incipient nuclei did not show lattice fringes in HRTEM images and lacked a visible crystalline structure. This might be caused by either (i) no close orientation of these particles to a crystallographic zone axis, or (ii) an amorphous structure, which seems more likely because of the weak diffraction contrast of the nuclei. Lattice fringes were observed in only two particles, and according to the Fourier transforms of the HRTEM images, the spacing between the fringes was ~3.71 Å (Figure 2B), which is very close to the d(012) spacing in hematite, whereas no other iron oxide has a d-spacing close to this value. For a second highly elongated particle only part of the crystal produced fringes with a distance of 2.72 Å, and showed again a value very close to that of hematite (d(014) = 2.70 Å) (Figure 2C). Thus, the few tiny electron dense particles seem to consist of hematite.

Complementation of mutant strains

Mutants carrying the respective insertion plasmids showed WT-like magnetosome biomineralization (Figure S3). Expression of WT alleles of *mms6* and *mmsF* from replicative plasmids pAL_*mms6* and pAL_*mmsF* was sufficient to restore phenotypes of Δ*mms6* and Δ*mmsF* at least in a significant fraction of cells (Figure S3). Complementation of ΔA10 with *mms6*, *mmsF* and *mgr4074* together (p*mmsF_mms6_4074*) led to crystals with 37 nm and 38 nm in size, but only 23 and 18 crystals per cell under control of the P_{mms6} and P_{mamDC} promoter, respectively. Only the entire *mms6* operon was able to fully restore both numbers and crystal size back to WT dimensions (Figure S3). Conjugative transfer of pAL_*mamIg* and pOR086 into mutants Δ*mamI* and Δ*mamQ* resulted in restoration of particle synthesis in 83% and 66% of cells, respectively. However, strain Δ*mamQ*_ pOR086 synthesized fewer particles than WT.

Table S1. Strains and plasmids used in this study.

Strains and plasmids	Description	References
MSR strains		
MSR-1 R3/S1	Rif^r Sm^r, spontaneous mutant	(1)
Δ*mamAB*	Δ*mamAB*	(2)
ΔA13	Δ*mms6* operon, Δ*mamGFDC,* Δ*mamXY*	(3)
ΔA12	Δ*mms6* operon, Δ*mamGFDC,*	(3)
ΔA10	Δ*mms6* operon	(3)
Δ*mamI*	deletion of *mgr4090*	this study
Δ*mamL*	deletion of *mgr4094*	this study
Δ*mamN*	deletion of *mgr4096*	this study
Δ*mamP*	deletion of *mgr4098*	this study
Δ*mamA*	deletion of *mgr4099*	this study
Δ*mamQ*	deletion of *mgr4100*	this study
Δ*mamR*	deletion of *mgr4101*	this study
Δ*mamS*	deletion of *mgr4103*	this study
Δ*mamT*	deletion of *mgr4104*	this study
Δ*mamU*	deletion of *mgr4105*	this study
Δ*mms48*	deletion of *mgr4070*	this study
Δ*mms36*	deletion of *mgr4071*	this study
Δ*mmsF*	deletion of *mgr4072*	this study
Δ*mms6*	deletion of *mgr4073*	this study
Δ*mmsF_mms6*	deletion of *mgr4072 and mgr4073*	this study
Δ*mmsF_mamF*	deletion of *mgr4072 and mgr4076*	this study
Δ*mamI::mamI*	Δ*mamI*+pAL_*mamIg,* Km^r	this study
Δ*mamL::mamL*	Δ*mamL*+pOR*mamL*	this study
Δ*mamN::mamN*	Δ*mamN*+pBam_*mamN,* Km^r	this study
Δ*mamP::mamP*	Δ*mamP*+pBam_*mamP,* Km^r	this study
Δ*mamA::mamA*	Δ*mamA*+pBam_*mamA,* Km^r	this study
Δ*mamQ::mamQ*	Δ*mamQ*+pOR86, Km^r	this study
Δ*mamR::mamR*	Δ*mamR*+pBam_*mamR,* Km^r	this study
Δ*mamS::mamS*	Δ*mamS*+pBam_*mamS,* Km^r	this study
Δ*mamT::mamT*	Δ*mamT*+pBam_*mamT,* Km^r	this study
Δ*mms48::mms48*	Δ*mms48*+pBam_*mms48,* Km^r	this study
Δ*mms36::mms36*	Δ*mms36*+pBam_*mms36,* Km^r	this study
Δ*mmsF::mmsF*	Δ*mmsF+pAL_mmsF,* Km^r	this study
Δ*mms6::mms6*	Δ*mms6+pAL_mms6,* Km^r	this study
Δ*mmsF_mms6::mms6*	Δ*mmsF_mms6+pAL_mms6,*	this study

	Km^r	
Δ*mmsF_mamF::mmsF*	Δ*mmsF_mamF+pAL_mmsF,* Km^r	this study
ΔA10::P_{mms6}_*mmsF,6,4074*	ΔA10+P_{mms6}_*mmsF,6,4074*+ pAL_P_{mms6}_*mmsF,6,4074*, Km^r	this study
ΔA10::P_{mamDC}_*mmsF,6,4074*	ΔA10+P_{mamDC}_*mmsF,6,4074* + pAL_P_{mamDC}_*mmsF,6,4074,* Km^r	this study
ΔA10::*mms6op*	ΔA10+pAL_P_{mamDC}_*mms6op* , Km^r	this study
Δ*mamI::mamCgfp*	Δ*mamI, gfp* fused to the chromosomal *mamC*	this study
Δ*mamN::mamCgfp*	Δ*mamN, gfp* fused to the chromosomal *mamC*	this study
Δ*mamP::mamCgfp*	Δ*mamP, gfp* fused to the chromosomal *mamC*	this study
Δ*mamA::mamCgfp*	Δ*mamA, gfp* fused to the chromosomal *mamC*	this study
Δ*mamQ::mamCgfp*	Δ*mamQ, gfp* fused to the chromosomal *mamC*	this study
Δ*mamR::mamCgfp*	Δ*mamR, gfp* fused to the chromosomal *mamC*	this study
Δ*mamS::mamCgfp*	Δ*mamS, gfp* fused to the chromosomal *mamC*	this study
Δ*mamT::mamCgfp*	Δ*mamT, gfp* fused to the chromosomal *mamC*	this study
WT::*mms36*	MSR-1, chromosomal integration of *mms36*	this study
WT::*mms48*	MSR-1, chromosomal integration of *mms48*	this study
***E. coli* strains**		
BW29427	*thrB1004 pro thi rpsL hsdS lacZDM15 RP4-1360D(araBAD)567DdapA 1341::[erm pir(WT)]trahsdR17 recA1-endA1gyrA96thi-1relA1*	Datsenko and Wanner, unpublished data
DH5a		Invitrogen
S17-1*λpir*	RPA-2, Tc::Mu-Km::Tn7 (λpir)	(4)
WM3064	*thrB1004 pro thi rpsL hsdS lacZDM15 RP4-1360D(araBAD) 567DdapA*::[*erm pir*]	(5)

Plasmids

pJet1.2	Ap^r, *eco47IR*, *rep* (pMB-1)	Fermentas
pCM184	Km^r, Ap^r, Tet^r	(6)
pBam1	*ori*R6K, Km^r, Ap^r	(7)
pBam_*mamGFDC*	pBam1, inserted mamGFDC operon	Lohße, Kolinko *et al*., in preparation
pBBR1MCS2	Mobilizable broad-host-range vector, Km^r	(8)
pCL6	pBBR1MCS2, 10-glycine linker, *egfp,* Km^r	(9)
pAP150	pBBR1MCS2, 10-glycine linker, *egfp*, Km^r	(10)
pORFM_*galK*	suicide vector, Km^r	Raschdorf *et al*., submitted for publication
pFM236	integrative plasmid, *gfp,* Km^r	Raschdorf *et al*., submitted for publication
pAL_*mamI* 3'5'	pORFM_*galK*, upstream and downstream fragments of *mamI*, Km^r	this study
pOR_Δ*mamL*	pORFM_*galK*, upstream and downstream fragments of *mamL,* Km^r	this study
pAL_*mamN* 3'5'	pORFM_*galK*, upstream and downstream fragments of *mamN,* Km^r	this study
pAL_*mamP* 3'5'	pORFM_*galK*, upstream and downstream fragments of *mamP,* Km^r	this study
pAL_*mamA* 3'5'	pORFM_*galK*, fragments of *mamA,* Km^r	this study
pAL_*mamQ* 3'5'	pORFM_*galK*, insertion of upstream and downstream fragments of *mamQ,* Km^r	this study
pAL_*mamR* 3'5'	pORFM_*galK*, upstream and downstream fragments of *mamR,* Km^r	this study
pAL_*mamS* 3'5'	pORFM_*galK*, upstream and downstream fragment of *mamS,* Km^r	this study
pAL_*mamT* 3'5'	pORFM_*galK*, upstream and downstream fragments of *mamT,* Km^r	this study
pAL_*mamU* 3'5'	pORFM_*galK*, upstream and	this study

	downstream fragments of *mamU,* Km^r	
pAL_*mamAB* 3'5'	pORFM_*galK*, upstream fragments of *mamH* and downstream fragment of *mamU,* Km^r	this study
pAL_*mmsF_mms6* 3'5'	pORFM_*galK*, downstream fragments of *mmsF* and upstream fragment of *mms6,* Km^r	this study
pCM184_*mmsF* 3'5'	pCM184, downstream and upstream fragment of *mmsF,* Km^r	this study
pCM184_*mms6* 3'5'	pCM184, downstream and upstream fragments of *mms6,* Km^r	this study
pCM184_*mamF* 3'5'	pCM184, downstream and upstream fragments of *mamF,* Km^r	this study
pAl_*mamIg*	pCL6, *mamI*, Km^r	this study
pBam_*mamN*	pBam_*GFDC*, *mamN*, Km^r	this study
pBam_*mamP*	pBam_*GFDC*, *mamP*, Km^r	this study
pBam_*mamA*	pBam_*GFDC*, *mamA,* Km^r	this study
pBam_*mamR*	pBam_*GFDC*, *mamR*, Km^r	this study
pBam_*mamS*	pBam_*GFDC*, *mamS*, Km^r	this study
pBam_*mamT*	pBam_*GFDC*, *mamT,* Km^r	this study
pOR086	pBBR1MCS2, *mamQ*, Km^r	this study
pBam_*mgr4074*	pBam_*GFDC*, *mgr4074,* Km^r	this study
pAL*g*	pAP150, 10-glycine linker, *egfp,* Km^r	this study
pAL_*mmsF*	pAP150, *mmsF,* Km^r	this study
pAL_*mms6*	pAP150, *mms6,* Km^r	this study
pAL_P$_{mamDC}$_*mms6op*	pAP150, *mms6* operon, P_{mamDC}, Km^r	this study
pAL_ P$_{mms6}$_*mms6,F,4074*	pAP150, *mms6, mmsF, mgr4074,* P_{mms6}, Km^r	this study
pAL_ P$_{mamDC}$_*mms6,F,4074*	pAP150, *mms6, mmsF, mgr4074,* P_{mamDC}, Km^r	this study

Table S2. DNA oligonucleotides used in this work.

Name	Sequence
AL251	GGATCCGGTTGGCGGAGCCTCCATT
AL252	CATAAACGTTCTCCAGTCTTGAT
AL253	ATCAAGACTGGAGAACGTTTATGCCTAACATCGATGGTTGATGAC
AL254	GGTACCACTTCATCCAGTGCGAAAAGG
AL255	GGATCCATTAAGCGCTGACATTCCATGC
AL256	CACCTAGTTATCCACCTTGGA
AL257	CCAAGGTGGATAACTAGGTGATCGCCGTTCTCGCAGGATG
AL258	GGTACCCATGGCCACAGTTTGGGCCG
AL259	GGATCCGGGCATGAATGTGGTGCAAG
AL260	CATTCCCGGCTAATCCCAAAAC
AL261	GTTTTGGGATTAGCCGGGAATGGAAGCTTGCCACGTGATAAATT
AL262	GGTACCGGGCATCCTCGTACATGGTG
AL263	GGATCCGGTGCTTATGTTGGCGGCAT
AL264	CATACTGTTCTCCAAAATCCCA
AL265	TGGGATTTTGGAGAACAGTATGGATGAACGTTCGGCCGTCTA
AL266	GCGGCCGCGCTATAGATGCGGTGCGGCAG
AL267	GGATCCTAAGGACAACCGTCCCGGCA
AL268	CATATCCGCCTCGTTGCTATC
AL269	ATAGCAACGAGGCGGATATGCATTCGCAGGAATCCAAGAATTG
AL270	GGTACCTATCGAACTGCACGTCCTCG
AL271	GGATCCGCAATCGCGTACAGCTACGA
AL272	GGTCATCAAGGCACTTCCCT
AL273	AGGGAAGTGCCTTGATGACCTGGAATACATGAACCGATGAAG
AL274	GGTACCCAGAATCAAGACTAGAGCGCC
AL275	GGATCCTGCAGGTGCTTGAGATGGTC
AL276	CATGATTCCCCTCTCCTGATC
AL277	ATCAGGAGAGGGGAATCATGTGGATGACCGTGCAGTGAG
AL278	GGTACCAACGATCATTGACCCGTCCC
AL279	GGATCCCGAGGACGTGCAGTTCGATA
AL280	CATGTTCACCCTCTCTGTCC
AL281	GGACAGAGAGGGTGAACATGGGCATTAAATGGCTGTTGTAAGC
AL282	GGTACCGCCATCCATCCGTTCACG
AL283	GGATCCTACCCGTGGGGAAGGCAAGA
AL284	CATCTTCCACACAGCCCCTG
AL285	CAGGGGCTGTGTGGAAGATGTCCATACTGGTTCCGAAATACG
AL286	GGTACCCGAGGCTACGGGCTTTTTCC
AL287	GGATCCCCGTCAATGGTTTCGTGAAGG
AL288	CATTCCCGTCACAATTCACCT
AL289	AGGTGAATTGTGACGGGAATGTCCATACTGGTTCCGAAATACG
AL364	GGATCCATTTCTGAACGGCAAAGGCA
AL365	TGATCCATGCTATTACGCCT

AL366	AGGCGTAATAGCATGGATCACGGTGCCTTTTCGTTGATGT
AL367	GGTACCACTACTTGATTGCTAAGGAGAA
AL368	GGATCCTAGCGCGCAGCAAAGTTGC
AL369	TGAGGGCATCGCGTTGTTTG
AL370	CAAACAACGCGATGCCCTCACAGGACGATCAGGCGTAATA
AL371	GGTACCGGTCCTGGTTCTGTATCTGG
AL372	GGATCCCTCGGTGCGTCTGATCAATA
AL373	TGAGGTTCGGCCTCGGGTGA
AL374	TCACCCGAGGCCGAACCTCAGGTTCCGACCGGAACCC
AL375	GGTACCCAAAATAGTCTCGGCCATTG
AL202	GAATTCCCATCGCCGACAATTCAGAC
AL203	CATATGCTGAGGTTCGGCCTCGGGTGATT
AL204	GGGCCCTTCATGTCCCCCCCCCCCCGTTCA
AL205	GAGCTCGCCTCAGCCTGCGCTTTGCG
AL208	GAATTCCGCGTTCCATTTCACCCAGG
AL209	CATATGTGCTTTGCCCTCGCTTAAGC
AL210	GGGCCCCGGCGAGCGATCTAACGGAC
AL211	GAGCTCAAACATCGGGAGCGCCATGG
AL240	GAATTCGCCTCCAGCCAGGGTTGGA
AL241	CATATGGCGACGCGCTGTCCTGAAC
AL242	GGGCCCCATTCCGTTGGCGATCTGAG
AL243	GAGCTCACTGACGAGACCGTCGCCGT
AL244	ATATGGAATTCGGAGGCGGAGGCGGTGGCGGAGGTGGCGGAGTGAGC AAGGGCGAGGAG
AL245	GGATCCTTACTTGTACAGCTCGTC
AL236	CATATGATGGTTTGCCCCCCTGGGGT
AL250	GAATTCGGACAGCGCGTCGCGCAG
AL398	CATATGATGAATAGCAAACTCGTCCT
AL464	GAATTCCTAATTTATCACGTGGCAAG
AL402	CATATGATGGACTTTCGGCCTGATCA
AL465	GAATTCTCACTGCACGGTCATCCAC
AL404	CATATGATGGGTACGCCAGGGGG
AL466	GAATTCTTACAACAGCCATTTAATGCC
AL406	CATATGATGACCTTTGTTCAGGGCG
AL467	GAATTCTCATCGGTTCATGTATTCCA
IB302	GGCGGTACCATGTCTAGCAAGCCG
IB303	GGCTCTAGATTAGACGGCCGAAC
AL414	CATATGGTGGTTGGATTTATCACCCT
AL469	TTAATTAATCATCCTGCGAGAACGGC
AL417	CATATGATGCTATTACGCCTGATCGT
AL487	GAATTCTCATGTACTGCGGAACAGTC
AL488	GAATTCTCACTCGTCTCGAGACGA
AL489	CATATGATGGACATCAACGAAAAGGC
AL499	GAATTCTCAAGTAGTGCGGGACTGAA

AL500	CATATGTTGGGCTTGTGGTTTTGGCG
AL220	GGATCCTCAGATCCGGTCGGCCACC
AL221	CATATGATGGTTGAAGCAATCCTTCGGA
AL134	GGATCCTCAGGACAGCGCGTCGCG
AL135	CATATGATGGTTTGCCCCCCTGGGGT
AL178	GGATCCTTCATGTACTGCGGAACAGTCG
AL179	CATATGTTGGGCTTGTGGTTTTGGCGG
AL234	GGATCCTCACCCGAGGCCGAACCTCA
AL394	CATATGATGCCAAGCGTGATTTTCGG
AL395	GAATTCACCATCGATGTTAGGGTCTG
OR252	GACAATGCATTGCTCAGCGAGATCAGTGACC
OR253	GTCAGCGCTTAATGACGATGTTTCCGATCACTCTTACCATACCAATG
OR254	CATTGGTATGGTAAGAGTGATCGGAAACATCGTCATTAAGCGCTGAC
OR255	ACTCACTAGTGTTCTGCACCGCCTCACC

Table S3. Oligonucleotides for amplification of sequences and genes important for gene deletions or complementation experiments.

Amplified region	Oligonucleotides
5' flanking sequence of *mamI*	AL251/AL252
3' flanking sequence of *mamI*	AL253/AL254
5' flanking sequence of *mamL*	OR252/OR253
3' flanking sequence of *mamL*	OR254/OR255
5' flanking sequence of *mamN*	AL255/AL256
3' flanking sequence of *mamN*	AL257/AL258
5' flanking sequence of *mamP*	AL259/AL260
3' flanking sequence of *mamP*	AL261/AL262
5' flanking sequence of *mamA*	AL263/AL264
3' flanking sequence of *mamA*	AL265/AL266
5' flanking sequence of *mamQ*	AL267/Al268
3' flanking sequence of *mamQ*	AL269/Al270
5' flanking sequence of *mamR*	AL271/AL272
3' flanking sequence of *mamR*	AL273/AL274
5' flanking sequence of *mamS*	AL275/AL276
3' flanking sequence of *mamS*	AL277/AL278
5' flanking sequence of *mamT*	AL279/AL280
3' flanking sequence of *mamT*	AL281/AL282
5' flanking sequence of *mamU*	AL283/AL284
3' flanking sequence of *mamU*	AL285/AL286
5' flanking sequence of *mms36*	AL364/AL365
3' flanking sequence of *mms36*	AL366/AL367
5' flanking sequence of *mms48*	AL368/AL369
3' flanking sequence of *mms48*	AL370/AL371
5' flanking sequence of *mmsF_mms6*	AL372/AL373
3' flanking sequence of *mmsF_mms6*	AL374/AL375
5' flanking sequence of *mmsF*	AL202/AL203
3' flanking sequence of *mmsF*	AL204/AL205
5' flanking sequence of *mamF*	AL208/AL209
3' flanking sequence of *mamF*	AL210/Al211
5' flanking sequence of *mms6*	AL240/AL241
3' flanking sequence of *mms6*	AL374/AL375
mamP	AL398/AL464
mamS	AL402/AL465
mamT	AL404/AL466
mamR	AL406/AL467
mamA	IB302/IB303
mamN	AL414/AL469
mms36	AL488/Al489
mms48	AL417/AL487
mgr4074	AL499/AL500
mmsF	AL220/AL221

mms6	AL134/AL135
mms6 operon	AL178/AL179
mms6, mmsF, mgr4074	AL179/AL234

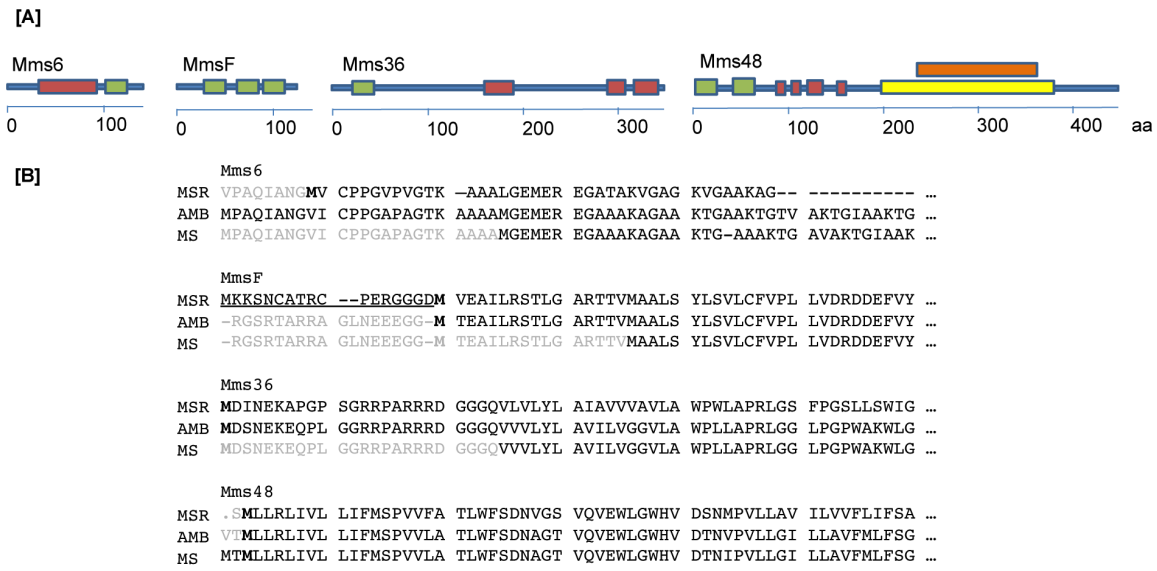

Figure S1. Domain structures and protein sequence analysis of proteins encoded by the *mms6* operon of MSR.

A: Predicted domain structure of Mms6, MmsF, Mms36 and Mms48 (11, 12). All proteins contain transmembrane domains (13), and except for MmsF the proteins have predicted regions of low complexity (red). Mms48 has a predicted C-terminal TPR-HemY domain (yellow), and a PEP-TPR domain (orange). B: Protein sequence comparison of magnetosome proteins encoded by the *mms6* operon of MSR, AMB, and MS. Black letters correspond to previous protein annotations; Bold letters mark the supposed start sequence; Grey letters illustrate sequences in front of previously annotated proteins; Underlined amino acids demonstrate potential false annotated sequences within the previous annotations of MSR.

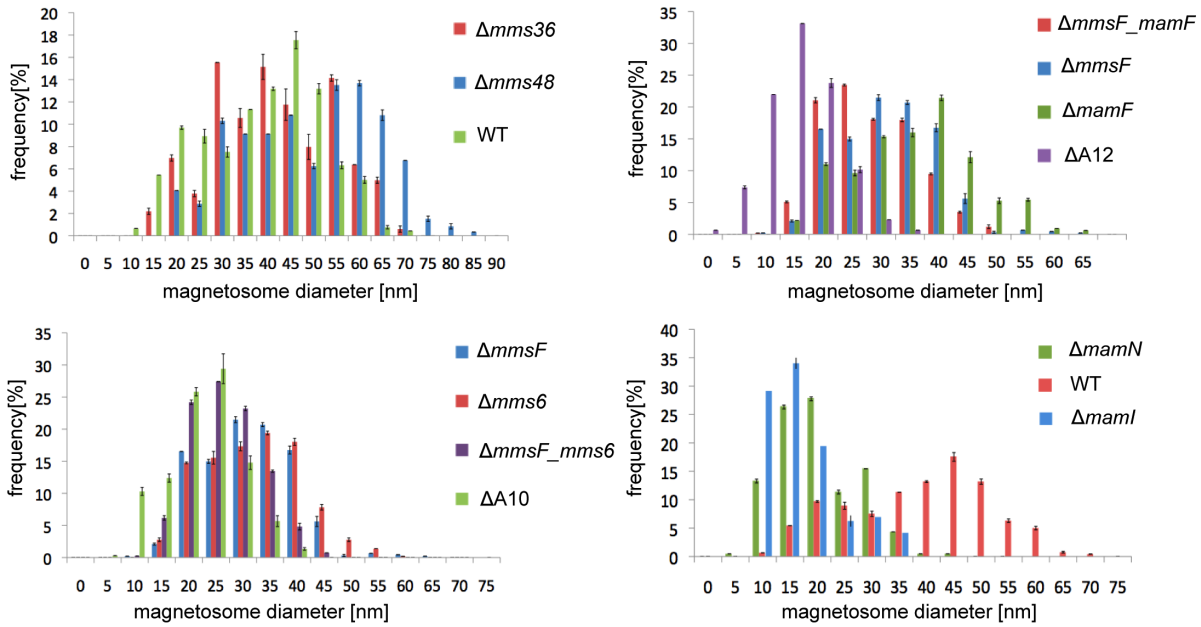

Figure S2. Magnetosome size distribution of various generated deletion strains of MSR. Magnetosome size distributions of electron dense particles within the mutants ΔA10, Δ*mms6*, Δ*mmsF*, Δ*mmsF_mms6,* Δ*mamF,* Δ*mmsF_mamF*, Δ*A12,* Δ*mms36*, Δ*mms48,* and WT.

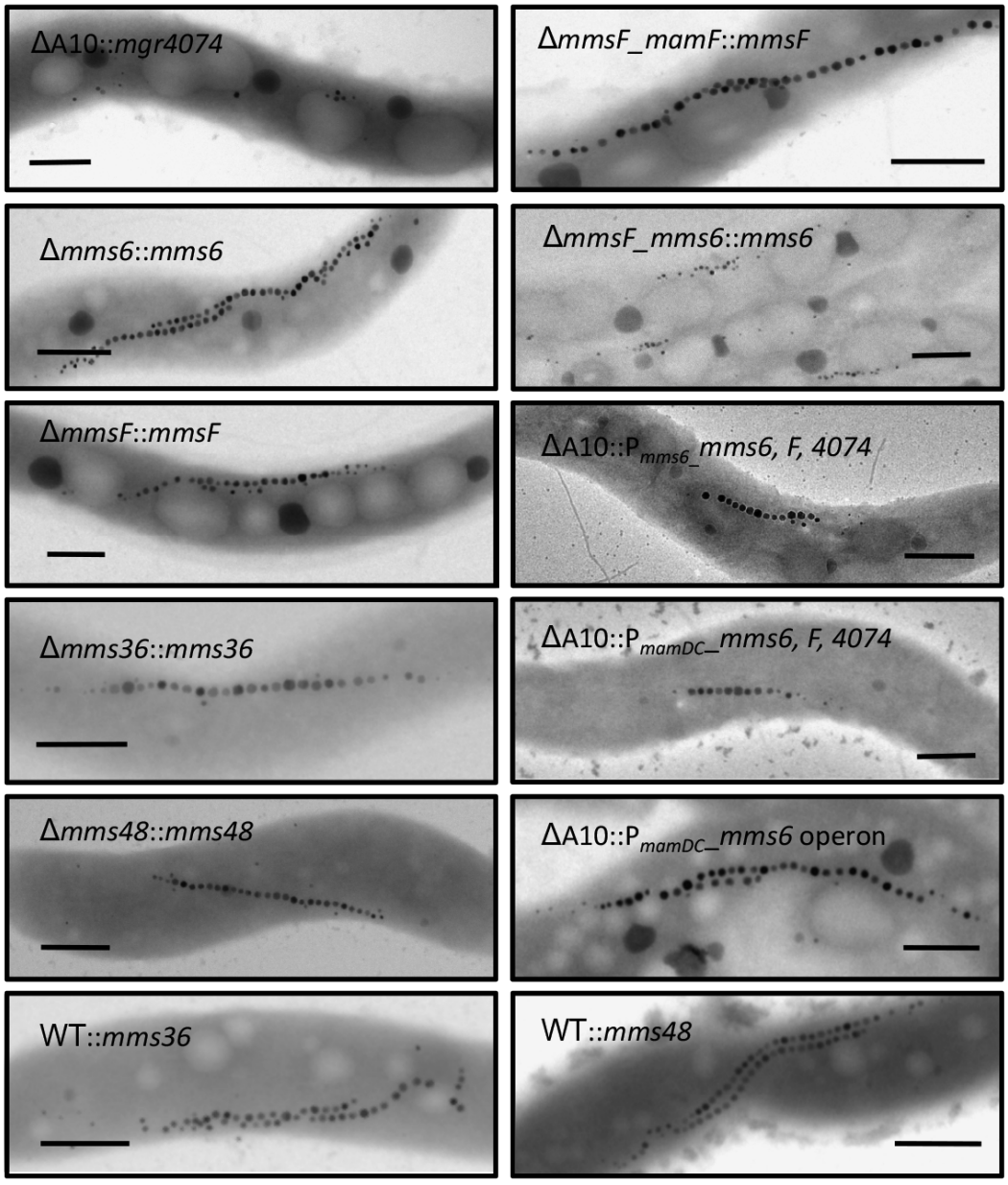

Figure S3. Overview about complementation experiments of various generated deletion strains of MSR and overexpression strains. TEM micrographs of ΔA10, Δ*mms6*, Δ*mmsF*, Δ*mms36*, Δ*mms48, ΔmmsF_mamF, and ΔmmsF_mms6* cells with indicated gene complementations and overexpression strains WT::*mms36* and WT::*mms48*. Scale bars: 500 nm.

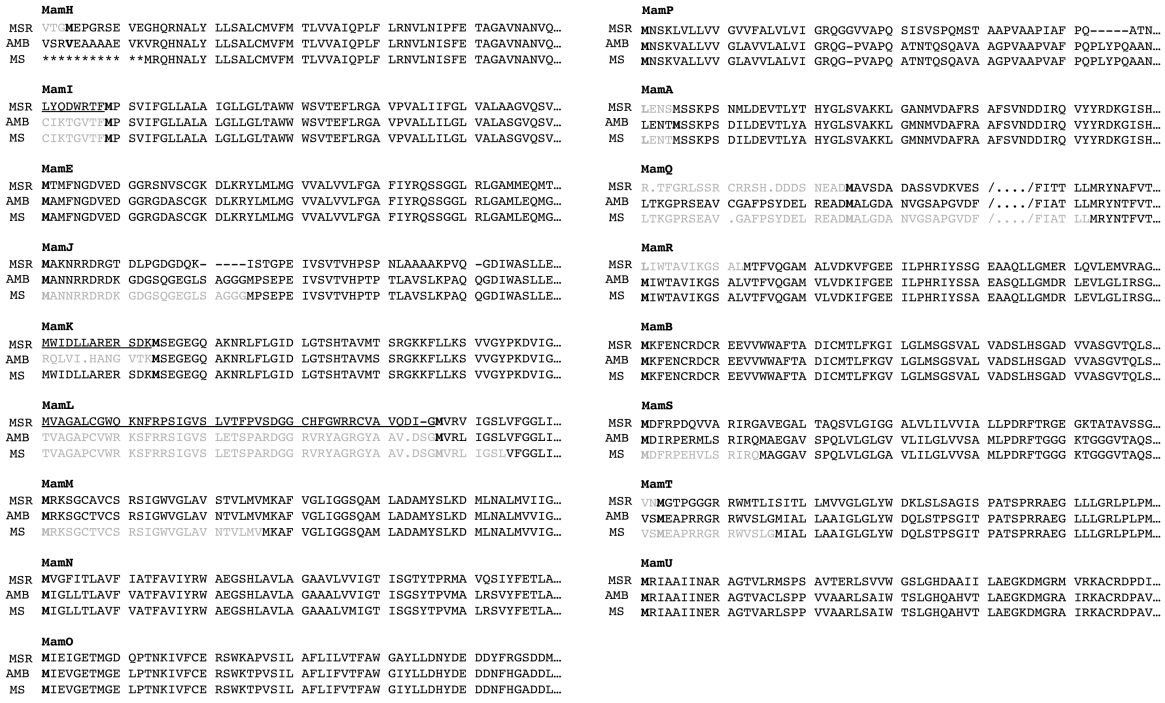

Figure S4. Protein sequence alignments of magnetosome proteins encoded by the *mamAB* operon of *M. gryphiswaldense* (MSR), *M. magneticum* (AMB), and *M. magnetotacticum* (MS). Asterisks mark amino acids that not part of the published geneome sequence; Black letters correspond to previous protein annotations; Bold letters mark the likely start codon; Grey letters indicate amino acids in front of previous protein annotations; Underlined amino acids demonstrate false sequences within the previous annotations of MSR.

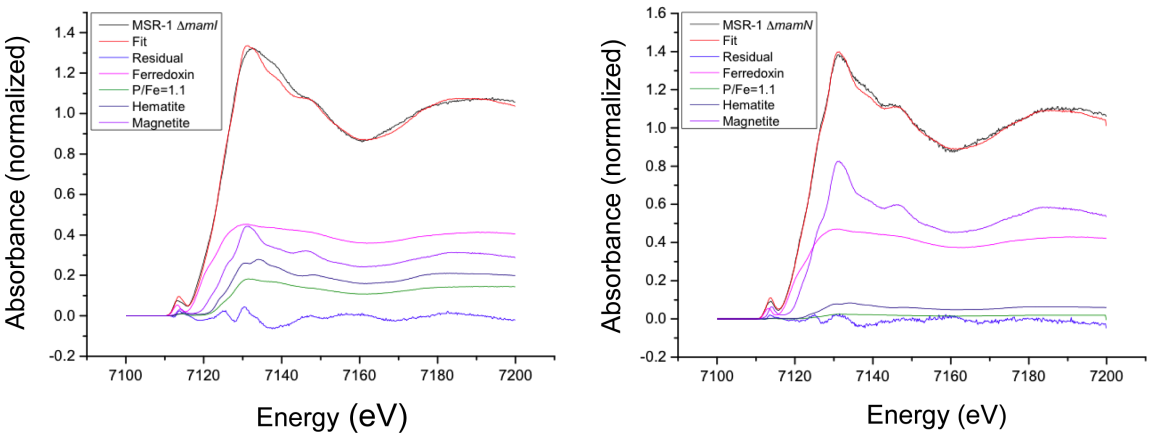

Figure S5: XANES (X-ray Absorption Near Edge Structure) analysis of mutants Δ*maml* and Δ*mamN*. XANES spectra obtained from Δ*maml* (A) and Δ*mamN* (B) are clearly distinct from those of pure magnetite as in the WT or phosphate-rich ferric hydroxides as observed in the early mineralization stages in induction experiments with MSR or AMB (14, 15). For both mutants the pre-edge peak and the low energy part of the edge are shifted towards lower energies with respect to a magnetite reference spectrum, which indicates the presence of higher ratios of ferrous iron in the cells than in the WT (33% Fe(II), 67% Fe(III)). Linear combination fitting with reference compounds (magnetite, hematite, ferrihydrite, phosphate-enriched ferric hydroxides, ferrous hexaphosphate, spinach ferredoxin) suggest that the ferrous compounds are predominantly Fe-S clusters (proteins) and account for around 40% of the total iron content in the cells. Magnetite is clearly present in the Δ*mamN* mutant (around 50% of total iron), whereas the low fit quality for Δ*maml* (large residue) does not allow us to reliable determine the structure of the Fe present in the bacteria apart from Fe-S. However, the overall line shape appears most consistent with an amorphous or only poorly ordered Fe compound as suggested by HRTEM.

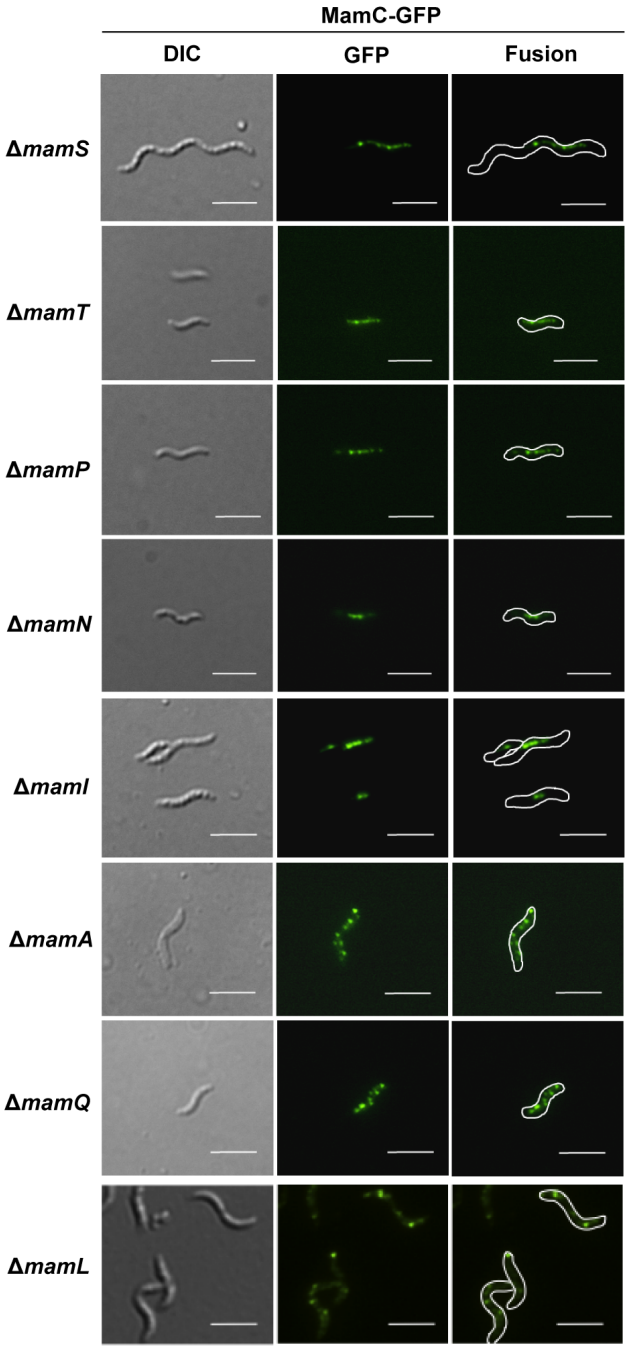

Figure S6. Fluorescence micrographs of MSR WT and various deletion strains expressing different MamC-GFP fusions. Scale bar: 4 µm.

References

1. **Schultheiss D, Schüler D.** 2003. Development of a genetic system for *Magnetospirillum gryphiswaldense*. Arch Microbiol **179:**89-94.
2. **Ullrich S, Schüler D.** 2010. Cre-lox-based method for generation of large deletions within the genomic magnetosome island of *Magnetospirillum gryphiswaldense*. Appl Environ Microbiol **76:**2439-2444.
3. **Lohsse A, Ullrich S, Katzmann E, Borg S, Wanner G, Richter M, Voigt B, Schweder T, Schüler D.** 2011. Functional analysis of the magnetosome island in *Magnetospirillum gryphiswaldense*: the *mamAB* operon is sufficient for magnetite biomineralization. PLoS One **6:**e25561.
4. **Simon R, Priefer U, Puhler A.** 1983. A Broad Host Range Mobilization System for In Vivo Genetic Engineering: Transposon Mutagenesis in Gram Negative Bacteria. Nat Biotech **1:**784-791.
5. **Saltikov CW, Newman DK.** 2003. Genetic identification of a respiratory arsenate reductase. Proceedings of the National Academy of Sciences **100:**10983-10988.
6. **Marx CJ, Lidstrom ME.** 2002. Broad-host-range cre-lox system for antibiotic marker recycling in gram-negative bacteria. Biotechniques **33:**1062-1067.
7. **Martinez-Garcia E, Calles B, Arevalo-Rodriguez M, de Lorenzo V.** 2011. pBAM1: an all-synthetic genetic tool for analysis and construction of complex bacterial phenotypes. BMC Microbiology **11:**38.
8. **Kovach ME, Elzer PH, Hill DS, Robertson GT, Farris MA, Roop RM, 2nd, Peterson KM.** 1995. Four new derivatives of the broad-host-range cloning vector pBBR1MCS, carrying different antibiotic-resistance cassettes. Gene **166:**175-176.
9. **Lang C, Schüler D.** 2008. Expression of green fluorescent protein fused to magnetosome proteins in microaerophilic magnetotactic bacteria. Appl Environ Microbiol **74:**4944-4953.
10. **Pollithy A, Romer T, Lang C, Muller FD, Helma J, Leonhardt H, Rothbauer U, Schüler D.** 2011. Magnetosome expression of functional camelid antibody fragments (nanobodies) in *Magnetospirillum gryphiswaldense*. Appl Environ Microbiol.

11. **Schultz Jr, Milpetz F, Bork P, Ponting CP.** 1998. SMART, a simple modular architecture research tool: Identification of signaling domains. Proceedings of the National Academy of Sciences **95:**5857-5864.
12. **Letunic I, Doerks T, Bork P.** 2012. SMART 7: recent updates to the protein domain annotation resource. Nucleic Acids Research **40:**D302-D305.
13. **Bolivar F, Rodriguez R, Greene P, Betlach M, Heyneker H, Boyer H, Crosa J, Falkow S.** 1977. Construction and characterization of new cloning vehicles. II. A multipurpose cloning system. Gene **2:**95 - 113.
14. **Fdez-Gubieda ML, Muela A, Alonso J, Garcia-Prieto A, Olivi L, Fernandez-Pacheco R, Barandiaran JM.** 2013. Magnetite biomineralization in *Magnetospirillum gryphiswaldense*: time-resolved magnetic and structural studies. ACS Nano **7:**3297-3305.
15. **Baumgartner J, Morin G, Menguy N, Perez Gonzalez T, Widdrat M, Cosmidis J, Faivre D.** 2013. Magnetotactic bacteria form magnetite from a phosphate-rich ferric hydroxide via nanometric ferric (oxyhydr)oxide intermediates. Proc Natl Acad Sci U S A **110:**14883-14888.

Acknowledgements

First of all, I wish to express my sincere gratitude to my supervisor, Prof. Dirk Schüler, for his continuous support, trust and encouragement in all stages of my PhD thesis, and his advices for my Post Doc applications.

I am also very grateful to Prof. Kirsten Jung for her interest in my work, for being the second examiner of this thesis, and for her advices about the social life and the time as Post Doc in the US.

I would like to thank Prof. Rolf Müller (Saarland University) and Prof. Youming Zhang (Shandong University, China) for the close collaboration and their supervision during the time I spent at the Helmholtz Institute for Pharmaceutical Research Saarland (HIPS). Also, I would like to thank Prof. Mihály Pósfai (University of Pannonia), Prof. Gerhard Wanner (LMU Munich), Prof. Jürgen M. Plitzko (Utrecht University, Netherlands) and Dr. Andreas Brachmann (LMU Munich) for the fruitful collaboration.

I feel highly indebted to many current and former members of the “Magnetolab”. In particular, I want to thank Dr. Christian Jogler, Dr. René Uebe, Anna Lohße, Oliver Raschdorf and Sarah Borg for many scientific and non-scientific discussions.

Many thanks go to my undergraduate students Pamela, Andreas and Felizitas. It was a great pleasure to work with you.

I sincerely thank my family for their encouragement and patience, and for taking care of our son Hannes, when my husband and I needed support.

My deepest gratitude goes to my husband Sebastian for his continuous support, inspiration and trust during all these years.

Eidesstattliche Erklärung

Ich erkläre hiermit an Eides statt, dass die vorgelegte Dissertation von mir selbständig und ohne unerlaubte Hilfe angefertigt ist. Des Weiteren erkläre ich, dass ich nicht anderweitig ohne Erfolg versucht habe, eine Dissertation einzureichen oder mich der Doktorprüfung zu unterziehen. Die vorliegende Dissertation liegt weder ganz, noch in wesentlichen Teilen einer anderen Prüfungskommission vor.

Isabel Kolinko, München